Studies of inherently conducting polymers in ionic liquids

Jakub Mazurkiewicz
University of Wollongong

STUDIES OF INHERENTLY CONDUCTING POLYMERS IN IONIC LIQUIDS

A thesis submitted to satisfy the requirements for the award

DOCTOR OF PHILISOPHY

from

THE UNIVERSITY OF WOLLONGONG

by

JAKUB MAZURKIEWICZ, BSc. (Hons)

DEPARTMENT OF CHEMISTRY – INTELLIGENT POLYMER RESEARCH INSTITUTE

January 2007

“I am enthusiastic over humanity's extraordinary and sometimes very timely ingenuities. If you are in a shipwreck and all the boats are gone, a piano top buoyant enough to keep you afloat may come along and make a fortuitous life preserver. This is not to say, though, that the best way to design a life preserver is in the form of a piano top. I think we are clinging to a great many piano tops in accepting yesterday's fortuitous contrivings as constituting the only means for solving a given problem.”

- Buckminster Fuller

ABSTRACT

In this dissertation, the effect of ionic liquid (IL) or classical electrolyte (CE) employed on the redox behaviour of many inherently conducting polymers (ICPs) was investigated with the ultimate goal of producing flexible batteries.

ICPs can be used in a range of unique applications, and also to replace many metal conductors or inorganic semiconductors. Commercialisation of ICPs has, however, been limited. Ion and solvent transport in ICPs during redox cycling almost universally leads to breakdown of redox activity and desired properties of the material. ILs comprise of neat ions in the form of a room temperature melt. ILs show great promise as novel electrolytes to enhance the stability of ICPs beyond that observed in CEs and paves the way to commercialisation of ICP devices.

Chapter 3 describes fundamental investigations of ICP / IL systems on Pt disk electrodes. The redox cycling stability of polypyrrole was increased over those of CE systems in the IL 1-butyl-3-methylimidazolium hexafluorophosphate ($BMIPF_6$). The electroactivity in this system showed no degradation over 900 redox cycles. The use of 1-ethyl-3-methylimidazolium (bis) trifluoromethanesulfonimide (EMITFSI) also improved the redox stability of polypyrrole in comparison to the CE systems. The stable potential windows of polypyrrole were significantly improved in both IL systems compared to CEs.

The transitional behaviour between ILs and CEs was investigated by diluting ILs in a common neutral solvent electrolyte, propylenecarbonate (PC). In such IL / CE mixtures,

differences were noted in the electrolyte conductivity profile and ICP electroactivity with respect to concentration of IL. $BMIPF_6$ exhibited a significantly higher degree of ion pairing than EMITFSI, and the strong ion pairing property of $BMIPF_6$ is thought to be responsible for unique electrochemical observations absent from the ICP in EMITFSI systems.

N-doping is an attractive feature of some ICPs and has promise in charge storage applications, providing significant driving potential differences of two or more volts against p-doped electrodes. As ILs were found to enhance redox stability of common p-doping processes in ICPs, investigations were conducted in Chapter 4 to see if the same was true for inherently unstable n-doping processes.

Poly-3-*p*-flourophenylthiophene (P3PFTh) was chosen as a model n-doping system, due to its well published n-doping behaviour in classical electrolytes. Surprisingly, n-doping responses of P3PFTh in EMITFSI were very poor. The reasons behind this were explored by testing other n-dopable polymers in EMITFSI to isolate whether EMITFSI was inherently preventing n-doping, and P3PFTh was tested with different ILs to investigate P3PFTh / EMITFSI incompatibility.

EMITFSI used as an electrolyte was found to decrease electroactivity of the n-doping processes in most polythiophenes, with the exception of polybithiophene (PBiTh). The stability of n-doping PBiTh in EMITFSI did not, however, improve to an extent that would allow derivative devices to be practical.

Spectroelectrochemical Raman studies of the n-doping processes of polythiophenes in EMITFSI were conducted *in-situ* to reveal behaviour that may be responsible for poor electrochemical responses. Raman studies showed that both the p-doping and n-doping process in polythiophenes occurred with a 'reverse' mechanism of ion expulsion upon doping (whereas doping processes of ICPs in CEs usually occur by ion insertion). The Raman studies also indicated that the physical structure of polythiophene had a large effect on the resulting electrochemistry, to an extent that impeded doping processes.

The structure-activity relationships of P3PFTh were investigated by CV using a range of growth and cycling electrolytes. Observations were analysed chemometrically to identify the effects on electrochemical parameters of electrolyte component (anion or cation), whether the dominating effect was from growth or cycling electrolyte, and which particular doping / dedoping process was affected by these parameters.

Chapter 5 describes electrochemical charge storage devices based on IL electrolytes using various substrates, polymers and configurations. The highest capacity device was based on polyaniline doped with ferrocene sulphonic acid on carbon fibre textile for both anode and cathode, with a polyvinylidene fluoride (PVDF) separator and EMITFSI electrolyte. The flexible charge storage device produced in this way had a maximum charge capacity of 58 mAh/g, but degraded quickly on cycling. The most stable device was constructed similarly to the highest capacity device, but used polypyrrole and poly-3-methylthiophene electrodes, with maximum charge capacity of 17 mAh/g, remaining unchanged for 60 cycles.

DECLARATION

This is to certify that the work described in this thesis has not been submitted for a higher degree at any other university or institution.

Jakub Mazurkiewicz

PUBLICATIONS

Journal Papers

1. Lu, Wen, G. Fadeev Andrei, Baohua Qi, Elisabeth Smela, R. Mattes Benjamin, Jie Ding, M. Spinks Geoffrey, **Jakub Mazurkiewicz**, Dezhi Zhou, G. Wallace Gordon, R. Macfarlane Douglas, A. Forsyth Stewart and Maria Forsyth. *"Use of ionic liquids for pi-conjugated polymer electrochemical devices."* Science, 2002 297: 983-7.

2. **Jakub Mazurkiewicz**, Peter Innis, Gordon Wallace, D. R. Macfarlane, M Forsyth *"Conducting polymer electrochemistry in ionic liquids."* Synthetic Metals, 2003 135-136: 31-32.

3. Peter Innis, **Jakub Mazurkiewicz**, T Nguyen, Gordon Wallace, D Macfarlane. *"Enhanced electrochemical stability of polyaniline in ionic liquids."* Current Applied Physics, 2004 4: 389-393.

Conference Proceedings

1. **Jakub Mazurkiewicz**, Gordon Wallace, Peter Innis, . *"Flexible fabric batteries from conductive polymers and ionic liquids."* ICSM 04: The role and impact of Nanoscience & Nanotechnologies, IPRI - University of Wollongong, 2004: 112.

2. **Jakub Mazurkiewicz**, Gordon Wallace, Peter Innis. *"p- and n-doping in poly (bithiophene) using ionic liquid electrolyte."* ICSM 04: The role and impact of Nanoscience & Nanotechnologies, IPRI - University of Wollongong, 2004: 112.

3. Wallace, G. G., D. Zhou, J. Ding, B. Xi, P. Innis, **J. Mazurkiewicz**, G. M. Spinks, J. Gillespie, D. R. Macfarlane and S. Forsyth. *"Ionic liquids and helical interconnects: Bringing the electronic Braille screen closer to reality."* EAP Actuators and Devices. SPIE. ,2003. 5051

ACKNOWLEDGEMENTS

I would like to thank my supervisors Prof. Gordon Wallace and Assoc. Prof. Peter Innis for providing me with an excellent opportunity to undertake study with them.

I would like to particularly thank Assoc. Prof. Peter Innis for his enthusiasm and encouragement, and also his vast technical expertise and knowledge without which little would be possible for others and myself in the department.

I would like to express gratitude to the Australian Government for an Australian Postgraduate Award Scholarship, the US Naval International Cooperative Opportunities in Science and Technology Program (NICOP) for additional funding and Schefenacker Vision Systems with the Commonwealth Research Council (CRC) for my pre-submission employment.

I would further like to thank my colleagues, co-workers and visitors alike who helped provide a working environment that was stimulating, fruitful and immensely enjoyable. In particular, I would like to thank Jenny (Causley) Halldorsson, Magnus Gustavsson, Scott McGovern, Lou Fox, Adrian and Meghan Gestos and Richard (Yanzhe / Tricky) Wu, for providing endless support, creative input and friendship.

A very special thankyou goes out to Prof. Leon Kane-Maguire, who helped with the final corrections of this dissertation by going through it word-by-word with me. Leon, you are a Saint.

Last but not least, I thank my parents for all of the support they have provided.

TABLE OF CONTENTS

LIST OF FIGURES

LIST OF ABBREVIATIONS

3MeTh	3-Methylthiophene
3PFTh	3-Parafluorophenylthiophene
A	Electrode area (cm^2)
ACN	Acetonitrile
A_{ox}	activity (concentration) of oxidised species
A_{red}	activity (concentration) of reduced species
AUX	auxillary electrode
B	Bipolaronic
BF_4	tetrafluoroborate
BiTh	2,2'-Bithiophene
BMI	1-Butyl-3-methylimidazolium
C	analyte's concentration (mol/L)
cet	Cetrimide
ClO_4	Perchlorate
c^o	Initial concentration
CV	Cyclic Voltammetry
D1	Dimension 1
D2	Dimension 2
D^o	Diffusion constant
E	Overpotential
E^0	Standard potential of reaction
EDOT	3,4-Ethylenedioxythiophene
EMI	1-Ethyl-3-methylimidazolium
F	Faraday's constant
FEM	Finite element method
GC	Glassy carbon
I	Current
ICP	Inherently conducting polymer
IL	Ionic liquid
IR	Internal resistance
Li	Lithium
MDS	Multidimensional scaling
n	Number of electrons involved in process
Ns	Density of conjugated chain segments.
P	Poly-
P	Polaronic
PC	Propylenecarbonate
PCA	Principal component analysis
PF_6	Hexafluorophosphate
Pt	Platinum
PVDF	Polyvinylidene fluoride

Py	Pyrrole
R	Gas constant
R	Universal gas constant (8.314 J / mol K)
RE	Reference electrode
RSQ	Proportion of variance
SEM	Scanning electron microscopy
t	time (seconds)
T	Temperature in Kelvin
TBA	Tetrabutylammonium
TEA	Tetraethylammonium
TerTh	2,2':5',2"-Terthiophene
TFSI	(bis)trifluoromethanesulfonimide
TMA	tetramethylammonium
V	Voltage / Volts
WE	Working Electrode
x	distance from electrode
E	applied potential.
$E_{ox}P$	mean potential of polaron formation.
σ	peak width at half height

CHAPTER 1

GENERAL INTRODUCTION

1.1 Overview

This thesis investigates the performance of inherently conducting polymers (ICPs) in the presence of novel electrolyte systems, namely ionic liquids (ILs). A general background on ICPs and a discussion of the novel electrolyte systems is therefore provided in this Chapter.

1.2 Conducting Polymers

In the year 2000, Hideki Shirakawa, Alan MacDiarmid, and Alan Heeger were awarded the Nobel Prize in Chemistry[1] for the discovery and development of conducting polymers[2]. The significance of conducting polymers was that plastics could now be created which could conduct electricity to a degree approaching that of copper[2]. Such properties were previously unheard of, as organic polymers are typically electrical insulators and commonly used as such.

Polyacetylene was the first generation material, but it is unstable in atmospheric conditions so other ICPs were soon developed. The next generation of ICPs were made from five-membered heterocycles and anilines. These conducting polymers possessed new characteristics, including increased stability and properties that could be custom tuned to specific applications.

The possible applications of conducting polymers vary widely, with reported uses including energy storage[3,4,5,6], electrical displays[7,8,9,10,11], sensors (pressure, temperature, chemical)[12,13,14,15,16,17], drug release systems[18,19,20], artificial muscles[21,22,23], active electronics[24,25,26], corrosion inhibitors[27,28,29], electromagnetic shielding[30], light emitting devices[31,32,33] and information storage[34,35].

Apart from polyacetylene, the polymers in Figure 1.1 provided further benefit from the fact that they could be synthesised simply in ambient conditions, using either chemical or electrochemical techniques.

Structure	Name	Abbreviation
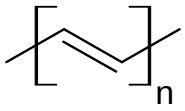	**polyacetylene**	**PAc**
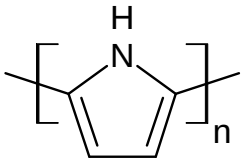	**polypyrrole**	**PPy**
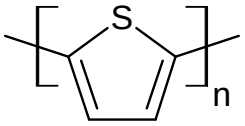	**polythiophene**	**PTh**
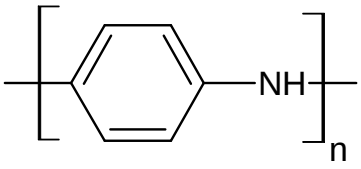	**polyaniline**	**PAn**

Figure 1.1- Structures and names of some common inherently conducting polymers (ICPs).

1.3 Limitations of Conducting Polymers

Simple syntheses from readily available starting materials have brought conductive polymers into the limelight, although few applications have achieved commercialisation to date. So why are materials with such fantastic possibilities so poorly exploited? The most general answer is the lack of stability to satisfy commercial requirements.

We know that polyacetylene reacts readily with atmospheric oxygen to destroy conjugation and render the material an insulator. Such ‘passive’ atmospheric sensitivity was mostly overcome when heterocyclic conducting polymers were discovered. Yet, stability issues still exist when it comes to systems relying on redox changes. Significant degradation still occurs during redox cycling, even when great care is taken to exclude water and oxygen.

1.4 Conductivity and Charge Transport in Conductive Polymers

To shed light on what makes conductive polymers conductive, the best starting point would be to look at what electrical conductivity actually is, and how it works. An electrical conductor has free or mobile electrons that convey charge. An insulator does not have free electrons, as its electrons are immobilised in bonds and such materials fall into the category of dielectric materials. At high potentials, however, even dielectrics allow current to pass. The notion of electronic bands is useful in conceptualising these properties and explaining the origins of electrical conductivity.

1.4.1 Electronic Bands and Electrical Conductivity

The concept of electronic bands has been applied to describe electrical conductivity, semiconducting properties and insulating properties. It stems from quantum theory, which states that electrons *cannot* occupy an arbitrary energy state. The energy states in a given material can be loosely grouped into the valence band (VB) and conduction band (CB) (Figure 1.2).

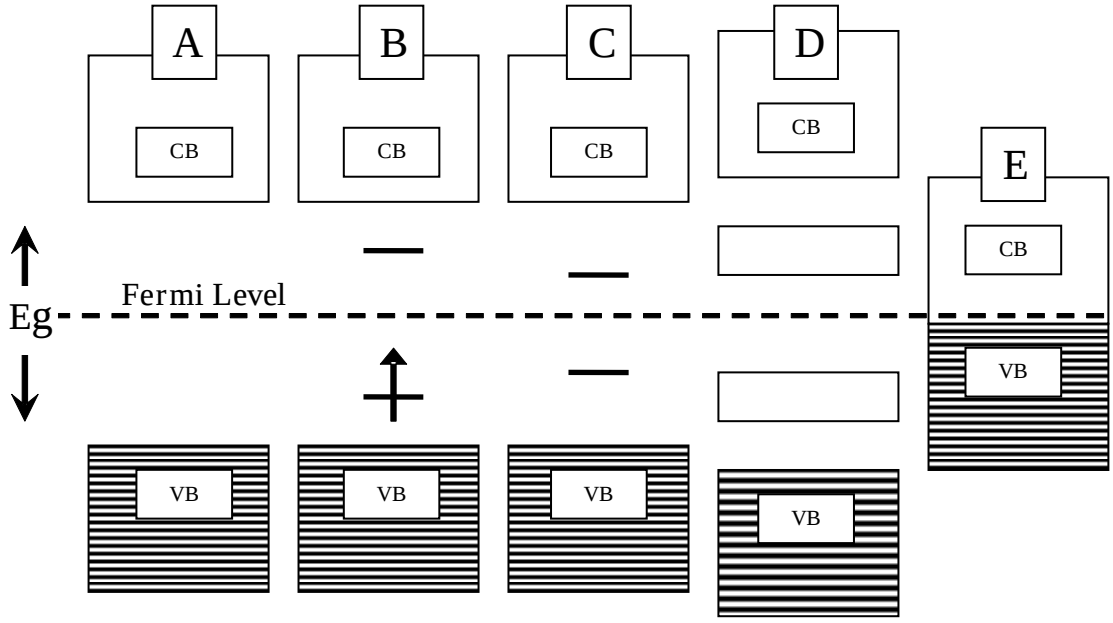

Figure 1.2- The electronic band structures of various classes of materials. (Eg)- band-gap, (CB)- conduction band, (VB)- valence band.

A	**-**	*insulator*
B	**-**	*conducting polymer with a polaron*
C	**-**	*conducting polymer with a bipolaron*
D	**-**	*highly doped conducting polymer*
E	**-**	*conductive metal.*

The VB represents the energies of electrons that are used to bind the molecule together; the uppermost level of the VB directly correlates to the highest occupied molecular orbital (HOMO). The lowest excitation energy level of a molecule or the lowest

unoccupied molecular orbital (LUMO) correspondingly correlates to the bottom of the CB. The energy required to move electrons from the VB to the CB is the band gap (Eg) displayed in Figure 1.2.

The limiting case, shown in Figure 1.2A, represents an insulator, because electrons need considerable energy to pass from the VB to the mobile region of the CB. Hence, electron movement cannot easily happen across the molecule if the energy jump is overly high. The opposite limit is shown in Figure 1.2E; the band structure is that of a metal. The VB electrons have easy access to the CB and are free to move around the material. In fact, there is a small Eg between the VB and CB, but this is usually regarded as insignificant.

Figure 1.2B, C and D show the energy state development upon doping a typical conducting polymer. Figure 1.2B denotes the energy levels of a polaron, which may be formed sequentially. On the formation of the first polaron state (by removal or addition of an electron), an electron of quantum spin 1/2 is raised to an energy level somewhere in what used to be the barren *'forbidden'* zone. This energetic stepping-stone in the band gap is essentially how silicon semiconductors are modelled, and thought to conduct electricity. The physical consequence is electrons gain easier access to the conduction band by negotiating lower energy vacancy sites (p-type) or by promoting polaron electrons to conduction (n-type).

In earlier studies of conducting polymers, the doped semiconductor model was thought to be sufficient to explain conductivity. Soon observations were made which did not

correspond to charge conduction via a polaron alone. If there are two polarons next to each other, thermodynamics, and quantum mechanics take over. A system like a polymer chain is no suitable place for two electrons with the same spin to co-exist at the same energy level, as dictated by the quantum Pauli Exclusion Principle. One of the electrons has to flip its spin so that the two electrons can carry opposing spins. Thermodynamically, this process is also favoured and the resulting state is called a bipolaron. Although the bipolaron state is higher in energy than an individual polaron state, it is lower in energy than two polaron states.

The result of two polarons coming together in energy states and forming a bipolaron is that the conduction state has spin of +1/2 and -1/2, resulting in a total spin of 0, unlike inorganic semiconductors. Inorganic semiconductors deal with the Pauli Exclusion Principle by dissipating the electrons as far away from each other as possible. Polymer chains can deal with the situation differently, by causing localised defects of lower energy.

This effect of removing electrons from the conjugated polymer can continue due to the nature of charge localisation, so much so that it is possible to form a cation, usually with up to one for every three monomeric units. Such populous bipolaronic formation results in the widening of bipolaronic bands as seen in Figure 1.2D, at the expense of removing states from the VB and CB. The presence of these bipolaron bands allows easy access for electrons to enter the CB, via a few small energy level jumps, and therefore, allowing for the flow of electric current.

1.4.2 Doping and Charge Conduction in ICPs

To facilitate free electron movement, there is a requirement that a conjugated polymer be reduced or oxidised for smaller band gap energies to be formed. This allows electrons simpler transitions into the conduction band. If a polymer is reduced or oxidised, a negative or positive charge is formed, respectively, upon the polymer chain. If this charge is both stable and mobile, which arises from the presence of long-range conjugation, such charges will be balanced by the incorporation of a counter ion, typically referred to as a dopant. In the case of ICP redox systems, this usually involves a small, mobile ion species present during synthesis, *i.e.* a spectator ion, such as the reduced form of a chemical oxidant or an electrolyte ion species used during electrochemical synthesis.

Application of an appropriate electrochemical current to a conjugated polymer system may result in reduction or oxidation of the polymer. The removal or addition of electrons from the chemical redox state of the polymer is complemented by the migration of ions resulting in charge conduction. This process is quite different to the electron conduction in section 1.4.1 above, but the processes are fundamentally inter-twined. Thus, the reduction or oxidation of an ICP is required for an ICP to be electron conductive, and the redox charge requires the presence of a dopant to balance the excess charge.

1.5 Ionic Liquids

1.5.1 What are Ionic Liquids?

Ionic liquids (ILs) are a class of compounds composed entirely of ionic species existing in the liquid state below 100 ºC. The name refers specifically to a class of compounds which are held together prevalently by ionic forces, such as common table salt; but whereas table salt is solid at or around room temperature, ILs are in a liquid state. This contrasts significantly to many alternative ionic compounds, which either decompose on heating or require temperatures of several hundred degrees to reach a molten state (e.g. common table salt [NaCl] melts at 803 ºC[36]).

ILs have been known since 1914[37], but the number of publications has exponentially increased only in the last five years. The interest has stemmed from the fact that ILs have some remarkable properties not present in other types of liquids or salts. ILs generally possess exceptionally low vapour pressure[38], high thermal stability[39], large electrochemical windows[40], powerful catalytic properties[41,42], as well as widely tuneable solvent properties[43], ranging from hydroscopic[44] to hydrophobic[45].

Much research has been carried out towards applying ILs as recyclable solvents in chemical reaction media[46], alternatives to volatile reaction solvents[47] and catalysts[48]. They also possess properties that make them very attractive as electrolytes. An IL that is environmentally stable, neither evaporating away or into being affected by moisture,

whilst having good ionic conductivity and a large electrochemical window, is particularly sought after.

One such IL is 1-ethyl-3-methylimidazolium (bis) trifluoromethanesulfonimide (EMITFSI). EMITFSI is liquid from -15 °C and decomposition occurs well above 100 °C [49]. It has no measurable vapour pressure, is immiscible with water and has an electrochemical window of approximately 4.5 V on glassy carbon[50].

1.5.2 Why are Ionic Liquids, liquid?

The fluidity of ILs stems from various structure and electronic properties. The characteristics usually required for fluidity to manifest are:

- Low symmetry of ions. This is most easily achieved by synthetic manipulation of the cation; the anion usually being more difficult to manipulate. Low symmetry discourages the system to collapse into an organised solid[51,52].

- Charge dissipation. A system which has its charge dispersed over several atoms of a molecule allows greater mobility and increased susceptibility to entropy[49].

- Steric hindrance. Parts of a molecule may prevent ionic centres coming too close together to form a very strong bond causing solidification[53].

1.6 Contrasts of Ionic Liquids and Classic Electrolytes

1.6.1 Introduction

The most striking and obvious difference between ILs and classical electrolyte (CEs) is that ILs lack any neutral solvent. This therefore results in different charge conduction mechanisms between ILs and CEs[54]. The conductivity of a CE is governed by diffusion of dissociated ions through a molecular liquid under the influence of an electrical field and the resulting concentration profiles of those ions[55]. As the concentration profile of ILs is essentially unchangeable in the neat system, simple diffusion cannot itself explain why these materials are conductive.

1.6.2 Charge Conduction in a Classical Electrolyte (CE)

Ion conduction in CEs often occurs when both the cation and anion become dissociated and surrounded by solvent molecules. Such a separated charge system would allow for ions to migrate under external influences, and to become the charge carriers of the system. When a potential field is applied, such as with biased electrodes, ions interact with the field and migration occurs. The charge on the electrode begins to play the role of the complementary charge. The migration of ions away from an arbitrary space further from the electrode causes a concentration deficiency in that region. Regions beyond, now having a thermodynamic excess of ions, equilibrate the situation by supplying more ions via diffusion (Figure 1.3). The Brownian motion and electrochemical drag stemming from ion size and its dissociative interaction with solvent determines the efficiency of charge transport in a given system.

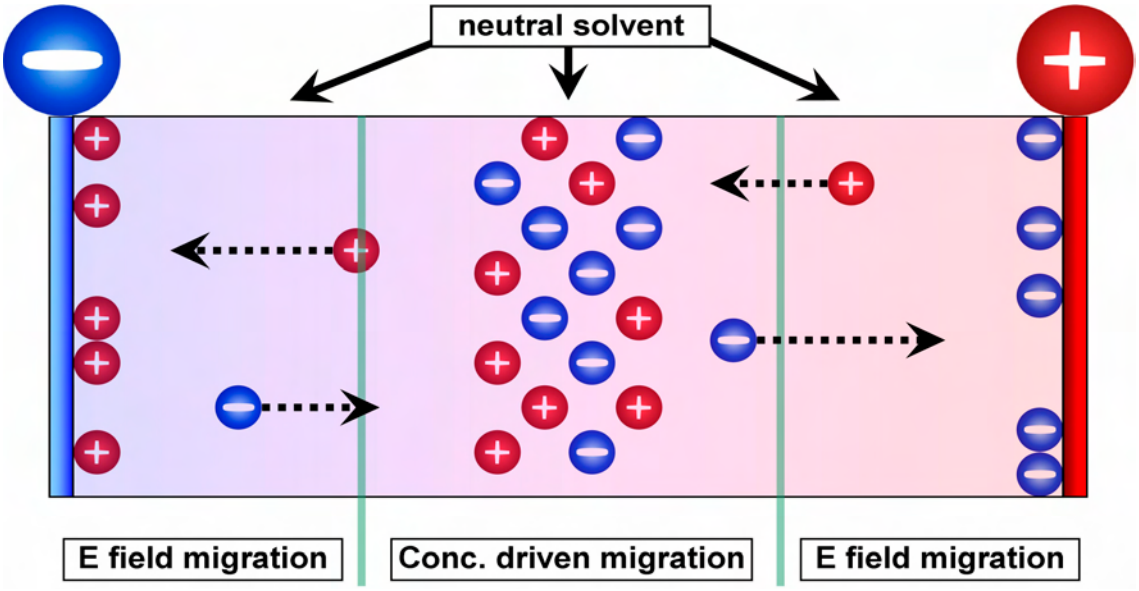

Figure 1.3- Ion migration in a classical electrolyte.

1.6.3 Charge Conduction in Ionic Liquids

Charge conduction in an IL is not driven by simple diffusion. The ion density points towards a hopping mechanism[56], illustrated in Figure 1.4. The mechanism resembles the conductivity behaviour of conducting polymers, as mentioned in Section 1.4. Ionic conductivity requires charge carriers.

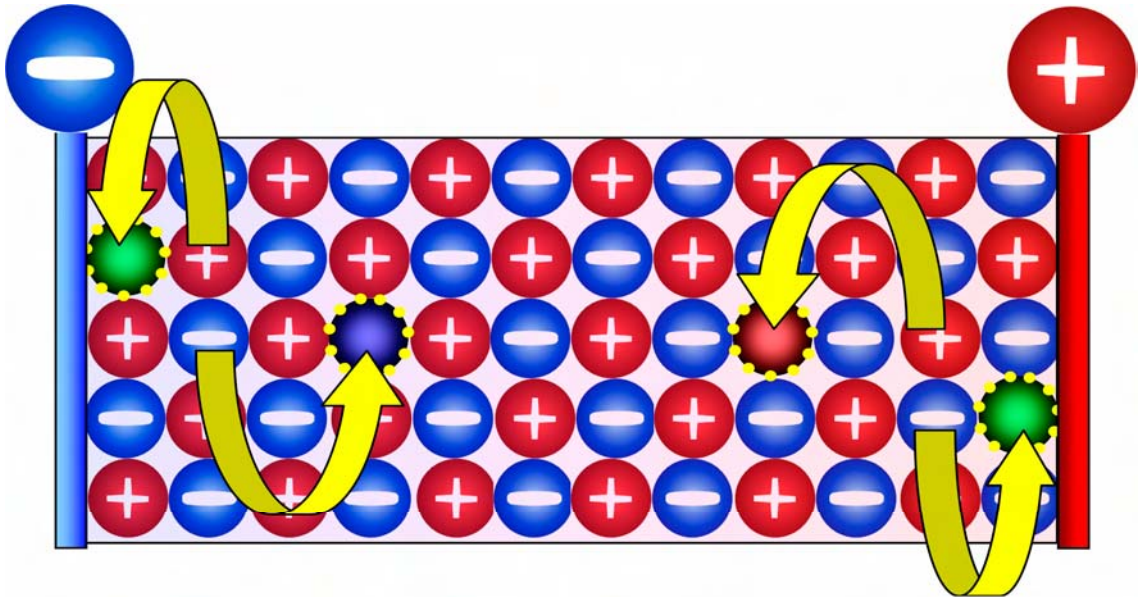

Figure 1.4- Charge conduction via hopping in ionic liquids.

A CE contains mostly dissociated ions, and the dissociated species in turn are the charge carriers. In a neat IL, the charge carriers are charged vacancies. When an IL is mixed with a neutral solvent or molecular liquid, we may find that the system can form intermediates between dissociation and dilution[43], depicted in Figure 1.5. Further evidence by MacFarlane[57] *et al*., towards ion-pairing scenarios is the lack of change of density when an IL is mixed with a molecular solvent. If ions become dissociated then one would expect a change in density, however, the density follows a simple mixture law.

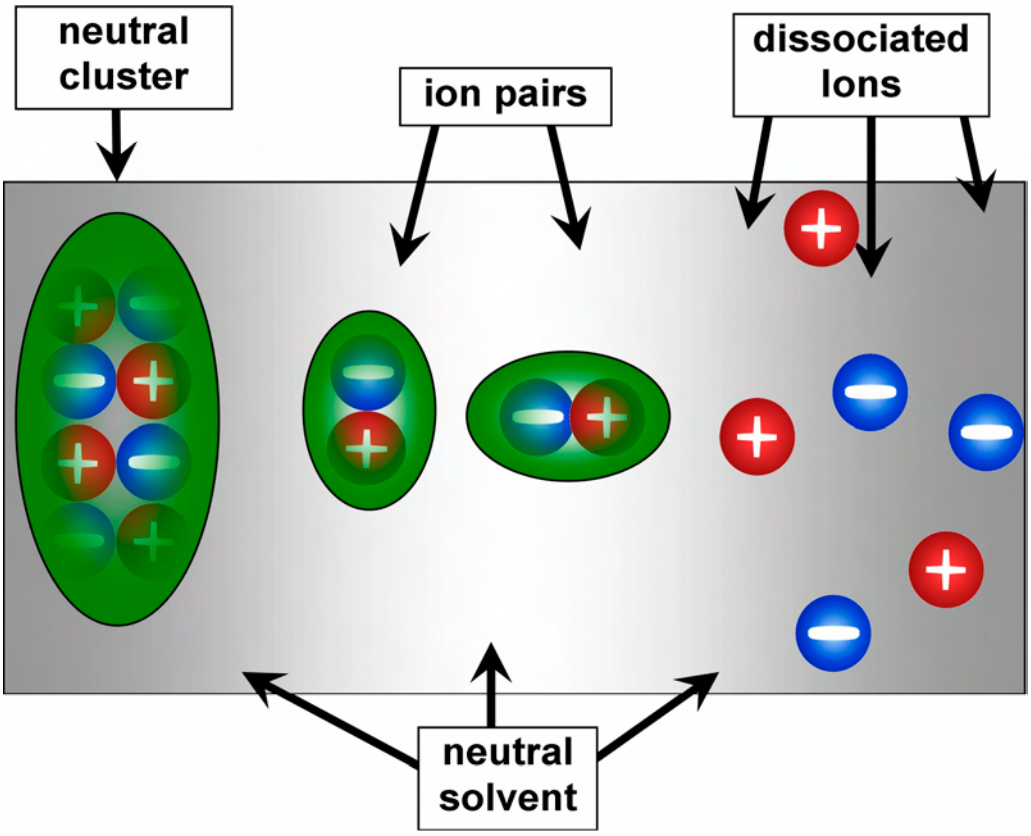

Figure 1.5- Possible phases of ionic liquid in a neutral solvent.

The determination of conductivity in an IL is usually limited by viscosity[43], and relates to the amount of charge carriers, which in turn relates to the ability of ILs to form vacancies and allow charge migration by hopping.

1.7 Interaction of Conducting Polymers with Electrolytes

This Chapter has focused on conducting polymers and the choice of two main kinds of electrolytes, ILs and CEs. The discussion in Section 1.5 indicate that the process of charge conduction in ILs is fundamentally different to charge conduction in CEs. In Section 1.4, distinctions were made between electrical conductivity of ICPs and the ionic conductivity during the redox process, although the two are closely related. We will now consider some of the possible interactions between conducting polymers and the two types of electrolytes discussed in this Chapter.

Figure 1.6 depicts the situation of an ICP in an oxidation process in a CE system. Figure 1.6a is the situation where the ICP is in the process of being oxidised. The dissociated ions are surrounded by a solvent sphere composed of the neutral solvent. A solvent sphere is necessary for the dissolution of the ionic species, and may interact sufficiently with the ion to be dragged into the conducting polymer. When the polymer is reduced to a neutral state, as in Figure 1.6b, it is possible that the ion will be ejected, leaving some of its solvent sphere behind; and a new solvent sphere will be created when the ion interacts with additional neutral solvent[58]. Neutral solvent cannot carry charge by itself, and the production of neutral pockets may prevent intermolecular electron conductivity, eventually playing a role in the degradation of the electroactivity of the polymer by segregation of conducting chains by dielectric species.

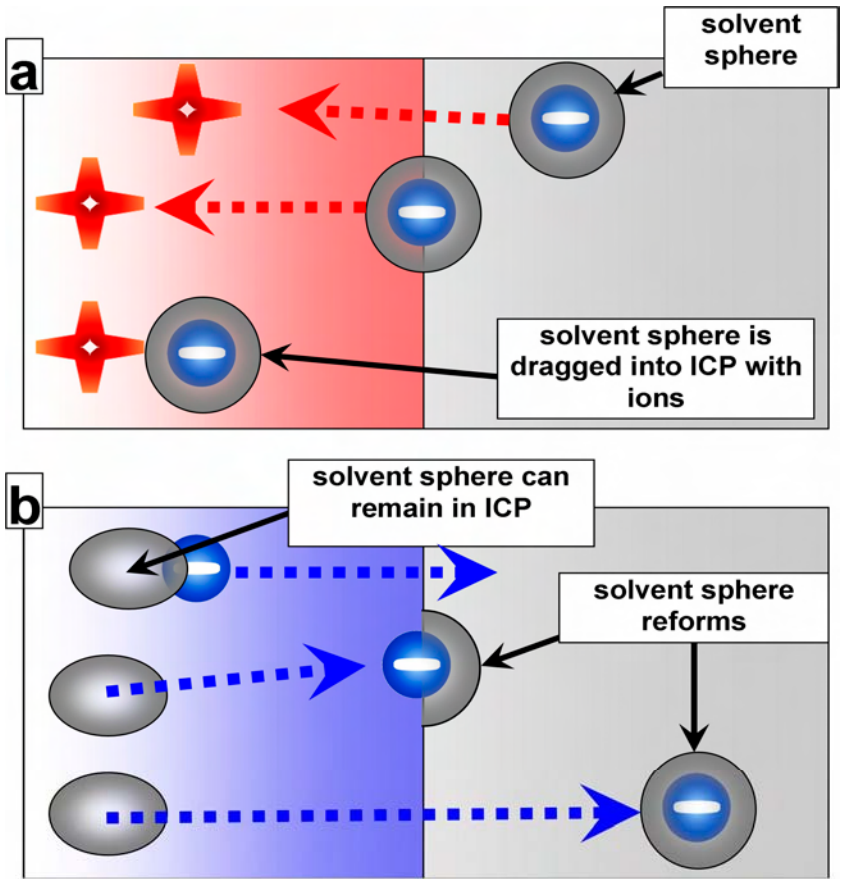

Figure 1.6- Proposed mechanism of ion and solvent movement into an ICP. (a)- initial oxidation, (b)- subsequent reduction to neutral state.

In IL / conducting polymer systems, cation diffusion has been found to dominate the charge-balancing requirements of p-doping / dedoping processes[59,60,61,62]. It has so far been discussed that ILs can only conduct charge via hole-hopping mechanisms. Therefore, the following discussion aims to reconcile how hole-hopping mechanisms may lead to the observation of cation expulsion upon oxidation of a conducting polymer in IL, rather than anion inclusion, as observed with most classical electrolyte / ICP systems.

Figure 1.7a shows an ICP / IL system where ion pairs infuse into the pores of the conducting polymer. (The system can be in an arbitrary oxidation state at this point, but a neutral state was chosen to clarify the diagram.)

If we look at the surface of an ICP film electrode under the application of positive charge in an ionic liquid (Figure 1.7b), we would expect that anions would eventually migrate to the electrode surface to balance the charge. The solid electrode surface has, however, fewer degrees of freedom than the bulk ionic liquid. Therefore, it would be difficult to force anions into that region without first displacing some cations. Cations are repelled from the charge of the positive electrode into the fluid ionic liquid, which can accommodate additional ions more readily than the surface of an electrode.

The resultant negative holes created at the IL interface may temporarily balance charge and provide vacancies for cations to occupy. Thus, the cation is expelled from the ICPs ion pairs from Figure 1.7a, into negatively charged vacancies, and the anion remains in the ICP to balance the positive charge from the oxidation of conducting polymer chains. When the polymer from Figure 1.7b is subsequently reduced to Figure 1.7c, positive holes can form at the IL interface when cations migrate into the polymer. The anions from the conducting polymer do not fill these positive holes, as the bulk IL anions can diffuse to these holes much faster.

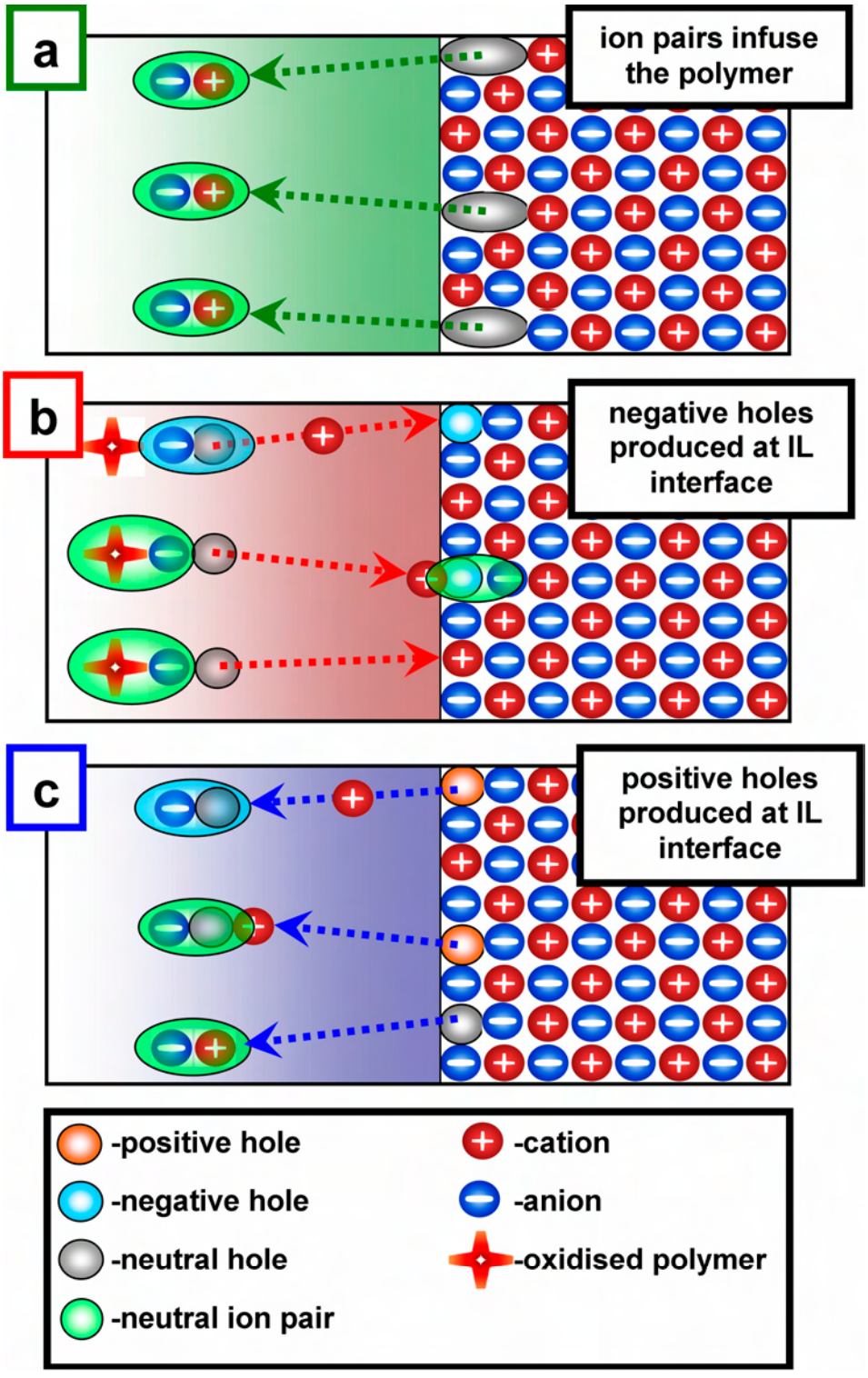

Figure 1.7- Proposed ion movement of an ionic liquid in a conducting polymer. (a)- ion pairs infuse the polymer by osmosis and capillary action, (b)- positive potential causes oxidation of polymer and produces negative holes for cations to occupy, (c)- subsequent reduction process produces positive holes which are rapidly occupied by anions from the bulk ionic liquid.

Such a mechanism requires cations or anions to first migrate away from the positive and negative electrodes, respectively, to initiate charge conduction and charge balance processes. In such a way, cation expulsion in p-doping and anion expulsion in n-doping processes may be rationalised in conducting polymer / ionic liquid systems.

1.8 Outline of Objectives

The specific aims of this project therefore are:

1- To investigate the interactions of ICPs with ILs. This will be compared with ICPs in CEs, and the differences observed discussed.

2- To explore novel characteristics that such systems may present. In comparison to CEs, ILs show characteristics of improved stability, both in cycling durability and the stable potential range over which ICPs may operate.

3- To find fundamental factors which differentiate ILs and CEs. Although ILs and CEs have obvious differences, the situation of diluting ILs in neutral solvents may give additional information on the inherent interactions within ILs.

4- To investigate and optimise electrochemical charge storage systems based on ILs and ICPs. The lack of volatility, increased environmental stability, and lack of corrosiveness of many ILs provides an opportunity to build more stable and safe batteries than current designs.

1.9 References

[1] Nobel, Foundation. *"For the discovery and development of conductive polymers."* http://nobelprize.org/chemistry/laureates/2000/, 2000 *The Nobel Prize in Chemistry 2000*.

[2] Hideki Shirakawa, Edwin J. Louis, Alan G. Macdiarmid, Chwan K. Chiang and Alan J. Heeger. *"Synthesis of electrically conducting organic polymers: Halogen derivatives of polyacetylene, (ch)x."* J. Chem. Soc., Chem. Commun., 1977: 577.

[3] Yossef Gofer, Haripada Sarker, Jeffrey G. Killian, Theodore O. Poehler, Peter C. Searson. *"An all-polymer charge storage device."* Appl. Phys. Lett., 1997 *71*: 1582-1584.

[4] S. A. Hashmi, R. J. Latham, R. G. Linford &W. S. Schlindwein. *"Conducting polymer-based electrochemical redox supercapacitors using proton and lithium ion conducting polymer electrolytes."* Polymer International, 1998 *47*: 28-33.

[5] Scrosati, Bruno. *"Conducting polymers: Advanced materials for new design, rechargeable lithium batteries."* Polymer International, 1998 *47*: 50-55.

[6] Gurunathan, K., A. Vadivel Murugan, R. Marimuthu, U. P. Mulik and D. P. Amalnerkar. *"Electrochemically synthesised conducting polymeric materials for applications towards technology in electronics, optoelectronics and energy storage devices."* Materials Chemistry and Physics, 1999 *61*: 173.

[7] Meng, Hong, Derald Tucker, Sterling Chaffins, Yongsheng Chen, Roger Helgeson, Bruce Dunn and Fred Wudl. *"An unusual electrochromic device based on a new low-bandgap conjugated polymer."* Advanced Materials (Weinheim, Germany), 2003 *15*: 146-149.

[8] Schneider, Martin J., Clemens Elster, Rolf Muelhaupt, Josef Honerkamp, Roland Nolte, Volker Wittwer and Konstantin Ledjeff. *"Synthesis of polymer electrolytes with high ion conductivity using experimental design of multicomponent polymer systems."* Industrial & Engineering Chemistry Research, 1993 *32*: 3128-34.

[9] Reeves, Benjamin D., Christophe R. G. Grenier, Avni A. Argun, Ali Cirpan, Tracy D. Mccarley and John R. Reynolds. *"Spray coatable electrochromic dioxythiophene polymers with high coloration efficiencies."* Macromolecules, 2004 *37*: 7559-7569.

[10] Schottland, Philippe, Kyukwan Zong, Carleton L. Gaupp, Barry C. Thompson, Christopher A. Thomas, Irina Giurgiu, Roberta Hickman, Khalil A. Abboud and John R. Reynolds. *"Poly(3,4-alkylenedioxypyrrole)s: Highly stable electronically conducting and electrochromic polymers."* Macromolecules, 2000 *33*: 7051-7061.

[11] Leventis, Nicholas and Young C. Chung. *"New complementary electrochromic system based on poly(pyrrole)-prussian blue composite, a benzylviologen polymer, and poly(vinylpyrrolidone)/potassium sulfate aqueous electrolyte."* Chemistry of Materials, 1992 *4*: 1415-22.

[12] H. Kaden, H. Jahn M. Berthold K. Jüttner K. M. Mangold S. Schäfer. *"Polypyrrole as the active material for potentiometric sensors."* Chemical Engineering & Technology, 2001 *24*: 1120-1124.

[13] H. Macit, S. Sen M. Saçak. *"Electrochemical synthesis and characterization of polycarbazole."* Journal of Applied Polymer Science, 2005 *96*: 894-898.

[14] Johan Bobacka, Ari Ivaska Andrzej Lewenstam. *"Potentiometric ion sensors based on conducting polymers."* Electroanalysis, 2003 *15*: 366-374.

[15] Milind V. Kulkarni, Annamraju Kasi Viswanath P. K. Khanna. *"Synthesis and characterization of poly(n-methyl aniline) doped with sulphonic acids: Their application as humidity sensors."* Journal of Applied Polymer Science, 2006 *99*: 812-820.

[16] Rahul Singhal, Asha Chaubey Keiichi Kaneto W. Takashima B. D. Malhotra. *"Poly-3-hexyl thiophene langmuir-blodgett films for application to glucose biosensor."* Biotechnology and Bioengineering, 2004 *85*: 277-282.

[17] Swati Unde, J. Ganu S. Radhakrishnan. *"Conducting polymer-based chemical sensor: Characteristics and evaluation of polyaniline composite films."* Advanced Materials for Optics and Electronics, 1996 *6*: 151-157.

[18] P. m. George, D. a Lavan J. a Burdick C. Y. Chen E. Liang R. Langer. *"Electrically controlled drug delivery from biotin-doped conductive polypyrrole."* Advanced Materials, 2006 *18*: 577-581.

[19] Zehava Weiss, Daniel Mandler Galit Shustak Abraham J. Domb. *"Pyrrole derivatives for electrochemical coating of metallic medical devices."* Journal of Polymer Science Part A: Polymer Chemistry, 2004 *42*: 1658-1667.

[20] B. Garner, A. Georgevich A. J. Hodgson L. Liu G. G. Wallace. *"Polypyrrole-heparin composites as stimulus-responsive substrates for endothelial cell growth."* Journal of Biomedical Materials Research, 1999 *44*: 121-129.

[21] Mitsuyoshi Onoda, Yoshiyuki Kato Hirokazu Shonaka Kazuya Tada. *"Artificial muscle using conducting polymers."* Electrical Engineering in Japan, 2004 *149*: 7-13.

[22] G.M. Spinks, L. Liu G. G. Wallace D. Zhou. *"Strain response from polypyrrole actuators under load."* Advanced Functional Materials, 2002 *12*: 437-440.

[23] Geoffrey M. Spinks, Gordon G. Wallace Lu Liu Dezhi Zhou. *"Conducting polymers electromechanical actuators and strain sensors."* Macromolecular Symposia, 2003 *192*: 161-170.

[24] Elsa Reichmanis, Howard Katz Christian Kloc Ashok Maliakal. *"Plastic electronic devices: From materials design to device applications."* Bell Labs Technical Journal, 2005 *10*: 87-105.

[25] Zhenan Bao, Andrew J. Lovinger Oksana Cherniavskaya. *"Material issues for construction of organic and polymeric driving circuits for display and electronic applications."* Macromolecular Symposia, 2000 *154*: 199-208.

[26] Richard D. Champion, Kai-Fang Cheng Chia-Ling Pai Wen-Chang Chen Samson A. Jenekhe. *"Electronic properties and field-effect transistors of*

thiophene-based donor-acceptor conjugated copolymers." Macromolecular Rapid Communications, 2005 *26*: 1835-1840.

[27] Sharif Ahmad, S. M. Ashraf Ufana Riaz. *"Corrosion studies of polyaniline/coconut oil poly(esteramide urethane) coatings."* Polymers for Advanced Technologies, 2005 *16*: 541-548.

[28] Y. Zhu, J. Zhang Y. Zheng Z. Huang L. Feng L. Jiang. *"Stable, superhydrophobic, and conductive polyaniline/polystyrene films for corrosive environments."* Advanced Functional Materials, 2006 *16*: 568-574.

[29] W. J. Hamer, L. Koene J. H. W. De Wit. *"Formation and electrochemical behaviour of poly(pyrrole) coatings on steel substrates."* Materials and Corrosion, 2004 *55*: 653-658.

[30] Yangyong Wang, Xinli Jing. *"Intrinsically conducting polymers for electromagnetic interference shielding."* Polymers for Advanced Technologies, 2005 *16*: 344-351.

[31] W. H. Kim, G. P. Kushto H. Kim Z. H. Kafafi. *"Effect of annealing on the electrical properties and morphology of a conducting polymer used as an anode in organic light-emitting devices."* Journal of Polymer Science Part B: Polymer Physics, 2003 *41*: 2522-2528.

[32] Paul w. M. Blom, Marc J. M. De Jong Coen T. H. F. Liedenbaum. *"Device physics of polymer light-emitting diodes."* Polymers for Advanced Technologies, 1998 *9*: 390-401.

[33] Benhu Fan, Qingjiang Sun Na Song Haiqiao Wang Huili Fan Yongfang Li. *"Electroluminescent properties of a partially-conjugated hyperbranched poly(p-phenylene vinylene)."* Polymers for Advanced Technologies, 2006 *9999*: n/a.

[34] Jianyong Ouyang, Chih-Wei Chu, Charles R. Szmanda, Liping Ma1 and Yang Yang. *"Programmable polymer thin film and non-volatile memory device."* nature materials, 2004 *3*: 918-922.

[35] Jianyong Ouyang, Chih-Wei Chu, Ricky Jia-Hung Tseng, Ankita Prakash, Yang Yang. *"Organic memory device fabricated through solution processing."* Proceedings of The IEEE, 2005 *93*: 1278-1296.

[36] Deetlefs, Maggel, Kenneth R. Seddon and Michael Shara. *"Predicting physical properties of ionic liquids."* Physical Chemistry Chemical Physics, 2006 *8*: 642-649.

[37] Walden, Paul. Bull Acad. Imper. Sci. (St Petersburg), 1914: 1800.

[38] Rebelo, Luis P. N., Jose N. Canongia Lopes, Jose M. S. S. Esperanca and Eduardo Filipe. *"On the critical temperature, normal boiling point, and vapor*

pressure of ionic liquids." Journal of Physical Chemistry B, 2005 *109*: 6040-6043.

[39] Ngo, H. L., K. Lecompte, L. Hargens and A. B. Mcewen. *"Thermal properties of imidazolium ionic liquids."* Thermochimica Acta, 2000 *357*: 97-102.

[40] Galinski, Maciej. Lewandowski, Andrzej. Stepniak, Izabela. *"Ionic liquids as electrolytes."* Electrochimica Acta, 2006 *In Press, Corrected Proof*: xxxx.

[41] Sheldon, R. *"Catalytic reactions in ionic liquids [review]."* Chemical Communications, 2001: 2399-2407.

[42] Lee, C. W. *"Diels-alder reactions in chloroaluminate ionic liquids: Acceleration and selectivity enhancement."* Tetrahedron Letters, 1999 *40*: 2461-2464.

[43] Comminges, Clement, Rachid Barhdadi, Michel Laurent and Michel Troupel. *"Determination of viscosity, ionic conductivity, and diffusion coefficients in some binary systems: Ionic liquids + molecular solvents."* Journal of Chemical & Engineering Data, 2006 *51*: 680-685.

[44] Dzyuba, Sergei V. and Richard A. Bartsch. *"Expanding the polarity range of ionic liquids."* Tetrahedron Letters, 2002 *43*: 4657-4659.

[45] Zhou, Zhi-Bin, Hajime Matsumoto and Kuniaki Tatsumi. *"Low-viscous, low-melting, hydrophobic ionic liquids: 1-alkyl-3-methylimidazolium trifluoromethyltrifluoroborate."* Chemistry Letters, 2004 *33*: 680-681.

[46] Driver, G. and K. E. Johnson. *"3-methylimidazolium bromohydrogenates(i): A room-temperature ionic liquid for ether cleavage."* Green Chemistry, 2003 *5*: 163-169.

[47] Ross, J. and J. L. Xiao. *"Friedel-crafts acylation reactions using metal triflates in ionic liquid."* Green Chemistry, 2002 *4*: 129-133.

[48] Fraga-Dubreuil, Joan, Khadidja Bourahla, Mustapha Rahmouni, Jean Pierre Bazureau and Jack Hamelin. *"Catalysed esterifications in room temperature ionic liquids with acidic counteranion as recyclable reaction media."* Catalysis Communications, 2002 *3*: 185.

[49] Pierre Bonhôte, Ana-Paula Dias, Nicholas Papageorgiou, Kuppuswamy Kalyanasundaram, and Michael Grätzel. *"Hydrophobic, highly conductive ambient-temperature molten salts."* Inorg. Chem., 1996 *35*: 1168 -1178.

[50] Zhang, Jie and M. Bond Alan. *"Practical considerations associated with voltammetric studies in room temperature ionic liquids."* The Analyst, 2005 *130*: 1132-47.

[51] Deetlefs, Maggel, R. Seddon Kenneth and Michael Shara. *"Predicting physical properties of ionic liquids."* Physical chemistry chemical physics: PCCP, 2006 *8*: 642-9.

[52] Zhao, Hua. *"Current studies on some physical properties of ionic liquids."* Physics and Chemistry of Liquids, 2003 *41*: 545-557.

[53] Anna S. Larsen, John D. Holbrey, Fook S. Tham, and Christopher A. Reed. *"Designing ionic liquids: Imidazolium melts with inert carborane anions."* J. Am. Chem. Soc., 2000 *122*: 7264 -7272.

[54] Xu, Wu and C. Austen Angell. *"Solvent-free electrolytes with aqueous solution-like conductivities."* Science (Washington, DC, United States), 2003 *302*: 422-425.

[55] Felmy, Andrew R. and John H. Weare. *"Calculation of multicomponent ionic diffusion from zero to high concentration: Ii. Inclusion of associated ion species."* Geochimica et Cosmochimica Acta, 1991 *55*: 133-44.

[56] Vila, J., P. Gines, J. M. Pico, C. Franjo, E. Jimenez, L. M. Varela and O. Cabeza. *"Temperature dependence of the electrical conductivity in emim-based ionic liquids: Evidence of vogel-tamman-fulcher behavior."* Fluid Phase Equilibria, 2006 *242*: 141-146.

[57] Every, H., A. G. Bishop, M. Forsyth and D. R. Macfarlane. *"Ion diffusion in molten salt mixtures."* Electrochimica Acta, 2000 *45*: 1279-1284.

[58] Elisabeth Smela, Xuezheng Wang, Benjamin Shapiro. *"Visualizing ion currents in conjugated polymers."* Advanced Materials, 2004 *16*: 1605-1609.

[59] Lu, Wen, Andrei G. Fadeev, Baohua Qi, Elisabeth Smela, Benjamin R. Mattes, Jie Ding, Geoffrey M. Spinks, Jakub Mazurkiewicz, Dezhi Zhou, Gordon G. Wallace, Douglas R. Macfarlane, Stewart A. Forsyth and Maria Forsyth. *"Use of ionic liquids for p-conjugated polymer electrochemical devices."* Science (Washington, DC, United States), 2002 *297*: 983-987.

[60] Ding, Jie, Dezhi Zhou, Geoffrey Spinks, Gordon Wallace, Stewart Forsyth, Maria Forsyth and Douglas Macfarlane. *"Use of ionic liquids as electrolytes in electromechanical actuator systems based on inherently conducting polymers."* Chemistry of Materials, 2003 *15*: 2392-2398.

[61] Zhou, Dezhi, Geoffrey M. Spinks, Gordon G. Wallace, Churat Tiyapiboonchaiya, Douglas R. Macfarlane, Maria Forsyth and Jiazeng Sun. *"Solid state actuators based on polypyrrole and polymer-in-ionic liquid electrolytes."* Electrochimica Acta, 2003 *48*: 2355-2359.

[62] Randriamahazaka, H., C. Plesse, D. Teyssie and C. Chevrot. *"Relaxation kinetics of poly(3,4-ethylenedioxythiophene) in 1-ethyl-3-methylimidazolium bis((trifluoromethyl)sulfonyl)amide ionic liquid during potential step experiments."* Electrochimica Acta, 2005 *50*: 1515-1522.

CHAPTER 2

ELECTROCHE ICAL ETHODS AND INTERPRETATION

2.1 Introduction

There are a large number of electrochemical methods available for the study of chemicals under the influence of potential[63,64,65,66]. In this chapter, some simple descriptions of theory and methods are presented with semi-quantitative interpretation of data.

2.2 easuring and Controlling Electrochemistry

Generally, electronic systems require a potential difference and electron flow (current) between two electrodes to provide useful work. The potential difference between two electrodes provides the driving force for electron movement and the current defines the population of charge passed over time. In an electrochemical apparatus, experimental cells are commonly designed to observe what occurs at an electrode of interest, known as the working electrode (WE). The potential required to drive a chemical reaction is applied to the WE by another electrode known as the auxiliary electrode (AUX). A third electrode known as the reference electrode (RE) monitors the potential at the surface of the WE.

The potential of the WE is particularly important due to a fundamental electrochemical relationship expressed by the Nernst Equation 2.1. This equation relates the activities of reactants, products and the standard potential of a reaction of interest (relating to the ability of the reaction to transfer electrons), to the overpotential (external driving force applied to the system).

Equation 2.1-

$$E = E^0 - \frac{RT}{nF} \ln\left[\frac{A_{red}}{A_{ox}}\right]$$

$\boldsymbol{E}$	-	*overpotential*
$\boldsymbol{E^0}$	-	*standard potential of reaction*
$\boldsymbol{R}$	-	*gas constant*
$\boldsymbol{T}$	-	*Temperature in degrees Kelvin*
$\boldsymbol{F}$	-	*Faraday's constant*
$\boldsymbol{A_{red}}$	-	*activity (concentration) of reduced species*
$\boldsymbol{A_{ox}}$	-	*activity (concentration) of oxidised species*
$\boldsymbol{n}$	-	*number of electrons involved in process*

If we were to apply, for example, an external potential of 5 V to an arbitrary cell, how would the potential distribute itself through the system? Would we expect -2.5 V at one electrode, and +2.5 V at the other? Alternatively, 0 V at one and +5 V at the other? These are both possible as potential difference is a relative quantity, and at this stage we can only tell the potential which is being applied to the whole system, rather than the subsystem of interest occurring at the WE. This can be further complicated if another process, commonly not of interest, occurs at the AUX electrode. Equation 2.1 requires the potential of the surface under investigation to be known, as it defines the overpotential driving the reaction.

The potential difference between the RE and WE can be used to define the overpotential of a reaction in absolute terms if the RE is defined against a universal standard. The RE ideally has a stable chemical potential present under small or negligible current flow conditions making it non-polarisable. The universal standard for potential, which defines 0 V under standard laboratory conditions, is the Standard Hydrogen Electrode (SHE). The SHE is not commonly used as an experimental RE, because it is a gas-liquid system, which requires the constant bubbling of hydrogen gas at atmospheric pressure across platinum. This can be expensive, difficult to operate, incompatible with many systems and potentially dangerous. More commonly, the RE of choice is Ag / AgCl or another solid / liquid system reference that is self-contained and easily maintained.

There are a large number of voltammetric techniques available, based around the current / potential / time (I / E / t) relationships depicted in Figure 2.1. Many methods work by providing a signal controlling current or potential, and observing how the system reacts to changes of potential or current, respectively.

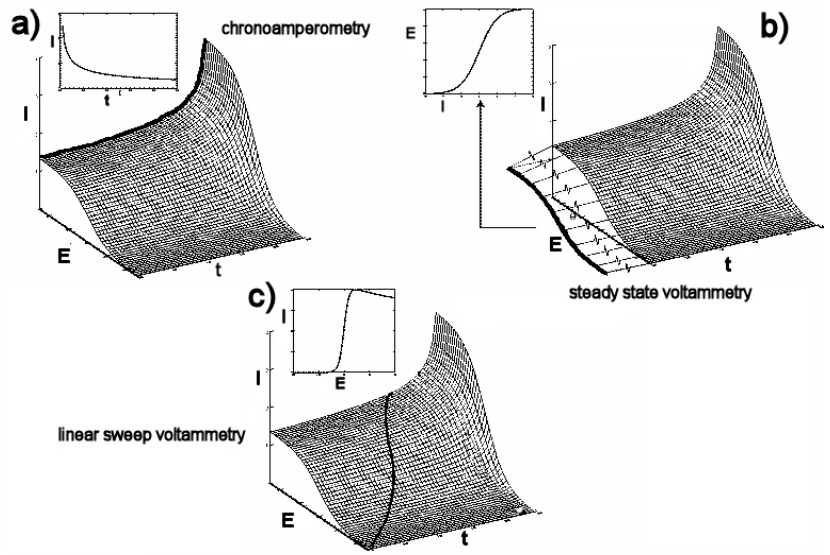

Figure 2.1- I / E / t surface for an arbitrary chemical reaction[67].

Chronoamperometry (Figure 2.1 a) and steady state voltammetry (Figure 2.1 b) both have an axis which remains constant (i.e. voltage and current, respectively), linear sweep methods vary parameters across two axes, increasing the amount of available information[67].

A potentiostat is used for control and observation of electrochemical processes and is usually employed in electrochemical investigations. Modern potentiostats interface with a computer, which takes readings and provides the necessary signal to investigate electrochemical reactions.

A three-electrode potentiostat has the general form outlined in Figure 2.2. Such a device is ideal for studying electrochemical reactions, as it can focus on and control the events occurring at the electrode of interest. The flexibility of a potentiostat controlled by a computer allows innumerable experiments by controlling either potential or current to any imaginable waveform or sequence of pulses. The data collected are in a digital form and recorded on a computer, expediting data analysis and manipulation to extract relevant experimental parameters.

In Figure 2.2, components marked with X1 are differential gain amplifiers, that is, they measure the potential difference between the RE and WE. If potential control of the WE is desired, the potential measured between the WE and the RE can pass through the electrometer to provide a feedback loop via the control amplifier. The feedback loop adjusts the potential difference between the AUX and WE, until the potential difference between the RE and WE match the desired potential difference input from the computer

or control device. The situation can be reversed so that current flow can be controlled, in which case the potential difference between the AUX and WE is adjusted to establish the desired current flow, and the RE can simply monitor the potential associated with the particular current.

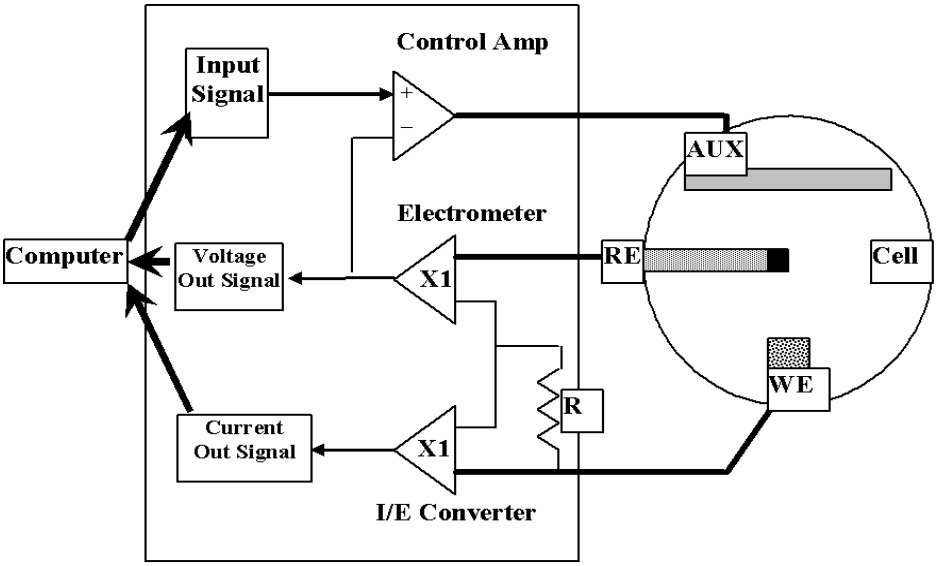

Figure 2.2- A general schematic of a potentiostat.

2.3 Cyclic Voltammetry

A major component of the studies carried out in this dissertation employ the method of cyclic voltammetry (CV). CV is a dynamic technique, commonly used to produce qualitative results for an electrochemical system. The method relies on linearly altering a potential through time, between positive and negative bounds, to produce a triangular potential wave and recording the resultant current flow as its function.

The main benefit of using CV is that results are generally quickly obtained and the voltammograms (I vs. E curves) produced are easy to interpret using visual inspection.

The CV technique can be used as a guide for the electrochemical events and system capabilities, providing information that can then be used to prepare more quantitative complementary experiments. CV data may also be subjected to computer-based analysis, allowing the possibility of obtaining increasingly meaningful quantitative data by shape deconvolution of signal peaks, or by overlay of simulation models incorporating the prevailing factors describing a particular system.

A typical CV response for a polypyrrole film in an ionic liquid with respect to time is shown in Figure 2.3. The positions of the arrows indicate that there were peak responses at about 160 mV and at -220 mV, which are the oxidation and reduction potentials of the polymer system, respectively. The direction of the arrows indicates that the peaks are increasing in magnitude, meaning the electrochemistry requires many cycles to reach maximum response.

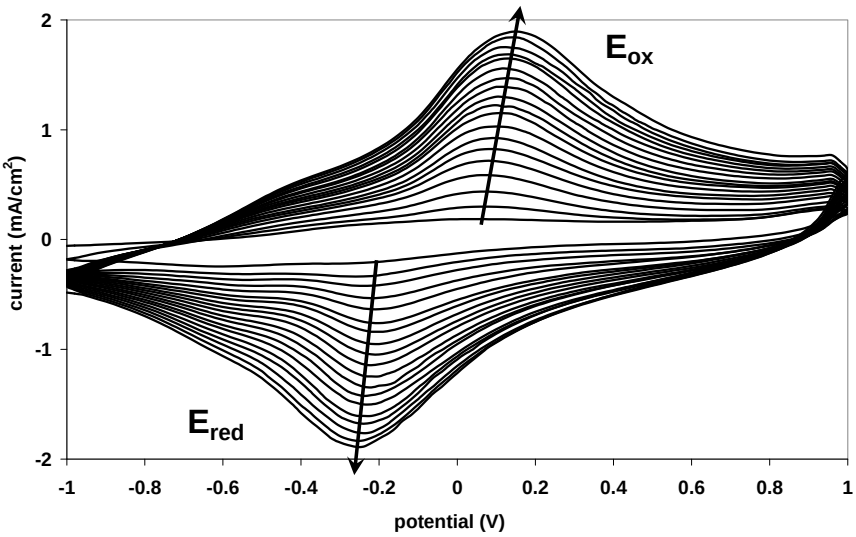

Figure 2.3- Example of cyclic voltammetry – PPy / PF_6 film in BMIPF_6 ionic liquid. E_{ox} = oxidation peak, E_{red} = reduction peak. Arrows indicate direction of peak growth from cycle 1. Scan rate = 200 mV/s, 20 cycles.

The direction of the arrows also strongly suggests that the system does not degrade electrochemically within this range of potentials, as the current magnitude (relating to the population of electroactive species) does not decrease. The CV appears to be quite symmetrical across the potential axis with respect to current magnitude. Although the peaks do not have a Nernstian theoretical potential separation of 59 mV (being *ca.* 380 mV), the magnitude of peak current response on both anodic and cathodic sides is the same suggesting the process is reversible, with the large peak separation influenced by factors described in the next section.

2.4 Factors Influencing CV

When investigating the electrochemistry of a system by CV we are usually interested in redox processes at an applied potential. The portion of current that is observed because of a redox process is referred to as the Faradaic current. Non-Faradaic processes are usually related to charged double layer formation (capacitance), where current drives ions to align themselves in alternating positive and negative layers. With non-Faradaic processes, no chemical change or redox processes occur, but in the CV, they are observed as a background current signal that can mask the presence of Faradaic processes.

Internal resistance (IR) causes other non-Faradaic effects commonly seen in CV. Large IR can delay the emergence of peaks, as the potential observed by the reference electrode will exhibit a potential offset. The above process may result in the CV suffering from distortion. Numerical deconvolution methods have been developed to separate these interferences to provide insight into the underlying redox processes of interest.

2.5 Deconvoluting Cyclic Voltammetry of ICPs

At any level of mathematical analysis or simulation, it should be noted that there are always assumptions made to make the problem manageable. Regardless of the sophistication of any model, there are always shortfalls and discrepancies between the realms of the experimental and theoretical. If we look at an ICP system and focus just on electron-ion transfer, solvent transport and polymer reconfiguration (neglecting all the other factors) we find that for a single redox cycle there are a large number of possible mechanistic sequences[68]. So at best, any simulation is a gross simplification, but can still yield much information on the dominating factors.

Fick's Laws adapted for electrochemistry (Equation 2.2 and Equation 2.3) represent the interplay of space, time, current and concentration in an electrochemical system with respect to diffusion.

Equation 2.2-

$$I = nFD_o \frac{\partial c_o}{\partial x} \qquad \text{(Fick's first law)}$$

Equation 2.3-

$$\frac{\partial c_o}{\partial t} = D_o \frac{\partial^2 c_o}{\partial x^2} \qquad \text{(Fick's second law)}$$

$\boldsymbol{I}$	–	*current*
$\boldsymbol{n}$	–	*molar ratio of electrons taking part in reaction*
$\boldsymbol{F}$	–	*Faraday's constant*
$\boldsymbol{D_o}$	–	*diffusion coefficient*
$\boldsymbol{c_o}$	–	*initial concentration*
$\boldsymbol{t}$	–	*time*
$\boldsymbol{x}$	–	*distance from electrode*

Fick's first law is a statement of conservation of matter as the current or ion flow relates directly to the concentration of ions moved through space. The second law indicates how the concentration profile propagates through space relative to time in a system with an unchanging diffusion coefficient. Fick's first law is hence considered to be correct for all diffusion type systems[69]. Fick's Laws combined with the Nernst Equation in the form of 'Finite Elements' can be input into a computer to model experimental observations and extract parameters[70]. The resulting finite element modelling (FEM) is an iterative method that simulates a system by dividing the modelled space into discrete (finite) regions (elements).

The modelled observations come from the difference of physical properties in adjacent finite elements. For example, if there are two adjacent finite elements and one has a concentration higher than the other, Fick's first law predicts a current will flow between them. Given defined starting and boundary conditions, the concentration profiles and flow of current can be determined by calculating the behaviour of every discrete element in sequence to give the emerging macroscopic behaviour.

The process of replicating an electrochemical system in this mathematical way produces large matrices, which have to be iterated across each discrete element to produce the final solution. Without involved mathematics this calculation can be quite time consuming, even for a modern desktop computer. In this dissertation, attempts were made to produce computer programs in Matlab to solve Fick's law for the studied electrochemical systems. However, to ensure accuracy with the solutions, only very time-consuming simulations could be produced. These simulations were also unsuitable for fitting to experimental data, due to the long time required to wait after any parameter was altered.

Commercial programs are available that utilize advanced algorithms to perform these calculations very rapidly[67]. However, it was soon realised that no commercial or pre-made software was actually suitable for applications with conducting polymers, as conducting polymers generally do not follow Fick's second law[68,69]. This stems from the dependence of conductivity upon oxidation state in conductive polymers. Therefore, if the polymer is dynamically reduced or oxidised, the diffusion constant will also alter, invalidating Fick's second law. It turns out that Fick's second law is in the form of a first order relationship in the case of conducting polymers[68,69].

Given the above challenges, is it still possible to deconvolute the CV of conducting polymers to extract useful information without complex iterative computing? An alternative approach is to model CV using statistical distribution functions that encompass the behaviour of a large population of discrete components, rather than focusing on the components individually.

2.6 Deconvolution of ICP CV s with Statistical Distribution Functions

Statistical distribution functions are used to describe a very broad range of phenomena[71]. These range from economics, epidemiology, classroom test results to irradiative spectra, behaviour of gases and quantum mechanics. In fact, statistical distribution functions are a good way of looking at almost any system with large amounts of components that may or may not be interdependent[71].

With such a broad choice of distribution functions, one may simply take the path of finding a function that fits most or part of the signal very well and extending the function to points where there may be interference from other processes, making the assumption that the function sufficiently predicts the required shape in the unknown region[72]. Alternatively, one can use statistical mathematics extended in context to try to interpret and apply theoretical distribution behaviour of a particular system[73,74,75,76,77].

2.6.1 The Statistical Gaussian Energy Dispersion Function for ICPs

The recent analysis by Bisquert *et al*.[77] applied a Gaussian statistical distribution function for ICP CV deconvolution, and fitted experimental data very well. This approach has been further examined in this thesis. Of note, some of the features produced in the present analysis provide further insight into some of the discrepancies between ICP systems and ordinary Nernstian type systems.

The Gaussian model strongly focuses on the expected distribution behaviour of polaronic (P) and bipolaronic (B) states, along with their mutual interactions[78,79] (Figure 2.4). Similar Nernstian type analyses were based on assumptions that all active sites are non-interacting, well separated and have the same energy. This would very rarely be the case in non-crystalline polymers, which are likely to be in twisted anisotropic bundles. A ‘fuzzy’ distribution of site separations and energies is far more likely. In fact, such a distribution of sites is an important characteristic of charge transport within these systems.

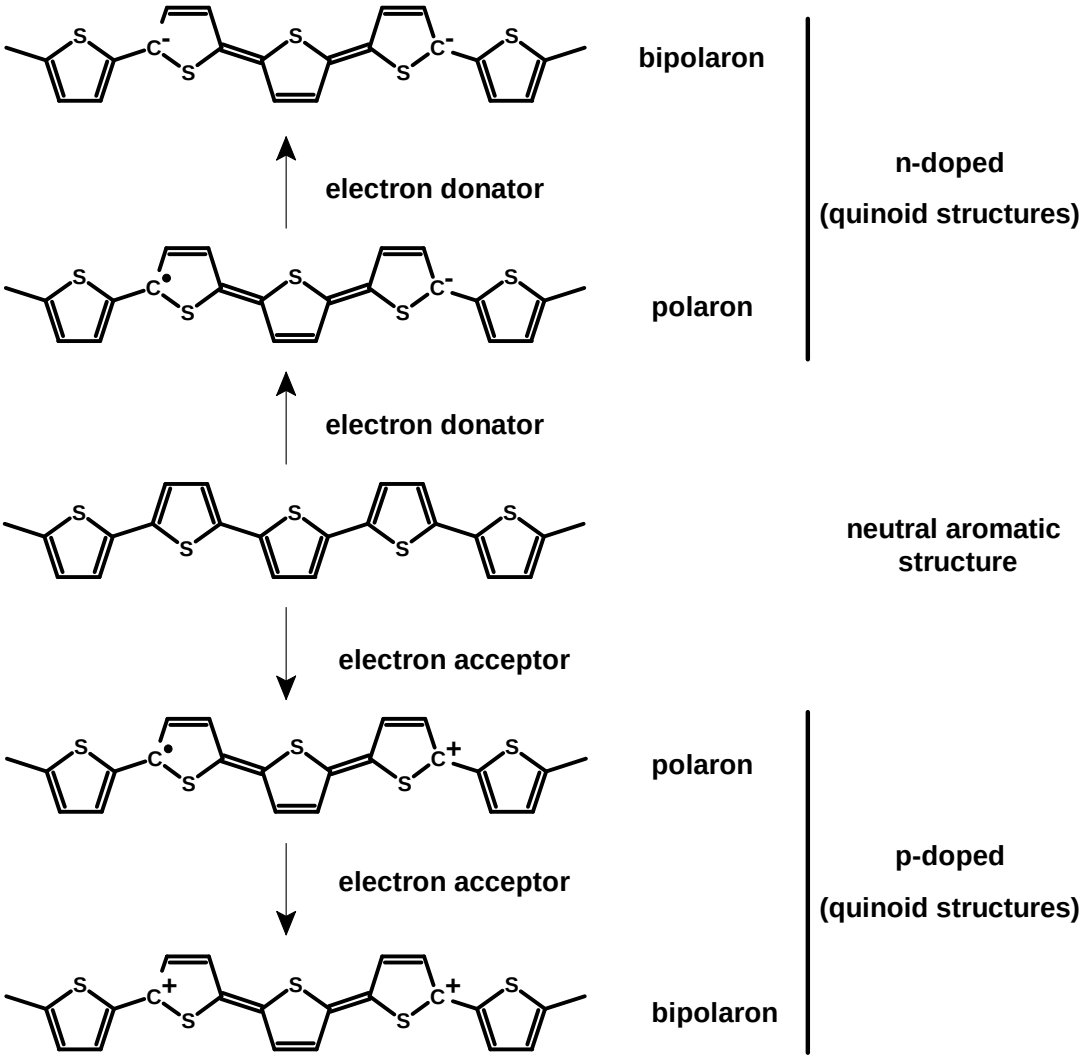

Figure 2.4- Structural diagrams of polythiophene in its polaronic and bipolaronic representations, for both p-doped and n-doped states.

The Gaussian distribution function for ICPs can be assembled in two weighted parts. Firstly, only the P state was taken into account. P states rapidly pair together to produce B states, because radicals are less stable than charged centres.

However, there is still an energetic separation between them, and this factor becomes important in describing apparent non-idealities , which make the ICP system produce results somewhat different to that of the Nernstian situation electrochemists are used to.

The Gaussian function takes the following form for polarons:

Equation 2.4-

$$I = \frac{N_s}{\sqrt{2\pi}\sigma_P} \exp\left[-\frac{(E - E_{ox}P)^2}{2\sigma_P^2} \right]$$

$\boldsymbol{N_s}$	-	*density of conjugated chain segments*
$\boldsymbol{\sigma_P}$	-	*peak width at half height for polaron distribution*
$\boldsymbol{E_{ox}P}$	-	*mean potential of polaron formation*
$\boldsymbol{E}$	-	*applied potential*

In order for charge to be carried in the polymer, the aromatic neutral structure takes on deformations, which can accommodate and propagate charge. When two polarons are present near each other, be it on the same chain or adjacent chains, their merging is possible and energetically favourable to form bipolarons[80].

Equation 2.4 would also apply to bipolarons, with adjusted notation for the unique variables σ_B and $E_{ox}B$, so combining the P and B functions, one obtains Equation 2.5.

Equation 2.5-

$$I = \frac{N_s}{2\pi\sigma_P\sigma_B} \exp\left[-\frac{(E - E_{ox}P)^2}{2\sigma_P^2} - \frac{(E - E_{ox}B)^2}{2\sigma_B^2} \right]$$

This function, in this particular form *could* be used in comparison to experimental data. However, manipulating five variables (*Ns, σ_P, σ_B, $E_{ox}P$, $E_{ox}B$*) in order to get a fit on an arbitrary curve can be tedious. In addition, so many loose variables have the potential of either producing ambiguities, or essentially being useless because the CV may not have

enough resolution to accurately express interpretable features. Alternatively, other effects may overly obscure the features of interest.

Equation 2.5 does, however, provide useful insights into how ICPs produce results constantly in discrepancy with Nernstian models. If we look at a simple series of theoretical experiments, altering one variable at a time, we can correlate the behaviour of variables with the result. Nernstian models make the following predictions[76]:

- A half height peak width (the width of an electrochemical signal peak at half of its height) of 91 mV is expected for a reversible one-electron process (182 mV for a two-electron process).
- The separation between oxidation and reduction peaks should be 58 mV for a one-electron reversible process.
- The difference in potential of a one-electron process should change by 58 mV per order of magnitude of electrolyte concentration change (29 mV for a two-electron process).
- The ratio of the peak currents of oxidation and reduction should be one for a reversible process.
- The potential of reversible peaks should not alter with respect to scan rate.

ICPs routinely stray from nearly all of these Nernstian predictions. The Gaussian model takes into consideration the factors previously discussed in this section and provides some useful insight to what may be occurring.

2.7 Theoretical experiments with the Gaussian odel

The distribution function of Equation 2.5 was programmed into Excel . The variables were referenced to stationary data cells and the function was plotted against linearly increasing values of potential. The variables were controlled with ‘spin button’ macro

controls, allowing the result to be viewed in real time as the variables were altered. All but one variable remained locked for each experiment, and the results were presented in the following four Figures (2.5 to 2.7). The base stationary variables were set to be non-zero, and P and B values were not identical. The base variables chosen were typical for ICP systems:

$$\begin{aligned} N_s &= 2.5x10^{21}\ cm^{-3} \\ \sigma_P &= 0.10\ V \\ \sigma_B &= 0.15\ V \\ E_{ox}P &= 0.05\ V \\ E_{ox}B &= 0.10\ V \end{aligned}$$

From Equation 2.4, when the potential of bipolaron formation ($E_{ox}B$) was altered, the distribution of current magnitude became asymmetrical. An increased energy gap between P and B formation caused decreasing peak current magnitude in the process reflecting the increased difficulty of transfer from one energy state to another. As expected, an increase in the potential energy separation between the P and B states caused the current magnitude peak to move to higher potentials (Figure 2.5).

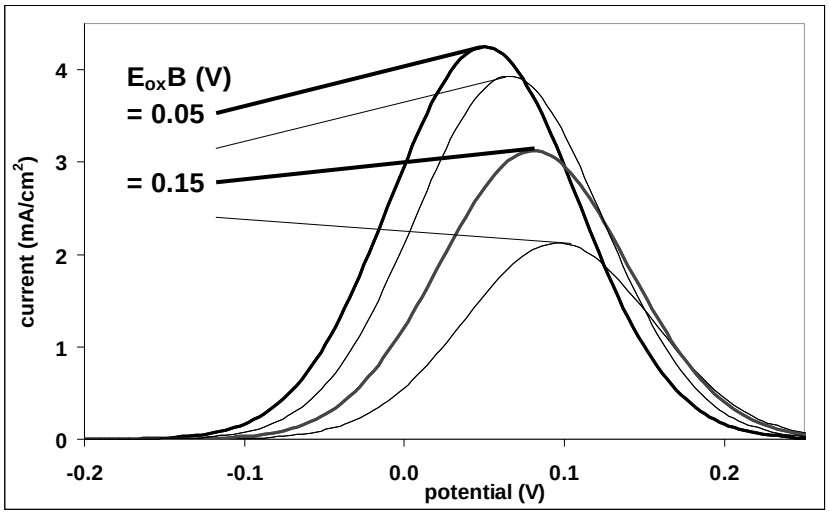

Figure 2.5- Current vs. potential plot of different $E_{ox}B$ values.

When the half peak width (σ_B) of the bipolaron distribution was increased, the Faradaic charge capacity decreased (Figure 2.6). The broadening of the curve by increasing the σ_B coefficient represented a less energetically favourable process, where the states were less accessible, due to inter- or intra-molecular barriers (Figure 2.6).

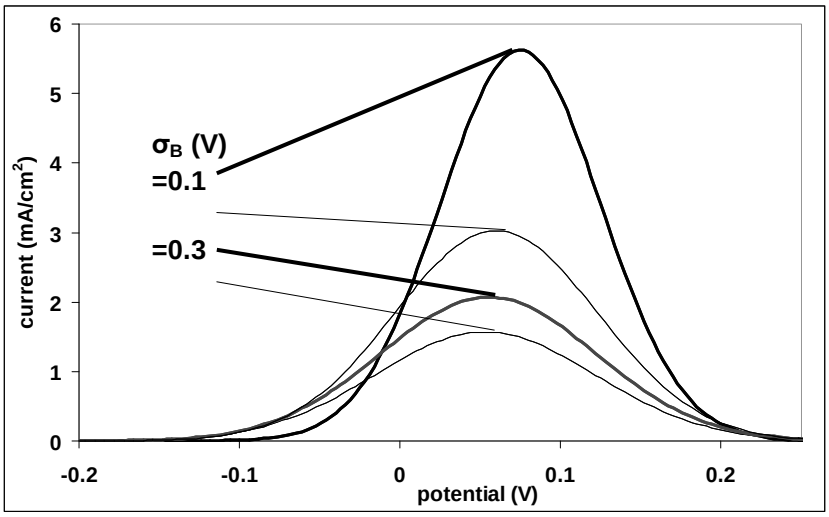

Figure 2.6- Current vs. potential plot of different σ_B values.

Altering the density of conjugated chain segments N_S produced intuitive results, such that an increase in conjugation sites resulted in an increase in current magnitude and charge (Figure 2.7 a). Figure 2.7 b clarifies features of Figure 2.7 a, showing that although the peak current magnitude of the response had been altered, all features apart from the density of chain segments have remained constant, including the potential width of the current magnitude peak at half its magnitude (half peak width). This example demonstrates the importance of half peak width in defining a process whose shape has been altered by changes in concentration, where all other parameters have remained unchanged.

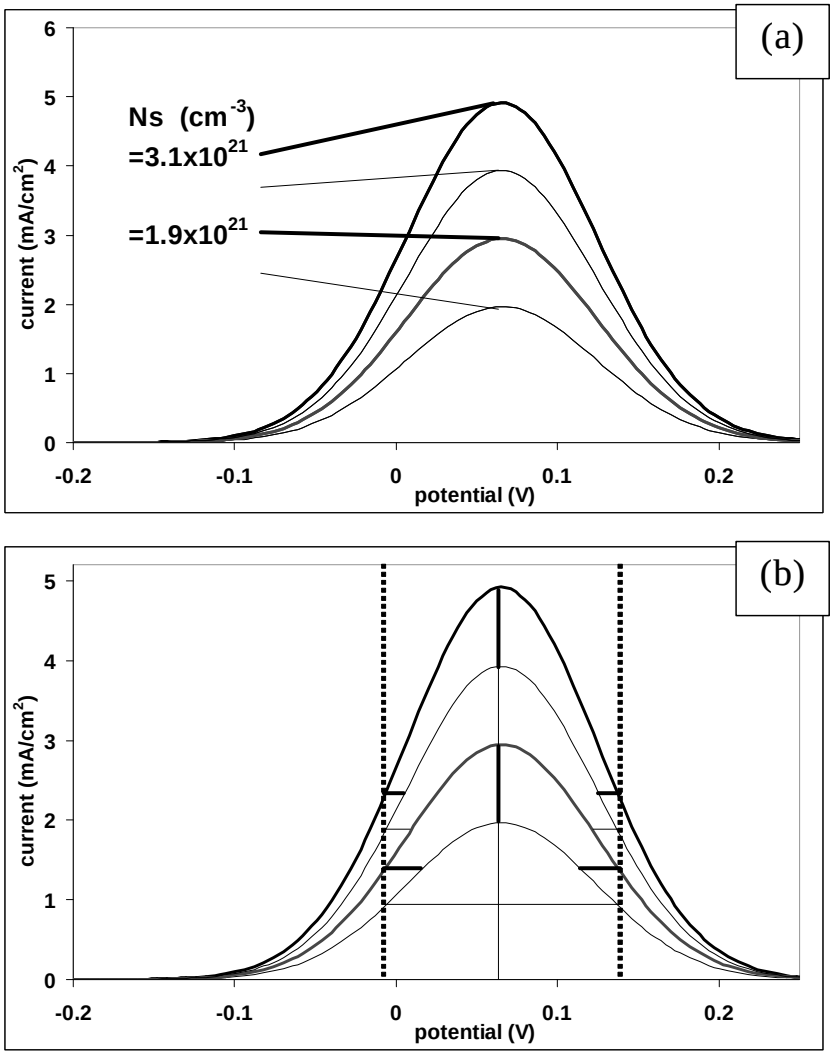

Figure 2.7- (a) current vs. potential plot of different N_s values, (b) the same plot as (a) showing how half peak width remains constant when kinetic parameters are not altered.

To simplify the Gaussian distribution hypothesis, we can assume that the mean potential of the P formation, $E_{ox}P$, is almost equal to B formation, $E_{ox}B$. This assumption should be valid as B in its zero spin state is considerably more stable than two isolated P states. Further, any P that is formed rapidly converts to B[81], usually in the time frame of femtoseconds[82]. Hence, there is validity in assuming σ_P and σ_B to have close to equal values. Literature suggests the value of mean potential separation of these states to be

between 50 to 100 mV[77]. However, the present simplification of assuming $\sigma_P \quad \sigma_B$ allows a more practical approach for use in deconvolution analysis[83].

If σ_P and σ_B were equal, Equation 2.5 would then reduce to the form of Equation 2.6:

Equation 2.6-

$$I = \frac{N_s}{2\pi\sigma^2} \exp\left[-\frac{(E - E_{ox})^2}{\sigma^2} \right]$$

Equation 2.6 fits data reasonably well (Figure 2.8), but only in those regions where the observed effect resulted from Faradaic processes. Commonly seen in the CV of ICPs is a large plateau soon after the polymer's oxidation peak[84]. This part of an ICP CV is often referred to as background current , and can be interpreted as a contribution from non-Faradaic capacitance effects.

The CV in Figure 2.8 was performed at 200 mV/s over potentials of -1.4 to 1.3 V. The green points represent the Gaussian functions, with parameters adjusted to fit the Faradaic regions of the polypyrrole CV. The edges of the latter regions are highlighted by the large black dots, and in the region of oxidation or reduction, the Gaussian function shows a good fit. The remainder of the scan where the calculated data does not fit experimental data, *i.e.* soon after the oxidation peak has been passed, may be attributed to capacitance effects[75].

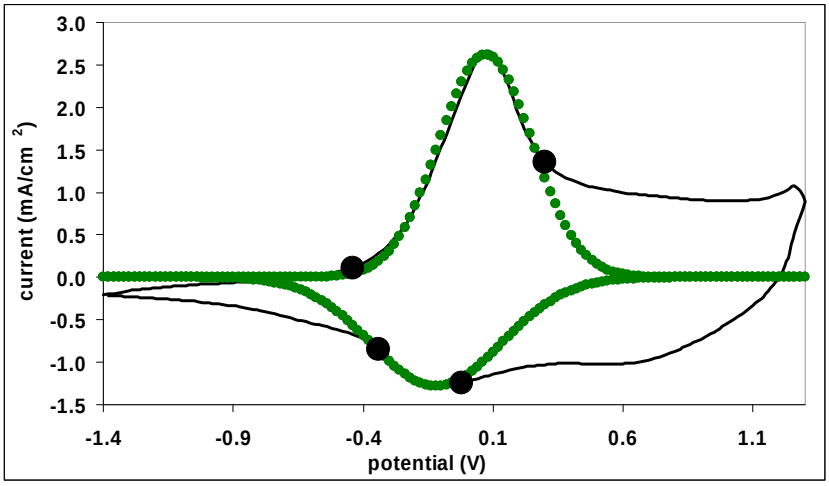

Figure 2.8- A CV of polypyrrole film (black) in propylenecarbonate solvent with tetrabutylammonium hexafluorophosphate as a dissolved electrolyte. The green dots represent a Gaussian distribution fit. Scan rate = 200 mV/s.

2.8 Capacitive Effects of Oxidised ICPs

The Gaussian distribution model appears to have an excellent general fit when used for deconvolution of Faradaic processes of ICPs. Outside of purely Faradaic regions, capacitance effects become apparent as plateaus. The plateaus only appear after a conducting polymer reaches a high conductivity. The plateau effect has therefore been interpreted as the polymer behaving as if it were a porous metal[75,84]. The interpretation by Feldberg[75] of this effect has led to Equation 2.7 describing the capacitive effect of a conducting polymer approaching its full oxidation state. Equation 2.7 is based on the assumption that differential capacitance effects are proportional to the amount of oxidised polymer. In this situation, the differential capacitance is unaffected by potential and the differential capacitance of the underlying bare working electrode is considered negligible.

Equation 2.7-

$$I = \frac{a\upsilon Q_s^0 \exp\left[\frac{F}{RT}(E - E_{ox})\right]}{1 + \exp\left[\frac{F}{RT}(E - E_{ox})\right]}$$

E	-	*applied potential (V)*
E_{ox}	-	*standard potential (V)*
a	-	*constant (units V^{-1})*
F	-	*Faraday's constant*
R	-	*universal gas constant*
T	-	*temperature in degrees Kelvin*
Q^0_s	-	*maximum Faradaic charge (C)*
υ	-	*scan rate (V/s)*

Combining Equation 2.6 and Equation 2.7 produces Equation 2.8, which describes both the observed effects of polarons / bipolarons and capacitive background current.

Equation 2.8-

$$I = \frac{N_s}{2\pi\sigma^2}\exp\left[-\frac{(E - E_{ox})^2}{\sigma^2}\right] + \frac{a\upsilon Q_s^0 \exp\left[\frac{F}{RT}(E - E_{ox})\right]}{1 + \exp\left[\frac{F}{RT}(E - E_{ox})\right]}$$

This formula was applied to the raw data presented in Figure 2.9, which is the same as in Figure 2.8. The large black circles represent regions of good correlation. On the cathodic portion, once the potential was returning to less positive values from the maximum of 1.3 V, the excess charge from the anodic portion was consumed causing current magnitude decease. In this case, the model equation did not fit until this charge was consumed. In this experiment, the effect that the capacitive contribution had on the Gaussian distribution was quite large. The peak potentials of the Gaussian functions were shifted higher, and the magnitude of the Faradaic component had to be decreased to accommodate the capacitive charge produced in the system.

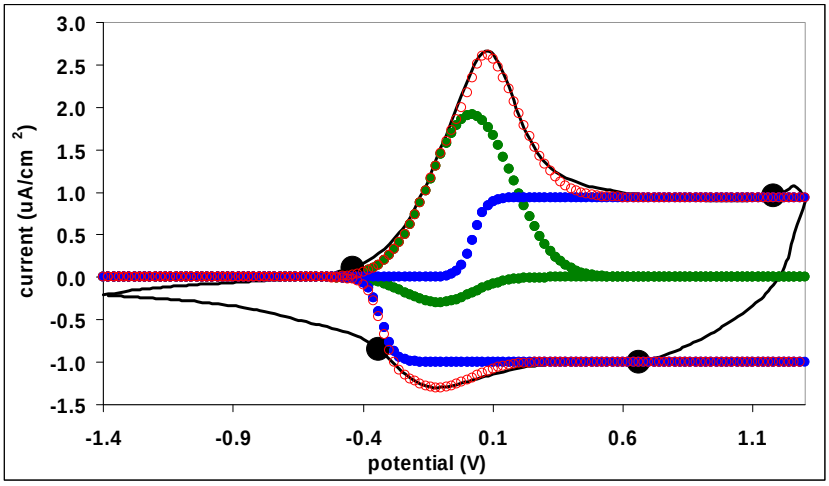

Figure 2.9- ***A CV of polypyrrole film (black) in propylene carbonate solvent with tetrabutylammonium hexafluorophosphate as a dissolved electrolyte. The red circles represent a combined Gaussian and capacitive fit using Equation 2.8. Green dots represent the Gaussian component and the blue dots represent the capacitive component. Scan rate = 200 mV/s.***

A main point made in the work by Feldberg[75] was the general inseparability of Faradaic and non-Faradaic process. The effect of the capacitive component on the positions and magnitudes of the Gaussian contributions was quite significant. Additionally, there may be ambiguities arising from the magnitude of the capacitive contribution with respect to the magnitude and position of polaron / bipolaron Gaussian distributions, where several solutions may closely satisfy the shape of signal denoted by experimental data. This can prove to be a difficult situation to resolve. Fortunately, the experimental data described in Chapter 4 had capacitive contributions significantly lower than what is observed in Figure 2.8 and Figure 2.9. For the purpose of simplification, the capacitive component was considered negligible in the specific CVs used in analysis.

2.9 References

[63] Blount, Paul F. Seelig and Henry N. *"Application of recursive estimation to the real time analysis of trace metal analytes by linear sweep, pulse, and differential pulse anodic stripping voltammetry."* Anal. Chem., 1979 *51*: 1129 -1134.

[64] Bond, H. Blutstein and A. M. *"Alternating current linear sweep and stripping voltammetry with phase-selective second harmonic detection."* Anal. Chem., 1974 *46*: 1531-1538.

[65] Bowden, E. F., M. F. Dautartas and J. F. Evans. *"Chemical and mechanical properties of redox polymer-modified electrodes. Part iii. Redox thermodynamics of linear polyvinylferrocene electrodes."* Journal of Electroanalytical Chemistry and Interfacial Electrochemistry, 1987 *219*: 91-115.

[66] Corry, Ben., Kuyucak, Serdar, and Shin-Ho Chungy. *"Dielectric self-energy in poisson-boltzmann and poisson-nernst-planck models of ion channels."* Biophysical Journal 3594 3606, 2003 *84*: 3594 3606.

[67] Alden, John. *"Computational electrochemistry."* Physical and Theoretical Chemistry Laboratories, Oxford University, 1998 *PhD Thesis*:

[68] I. Prigogine, Stuart A. Rice. *"Polymeric systems."* Advances in chemical physics, 1996 *XCIV*: 439.

[69] Elisabeth Smela, Xuezheng Wang, Benjamin Shapiro. *"Visualizing ion currents in conjugated polymers."* Advanced Materials, 2004 *16*: 1605-1609.

[70] Geiger, David T. Pierce and William E. *"Electrochemical kinetic discrimination of the single-electron-transfer events of a two-electron-transfer reaction: Cyclic voltammetry of the reduction of the bis(hexamethy1benzene)ruthenium dication."* J. Am. Chem. Soc., 1992 *114*: 6063-6073.

[71] Evans, M.; Hastings, N.; and Peacock, B. *"Statistical distributions."* 2000.

[72] Nie, Lei. Wu Shouguo, Wang Jianwei, Zheng Longzhen, Lin Xiangqin, Rui Lei. *"Continuous wavelet transform and its application to resolving and quantifying the overlapped voltammetric peaks."* Analytica Chimica Acta, 2001 *450*: 185 192.

[73] Susanne M. Dana, Matthew E. Jablonski, and Mark R. Anderson . *"Quantitative determination of surface excess by the semiintegral method."* Anal. Chem., 1993 *65*: 1120-1122.

[74] Mao, Huanyu and Peter G. Pickup. *"In situ measurement of the conductivity of polypyrrole and poly[1-methyl-3-(pyrrol-1-ylmethyl)pyridinium]+ as a function of potential by mediated voltammetry. Redox conduction or electronic conduction?"* Journal of the American Chemical Society, 1990 *112*: 1776-82.

[75] Feldberg, Stephen W. *"Reinterpretation of polypyrrole electrochemistry. Consideration of capacitive currents in redox switching of conducting polymers."* J. Am. Chem. Soc., 1984 *106*: 4671 - 4674.

[76] Hendrik A. Heering, Joel H. Weiner, and Fraser A. Armstrong. *"Direct detection and measurement of electron relays in a multicentered enzyme: Voltammetry of electrode-surface films of e. Coli fumarate reductase, an iron-sulfur flavoprotein."* J. Am. Chem. Soc. 119, 1997 *119*: 11628-11638.

[77] Bisquert, Juan. Garcia-Belmonte, Germa. Garcia-Canadas, Jorge. *"Effects of the gaussian energy dispersion on the statistics of polarons and bipolarons in conducting polymers."* Journal of Chemical Physics, 2004 *120*: 6726-6733.

[78] Murray, Christopher E. D. Chidsey and Royce W. *"Redox capacity and direct current electron conductivity in electroactive materials."* J. Phys. Chem., 1986 *90*: 1479 - 1484.

[79] Vorotyntsev, M. A. and J. Heinze. *"Charging process in electron conducting polymers: Dimerization model."* 2001 *46*: 3309.

[80] Magela E Silva, Geraldo. *"Electric-field effects on the competition between polarons and bipolarons in conjugated polymers."* Physical Review B: Condensed Matter and Materials Physics, 2000 *61*: 10777-10781.

[81] G. Paasch, P.H. Nguyen, A.J. Fisher. *"Potential dependence of polaron and bipolaron densities in conducting polymers: Theoretical description beyond the nernst equations."* Chemical Physics, 1998 *227*: 219-241.

[82] E Silva, G. M. and P. H. Acioli. *"Dynamical effects on the competition between polarons and bipolarons in conjugated polymers."* Theochem, 2001 *539*: 45-53.

[83] Juska, G., K. Arlauskas, M. Viliunas, K. Genevicius, R. Osterbacka and H. Stubb. *"Charge transport in p-conjugated polymers from extraction current transients."* Physical Review B: Condensed Matter and Materials Physics, 2000 *62*: R16235-R16238.

[84] Bull, R. A.; Fan, F.-R. F.; Bard, A. J. *"Polymer films on electrodes vii. Electrochemical behavior at polypyrrole-coated platinum and tantalum electrodes."* J. Electrochem. Soc, 1982 *129*: 1009-1015.

CHAPTER 3

EFFECTS OF IONIC LIQUID AS AN ELECTROLYTE IN CONDUCTING POLYMER SYSTEMS

3.1 Introduction

The role of an electrolyte in an electrochemical cell is to provide mobile ions for the migration of charge inside the cell and to balance the charge of species that may be produced by redox or other processes at the electrodes. There are many applications for conducting polymers that require charge balance from an electrolyte when redox reactions occur on the application of an electrical field[85,86,87].

Until recently, studies into the electrochemistry of conducting polymers have put much focus on the polymer itself, while generally neglecting the fundamental importance of the electrolyte. Focusing on the conducting polymer alone, however, has not been without great benefit, as conducting polymers have been developed with their own inherent properties[88], as well as a myriad of other properties that particular applications may require.

Conducting polymers are now much more functional and inherently durable than they were in the early days of development, although for polyacetylene this stability is still an issue. Opportunities therefore exist to extend the redox lifetime and potential window, and to enhance other properties of conducting polymers by tailoring the

interacting electrolyte. Desired properties for an ICP electrolyte may include high ionic conductivity, a large electrochemical window, limited chemical reactivity with electrodes and inherent hydrophobicity.

Ionic liquids are an attractive medium as electrolytes for many applications[89]. They can have a large electrochemical window[90], be hydrophobic[91] and highly conductive[92]. ILs are well known to catalyse many reactions[93,94,95,96]. This may suggest that electrochemistry performed in ILs with ICPs could possibly accelerate the degradation of the polymeric system, especially via nucleophilic attack[97,98] and possible overoxidation[99,100] reactions which are known to proceed well in ionic liquids. It should be noted that many IL catalysed reactions proceed with a very high degree of regio-specificity[101,102]. A high level of selection may in fact have protective properties for ICPs, especially if vulnerable centres are not favoured by the catalysis effect.

The work in this thesis is focussed on two ionic liquids, $BMIPF_6$ and EMITFSI, which both posses hydrophobic characteristics[91,103]. Upon exposing $BMIPF_6$ to moisture, the PF_6^- anion slowly hydrolyses to form HF, as evidenced by the irreversible frosting of the glass in electrochemical cells that were used for experimental work. The HF hydrolysis by-product of $BMIPF_6$ is a dangerous material capable of dissolving glass and human flesh.

A substitute was therefore sought using a more stable anion. The $TFSI^-$ anion was found suitable due to its hydrolysis stability, and also produced ILs with increased hydrophobicity. BMITFSI was considered as a replacement, but another cation, EMI^+, was chosen instead in these studies due to the superior ionic conductivity and corresponding increased liquid temperature range of the EMITFSI ionic liquid[89].

3.2 Experimental Procedure

3.2.1 General Electrochemistry

All electrochemistry was performed with a Radiometer Analytical® VoltaLab 50® (PST050) and VoltaMaster 4® software running on a personal computer installed with the Microsoft® Windows XP® operating system.

All electrochemical experiments were performed using a three electrode cell consisting of a platinum disk electrode with a surface area of 0.02 cm^2 (BASi Stationary Voltammetry Electrode®), or where noted, a glassy carbon electrode (GC) with a surface area of 0.07 cm^2). The working electrode was placed into a vessel containing a counter electrode made of platinum mesh measuring 4 cm^2 (Goodfellow®), and a specially constructed ionic liquid reference electrode[104] made with Ag / AgCl wire in $BMIPF_6$ and periodically calibrated to the ferrocene redox couple in acetonitrile. The ionic liquid reference electrode was determined to have a very stable potential of +222 mV versus the standard hydrogen electrode, remaining un-shifted in potential after several years of daily usage.

All cyclic voltammetry was performed at 200 mV/s except where noted. All working electrodes were cleaned before any polymer was deposited by polishing on 5 μm alumina / water paste on mineralogical polishing felt pads. The polished electrodes were washed with water, then acetone and wiped dry by hand, pressing the electrode surface against a fresh KimWipe® tissue and twisting axially until no alumina residue was visible.

Once the electrodes were thoroughly cleaned, ICPs were grown galvanostatically for 60 seconds applying a current of 0.1 mA/cm^2, unless stated otherwise. The deposited polymers were washed with acetone to remove excess electrolyte and gently dried with a hair dryer before continuing experimentation. The potential windows of cyclic voltammetry are noted in the respective Figures.

3.2.2 Materials

Pyrrole (Merck®), 3-methylthiophene (Aldrich®) and aniline (Aldrich®) were distilled under N_2 prior to use. Acetonitrile (Ajax®), Propylene carbonate (Aldrich®), tetrabutylammonium hexafluorophosphate (Aldrich®) terthiophene (Aldrich®) and bithiophene (Aldrich®) were of analytical or electrochemical grade and used as received.

Ionic liquids were synthesised via a solvent-free route based on the work of Geeta *et al.*[105], except that it was found that neither microwaves, nor sealed vessel systems were required. The precursor reagents for synthesis, namely 1-methylimidazole (Aldrich®), 1-bromobutane (Aldrich®), bromoethane (Aldrich®), sodium hexafluorophosphate (Aldrich®) and lithium (bis) trifluoromethanesulfonimide (Fluorad HQ115 by 3M®), were all analytical or electrochemical grade and were used as received.

3.2.3 Conductivity Measurements

Conductivity measurements were made using a Dallas Instruments two-point liquid conductivity probe at 24.5°C, pre-calibrated to known electrolyte conductivity standards.

3.3 Results and Discussion

3.3.1 Cyclic Voltammetry of Various Electrolyte Systems

In order to establish the most suitable range and gain a perspective on ILs as electrolytes, some ionic liquid systems were compared directly to a common electrolyte, 0.25 M tetrabutylammonium hexafluorophosphate ($TBAPF_6$) in propylene carbonate (PC). The various structures of other chemicals and electrolytes used are depicted in Table 3.1.

Propylene carbonate has a slightly hydrophobic character, a high dielectric constant[106], low melting point[106], low vapour pressure[106] and relatively low toxicity[106]. As an electrolyte solvent it is appealing because of low background currents and low decomposition due to oxidation[107].

Structure	Name	Acronym	Type	State (20°C)
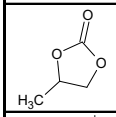	Propylene Carbonate	PC	supporting electrolyte	liquid
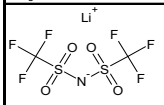	Lithium (bis) trifluoromethane sulfonimide	LiTFSI	ionic salt	solid
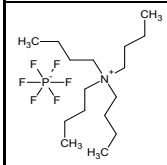	tetrabutylammonium hexafuorophosphate	$TBAPF_6$	ionic salt	solid
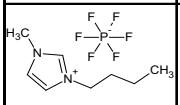	1-butyl-3-methylimidazolium hexafluorophosphate	$BMIPF_6$	ionic liquid	liquid
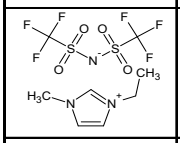	1-ethyl-3-methylimidazolium (bis) trifluoromethane sulfonimide	EMITFSI	ionic liquid	liquid
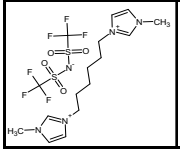	1-hexyl(bis)-3-methylimidazolium (bis) trifluoromethane sulfonimide	HbMITFSI	ionic liquid	liquid

Table 3.1- Structures of electrolyte components.

Tetrabutylammonium hexafluorophosphate is readily soluble in propylene carbonate, and the combination has gained popularity due to its wide electrochemical window of stability, as depicted in Figure 3.1.

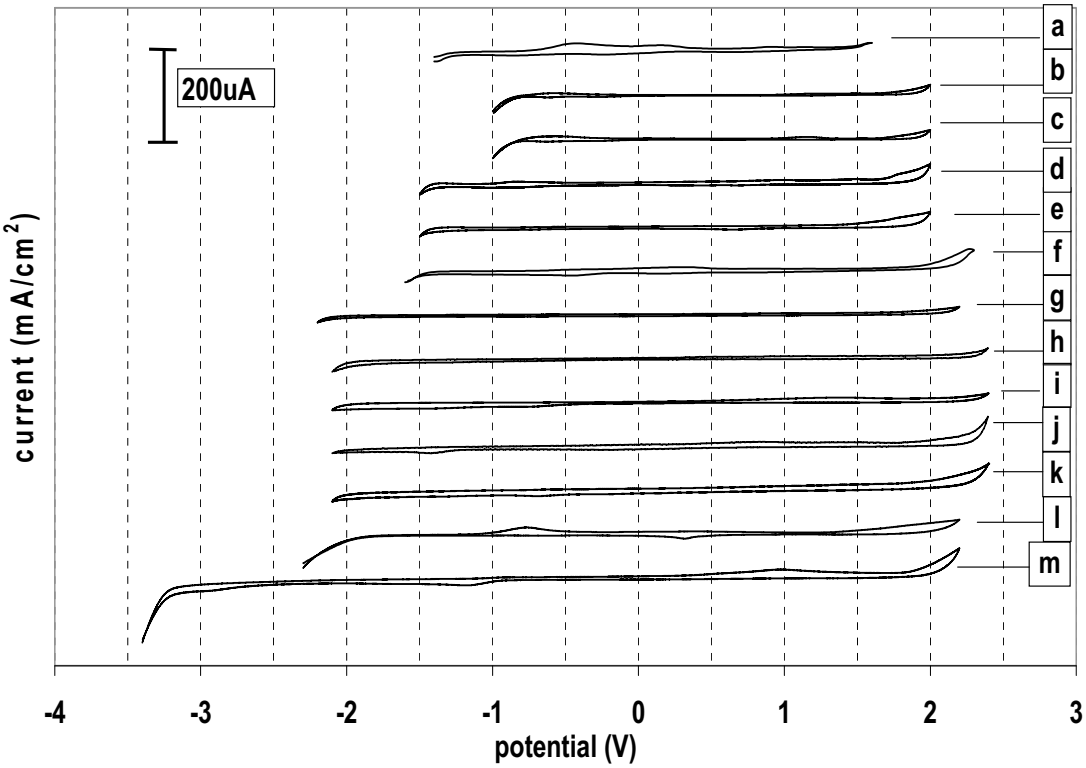

Figure 3.1- Cyclic voltammetry of various electrolytes. Scan rate = 200 mV/s

a- *20 % w/w $BMIPF_6$ in PC, on Pt disk*
b- *1 M LiTFSI in EMITFSI on Pt disk, with N_2 purging*
c- *1 M LiTFSI in EMITFSI on Pt disk, non-purged*
d- *Pure EMITFSI on Pt disk, with N_2 purging*
e- *Pure EMITFSI on Pt disk, non-purged*
f- *Pure $BMIPF_6$ on Pt disk, with N_2 purging*
g- *Pure $HbMIPF_6$ on GC disk, with N_2 purging*
h- *1 M LiTFSI in EMITFSI on GC disk, with N_2 purging*
i- *1 M LiTFSI in EMITFSI on GC disk, non-purged*
j- *Pure EMITFSI on GC disk, with N_2 purging*
k- *Pure EMITFSI on GC disk, non-purged*
l- *0.25 M $TBAPF_6$ in PC on Pt disk*
m- *0.25 M $TBAPF_6$ in PC on GC disk*

From Figure 3.1 it may be concluded that 0.25 M $TBAPF_6$ in PC with a GC disk electrode gives the largest potential range. However, PC as a supporting electrolyte has its drawbacks. It is miscible with water (240 g water dissolves in 1 L of PC) and it is prone to evaporation. In addition, as we shall see later, even though the $TBAPF_6$ / PC system has the widest electrochemical potential window in Figure 3.1, this cannot be exploited with conducting polymers due to redox cycling driven degradation.

Figure 3.1 *a* and 3.1 *f* depict the systems of 20 % w/w $BMIPF_6$ in PC and pure $BMIPF_6$ respectively. It was noted that there was a significant decrease in the potential window of stability when PC was added. The $BMIPF_6$ / PC had a lower potential window than either the pure $BMIPF_6$ system, or the 0.25 M $TBAPF_6$ / PC system of Figure 3.1 *m*.

3.3.2 Cyclic Voltammetry of Polypyrrole / PF_6 Film in $BMIPF_6$ and EMITFSI

Polypyrrole (PPy) was chosen for studies as an initial test candidate because it is a common and widely studied conducting polymer. All PPy electrode films were grown from 0.1 M pyrrole solution in 0.25 M $TBAPF_6$ / PC as the electrolyte. A 'reference' scan was conducted on a PPy / PF_6 film to define a typical PPy CV response (Figure 3.2). The position of the anodic peak shifted from -220 mV on the initial cycle, to 0 V after 20 cycles, with a corresponding rise in the cathodic peak potential of +100 mV, from -60 mV to +40 mV. The magnitudes of peak currents also increased with respect to cycle number from +0.1 mA/cm^2 to +2.2 mA/cm^2 for the anodic peak, and from -0.1 mA/cm^2 to -1.5 mA/cm^2 for the cathodic peak.

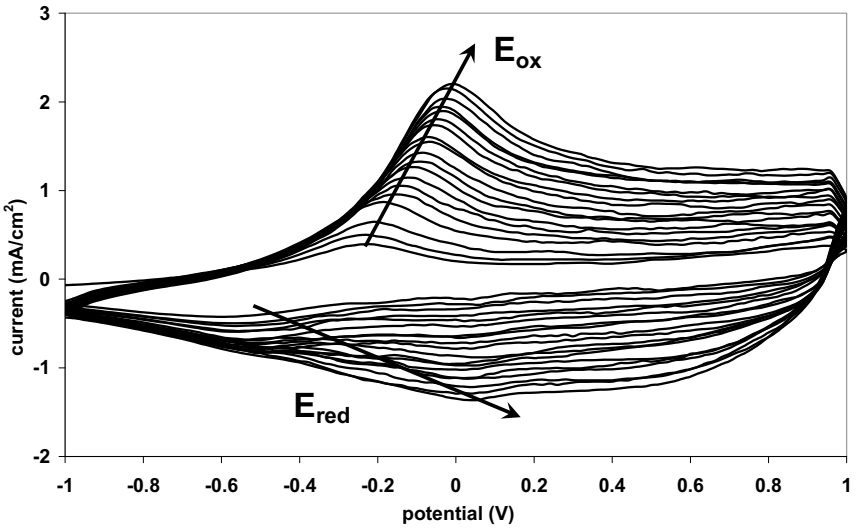

Figure 3.2- CVs of PPy / PF_6 film in a classical electrolyte, 0.25 M $TBAPF_6$ in PC. E_{ox} = oxidation peak, E_{red} = reduction peak. Arrows indicate direction of peak growth from cycle 1. Scan rate = 200 mV/s, 20 cycles.

This behaviour demonstrated that a higher population of electroactive polymer was accessible on subsequent scans, due to the effect of ion movement, although a higher electrical potential was required to access this population. The origin of the responses has been described in Chapter 2 in detail. Additional explanation of polypyrrole redox processes in classical electrolytes (CE) is provided by Equation 3.1 and simply shows how the polymer charge is balanced by mobile ions.

Equation 3.1-

anodic reaction (E_{ox}) : $PPy^0 + An^- \longrightarrow [PPy^+An^-] + e^-$

cathodic reaction (E_{red}) : $[PPy^+An^-] + e^- \longrightarrow PPy^0 + An^-$

PPy^0	-	*neutral polymer*
PPy^+	-	*oxidised polymer*
An^-	-	*anion*
e^-	-	*electron*

Initially, CVs of PPy / PF_6 films obtained in $BMIPF_6$ had poor reproducibility on a day-to-day basis. If the film was cycled in $BMIPF_6$ for 5 cycles and left in the air for a few hours, then cycled again, the second set of CV's did not resemble the first, even after $BMIPF_6$ was carefully purified. It was found that the results obtained were critically dependent on the amount of time taken between purging the $BMIPF_6$ with dry N_2 and running the CV.

The effect of N_2 purging during CV of PPy / PF_6 films in $BMIPF_6$ was therefore investigated. N_2 is commonly used in CV studies to displace other more reactive gases such as oxygen and carbon dioxide from sensitive systems. When a PPy / PF_6 film in $BMIPF_6$ was exposed to the atmosphere (Figure 3.3), two redox peaks were observed. Peak E_{ox} increased in potential from 0 mV to +260 mV, and peak E_{red} underwent a shift towards higher potentials from -600 mV to -300 mV during 20 scans. The magnitude of final peak currents was *ca.* ±4 mA/cm^2 for both processes.

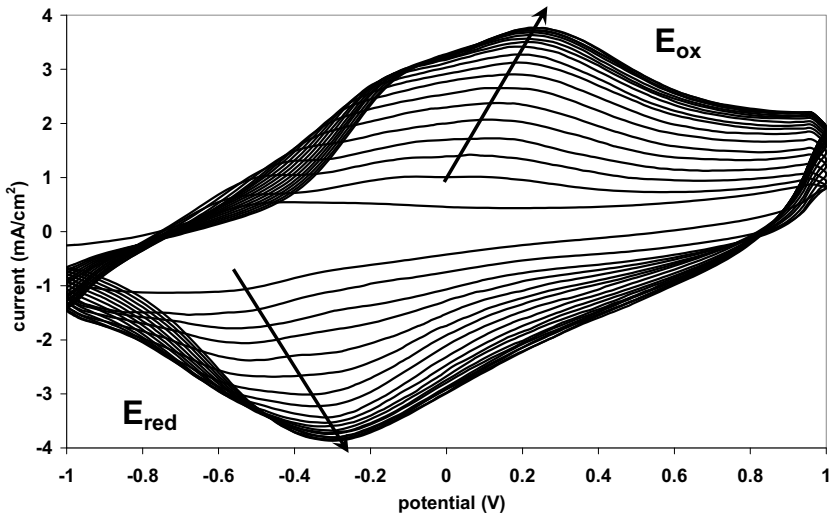

Figure 3.3- CVs of PPy / PF_6 film in $BMIPF_6$ under non-purged conditions. E_{ox} = oxidation peak, E_{red} = reduction peak. Arrows indicate direction of peak growth from cycle 1. Scan rate = 200 mV/s, 20 cycles.

When the PPy / PF_6 film in $BMIPF_6$ system was purged with N_2 (Figure 3.4), a significant decrease in the peak current magnitudes was observed compared to the non-purged system in Figure 3.3, decreasing by *ca.* 2 mA/cm^2. Two redox processes were also observed, but with different electrical potential behaviour on subsequent cycles compared to the non-purged system. The E_{ox} peaks increased in potential from 0 mV to +160 mV, and the E_{red} peaks decreased in potential from -200 mV to -260 mV during 20 cycles. These changes showed that the potential energies of species increased on subsequent cycling, with more energy required to drive the process as higher electroactive populations were accessed. The potential separations of E_{ox} and E_{red} potential separations were 420 mV on the 20^{th} cycle.

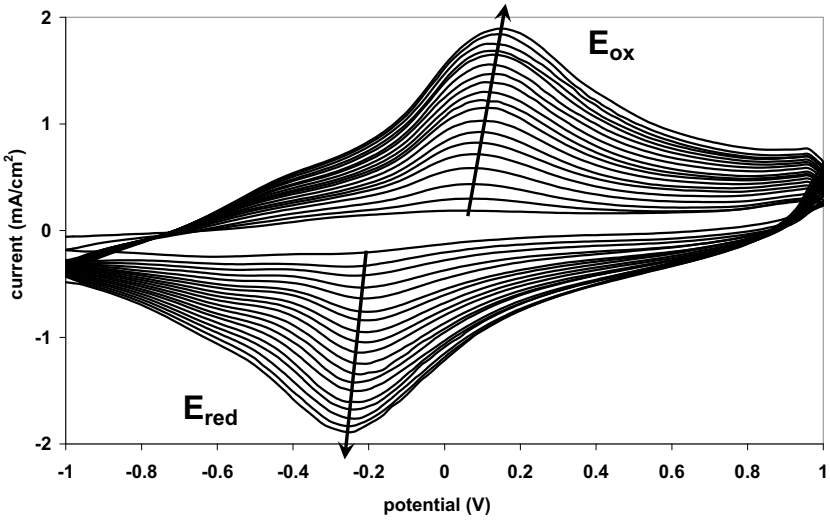

Figure 3.4- CVs of PPy / PF_6 film in $BMIPF_6$ under constant N_2 purging. E_{ox} = oxidation peak, E_{red} = reduction peak. Arrows indicate direction of peak growth from cycle 1. Scan rate = 200 mV/s, 20 cycles.

The possible influence of moisture on the system was investigated by purging samples during CV with 'wet' N_2 (Figure 3.5) and air dried through silica gel (Figure 3.6). Interestingly Figure 3.5 (wet N_2) and Figure 3.6 (dry air), when compared to Figure 3.4

(dry N_2) suggested that atmospheric moisture is not the only variable that affects the performance of the $BMIPF_6$ electrolyte, although it does have a dominant effect on the evolution of the CV.

The wet N_2 purged film from Figure 3.5 has E_{ox} peaks that increased in potential from 100 mV to 200 mV, and the E_{red} peaks increased in potential from -600 mV to -360 mV during 20 cycles, placing the observed potentials close to those observed in the non-purged example. The peak current magnitudes were *ca.* ±2.5 mA/cm^2 on the 20th cycle, which were similar values to those observed in the N_2 purged example.

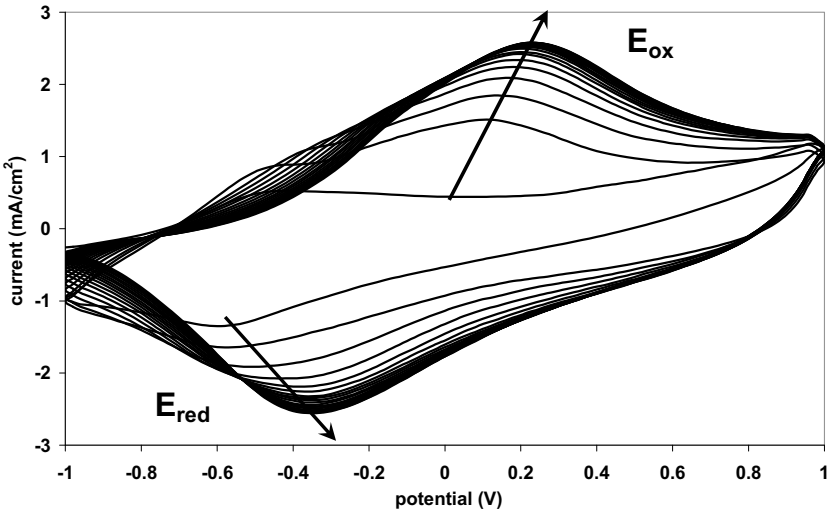

Figure 3.5- CVs of PPy / PF_6 film in $BMIPF_6$ with constant wet N_2 purging. E_{ox} = oxidation peak, E_{red} = reduction peak. Arrows indicate direction of peak growth from cycle 1. Scan rate = 200 mV/s, 20 cycles.

The dry air purged film from Figure 3.6 has E_{ox} peaks that increased in potential from -100 mV to +220 mV, and the E_{red} peaks increased in potential from -660 mV to -460 mV during 20 cycles resulting in values similar to those observed in the non-purged example. The peak current magnitudes were *ca.* ±3.5 mA/cm^2 on the 20th cycle, which were values closely resembling the non-purged PPy / PF_6 in $BMIPF_6$.

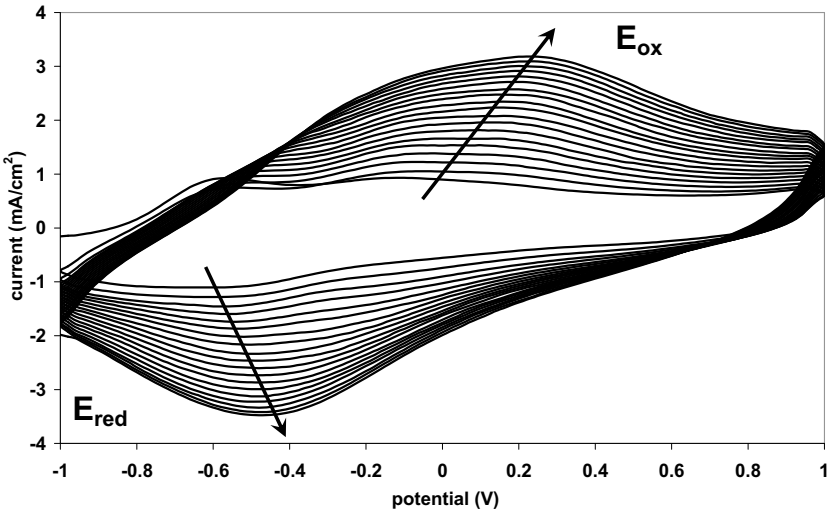

Figure 3.6- CVs of PPy / PF_6 film in $BMIPF_6$ with constant dry air purging. E_{ox} = oxidation peak, E_{red} = reduction peak. Arrows indicate direction of peak growth from cycle 1. Scan rate = 200 mV/s, 20 cycles.

As such, it appeared that moisture, and at least one other atmospheric gas played a role in determining the potentials of peak current CV responses of the PPy / PF_6 in $BMIPF_6$ systems. The magnitude of CV response was affected by an unidentified atmospheric gas that was not water.

The PPy / PF_6 film in EMITFSI CVs are depicted in Figure 3.7 to Figure 3.10, and represent the analogues of the preceding $BMIPF_6$ based studies. Many observations of the PPy / PF_6 film in $BMIPF_6$ CV were not present when EMITFSI was used as the electrolyte. Most notably there was a large difference of peak current redox potentials in the EMITFSI system versus the $BMIPF_6$ system. In addition, the EMITFSI system appeared to have negligible sensitivity to atmospheric gases. The apparent lack of influence of atmospheric reactants on the electrochemistry of PPy / PF_6 films in EMITFSI to may be due to EMITFSI having more pronounced hydrophobicity than $BMIPF_6$[108]. Alternatively, there may have been trace production of hydrofluoric acid caused by atmospheric oxygen or moisture in the $BMIPF_6$ electrolyte that may have interacted with the PPy / PF_6 polymer film.

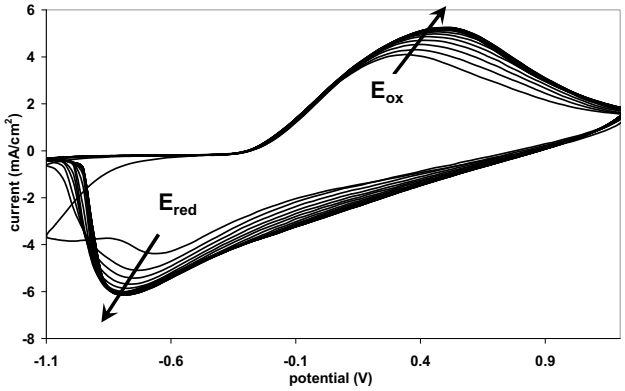

Figure 3.7- CVs of PPy / PF_6 film in EMITFSI under non-purged conditions. E_{ox} = oxidation peak, E_{red} = reduction peak. Arrows denote direction of peak growth from cycle 1. Scan rate = 200 mV/s, 20 cycles.

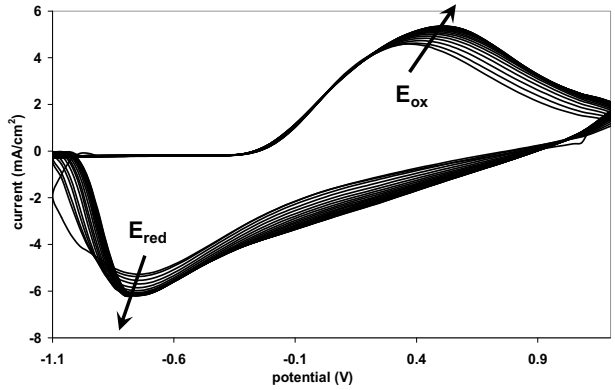

Figure 3.8- CVs of PPy / PF_6 film in EMITFSI under constant N_2 purging. E_{ox} = oxidation peak, E_{red} = reduction peak. Arrows indicate direction of peak growth from cycle 1. Scan rate = 200 mV/s, 20 cycles.

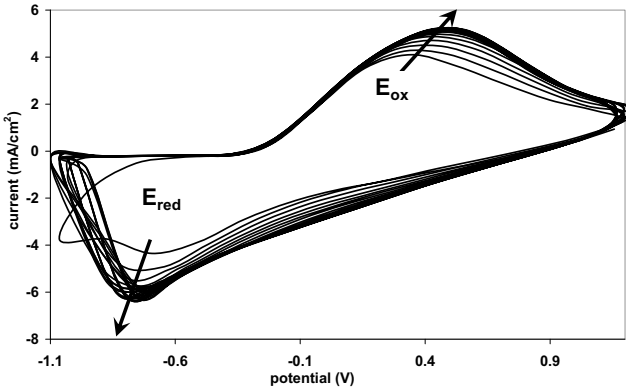

Figure 3.9- CVs of PPy / PF_6 film in EMITFSI with constant wet N_2 purging. E_{ox} = oxidation peak, E_{red} = reduction peak. Arrows indicate direction of peak growth from cycle 1. Scan rate = 200 mV/s, 20 cycles.

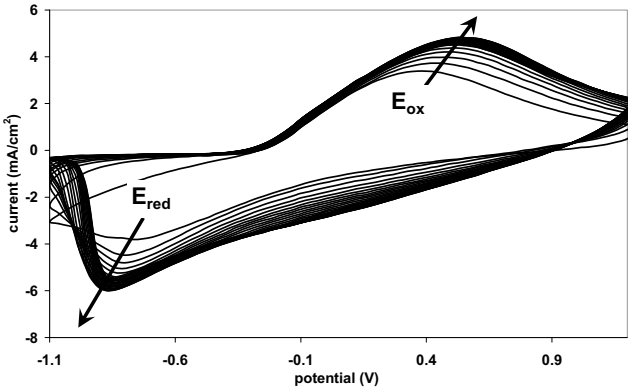

Figure 3.10- CVs of PPy / PF_6 film in EMITFSI with constant dry air purging. E_{ox} = oxidation peak, E_{red} = reduction peak. Arrows indicate direction of peak growth from cycle 1. Scan rate = 200 mV/s, 20 cycles.

The peak current magnitude potentials from the CVs of PPy / PF_6 film in $BMIPF_6$ and EMITFSI under different conditions are shown in Table 3.2. Comparison of the peak redox potentials revealed that the average separation of anodic and cathodic processes was 1300 mV for the PPy / PF_6 film in EMITFSI contrasting with a much lower separation range for the PPy / PF_6 film in $BMIPF_6$, from 200 to 700 mV.

Condition of IL	Peak current potentials (mV)			
	$BMIPF_6$ electrolyte		EMITFSI electrolyte	
	E_{ox}	E_{red}	E_{ox}	E_{red}
non-purged	260	-300	490	-840
N_2 purge	160	-260	530	-760
wet N_2 purge	200	-360	490	-800
dry air purge	220	-460	530	-880

Table 3.2 - Peak redox potentials of PPy / PF_6 films in various conditions of EMITFSI and $BMIPF_6$

The oxidation and reduction peak potentials of PPy / PF_6 in $BMIPF_6$ were the closest together in the N_2-purged situation, appearing at +160 mV and -260 mV, respectively.

These potentials were far more negative than observed in experiments using EMITFSI case, where oxidation and reduction peaks occurred at +530 mV and -760 mV, respectively. This observation appeared counter-intuitive in the light of the work by Wallace *et al.*[109]. They showed with PPy-based artificial muscles that the most mobile species in a PPy / PF_6 film in $BMIPF_6$ or EMITFSI are the cations. Actuation occurred as contraction on oxidation of the polymer, suggesting the expulsion of cations, with anions remaining immobile. Such behaviour is summarised in Equation 3.2

Equation 3.2-

cathodic reaction: $[PPy^0Cat^+An^-] \longleftrightarrow [PPy^+An^-] + Cat^+ + e^-$

anodic reaction: $[PPy^+An^-] + Cat^+ + e^- \longleftrightarrow [PPy^0Cat^+An^-]$

PPy^0	-	*neutral polymer*
PPy^+	-	*oxidised polymer*
An^-	-	*anion*
Cat^+	-	*cation*
e^-	-	*electron*

Other rationalisations may account for the unexpected behaviour of a larger cation being more mobile than a smaller one. In particular, a different anion was used in the two PPy / IL systems studied, and even though it is thought that the anion in ionic liquid systems remains essentially immobile, it still does have strong affinity for the cation. The charge dissipation or shielding of a larger cation may also play a role in its apparent increased electrochemical mobility. Decreased charge concentration reduces the strength of ionic bonds, and may increase the mobility of the cation to a greater extent than the related steric mobility impairment.

Ionic conductivity for $BMIPF_6$ is 1.8 mS/cm compared to 8.8 mS/cm for EMITFSI. EMITFSI is thus nearly five times more conductive than $BMIPF_6$. Typically, a low conductivity electrolyte causes increasing separations between E_{ox} and E_{red}. One would therefore expect the lower conducting $BMIPF_6$ to produce E_{ox} and E_{red} peak separation than in EMITFSI. However, the opposite is observed, meaning other factors dominate over ionic conductivity.

3.3.3 Potential Window of Polypyrrole / PF_6 Film in $BMIPF_6$ and EMITFSI

As EMITFSI and $BMIPF_6$ have relatively large potential windows, the effect of increasing the potential range used during cyclic voltammetry on a PPy / PF_6 film was investigated. All polymers were first cycled from +1.0 V to increasingly negative potentials, until decomposition began. When the most negative stable potential was obtained, a fresh PPy / PF_6 film was cycled from the lowest stable potential in a series of CVs with increasing positive potential limits until decomposition occurred. A 'reference' scan of a PPy / PF_6 film in 0.25 M $TBAPF_6$ / PC (Figure 3.11) was also produced in this way to compare the IL systems to a classical electrolyte. The PPy / PF_6 film was found to decompose rapidly beyond potentials of -1.5 or +1.4 V, demonstrated by the collapse in current magnitude in the CV.

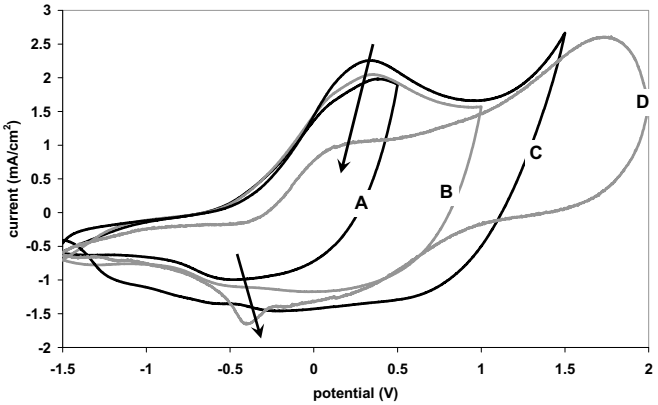

Figure 3.11- CVs obtained for potential window of PPy / PF_6 film in 0.25 M $TBAPF_6$ / PC. With a constant negative potential limit of -1.5 V, positive potential limits were (A) = +0.4 V, (B) = +0.8 V, (C) = +1.4 V, (D) = +2.0 V. Arrows indicate direction of peak current migration with progressively higher positive potential limits. Scan rate = 200 mV/s.

The potential window experiment using non-purged $BMIPF_6$ (Figure 3.12) showed decreased potential window stability when compared to the 0.25 M $TBAPF_6$ / PC system at -1.4 to +1.4 V. The system appeared to be sensitised by atmospheric gases and / or moisture, resulting in rapid degradation. Both the anodic and cathodic peaks shifted in a positive potential direction on application of increasing potential energy limits.

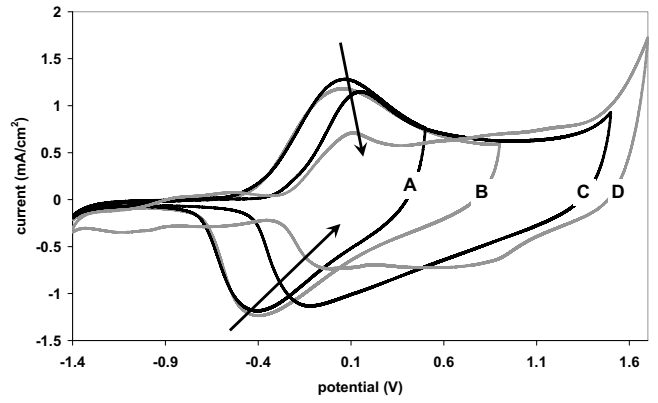

Figure 3.12- CVs obtained for potential window of PPy / PF_6 film in non-purged $BMIPF_6$. With a constant negative potential limit of -1.4 V, positive potential limits were (A) = +0.4 V, (B) = +0.8 V, (C) = +1.5 V, (D) = +1.7 V. Arrows indicate direction of peak current migration with progressively higher positive potential limits. Scan rate = 200 mV/s.

PPy / PF_6 film cycled in non-purged EMITFSI (Figure 3.13), had significantly increased potential stability (-1.5 to +2.0V) when compared to either the non-purged $BMIPF_6$ or PC based electrolyte. As the positive potential was increased, the magnitude of the anodic peak current decreased but its potential remained almost constant. The cathodic peak, however, increased in current magnitude and moved to lower potentials. Such behaviour suggests that the time constants for ion insertion and expulsion are different, with the oxidative process being faster.

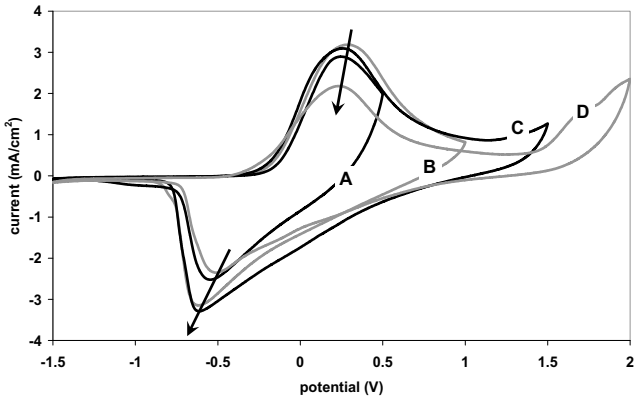

Figure 3.13- CVs obtained for potential window of PPy / PF_6 film in non-purged EMITFSI. With a constant negative potential of -1.5 V, positive potential limits were (A) = +0.4 V, (B) = +0.8 V, (C) = +1.4 V, (D) = +2.0 V. Arrows indicate direction of peak current migration with progressively higher positive potential limits. Scan rate = 200 mV/s.

When the PPy / PF_6 film in $BMIPF_6$ system was purged with N_2, the electrochemistry changed significantly. The range of potential stability, where significant current peak magnitudes do not drop, nearly doubled compared to the non-purged system (Figure 3.14). This observation reemphasises the high level of sensitivity of the PPy / PF_6 film in $BMIPF_6$ to reactive atmospheric gases. It should also be noted that the polymer appeared to be stable beyond the potential window of a Pt disk in $BMIPF_6$, suggesting that the polypyrrole is protecting the underlying Pt from reacting with the $BMIPF_6$. The oxidation and reduction peaks migrated in the positive and negative potential directions, respectively, as positive potential limits were increased, suggesting that the polymer was becoming harder to reduce and oxidise.

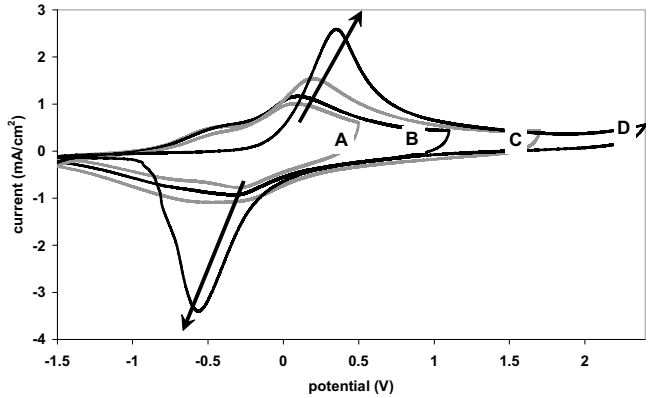

Figure 3.14- CVs obtained for potential window of PPy / PF_6 film in BMIPF_6 with N_2 purging. With a constant negative potential of -1.5 V, positive potential limits were (A) = +0.4 V, (B) = +1.0 V, (C) = +1.6 V, (D) = +2.4 V. Arrows indicate direction of peak current migration with progressively higher positive potential limits. Scan rate = 200 mV/s.

Figure 3.15 shows the CV of the PPy / PF_6 cycled in N_2 purged EMITFSI. Unlike the analogous non-purged system, the peak currents both grew at larger positive cycling voltages and peak potentials migrated closer together. This indicated that the electrochemical processes became more favourable. This may be due to improvement of ion migration pathways in the PPy /PF_6 film from driving ions through the material at increasing voltage.

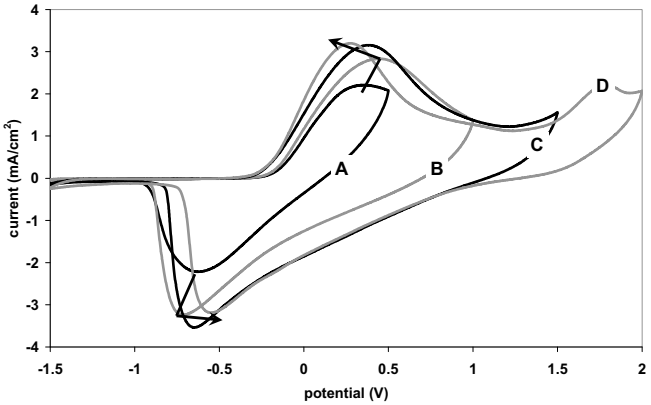

Figure 3.15- CVs obtained for potential window of PPy / PF_6 film in EMITFSI with N_2 purging. With a constant negative potential limit of -1.5 V, positive potential limits were (A) = +0.4 V, (B) = +1.0 V, (C) = +1.4 V, (D) = +2.0 V. Arrows indicate direction of peak current migration with progressively higher positive potential limits. Scan rate = 200 mV/s.

3.3.4 Redox Cycling Stability of Polypyrrole / PF_6 Film in $BMIPF_6$ and EMITFSI

Many ICPs degrade rapidly on redox cycling in conventional electrolytes. The effect of redox cycling on the stability of PPy / PF_6 films in $BMIPF_6$ and EMITFSI electrolytes was investigated and compared to a conventional electrolyte system consisting of 0.25 M $TBAPF_6$ in PC. Potential ranges were chosen to encompass the full doping / dedoping region of each system.

Figure 3.16 depicts CVs obtained of PPy / PF_6 films in the conventional electrolyte, 0.25 M $TBAPF_6$ / PC, showing intermittent cycles up to cycle number 300. The system degraded rapidly, current magnitude fell in intensity, and the redox peaks corresponding to oxidation and reduction shifted in negative potential directions.

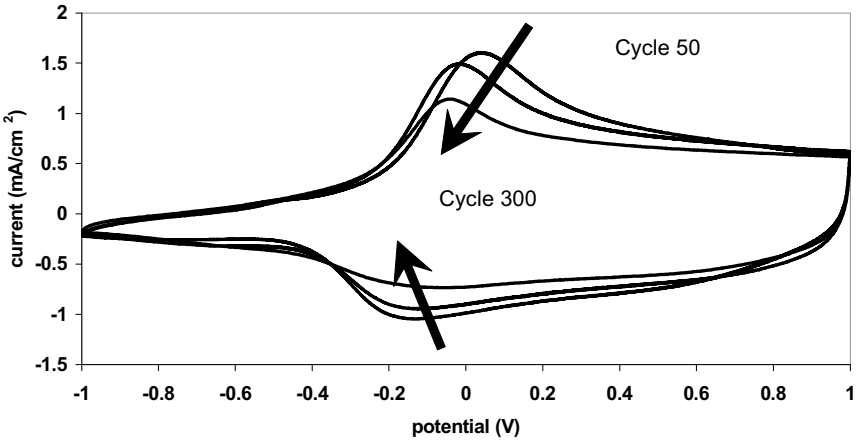

Figure 3.16- CVs of PPy / PF_6 film in 0.25 M $TBAPF_6$ / PC. Obtained after 50, 200 and 300 cycles. Arrows indicate direction of peak current migration on successive cycles. Scan rate = 200 mV/s.

When PPy / PF_6 film was cycled in non-purged $BMIPF_6$ (Figure 3.17), the electrochemistry took more than 50 cycles to establish, and once it did, the system did

not change for 900 cycles (Figure 3.17). Even without purging of electrolyte, stable electrochemistry was observed. Such a high degree of stability may allow for the use of polypyrrole in commercial devices that rely on redox cycling such as batteries or capacitors.

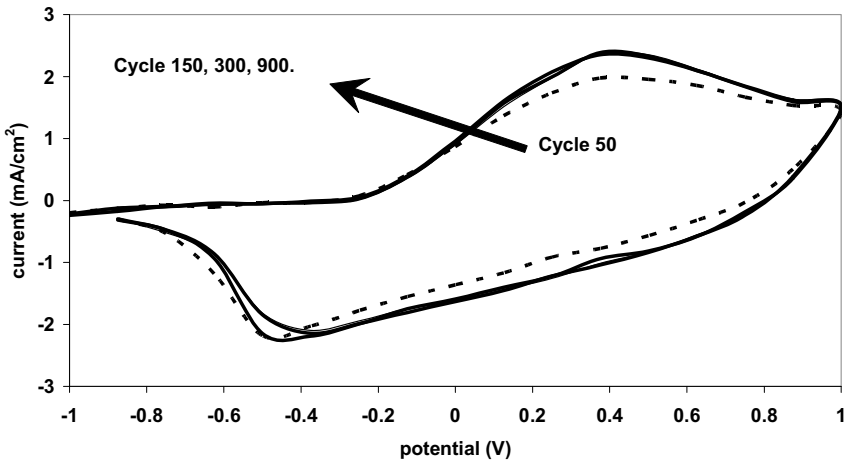

Figure 3.17- CVs of PPy / PF_6 film in non-purged $BMIPF_6$. Obtained after 50, 150, 300 and 900 cycles. Arrows indicate direction of peak current migration on successive cycles. Scan rate = 200 mV/s.

PPy / PF_6 film in non-purged EMITFSI was subjected to prolonged cycling by CV (Figure 3.18). The system exhibited considerably lower stability to redox cycling compared to the $BMIPF_6$ electrolyte analogue. Current magnitude decreased rapidly in the first 300 cycles; but thereafter the degradation significantly slowed down, cycle 900 being only marginally smaller than cycle 300. The redox peaks also moved closer together, reduction peak potentials increased from -0.8 V to -0.6 V, and oxidation peak potentials decreased from +0.5 V to +0.3 V. This may signify that ion migration pathways in the ICP have been improved during cycling, or that atmospheric gases have integrated into the PPy and may be mediating the redox switching of the PPy film.

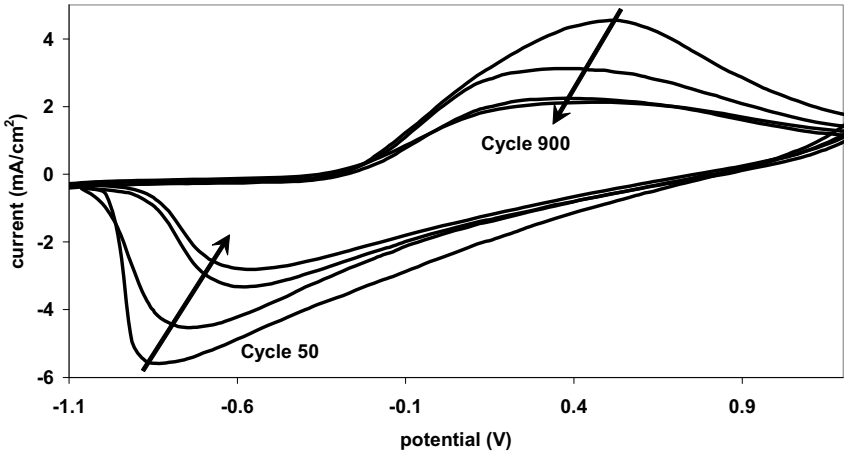

Figure 3.18- CVs of PPy / PF_6 film in EMITFSI, non-purged. Cycles 50, 150, 300 and 900 shown. Arrows indicate direction of peak current migration on successive cycles. Scan rate = 200 mV/s.

When the $BMIPF_6$ electrolyte was purged with N_2 (Figure 3.19), significant changes occurred to the electrochemistry, as observed in previous sections. Interestingly, the electrochemistry took a considerably longer time to establish. After 300 cycles the current magnitude was still increasing up to the 900^{th} cycle.

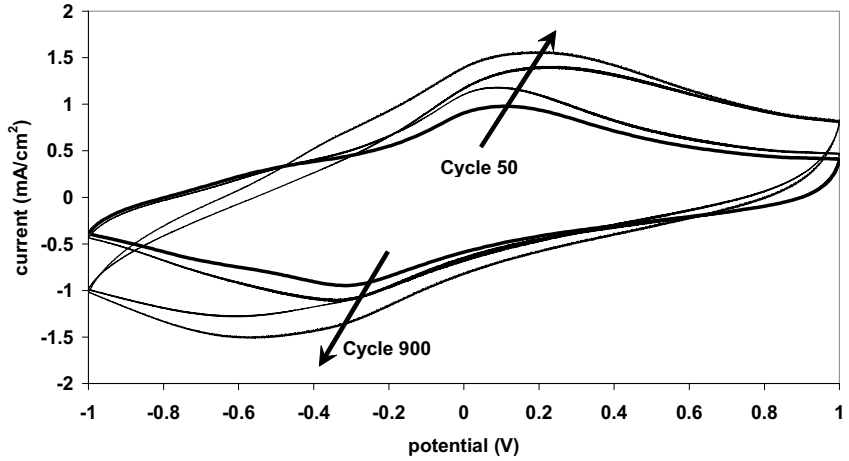

Figure 3.19- CVs of PPy / PF_6 film in N_2 purged $BMIPF_6$. Cycles 150, 300 and 900 shown. Arrows indicate direction of peak current migration on successive cycles. Scan rate = 200 mV/s.

On purging the EMITFSI system with N_2 (Figure 3.20), the decrease in current magnitude still happened rapidly until cycle 300, after which time the system appeared relatively stable, with little decrease in current magnitude between cycles 300 and 900. The effect of removing reactive atmospheric gases from the system was to slow down degradation of the PPy / PF_6 when using EMITFSI electrolyte, as the current peak magnitudes were larger in the N_2-purged case. The position of the redox peaks was unaltered throughout 900 cycles, providing some evidence that reactive atmospheric gases may have provided redox mediation in the non-purged system.

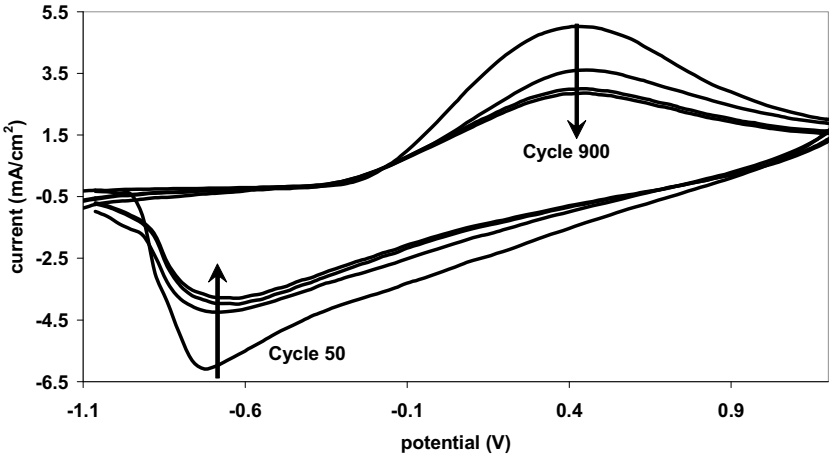

Figure 3.20- CVs of PPy / PF_6 film in EMITFSI, N_2 purged. Cycles 50, 150, 300 and 900 shown. Arrows indicate direction of peak current migration on successive cycles. Scan rate = 200 mV/s.

Of the systems investigated here for electrochemical stability, the PPy / PF_6 film cycled in $BMIPF_6$ electrolyte under N_2 purging showed the greatest stability, with the current magnitude still increasing after 900 cycles. The CVs for PPy / PF_6 film cycled in EMITFSI were similar for the N_2 purged and non-purged examples. However, the absence of reactive atmospheric gases in the system resulted in slightly improved stability and prevented the shifting of peak potentials. It is believed that shifting peak potentials might be due to electron mediation by reactive atmospheric constituents, due to the magnitude decrease of redox potentials.

3.3.5 Kinetic Studies of Polypyrrole / PF_6 Film in $BMIPF_6$ and EMITFSI

Kinetic studies were performed on PPy / PF_6 films in $BMIPF_6$, EMITFSI and conventional electrolyte. The Randles-Sevcik equation (Equation 3.3) was used to determine diffusion constants. This approach makes a number of assumptions that must be reconciled in a conducting polymer system and are discussed below.

The Randles-Sevcik equation applies to reversible reactions under semi-infinite linear diffusion (unrestricted diffusion to a large planar electrode). If we assume that diffusion within the polymer is slower than diffusion through the mobile electrolyte surrounding it, the effect of diffusion within the polymer will become the limiting factor.

Equation 3.3-

$$i_p = 0.4463\ n\ F\ A\ C\ (n\ F\ v\ D\ /\ R\ T)^{-1/2}$$

i_p	-	*peak current*
n	-	*electron population from redox process*
v	-	*scan rate (V / sec)*
F	-	*Faraday's constant (96485 C / mol)*
A	-	*electrode area (cm^2)*
R	-	*universal gas constant (8.314 J / mol K)*
T	-	*temperature (K)*
D	-	*analyte's diffusion coefficient (cm^2/sec)*
C	-	*analyte's concentration (mol/L)*

Substituting for constants this can be expressed as:

Equation 3.4-

$$i_p = (2.687x10^5 \cdot n^{3/2}\ v^{1/2}) D^{1/2}\ A\ C$$

Rearranging Equation 3.4 gives a form where the charge transport rate D1/2C can be extracted from the slope of the line to give:

Equation 3.5-

$$D^{1/2}C = \left(\left(\frac{i_p}{\sqrt{v}}\right)\left(\frac{1}{\left(2.687\times10^5\right)n^{3/2}A}\right)\right)$$

where the charge transport rate is given in mol cm $s^{-1/2}$ L^{-1}.

Figure 3.21 depicts a plot of the peak current (i_p) versus the square root of scan rate (v) for PPy / PF_6 films in PC containing 0.25 M $TBAPF_6$ as well as in non-purged and N_2 purged $BMIPF_6$ and EMITFSI. As predicted by Equation 3.5, a linear relationship was found in each case, with reasonable R^2 values (0.99 to 0.97) from the fit of straight lines to the data points.

From the slopes of the plots in Figure 3.21, the charge transport rates were calculated using Equation 3.5. The calculated diffusion rates are shown in Table 3.3. When the relative conductivities of $BMIPF_6$ and EMITFSI, measured to be 1.8 and 8.8 mS/cm, respectively, are taken into account, it suggests that the rate limiting step of the electrochemical response is due to ion diffusion through the PPy / PF_6 polymer. One would expect that higher electrolyte conductivity would result in better charge transport rates. What was seen, however, was the rate of ion transport inside the polymer did not correlate to the conductivity of surrounding electrolyte.

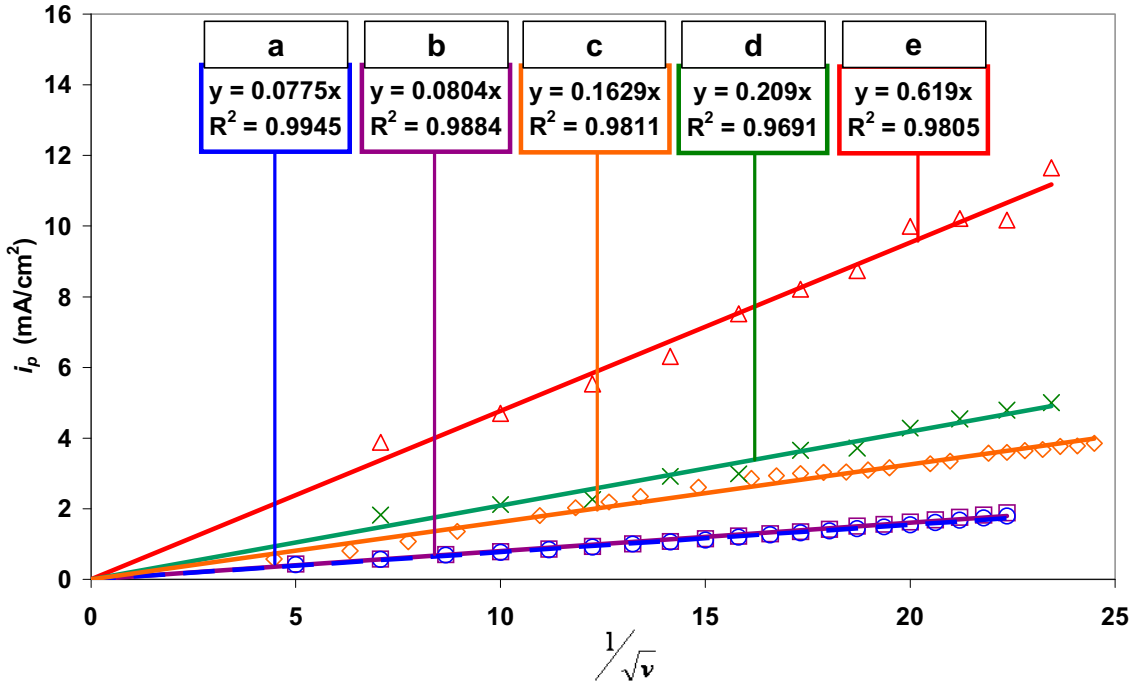

Figure 3.21- Square root of scan rate vs. peak current for PPy / PF_6 films in various electrolytes: (a) N_2 purged EMITFSI, (b) non-purged EMITFSI, (c) N_2 purged $BMIPF_6$, (d) 0.25 M $TBAPF_6$ in PC, (e) non-purged $BMIPF_6$. Potential range = -1.0 to +1.0 V, 3rd cycle from CV taken to determine peak current.

From Table 3.3 it may be observed that the charge transport rates obtained from PPy / PF_6 in N_2 purged $BMIPF_6$ and 0.25 M $TBAPF_6$ in PC were comparable at 3.0 x 10^{-5} and 3.9 x 10^{-5} mol cm $s^{-1/2}$ L^{-1} respectively. However, when atmospheric gases were allowed into the PPy / PF_6 film in $BMIPF_6$ system, the charge transport rates rose sharply by almost a factor of five to 1.2 x 10^{-4} mol cm $s^{-1/2}$ L^{-1}. It was also noted from Table 3.3 that the PPy / PF_6 film in EMITFSI electrolyte system was generally unaffected by atmospheric gases, producing charge transport rates comparable to N_2 purged PPy / PF_6 film in $BMIPF_6$, *ca.* 1.5 x 10^{-5} mol cm $s^{-1/2}$ L^{-1}.

System	Slope	Charge Transport Rate (mol cm $s^{-1/2}$ L^{-1})
PPy / PF_6 in 0.25M $TBAPF_6$ in PC	0.209	$3.9x10^{-5}$
PPy / PF_6 in non-purged $BMIPF_6$	0.619	$1.2x10^{-4}$
PPy / PF_6 in N_2 purged $BMIPF_6$	0.163	$3.0x10^{-5}$
PPy / PF_6 in non-purged EMITFSI	0.080	$1.5x10^{-5}$
PPy / PF_6 in N_2 purged EMITFSI	0.078	$1.4x10^{-4}$

Table 3.3- Charge transport rates of PPy / PF_6 films in various systems.

3.3.6 Electrochemistry of Conducting Polymers with Respect to $BMIPF_6$ and EMITFSI Quantity in PC

The most striking difference between ILs and classical electrolytes is that ILs are pure substances, while classical electrolytes consist of dissociated ions surrounded and solvated by a neutral solvent. Classical electrolyte (CE) systems are therefore considerably more complex due to the possibilities of internal interactions between solvent and solute. The contrast between the two systems may also provide clues as to the nature of "neutral" solvent interaction in electrochemical processes. ILs provide a unique opportunity where the electrolyte system can have the ion concentration varied in a neutral solvent across a range of 0 to 100 %.

3.3.7 Ionic Conductivity as a Function of $BMIPF_6$ and EMITFSI Quantity in PC

To determine the effect on the CVs of ICP films in varied IL / ICP mixtures, the conductivity of these mixed solutions was first determined. Higher electrolyte conductivity may be expected to increase the magnitude of current observed in CVs.

Pure $BMIPF_6$ and EMITFSI were recorded to have values of 1.8 and 8.0 mS/cm, respectively. This corresponded closely to the values reported by Maciej *et. al.*[89]. Ionic conductivity as a function of IL percentage in PC is shown in Figure 3.22 (% mol/mol) and Figure 3.23 (% w/w). The ionic conductivity of the $BMIPF_6$ and EMITFSI systems peaked at *ca.* 15 % mol/mol, and. 90 % mol/mol IL composition, respectively (Figure 3.22). As such the conductivity profiles were essentially mirrored, suggesting quite different solvation / conductivity mechanisms, even though the two ILs have many other physical properties that are similar.

Interestingly, the $BMIPF_6$ conductivity profile (Figure 3.22) closely matched to the work published by Lewandowski *et al*[110] for $EMIBF_4$ conductivities in water mixtures. Similarly, the conductivity profile for EMITFSI / PC mixtures (Figure 3.22) closely resembled that of published work by Barhdadi *et al.*[111] for BMITFSI in dimethylformamide. Barhdadi *et al.*[111] also published viscosity data for the system, finding a linear relationship of viscosity rising logarithmically with increasing IL composition.

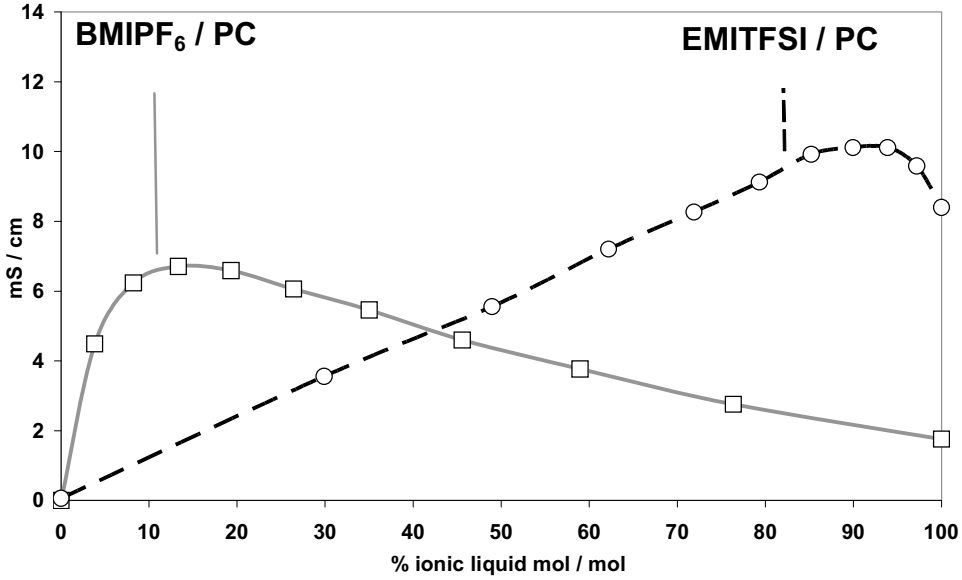

Figure 3.22- Conductivity of $BMIPF_6$ in PC and EMITFSI in PC at different concentrations of IL, % mol/mol.

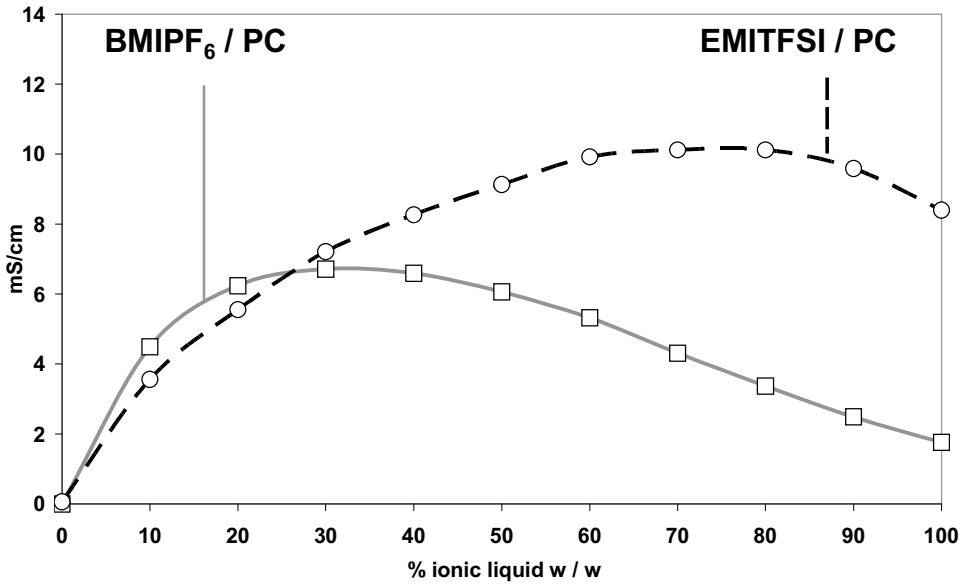

Figure 3.23- Conductivity of $BMIPF_6$ in PC and EMITFSI in PC at different concentrations of IL, % w/w.

Barhdadi *et al*. argued that lower viscosity produced higher conductivity, and the viscosity closely correlated with the conductivity. In fact, such an interpretation conflicted with the data they presented - the peak value of conductivity existed at a

composition with very high relative viscosity. The system therefore appears to be more complicated than just simple ion migration.

As was discussed in Chapter 1, conductivity requires charge carriers. Charge carriers cannot be neutral species, as these will not directly feel the effect of an electrical field. Viscosity also plays a role in the effectiveness of ion migration. The viscosity of binary mixtures of various ionic liquids and neutral solvents has been studied by others[110,111,112,113,114], and found to invariably follow a logarithmic relationship.

Viscosity data were re-constructed from the viscosities of pure PC (2.5 mPa s), pure EMITFSI (28 mPa s), and pure $BMIPF_6$ (270 mPa s) as starting points. It was assumed that the relationship between molar composition and the natural log of viscosity for the $BMIPF_6$ and EMITFSI would produce a straight line[110,111,112,113,114]. Converting these data to a plot of viscosity as a function of molar percentage IL in PC resulted in Figure 3.24.

From the Stokes Einstein equation, conductive diffusion is inversely proportional to viscosity[110]. Therefore, a plot of the reciprocal of viscosity vs. the percentage ionic liquid (% mol/mol) was made, to obtain an idea of how the conductivity due to only viscosity would vary upon increasing the molar percentage of IL, as depicted in Figure 3.25. The predicted conductivity profiles in Figure 3.25 are quite different to those observed experimentally, but the two profiles of EMITFSI and $BMIPF_6$ are similar to each other. Therefore, if one assumes that the conductivity changes in a similar way for both systems, one may expect that the differences in observed conductivity profiles for the two systems are caused by the mechanisms of charge carrier evolution overwhelming the effects from viscosity on conductivity.

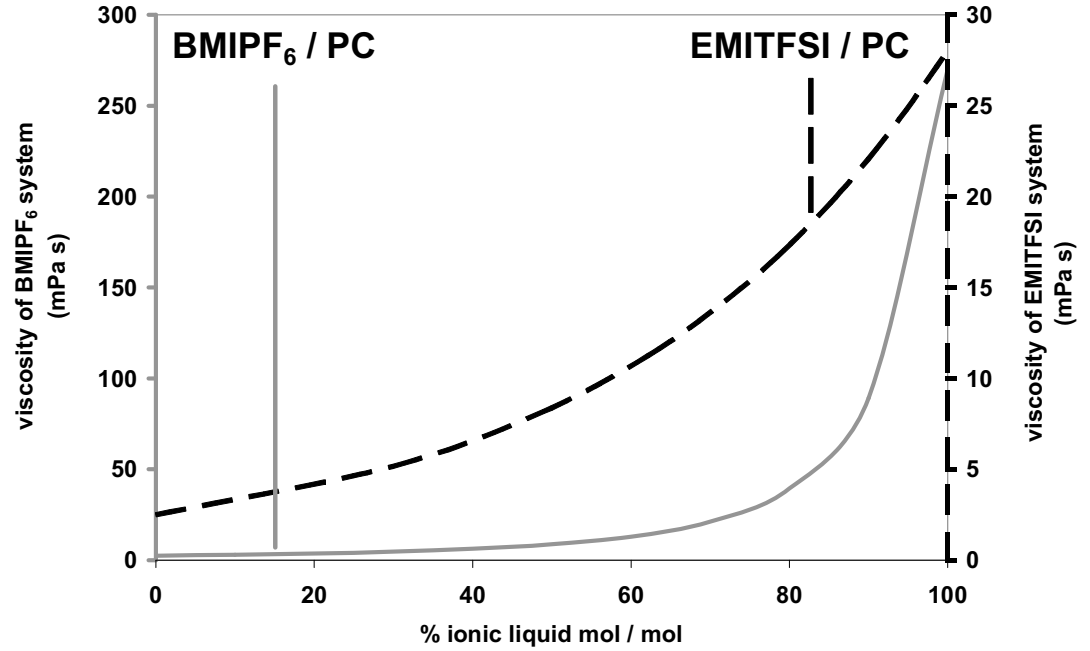

Figure 3.24- Predicted viscosities of $BMIPF_6$ and EMITFSI at different concentrations in PC.

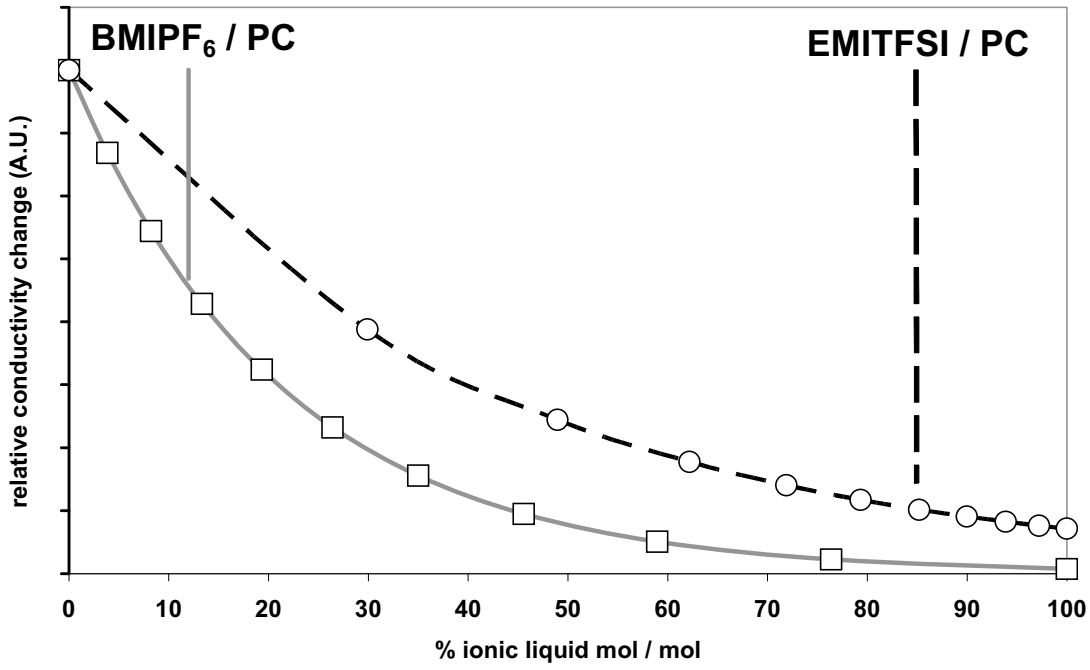

Figure 3.25- Relative conductivity changes predicted due to viscosity only.

As the different profiles are considered to be due to charge carrier population (without the effects of viscosity being visible), this may shed light on the tendencies of each IL to ion pair, dissociate or form overall neutral ion clusters.

The EMITFSI conductivity profile of Figure 3.22 showed a linear rise in conductivity as concentration of EMITFSI was gradually raised up to approximately 85 % mol/mol. Such behaviour suggested that the ions of EMITFSI were readily dissociating in PC, resulting in behaviour of simple dilution of a dissociable salt. Above 90 % mol/mol EMITFSI, the conductivity dropped slightly, presumably as ion pairing began to re-establish. This ease of ion dissociation also helps explain why EMITFSI is considerably more conductive than $BMIPF_6$.

The $BMIPF_6$ conductivity profile of Figure 3.22 told a different story. Conductivity rose very sharply from 0 to 15 % mol/mol $BMIPF_6$, and then gradually decreased in a nearly linear manner above 20 % mol/mol $BMIPF_6$. Such behaviour suggested that below 15 % mol/mol $BMIPF_6$, the concentration of PC was sufficiently high to encourage dissociation and produce charge-carrying ions. The almost linear drop beyond 20 % mol/mol $BMIPF_6$ could be attributed to the system's tendency to form neutral ion pairs[115]. As the concentration of PC was decreased in $BMIPF_6$, there was less material to support ion dissociation and charge carrier formation.

3.3.8 Conducting Polymer CVs as a Function of $BMIPF_6$ and EMITFSI Quantity in PC

To enable interpretation of data sets obtained for the CVs of ICPs in IL / PC dilutions, an alternative means of presentation was developed (Figure 3.26). CV produces data displayed in two dimensions (current vs. potential). Incorporating changes in IL / PC solvent composition produces another dimension. Hence, it was possible to plot the evolution of two-dimensional cyclic voltammetry against a third variable of electrolyte concentration. Separation of the anodic and cathodic components of the CV was also carried out to allow the effect of electrolyte composition to be clearly determined. The data could also be presented as a contour plot, using changes in colour to present current density.

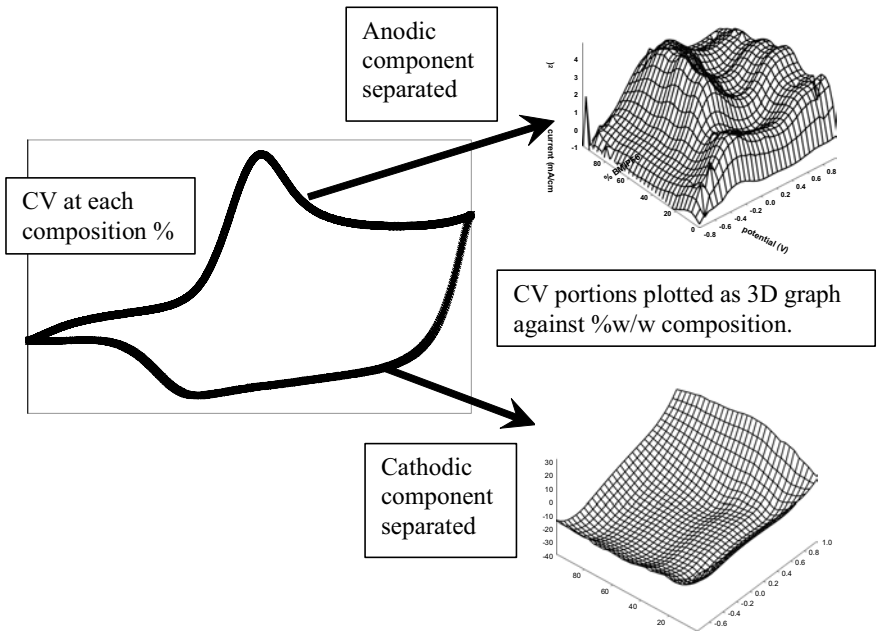

Figure 3.26- Diagram of the procedure used to develop CV contour plots obtained for ICP films in $BMIPF_6$ / PC and EMITFSI / PC of varying composition. 10 CVs used for each plot.

3.3.9 Polypyrrole / PF_6 CVs as a Function of $BMIPF_6$ and EMITFSI Quantity in PC

Figure 3.27 shows the CV obtained for PPy / PF_6 in $BMIPF_6$ / PC and EMITFSI / PC at 50 % w/w concentration to assist with the visualisation of the three-dimensional data presented in Figure 3.28 and Figure 3.29.

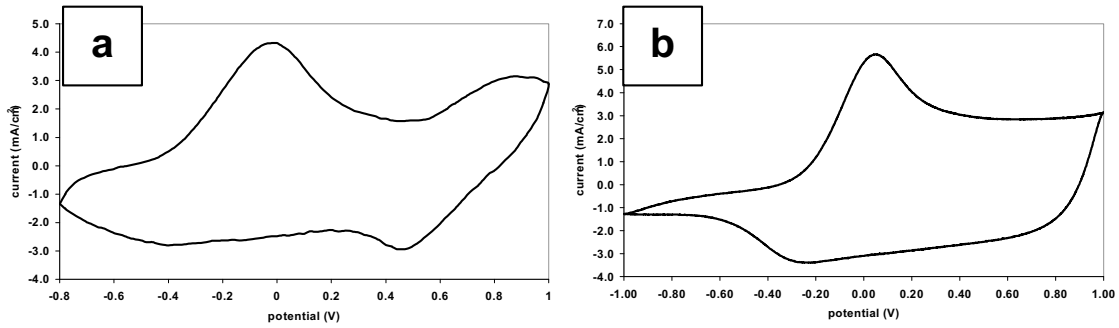

Figure 3.27- CV of PPy / PF_6 film in (a) $BMIPF_6$ / PC and (b) EMITFSI / PC electrolyte at 50 % w/w composition. Scan rate = 200 mV/s.

Figure 3.28 depicts the full range of PPy / PF_6 CVs in $BMIPF_6$ / PC mixtures. Counter-intuitively, a dip in the magnitude of redox response was noted at the point where the electrolyte was most conductive. The decreasing electrolyte conductivity at higher $BMIPF_6$ concentrations did not appear to follow the decrease of cathodic current in the polymer species. The general trend in the cathodic portion of the electrochemistry (omitting what occurred at maximum conductivity) was different to that shown by the conductivity itself. The broadest cathodic CV was seen at *ca.* 50 % w/w $BMIPF_6$ / PC.

In the anodic portion of Figure 3.28 other trends were observed. At zero percent w/w ionic liquid there was obviously poor electrochemistry as ions were not available to

interact with the polymer, line "d". Again, a lack of current was observed near the maximum point of ionic conductivity, line "c". The polymer's peak current oxidation potentials were noted to shift linearly towards more positive potentials as the $BMIPF_6$ concentration was increased, see line "a" and line "b" in Figure 3.28.

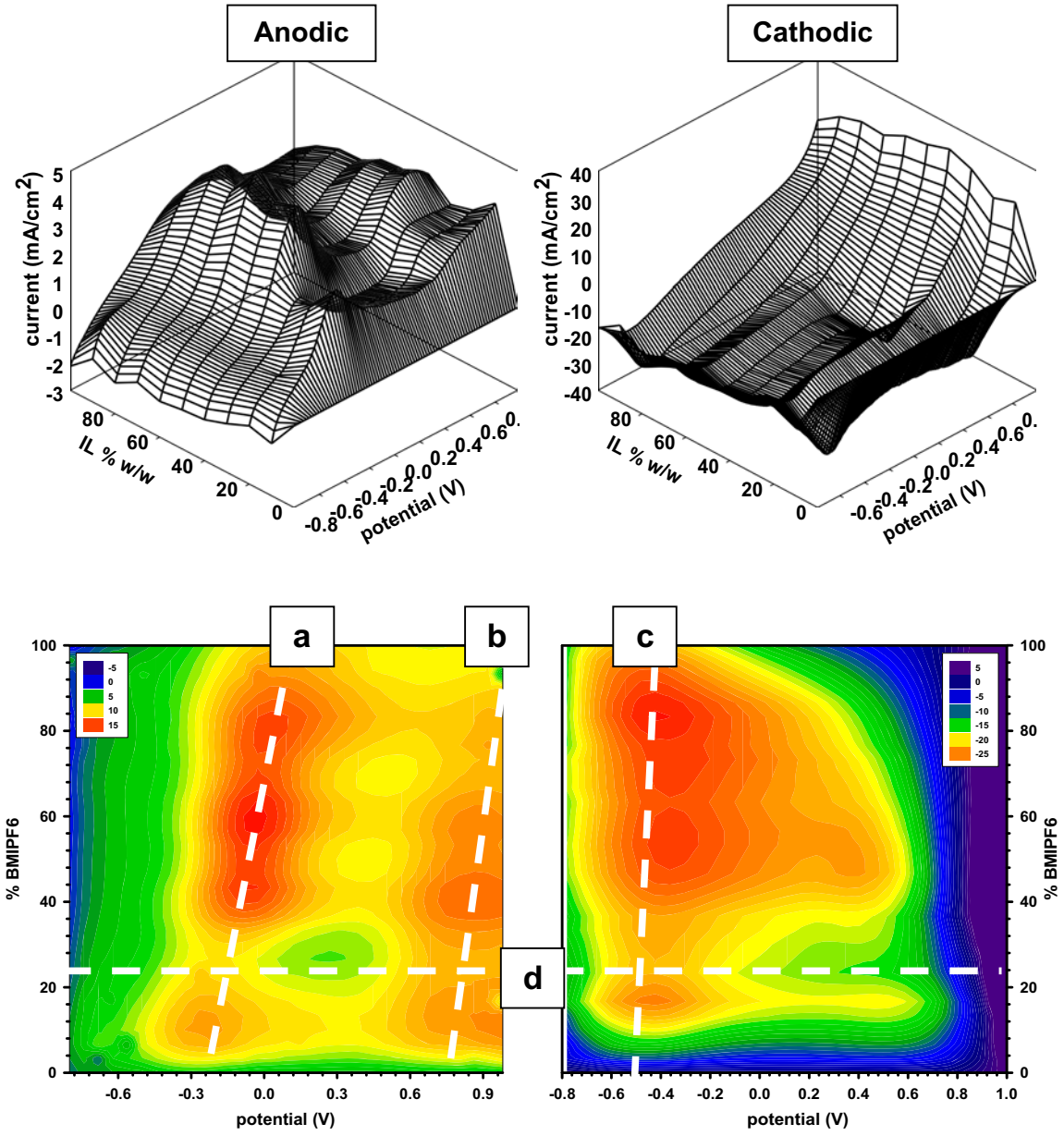

Figure 3.28 - Three-dimensional (top) and contour plots (bottom) of PPy / PF_6 CVs at varying concentrations of $BMIPF_6$ in PC. (a) , (b) (c) and (d) are lines drawn to guide the eye along trends of the current magnitudes and composition plots.

For the PPy / PF_6 film in EMITFSI / PC electrolyte, the three-dimensional CVs shown in Figure 3.29, exhibit a reversal of certain trends observed $BMIPF_6$ / PC electrolyte. In the PPy / PF_6 films in $BMIPF_6$ / PC electrolyte, increasingly positive oxidation peak potentials were observed at higher $BMIPF_6$ concentrations, denoting that $BMIPF_6$ may play a role in increasing oxidation potentials.

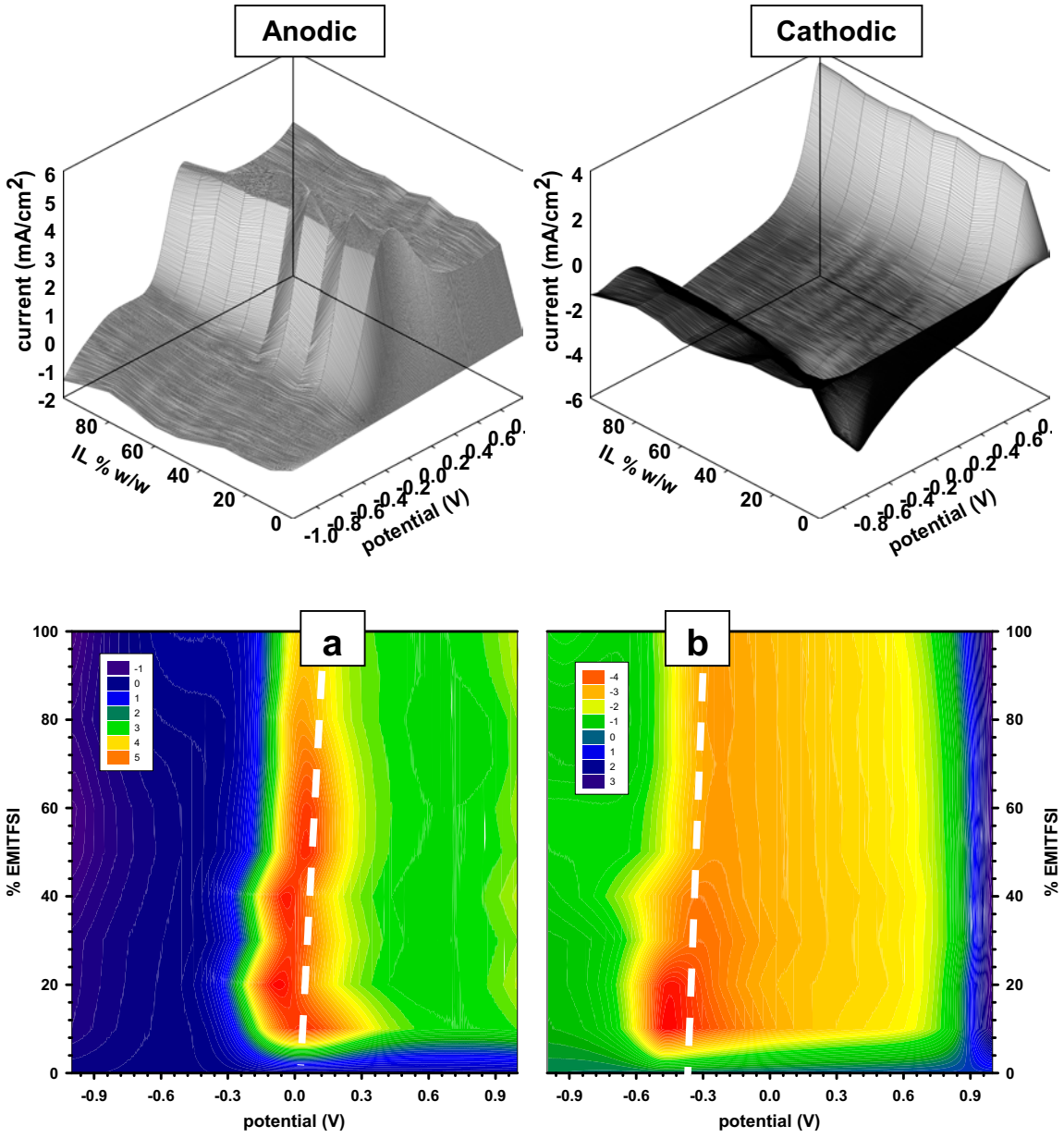

Figure 3.29- Three-dimensional (top) and contour plots (bottom) of PPy / PF_6 CVs at varying concentrations of EMITFSI in PC. (a) and (b) are lines drawn to guide the eye along trends of the current magnitudes and composition plots.

In EMITFSI / PC electrolyte, however, less positive potentials were required to reduce the polymer (see Figure 3.29 line "b"). The oxidation potentials were generally unaffected (Figure 3.29 line "a"). Although the anodic and cathodic current peaks of the PPy / PF_6 film in EMITFSI / PC electrolyte intensified and broadened in a way consistent with following the ionic conductivity profile, it was found that peak intensity was highest at the lowest ion conductivity, and dropped steadily as ionic conductivity was increased.

3.3.10 Poly-3-methylthiophene (P3MeTh) / PF_6 CVs as a Function of $BMIPF_6$ and EMITFSI Quantity in PC

Figure 3.30 shows the CV obtained for P3MeTh / PF_6 in $BMIPF_6$ / PC and EMITFSI / PC at 50 % w/w concentration to assist with the visualisation of the three-dimensional data presented in Figure 3.31 and Figure 3.32.

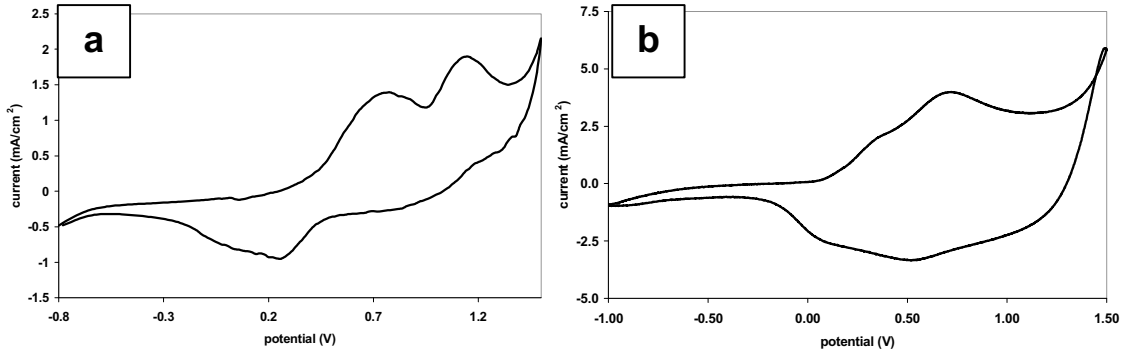

Figure 3.30- CV of P3MeTh / PF_6 film in (a) BMIPF6 / PC and (b) EMITFSI / PC electrolyte at 50 % w/w composition. Scan rate = 200 mV/s.

The three-dimensional plots for P3MeTh / PF_6 films in $BMIPF_6$ / PC mixtures are shown in Figure 3.31. From zero to 30 % w/w $BMIPF_6$ / PC, the anodic peak current, line "d" showed a decrease in electroactivity, with little corresponding effect on the cathodic portion at the same $BMIPF_6$ concentration below line "c". Between the lines "b" and "c" of Figure 3.31 (30-70 % w/w), the electrochemistry remained mostly unaffected. At composition of $BMIPF_6$ above 70 % w/w, line "b", the anodic current

also appeared mostly unaffected, but the cathodic current underwent a broadening, opposite to the decreased current magnitude profile denoted by line "a" in the anodic region.

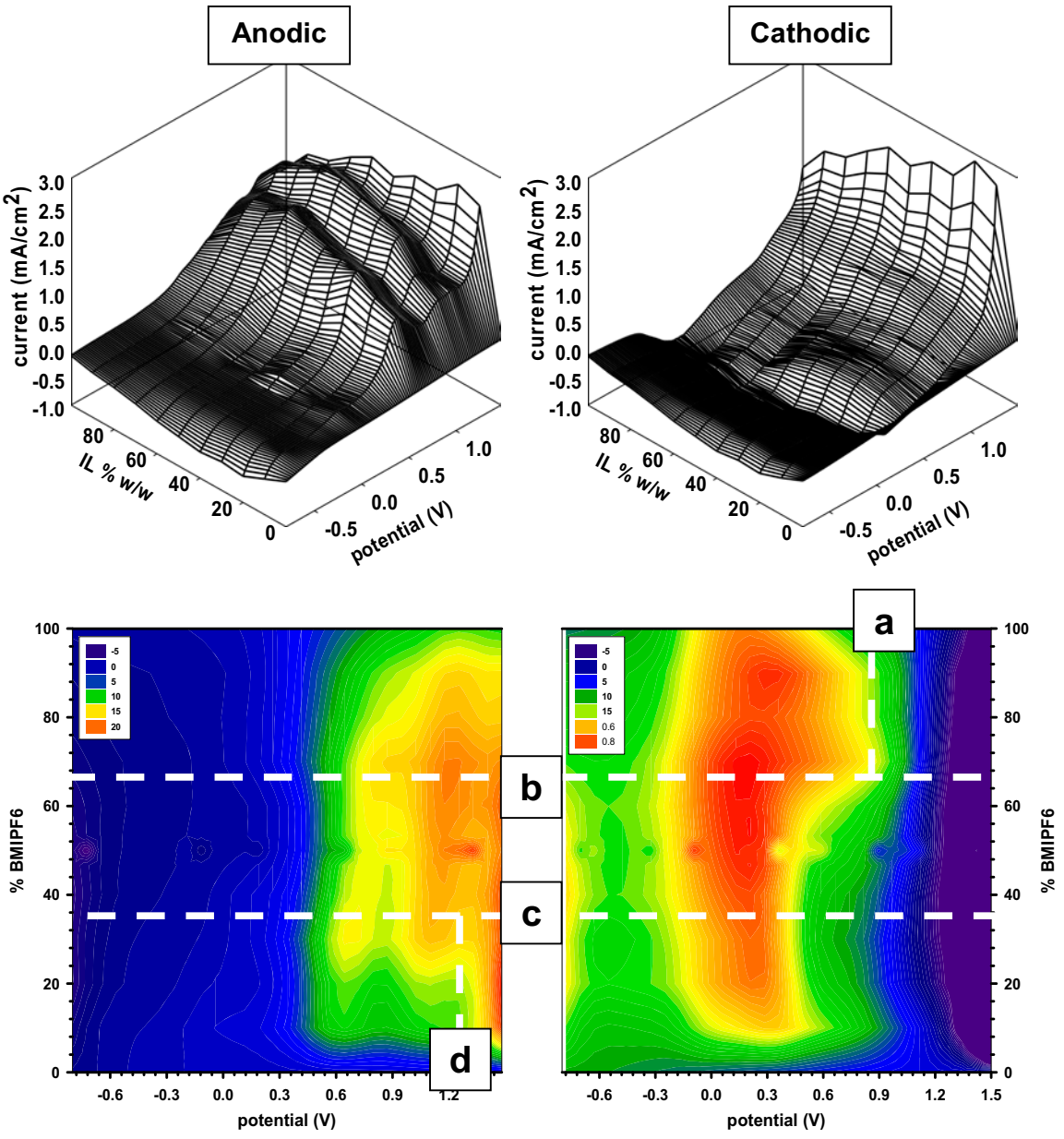

Figure 3.31- Three-dimensional (top) and contour plots (bottom) of P3MeTh / PF_6 CVs at varying concentrations of $BMIPF_6$ in PC. (a) , (b) (c) and (d) are lines drawn to guide the eye along trends of the current magnitudes and composition plots.

The analogous system of P3MeTh / PF_6 film in EMITFSI / PC electrolyte showed a linear transition throughout the sets of CV cycling with respect to EMITFSI

concentration (Figure 3.32). The unusual behaviour of increasing electroactivity with decreasing ionic conductivity of electrolyte was again observed, at approximately 20 % w/w EMITFSI, as denoted by Figure 3.32, line "c". The P3MeTh / PF_6 film became easier to oxidise and reduce as the EMITFSI concentration was increased, denoted by lines "a" and "b". This is opposite to the behaviour observed earlier in the polypyrrole equivalent system (see Section 3.3.9).

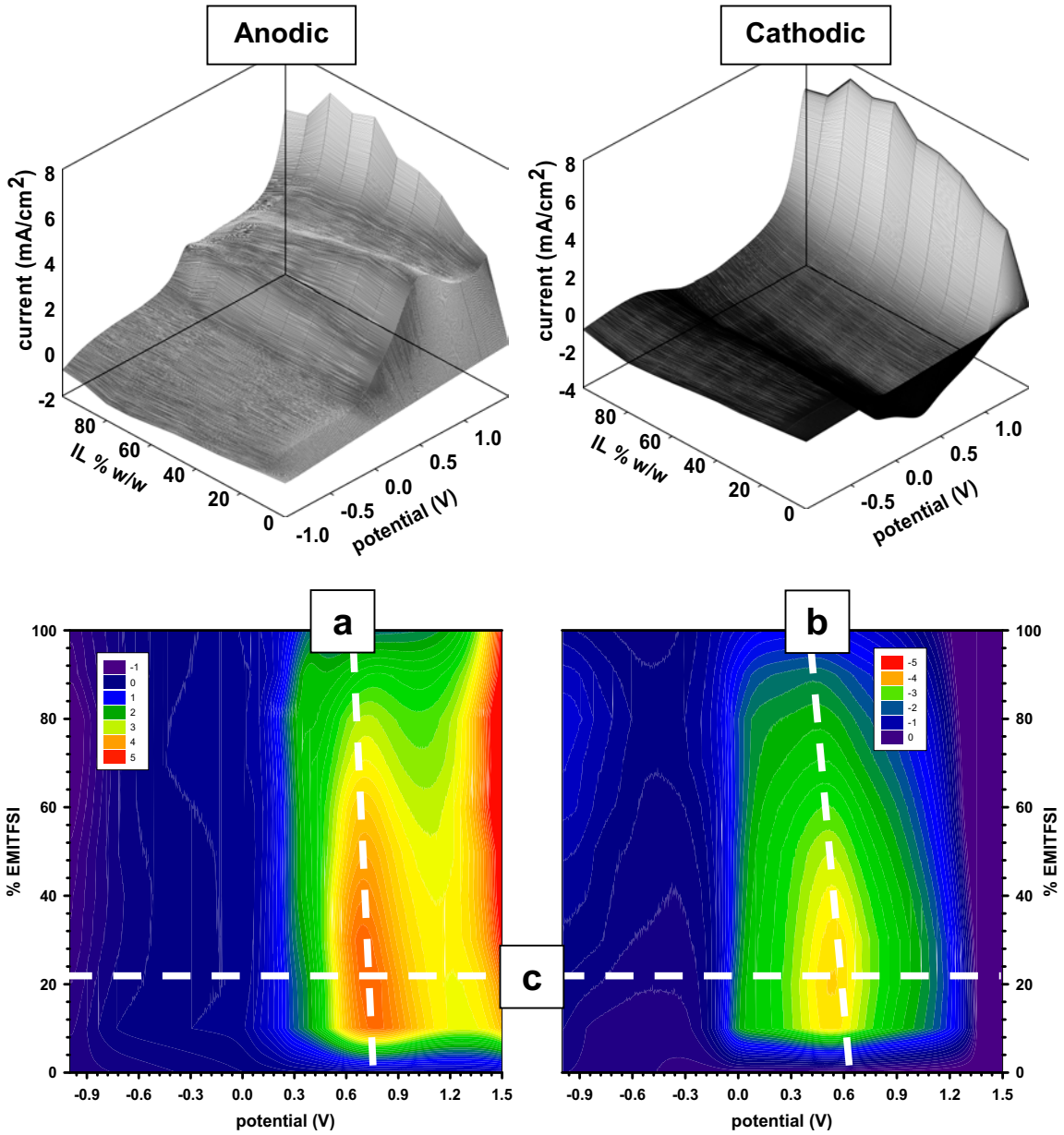

Figure 3.32- Three-dimensional (top) and contour plots (bottom) of P3MeTh / PF_6 CVs at varying concentrations of EMITFSI in PC. (a) , (b) and (c) are lines drawn to guide the eye along trends of the current magnitudes and composition plots.

3.3.11 Polybithiophene (PBiTh) / PF_6 CVs as a Function of $BMIPF_6$ and EMITFSI Quantity in PC

Figure 3.33 shows the CV obtained for PBiTh / PF_6 in $BMIPF_6$ / PC and EMITFSI / PC at 50 % w/w concentration to assist with the visualisation of the three-dimensional data presented in Figure 3.34 and Figure 3.35.

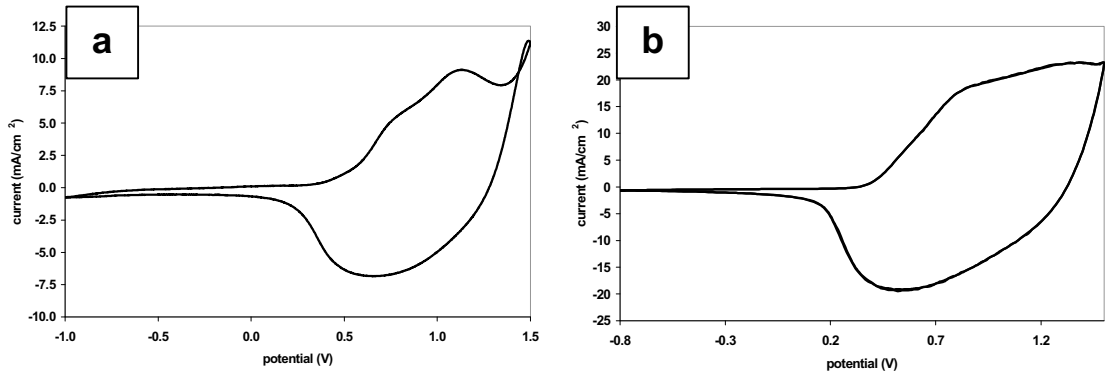

Figure 3.33- CV of PBiTh / PF_6 film in (a) $BMIPF_6$ / PC and (b) EMITFSI / PC electrolyte at 50 % w/w composition. Scan rate = 200 mV/s.

From the three-dimensional plots shown in Figure 3.34 for PBiTh / PF_6 films in $BMIPF_6$ / PC mixtures, the effect on the current magnitudes in 50 % w/w $BMIPF_6$ denoted by line "d", was very pronounced in both the anodic and cathodic portions of the CVs. However, polypyrrole only showed a major broadening at 50 % w/w composition for the cathodic portion of the CVs. Polybithiophene exhibited a clear increase in current intensity at around 50 % w/w $BMIPF_6$ for both the anodic and cathodic portions. In the cathodic portion, the reduction potential moved to more negative values at higher percentages of $BMIPF_6$, whereas this trend was seen in the anodic portion of PPy / PF_6 film in $BMIPF_6$ / PC electrolyte.

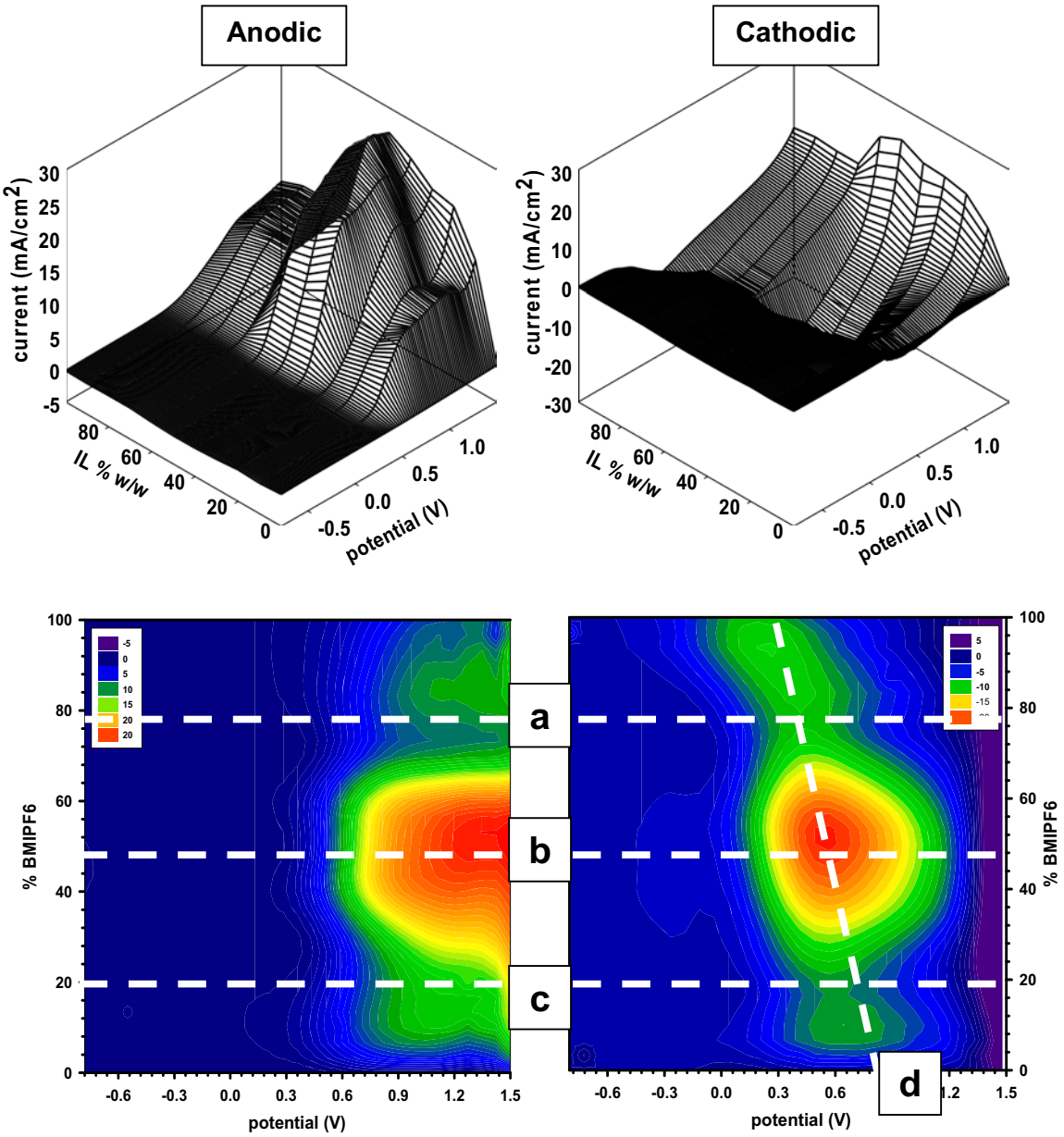

Figure 3.34- Three-dimensional (top) and contour plots (bottom) of PBiTh / PF_6 CVs at varying concentrations of $BMIPF_6$ in PC. (a) , (b) (c) and (d) are lines drawn to guide the eye along trends of the current magnitudes and composition plots.

The corresponding three-dimensional plots for PBiTh / PF_6 film in EMITFSI / PC electrolyte is depicted in Figure 3.35. The PBiTh / PF_6 film exhibited lower oxidation potentials at higher concentrations of EMITFSI up to *ca.* 60 % w/w, denoted by line "b". As the EMITFSI concentration rose above 60 % w/w, the magnitude of oxidation currents rapidly decreased.

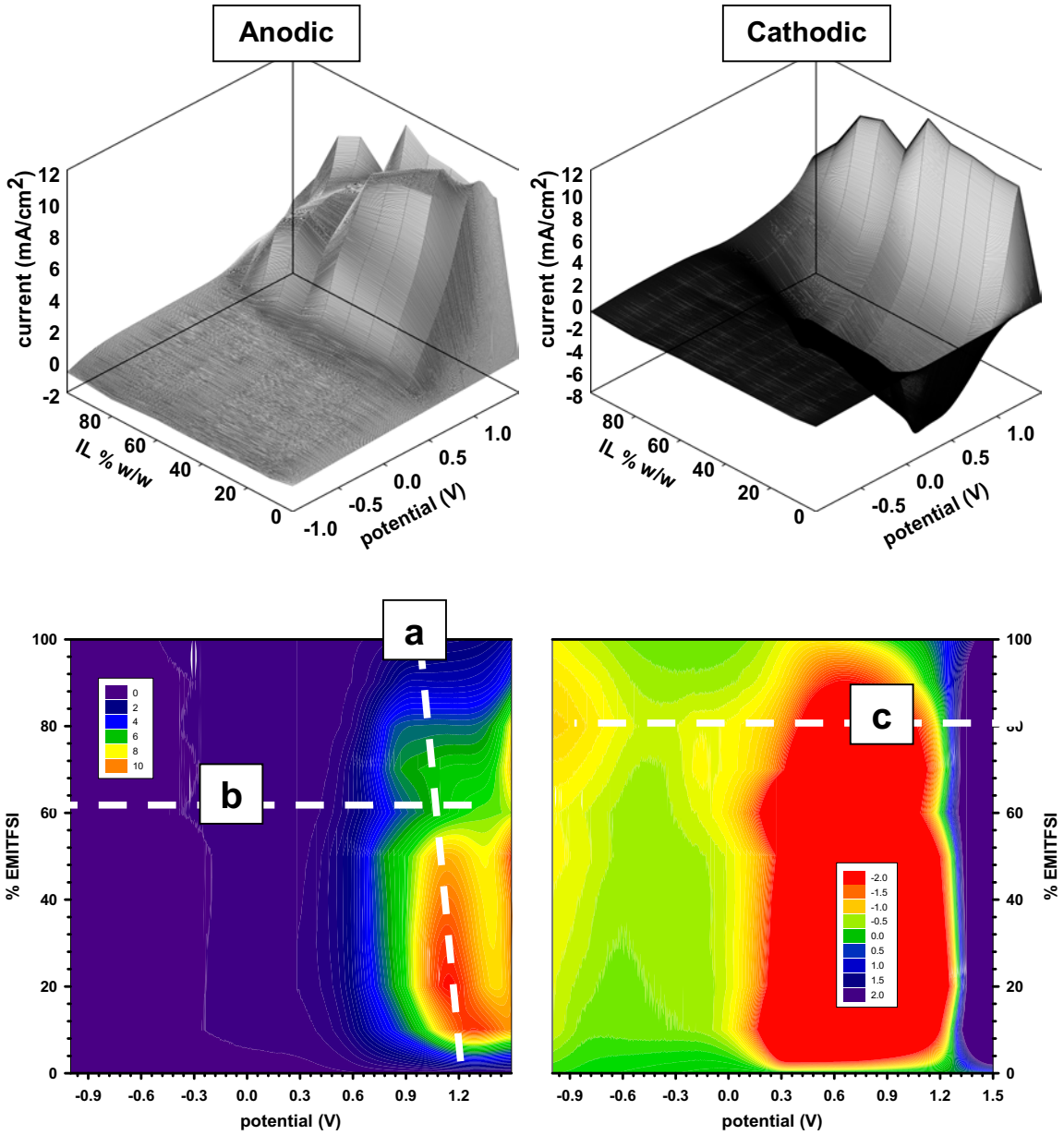

Figure 3.35- Three-dimensional (top) and contour plots (bottom) of PBiTh / PF_6 CVs at varying concentrations of EMITFSI in PC. (a) , (b) (c) and (d) are lines drawn to guide the eye along trends of the current magnitudes and composition plots.

Unlike the PBiTh / PF_6 film in $BMIPF_6$ / PC electrolyte, there was no region of EMITFSI concentration that produced increased magnitude of currents with respect to composition. The decrease in the oxidation current above the 60 % w/w EMITFSI line was not reflected in the same region of the reduction. In fact, the reduction currents in

the cathodic portion were generally unaffected by varying concentrations of EMITFSI until a very high concentration of 90 % w/w was reached.

3.3.12 Polyaniline (PAn) / PF_6 CVs as a Function of $BMIPF_6$ and EMITFSI Quantity in PC

Figure 3.36 shows the CV obtained for PAn / PF_6 in $BMIPF_6$ / PC and EMITFSI / PC at 50 % w/w concentration to assist with the visualisation of the three-dimensional data presented in Figure 3.37 and Figure 3.38.

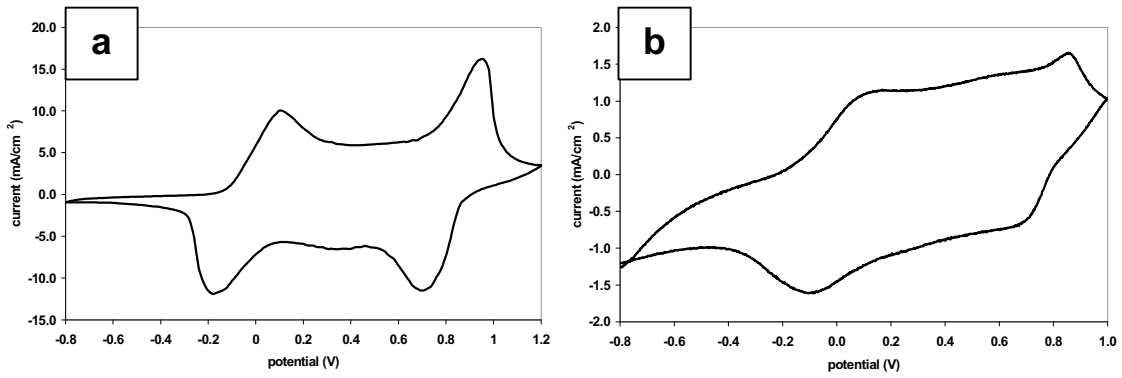

Figure 3.36- CV of PAn / PF_6 film in (a) $BMIPF_6$ / PC and (b) EMITFSI / PC electrolyte at 50% w/w composition. Scan rate = 200m V/s.

For the PAn / PF_6 film in $BMIPF_6$ / PC electrolyte, the 50 % w/w $BMIPF_6$ in PC held significance (Figure 3.37). A dip in the magnitude of currents was observed around the 50 % w/w $BMIPF_6$ composition mark, unlike the PBiTh / PF_6 film, although other aspects of the polyaniline system showed resemblance to the other studied systems. On the anodic portion, when the $BMIPF_6$ composition rose above about 70 % w/w (Figure 3.37 line "b"), the oxidation peaks shifted towards higher potential as seen with polypyrrole. Below approximately 30 % w/w $BMIPF_6$ on the cathodic portion, line "d",

the reduction peaks shifted to more negative potentials. Within the 30-70 % w/w region, no definite variation in the peak potentials was seen.

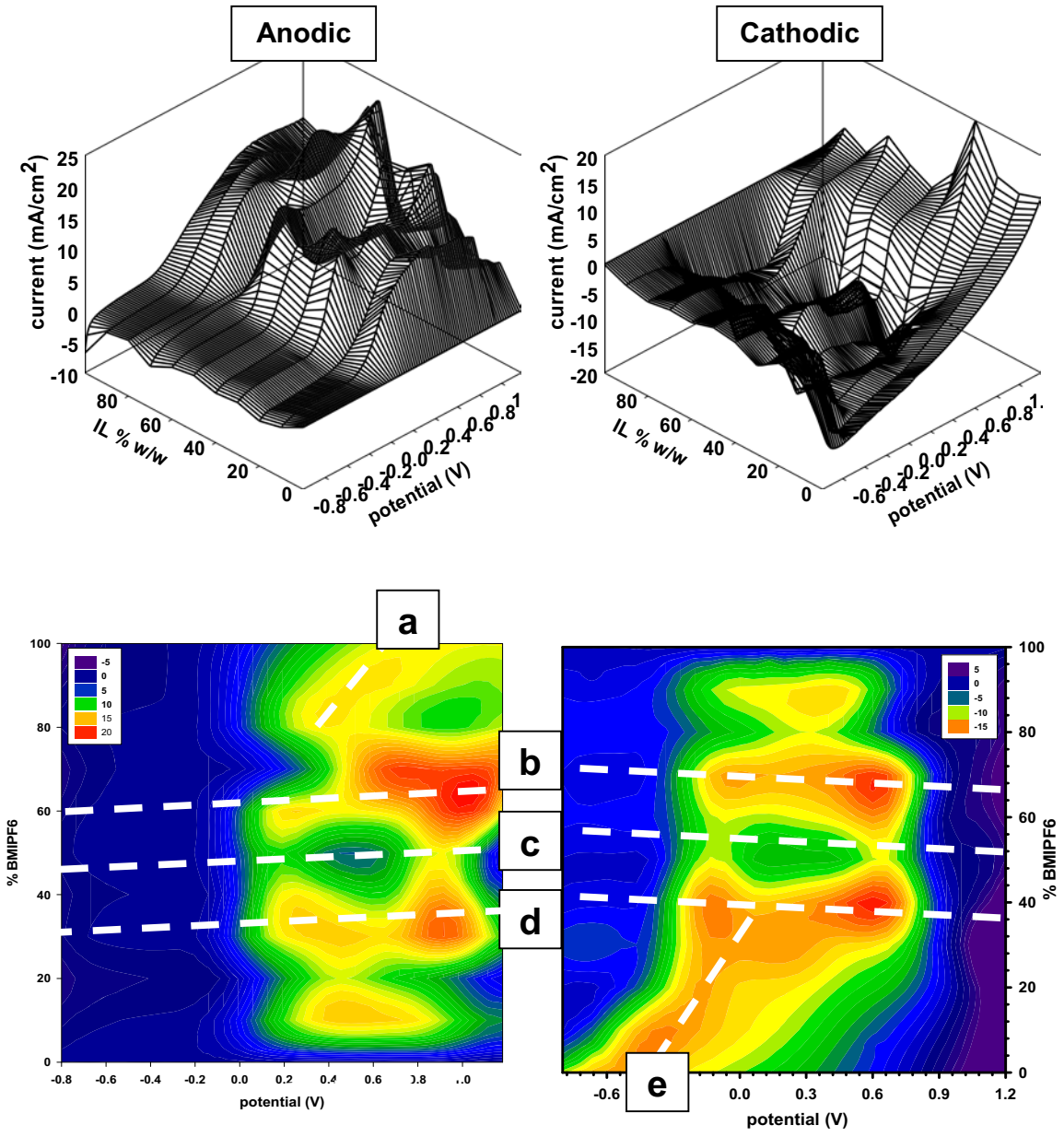

Figure 3.37- Three-dimensional (top) and contour plots (bottom) of PAn / PF_6 CVs at varying concentrations of $BMIPF_6$ in PC. (a) , b,) (c), (d) and (e) are lines drawn to guide the eye along trends of the current magnitudes and composition plots.

For the PAn / PF_6 film in EMITFSI / PC electrolyte (Figure 3.38) only minor trends were observed in the three-dimensional plots, with small peak currents and widths noted

as the electrolyte reached higher conductivity. $BMIPF_6$ was an electrolyte more suited for use with polyaniline, as its gradual decomposition into hydrofluoric acid may lower pH and provide a more suitable environment for electrochemical processes in this particular polymer.

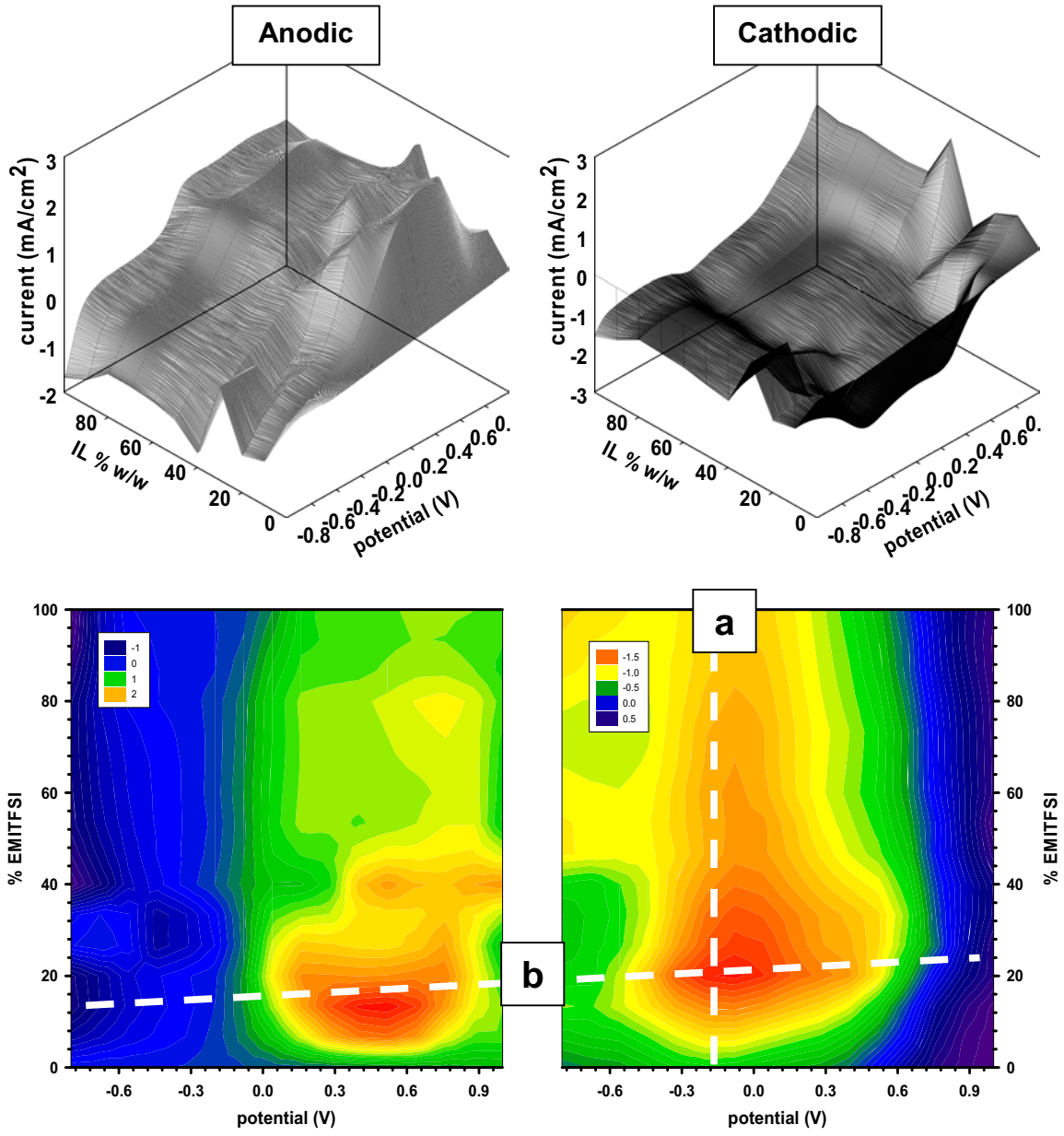

Figure 3.38- Three-dimensional (top) and contour plots (bottom) of PAn / PF_6 CVs at varying concentrations of EMITFSI in PC. (a) and (b) are lines drawn to guide the eye along trends of the current magnitudes and composition plots.

3.4 General Conclusions

- Moisture and other atmospheric gases have been shown to have significant effect on the electrochemistry of PPy / PF_6 films in the ionic liquid, $BMIPF_6$, but not in EMITFSI.

- The electrochemical current produced in the CV of PPy / PF_6 film in $BMIPF_6$ halved when the atmospherically exposed electrolyte was purged with N_2 while recording CV. Moisture is known to hydrolyse the PF_6^- anion into hydrofluoric acid and it was found that the presence of moisture did contribute to observations in the corresponding CVs.

- The potential windows (*ca*. 3.5 V or less) observed for PPy / PF_6 films in non-purged $BMIPF_6$ and all examples with EMITFSI were comparable to those found for the related propylene carbonate based system, whereas N_2 purged $BMIPF_6$ electrolyte improved the stable potential range to 3.9 V.

- When the PPy / PF_6 systems were exposed to 900 CV cycles, the $BMIPF_6$ systems produced the greatest level of stability, showing little change in their CVs during successive cycling. The PPy / PF_6 film in EMITFSI systems showed lesser cycling durability than for $BMIPF_6$ electrolyte, although stability was better than that observed in PC electrolyte.

- A systematic CV study of various conducting polymers in various $BMIPF_6$ / PC electrolyte mixtures indicated a range of dependencies on the electrolyte composition for the different polymers. Polypyrrole, polybithiophene,

polyaniline and poly-3-methylthiophene all behaved differently with respect to the percentage of $BMIPF_6$ in PC.

- Corresponding studies of ICPs in EMITFSI / PC electrolyte mixtures did not reveal significant changes on varying EMITFSI percentage compared to the $BMIPF_6$ equivalent. This is believed to be due to differences in ion pairing interactions within EMITFSI and $BMIPF_6$, as suggested by the conductivity profiles for IL / ICP mixtures.

3.5 References

[85] G.M. Spinks, L. Liu G. G. Wallace D. Zhou. *"Strain response from polypyrrole actuators under load."* Advanced Functional Materials, **2002** *12*: 437-440.

[86] Gazotti, W. A., Jr., M. A. De Paoli, G. Casalbore-Miceli, A. Geri and G. Zotti. *"A solid-state electrochromic device based on complementary polypyrrole/polythiophene derivatives and an elastomeric electrolyte."* Journal of Applied Electrochemistry, **1999** *29*: 753-757.

[87] Jianyong Ouyang, Chih-Wei Chu, Charles R. Szmanda, Liping Ma1 and Yang Yang. *"Programmable polymer thin film and non-volatile memory device."* nature materials, **2004** *3*: 918-922.

[88] Winther-Jensen, Bjorn. West, Keld. *"Stability of highly conductive poly-3,4-ethylene-dioxythiophene."* Reactive and Functional Polymers, **2005** *In Press, Corrected Proof*.

[89] Galinski, Maciej. Lewandowski, Andrzej. Stepniak, Izabela. *"Ionic liquids as electrolytes."* Electrochimica Acta, **2006** *In Press, Corrected Proof*: xxxx.

[90] Egashira, Minato, Shigeto Okada and Junichi Yamaki. *"The improvement of the electrochemical stability of room-temperature molten salt by dual anion system."* Kyushu Daigaku Kino Busshitsu Kagaku Kenkyusho Hokoku, **2000** *14*: 127-131.

[91] Zhou, Zhi-Bin, Hajime Matsumoto and Kuniaki Tatsumi. *"Low-viscous, low-melting, hydrophobic ionic liquids: 1-alkyl-3-methylimidazolium trifluoromethyltrifluoroborate."* Chemistry Letters, **2004** *33*: 680-681.

[92] Xu, Wu and C. Austen Angell. *"Solvent-free electrolytes with aqueous solution-like conductivities."* Science (Washington, DC, United States), **2003** *302*: 422-425.

[93] Earle, M. J., P. B. Mccormac and K. R. Seddon. *"The first high yield green route to a pharmaceutical in a room temperature ionic liquid."* Green Chemistry, **2000** *2*: 261-262.

[94] Handy, S. T. and X. L. Zhang. *"Organic synthesis in ionic liquids: The stille coupling."* Organic Letters, **2001** *3*: 233-236.

[95] Rebeiro, G. L. and B. M. Khadilkar. *"Chloroaluminate ionic liquid for fischer indole synthesis."* Synthesis-Stuttgart, **2001**: 370-372.

[96] Peng, J. J. and Y. Q. Deng. *"Ionic liquids catalyzed biginelli reaction under solvent-free conditions."* Tetrahedron Letters, **2001** *42*: 5917-5919.

[97] Kantam, M. Lakshmi, B. Neelima, Ch Venkat Reddy and V. Neeraja. *"N-arylation of imidazoles, imides, amines, amides and sulfonamides with boronic acids using a recyclable cu(oac)2[middle dot]h2o/[bmim][bf4] system."* Journal of Molecular Catalysis A: Chemical, *In Press, Corrected Proof.*

[98] Muller, Erno, Gabor Peczely, Rita Skoda-Foldes, Eszter Takacs, George Kokotos, Evagelos Bellis and Laszlo Kollar. *"Homogeneous catalytic aminocarbonylation of iodoalkenes and iodobenzene with amino acid esters under conventional conditions and in ionic liquids."* Tetrahedron, **2005** *61*: 797.

[99] Wang, Jia-Rui, Lei Liu, Ye-Feng Wang, Ying Zhang, Wei Deng and Qing-Xiang Guo. *"Aerobic oxidation with n-hydroxyphthalimide catalysts in ionic liquid."* Tetrahedron Letters, **2005** *46*: 4647.

[100] Ansari, I. A., Sipak Joyasawal, Manoj K. Gupta, J. S. Yadav and R. Gree. *"Wacker oxidation of terminal olefins in a mixture of [bmim][bf4] and water."* Tetrahedron Letters, **2005** *46*: 7507.

[101] Le, Zhang-Gao, Zhen-Chu Chen, Yi Hu and Qin-Guo Zheng. *"Organic reactions in ionic liquids: A simple highly regioselective or regiospecific substitutions of benzotriazole."* Heterocycles, **2004** *63*: 1077-1081.

[102] Palimkar Sanjay, S., A. Siddiqui Shapi, Thomas Daniel, J. Lahoti Rajgopal and V. Srinivasan Kumar. *"Ionic liquid-promoted regiospecific friedlander annulation: Novel synthesis of quinolines and fused polycyclic quinolines."* The Journal of organic chemistry, **2003** *68*: 9371-8.

[103] Holbrey, K.R. Seddon. *"Ionic liquids."* Clean Products and Processes, **1999** *1*: 223–236.

[104] Saheb, Amir, Jiri Janata and Mira Josowicz. *"Reference electrode for ionic liquids."* Electroanalysis, **2006** *18*: 405-409.

[105] Rebeiro, Bhushan M. Khadilkar and Geeta L. *"Microwave-assisted synthesis of room-temperature ionic liquid precursor in a closed vessel."* Organic Process Research & Development, **2002** *web*.

[106] Donald T. Sawyer, Andrzej Sobkowiak, Julian L. Roberts Jr. *"Electrochemistry for chemists."* **1995**.

[107] Clark, D. B., M. Fleischmann and D. Pletcher. *"The partial anodic oxidation of aliphatic hydrocarbons in aprotic solvents."* Journal of Electroanalytical Chemistry, **1973** *42*: 133-138.

[108] Widegren, Jason A., Eric M. Saurer, Kenneth N. Marsh and Joseph W. Magee. *"Electrolytic conductivity of four imidazolium-based room-temperature ionic liquids and the effect of a water impurity."* Journal of Chemical Thermodynamics, **2005** *37*: 569-575.

[109] Ding, Jie, Dezhi Zhou, Geoffrey Spinks, Gordon Wallace, Stewart Forsyth, Maria Forsyth and Douglas Macfarlane. *"Use of ionic liquids as electrolytes in electromechanical actuator systems based on inherently conducting polymers."* Chemistry of Materials, **2003** *15*: 2392-2398.

[110] Jarosik, Anna, Sebastian R. Krajewski, Andrzej Lewandowski and Przemyslaw Radzimski. *"Conductivity of ionic liquids in mixtures."* Journal of Molecular Liquids, **2005** *123*: 43-50.

[111] Comminges, Clement, Rachid Barhdadi, Michel Laurent and Michel Troupel. *"Determination of viscosity, ionic conductivity, and diffusion coefficients in some binary systems: Ionic liquids + molecular solvents."* Journal of Chemical & Engineering Data, **2006** *51*: 680-685.

[112] Purjari, B. R., G. Dixit and B. Behera. *"Conductivity of n-ethylpyridinium iodide in water-dioxan mixtures."* Indian Journal of Chemistry, Section A: Inorganic, Bio-inorganic, Physical, Theoretical & Analytical Chemistry, **1995** *34A*: 838-9.

[113] Seddon, Kenneth R., Annegret Stark and Maria-Jose Torres. *"Influence of chloride, water, and organic solvents on the physical properties of ionic liquids."* Pure and Applied Chemistry, **2000** *72*: 2275-2287.

[114] Wang, Jianji, Anlian Zhu, Yang Zhao and Kelei Zhuo. *"Excess molar volumes and excess logarithm viscosities for binary mixtures of the ionic liquid 1-butyl-3-methylimidazolium hexaflurophosphate with some organic compounds."* Journal of Solution Chemistry, **2005** *34*: 585-596.

[115] Behar, D., C. Gonzalez and P. Neta. *"Reaction kinetics in ionic liquids: Pulse radiolysis studies of 1-butyl-3-methylimidazolium salts."* Journal of Physical Chemistry, **2001** *105*: 7607-7614.

CHAPTER 4

STUDIES OF N-DOPING POL THIOPHENES

4.1 General Introduction

All electronic devices rely on the movement of electrons to function. Electrical potential provides the driving force for electron movement, allowing work to be performed. Conducting polymers are attractive materials for use in battery cells because of their physical properties, environmental benignness (when compared to lithium, acids and hydrides), and lightweight. To be able to gain full benefit from ICP batteries, they should produce a potential of at least 1.2 V, and preferably higher, so that they can be applied in portable electronics directly.

A way to gain maximum driving potential in an ICP charge storage device is to use separate p- and n-doping[116] electrodes. N-doping occurs when an ICP material holds negative charges on the polymer backbone, instead of the more common p-doping where positive charges manifest[117]. Polythiophenes are attractive materials in this regard for charge storage applications as they can be both p-doped and n-doped[118,119].

The electrochemical stability of n-doping polythiophene systems is usually very poor[120], preventing practical applications of the materials. The effects of ionic liquid (IL) and classical electrolyte (CE) interactions with n-doping polythiophenes were investigated so that suitable characteristics can be identified and developed for battery applications.

4.2 Experimental

4.2.1 General Electrochemistry

The monomer 3-methylthiophene (Aldrich) was distilled prior to use. Acetonitrile (Ajax), $TBABF_4$ (Aldrich), terthiophene (Aldrich) and bithiophene (Aldrich) were used as received. 3-Paraflourophenylthiophene was synthesised following a published procedure[121] and further purified by vacuum sublimation. All electrochemical measurements were performed with continual nitrogen purging of the EMITFSI ionic liquid electrolyte. Electrochemistry was performed with a Radiometer Analytical potentiostat P050, using Voltamaster 4 software.

Conducting polymers shown in Table 4.1 were grown from analytical grade acetonitrile (Ajax) solutions containing 0.1 M electrolyte salt and 0.01 M monomer. The working electrode consisted of a 0.02 cm^2 Pt disk. Growth was performed galvanostatically for 60 seconds at a current of 0.1 mA/cm^2. Polymers were also grown in ionic liquid electrolyte instead of 0.1 M salt in acetonitrile.

Structure	Name	Acron m
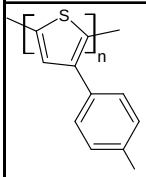	n n	
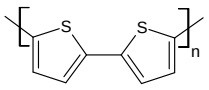	n	
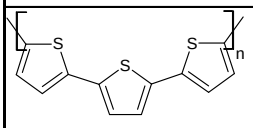	n	
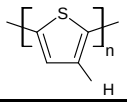	n	

Table 4.1 Structures and names of some n-dopable polythiophenes.

4.2.2 In-Situ Raman

Various polythiophenes were grown electrochemically onto a platinum disc electrode in a sealed electrochemical in-situ surface Raman cell, Figure 4.1. The polymers were first cycled in the ionic liquid EMITFSI to equilibrate the materials before spectroscopic investigations were initiated. Spectroscopy was performed using a Jobin Yvonne HR800 Raman spectrophotometer employing a 632.8 nm excitation laser and a working objective (x 50). The Raman signal was resolved on a 300 line / mm grating to give a resolution of 1 cm^{-1}. In order to effectively measure the Raman signal and reject interference from the electrolyte or ionic liquid, the imaging microscope was configured in a confocal mode using a confocal pinhole of 250 μm.

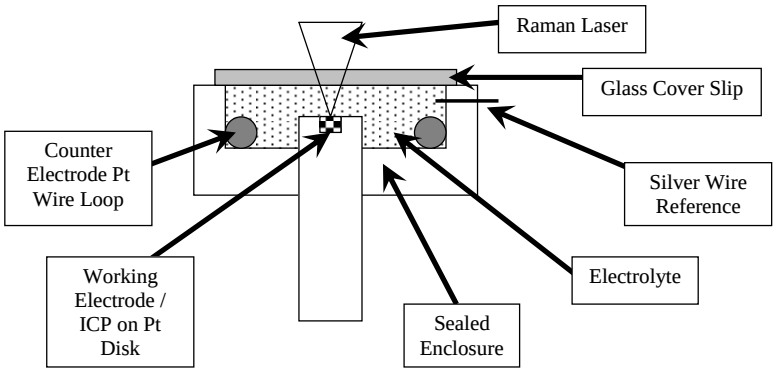

Figure 4.1- Spectroelectrochemical cell for the in-situ study of polythiophenes.

4.2.3 Theoretical Calculations of Raman Spectral Features

Theoretical Raman spectra calculations were performed using Gaussian03W Revision D.01-SMP[122] for Symmetrical Multiple Processors. Calculations were performed on either of two systems:

Compaq Proliant 6400R server

- 4 x SMP 2 Mb cache, 550 MHz Xeon Pentium(III) processors
- 4 Gb of RAM
- Windows 2000 Server Edition ,

IBM xSeries 350 eServer with

- 4 x SMP 2 Mb cache, 700 MHz Xeon Pentium(III) processors
- 4 Gb of RAM
- Windows 2003 Server Edition

All calculations used the Density Field Theory (DFT), on a restricted B3LYP method with a 3-21G basis set. All molecules were first optimised with the above conditions, and then Raman activity calculated from those results.

4.2.4 Structure-Electroactivity Relationships for Poly-3-Paraflourophenylthiophene (P3PFTh)

An experimental matrix was produced to investigate the doping processes in P3FPTh a range of electrolytes consisting of those listed in Table 4.2b. $BMIBF_4$, $BMIPF_6$ and EMITFSI were studied in their pure form, and also as 0.1 M dilutions in acetonitrile.

The experimental matrix was produced by first growing P3PFTh in one electrolyte (for example, $TBAClO_4$ / acetonitrile), removing the polymer, rinsing in acetone, drying and placing it in a cycling electrolyte (for example $TBAPF_6$ / acetonitrile) and recording its CV. This would produce one data set in the experimental matrix, namely $TBAClO_4$ grown $TBAPF_6$ cycled. To continue in the $TBAClO_4$ grown series, a fresh polymer on a clean electrode would then be grown from $TBAClO_4$ / acetonitrile, washed, dried, and its CV recorded in a new cycling electrolyte (for example $TBABF_4$ / acetonitrile), giving another data point in the experimental matrix, namely $TBAClO_4$ grown $TBABF_4$ cycled . This procedure was repeatedly performed to obtain every possible

combination of the available monomer solution and cycling electrolyte in the CVs measured.

a

Cations		Anions	
S	n	S	n
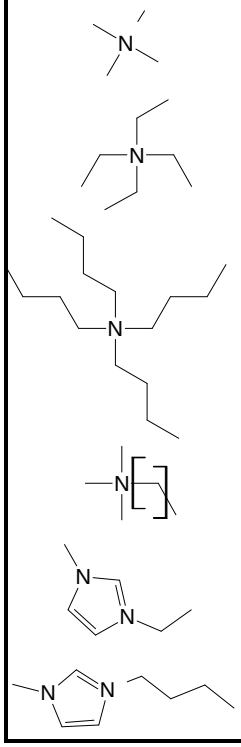		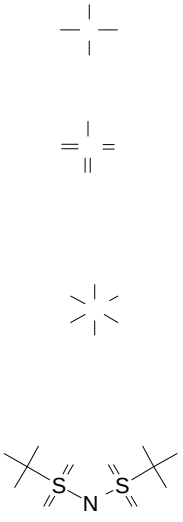	S

b

Combinations sed
S
S
S

Table 4.2- Structure, acronyms and composition of studied electrolytes.

Statistical Gaussian functions described in Chapter 2 were overlayed with experimental data and parameters adjusted until the function and data correlated to 0.95 residual sum of squares. The extracted parameter sets were analysed with multidimensional scaling to reveal dependencies between doping states, ion sizes, and nature of electrolyte. Analysis was performed using Windows XP operating system running SYSTAT 11 by SYSTAT Software .

4.3 Results and Discussion

4.3.1 CV and In-Situ Raman Spectral Studies of Polythiophenes in E ITFSI

4.3.1.1 Poly-3-paraflourophenylthiopene (P3PFTh) in E ITFSI

P3PFTh was chosen as an n-doping candidate for batteries on reviewing the work of others[116,123,124]. The electron withdrawing group (parafluorophenyl) on the thiophene ring is thought to assist negative charge stabilisation during n-doping. To provide an illustrative example of the type of CV that may be produced during n-doping, CV's were first obtained on P3PFTh / TFSI in an acetonitrile based electrolyte using published procedures[121] (Figure 4.2). The current peaks in Figure 4.2 are annotated with letters corresponding to possible dominant processes shown in Equations 4.1.

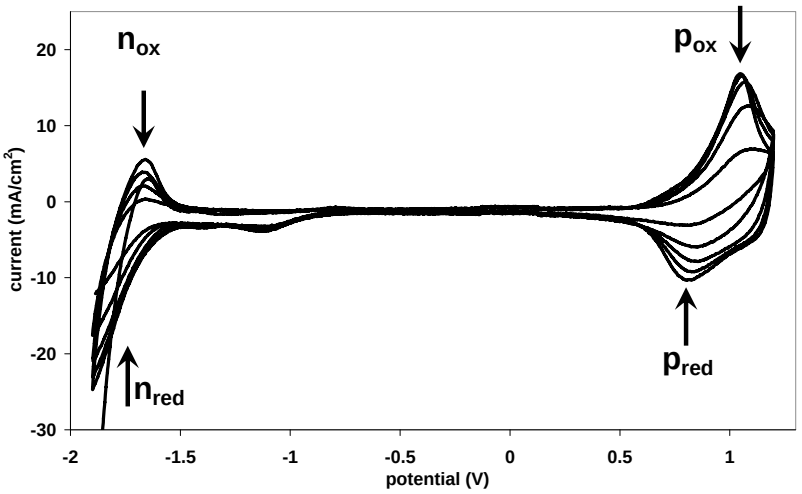

Figure 4.2- CV of a P3PFTh / TFSI film grown from and cycled in 0.1 M EMITFSI / acetonitrile. n_{ox}, p_{ox}, p_{red} and n_{red} refer to p- and n-doping processes described in Equations 4.1. Arrows indicate change in CV magnitude on subsequent cycles. Scan rate = 200 mV/s, 5 cycles.

Equations 4.1

p_{ox} p-doping oxidation

4.1 a ***insertion-*** ***Poly^0*** ***An$^-_{diss}$*** → ***(Poly An$^-$)*** ***e$^-$***

4.1 b ***expulsion-*** ***(Poly^{0}Cat An$^-$)*** → ***(Poly An$^-$)*** ***Cat $_{diss}$*** ***e$^-$***

p_{red} p-doping reduction

4.1 c ***expulsion-*** ***(Poly An$^-$)*** ***e$^-$*** → ***Poly^0*** ***An$^-_{diss}$***

4.1 d ***insertion-*** ***(Poly An$^-$)*** ***Cat$^+_{diss}$*** ***e$^-$*** → ***(Poly^{0}Cat An$^-$)***

n_{red} n-doping reduction

4.1 e ***insertion-*** ***Poly^0*** ***Cat $_{diss}$*** ***e$^-$*** → ***(Poly$^-$Cat$^+$)***

4.1 f ***expulsion-*** ***(Poly^{0}Cat An$^-$)*** ***e$^-$*** → ***(Poly$^-$Cat$^+$)*** ***An$^-_{diss}$***

n_{ox} n-doping oxidation

4.1 g ***expulsion-*** ***(Poly$^-$Cat)*** → ***Poly^0*** ***Cat$^+_{diss}$*** ***e$^-$***

4.1 h ***insertion-*** ***(Poly$^-$Cat$^+$)*** ***An$^-_{diss}$*** → ***(Poly^{0}Cat An$^-$)*** ***e$^-$***

equations in blue occur for many conventional solvent / electrolyte systems
equations in green are potential processes for neat ionic liquid systems

Poly^0	-	*neutral polymer*
Poly	-	*p-doped polymer*
Poly$^-$	-	*n-doped polymer*
Cat	-	*cation*
An$^-$	-	*anion*
( )	-	*encompassed in polymer*
diss	-	*dissociated ion*

Figure 4.2 exhibits two quite separate doping / dedoping processes, the n-doping occurring at *ca.* -1.7 V and the p-doping at *ca.* 1.0 V. Such large separations in redox potentials (2.7 V) are ideal for charge storage applications. The current magnitudes of the p- and n-doping regions are similar, which can benefit battery device construction by allowing the use of a single polymer at both the anode and cathode to work at optimum efficiency.

However, the CV depicted in Figure 4.2 suggests serious drawbacks with respect to cycle stability if the system was applied in a charge storage device. After only 5 electrochemical cycles there was a near complete loss of current magnitude, making the system unsuitable for battery devices.

In an attempt to improve cycle stability, the CV of an equivalent P3PFTh / TFSI was performed in pure EMITFSI. However, as seen in Figure 4.3, the magnitude of CV response again degraded extremely rapidly over 5 cycles. In addition, the P3PFTh / TFSI in EMITFSI electrolyte did not produce discrete current peaks in the n-doping region.

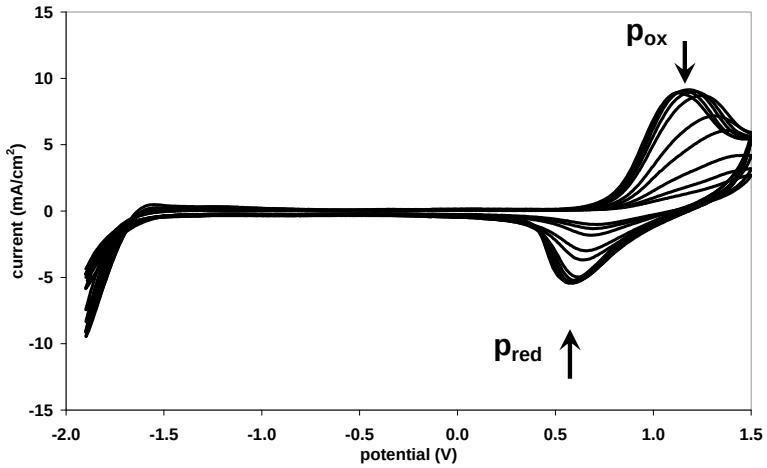

Figure 4.3- P3PFTh / TFSI grown from 0.1 M EMITFSI / acetonitrile, and cycled in pure EMITFSI. p_{ox}, and p_{red} refer to p-doping processes described in Equations 4.1. Arrows indicate change in CV magnitude on subsequent cycles. Scan rate = 200 mV/s, 10 cycles.

In order to investigate structural characteristics of doping processes in the polythiophene P3PFTh / TFSI in EMITFSI electrolyte, Raman studies were conducted. The Raman spectra of the P3PFTh system in EMITFSI at p-, n-doping and undoped potentials are shown in Figure 4.4. The lack of change in the Raman response at various potentials indicates insignificant structural change in the polymer.

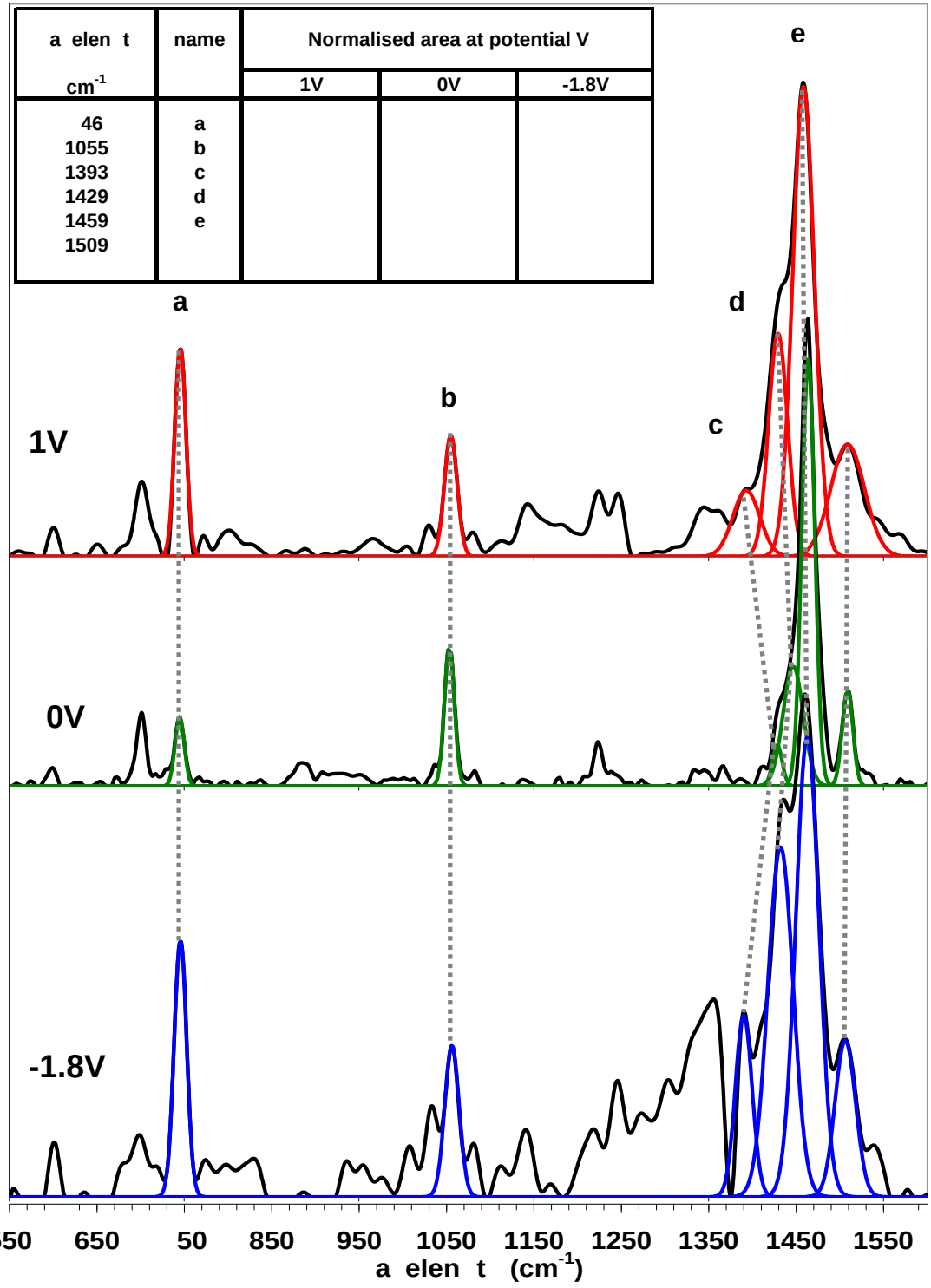

Figure 4.4- Raman spectra of P3PFTh / TFSI in EMITFSI at various potentials. 635 nm excitation. Assignments of bands a-f are described in greater detail in polymer systems studied later in this Chapter, where spectral changes were visible on application of varied potentials.

Several factors may be responsible for the poor current responses of P3PFTh / TFSI in EMITFSI:

- Chemical purity. EMITFSI was exceptionally clean from rigorous purification of starting materials, intermediates, and end product, to produce a completely colourless liquid. 3PFTh monomer was also exceptionally pure, as the result of patient vacuum sublimation of the crude product to produce long, colourless, needle-shaped crystals. Acetonitrile was analytical grade and all apparatus was thoroughly cleaned prior to use.
- EMITFSI may be an unsuitable electrolyte support for n-doping in general.
- The polymer synthesis conditions formed a polymer that did not have suitable structural characteristics to allow ion movement, thereby impeding electrochemical response.

These factors are investigated in the following sections of this Chapter to establish how resulting electrochemical responses may be customised into desirable specifications.

4.3.1.2 CV and Raman Studies of P3 eTh in E ITFSI

To investigate whether EMITFSI electrolyte was inherently spoiling n-doping observations in ICPs, three other thiophene-based polymers were examined by CV and *in-situ* Raman spectroscopy in EMITFSI. The CV of P3MeTh / TFSI film in pure EMITFSI is shown in Figure 4.5. Although a small current was observed below -1.3 V, this could not be clearly interpreted as a region of n-doping. The p-doping region did produce a large current response, with a significantly larger magnitude for the anodic

then cathodic process. The cathodic p-doping process, p_{red}, is likely to be due to ion insertion (Equation 4.1d), which may be less favoured than ion expulsion (p_{ox}), resulting in a lower current response. The anodic peak of the p-doping region was noted to shift to positive potentials by 150 mV over 10 cycles, without decay in peak current. The cathodic region of the p-doping process, however, was generally unaltered by successive cycling.

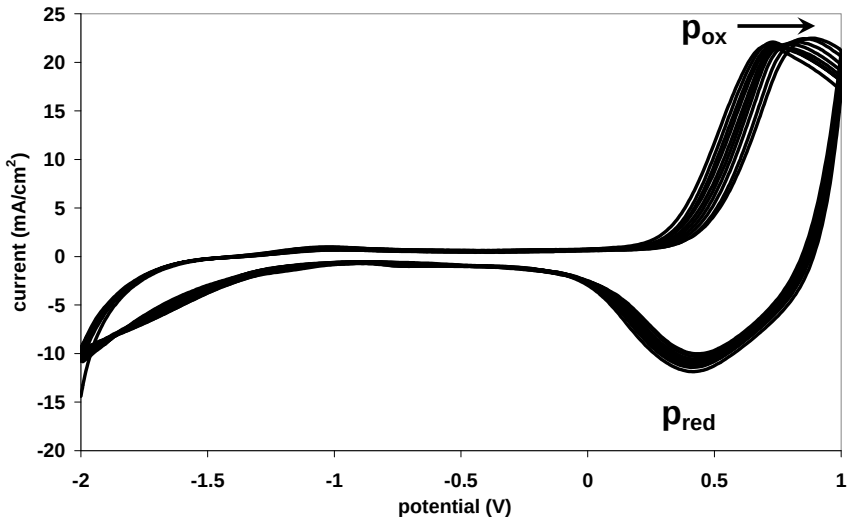

Figure 4.5- CV of P3MeTh film grown from 0.1 M EMITFSI / acetonitrile, and cycled in pure EMITFSI. p_{ox}, and p_{red} refer to p-doping processes described in Equations 4.1. Arrows indicates change in CV peak position on subsequent cycles. Scan rate = 200 mV/s, 10 cycles.

The Raman spectra of the P3MeTh / TFSI film in EMITFSI electrolyte at various applied potentials are shown in Figure 4.6. All peaks were normalised to the area of peak b at 992 cm^{-1}, which has been assigned to the C-H group stretch[125] which is un-influenced by the doping state of the polymer. Peak a at 726 cm^{-1} has been previously assigned as a C-S-C ring deformation[125,126,127], and corresponds to the eigenvector result of computer simulation of decathiophene in these studies (Figure 4.7).

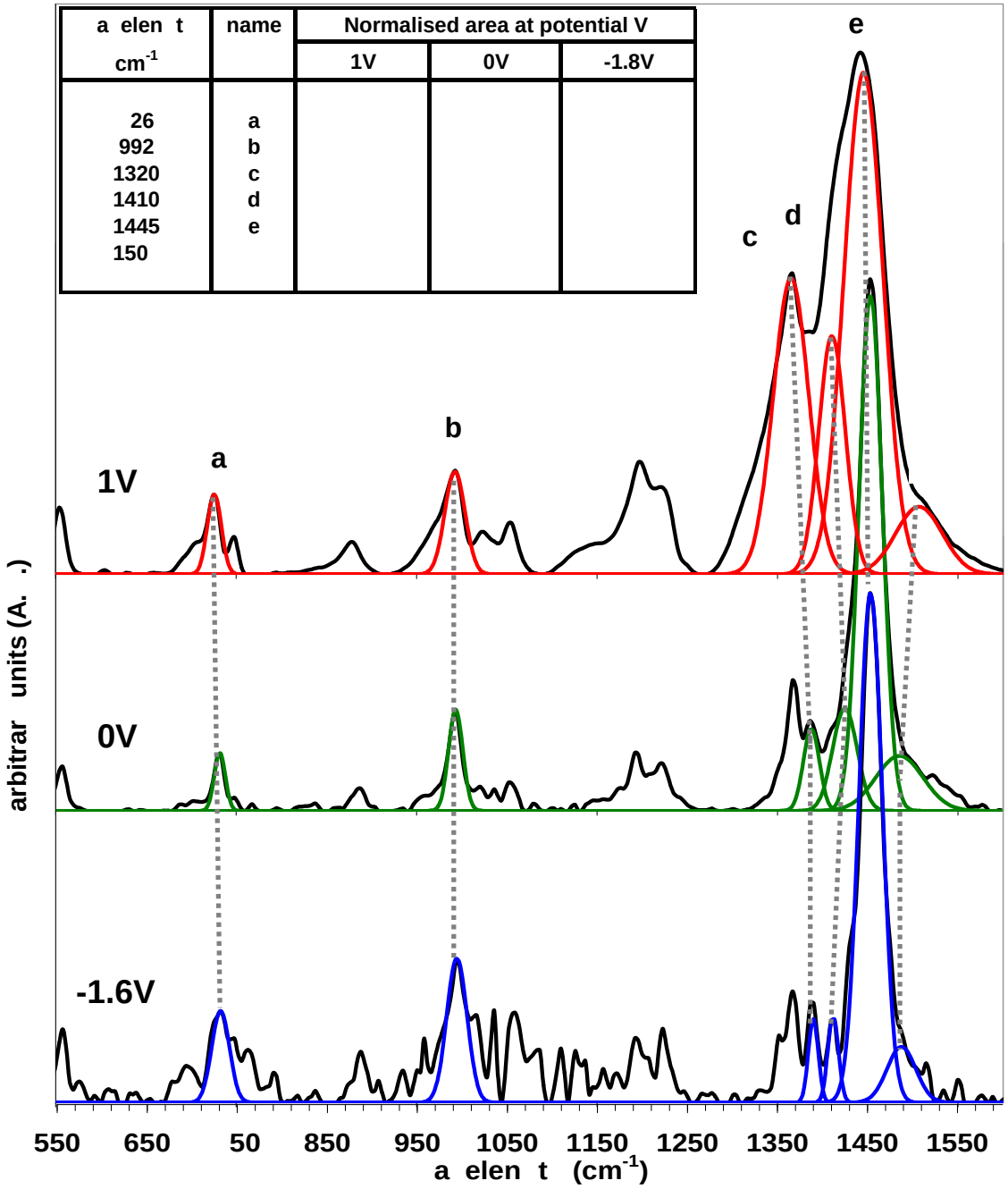

Figure 4.6- Raman spectra of P3MeTh in EMITFSI at various potentials. 635 nm excitation. Table inset shows peak areas at various applied potentials.

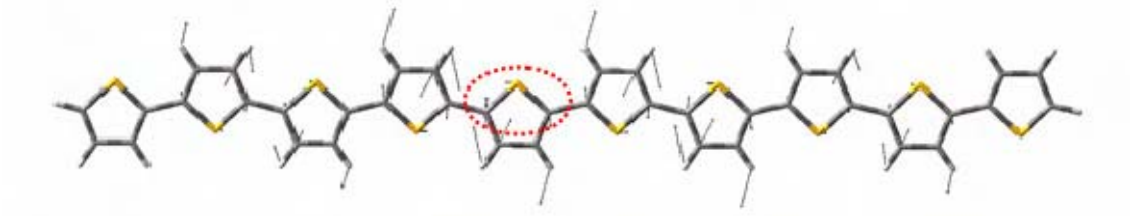

Figure 4.7- Eigenvector diagram of decathiophene in a C-S-C deformation found in Raman spectra at circa 730 cm^{-1}. Red dotted circle shows region of activity.

Band a in Figure 4.6 has been reported to be sensitive to the amount of deformations on a polythiophene chain, increasing in intensity with an increase in chain order[128]. The results in Figure 4.6 therefore indicate that there was a slight increase in order at both p- and n-doping potentials relative to the neutral state. Such an increase in chain order is likely to be due to ion expulsion during both p- and n-doping processes, allowing chains to straighten as there are fewer ions causing obstacles that bend the chains.

Bands c d and f have been assigned as originating from quinoid cations[128], so unsurprisingly these bands reduce in magnitude as the polymer chains approach electrical neutrality. In addition, the c and d bands are blue shifted as the polymer chains approach neutrality. Blue shifting of these equivalent bands is observed in many polythiophene systems[125,126,129,130,131], and occurs when the polymer is doped or forced into a less ordered state, such as by packing with ions from a classical electrolyte. The apparent reverse behaviour in EMITFSI indicated that additional ions are packed into the polymer as chain neutrality is approached, supporting a hypothesis of ion expulsion upon doping.

4.3.1.3 Polyterthiophene in E ITFSI

The CV of a PTerTh / TFSI film in EMITFSI electrolyte is depicted in Figure 4.8. The magnitude of current responses in doping regions was comparatively small, and only one definable peak at -1.1 V, indicating resilience of the material to ion migration and doping processes.

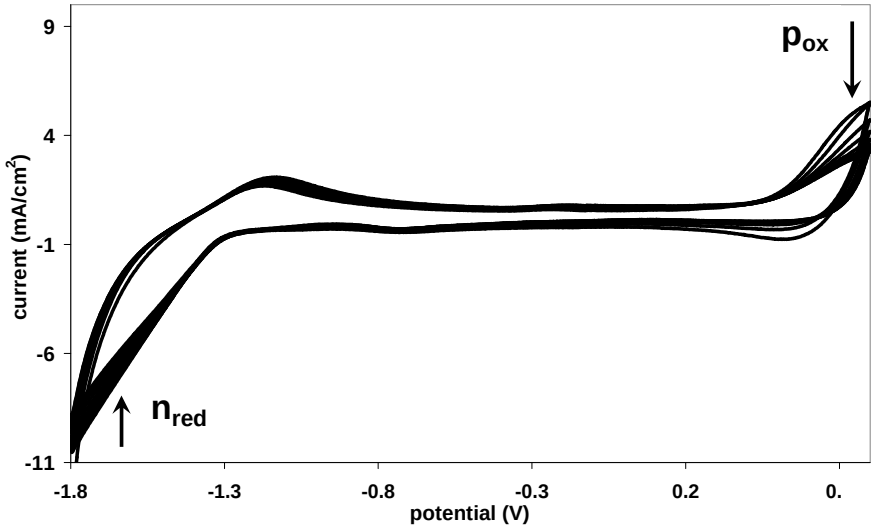

Figure 4.8- CV of PTerTh / TFSI film grown from 0.1 M EMITFSI / acetonitrile, and cycled in pure EMITFSI. p_{ox}, and p_{red} refer to p-doping processes described in Equations 4.1. Arrows indicate change in CV magnitude on subsequent cycles. Scan rate = 200 mV/s, 10 cycles.

The Raman spectra of PTerTh / TFSI in EMITFSI at various applied potentials are shown in Figure 4.9. All peak intensity areas have been normalised to the in-plane C-H bends of the polymer backbone expressed by the eigenvector diagram of Figure 4.10. The effect on the a band is seen very clearly as a result of the doping processes. The a band is at a minimum when the polymer is in its neutral state, meaning that the polymer has maximum defects at neutrality. At both the p- and n-doping potentials, the polymer becomes significantly more ordered, suggesting that these doping processes proceed via ion expulsion processes.

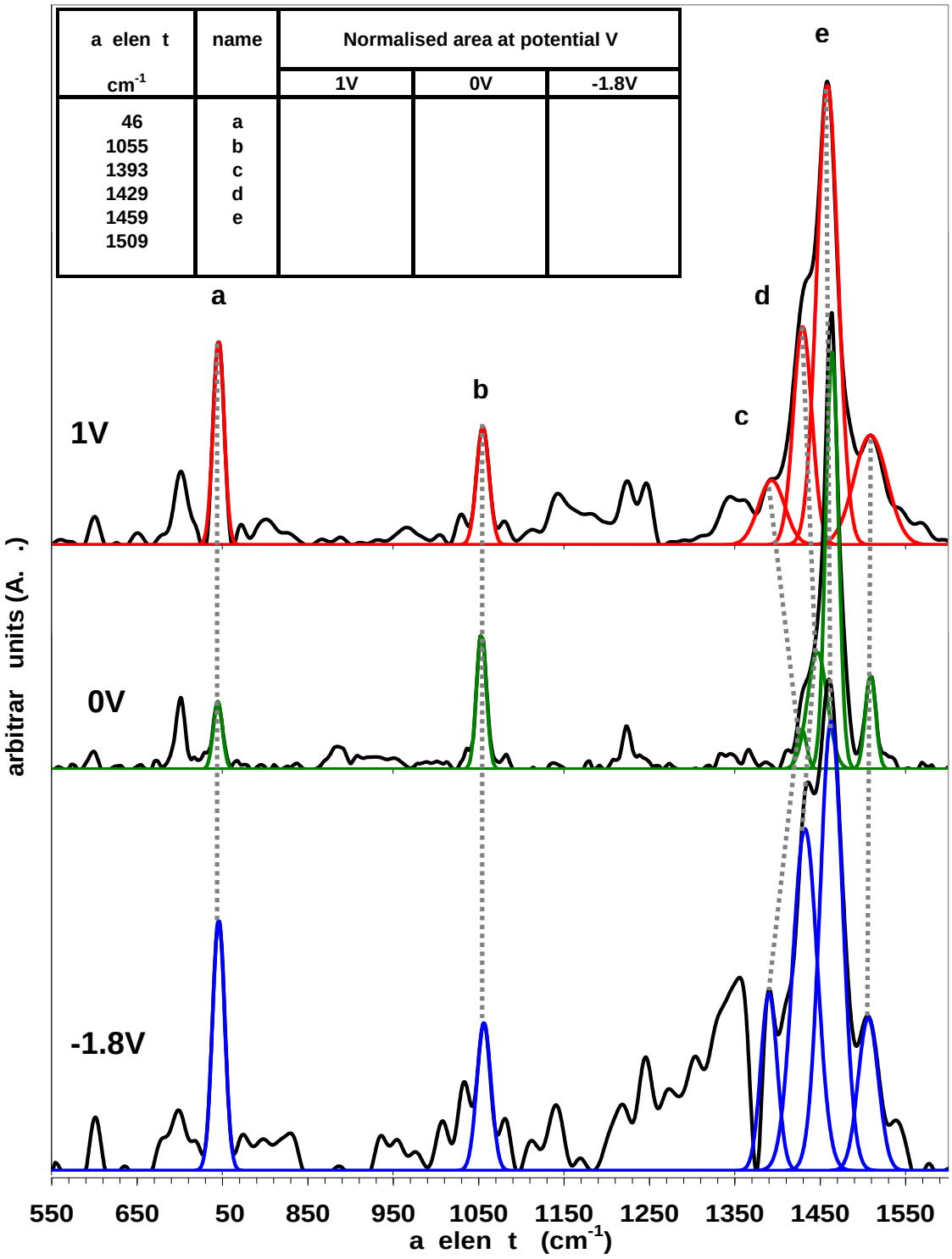

Figure 4. - Raman spectra of PTerTh / TFSI film in EMITFSI at various potentials. 635 nm excitation. Table inset shows peak areas at various applied potentials.

Figure 4.10- Eigenvector diagram of in plane C- bends of decathiophene found in Raman spectra circa 1040 cm^{-1}. Red dotted circle shows region of activity.

From Figure 4.9, it is also seen that bands c , d and f re-emerge in the n-doping process, assignments previously given to quinoidial radical dications at p-doping potentials[128]. The migration patterns of the c and d bands on application of potential also further support ion expulsion processes upon doping, as it is the reverse of that observed in classical electrolyte studies[125,126,129,130,131] (more ions in the polymer causes blue shift). In the present study with EMITFSI, the state created at n-doping potentials would probably be in the form of quinoidial radical dianions, producing an analogous state to p-doping. The Raman spectra have therefore divulged processes not clearly visible in the CV, but occurring on the surface of the polymer.

4.3.1.4 Polybithiophene (PBiTh) in E ITFSI

The CV of PBiTh in EMITFSI electrolyte (Figure 4.11) did produce an observable n-doping response *ca.* -1.6 V and p-doping response *ca.* 0.6 V. Unfortunately, the rate of current degradation was too rapid to apply this system in a practical battery.

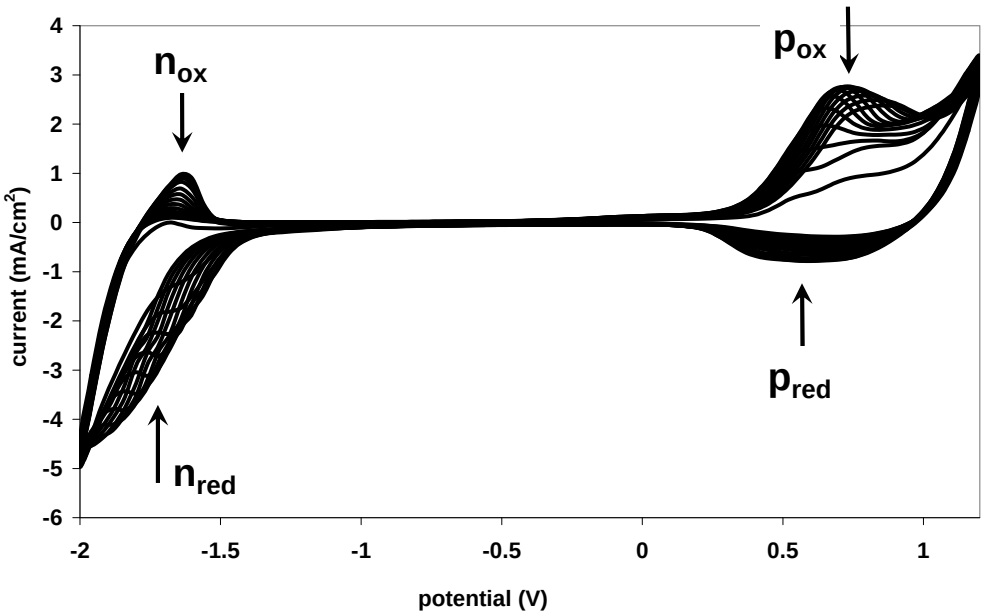

Figure 4.11- PBiTh / TFSI film grown from 0.1 M EMITFSI / acetonitrile, and cycled in pure EMITFSI. n_{ox}, p_{ox}, p_{red} and n_{red} refer to p and n-doping processes described in Equations 4.1. Arrows indicate change in CV magnitude on subsequent cycles. Scan rate = 200 mV/s, 10 cycles.

The Raman spectra of a PBiTh film in EMITFSI at various applied potentials are presented in Figure 4.12. After normalisation to the C-H bending band of b , the distortion sensitive a band changes little when p- and n-doping potentials are applied. This means that little if any structural change occurs in the doping regimes. Further evidence in support of the p- and n-doping processes comes from significant increases observed in intensity of the quinoidial c , d and f bands. Lack of structural change is supported by an insignificant blue or red shifting of the c and d bands.

The Raman spectra and corresponding CVs of the studied polythiophenes show that n-doping in pure EMITFSI is possible and proceeds via ion expulsion processes typical of p-doping mechanisms in ionic liquids (and the reverse of the process observed with classical electrolytes). Doping is limited, however, by the structural characteristics of the polymer causing physical resistance to ion movement within the polymer. If this is the reason for lack of CV current in P3PFTh, it may still be possible to exploit the n-

doping characteristics of the polymer by finding the correct monomer solution and cycling ionic liquid. This possibility is explored in the next Section using a range of ionic liquids.

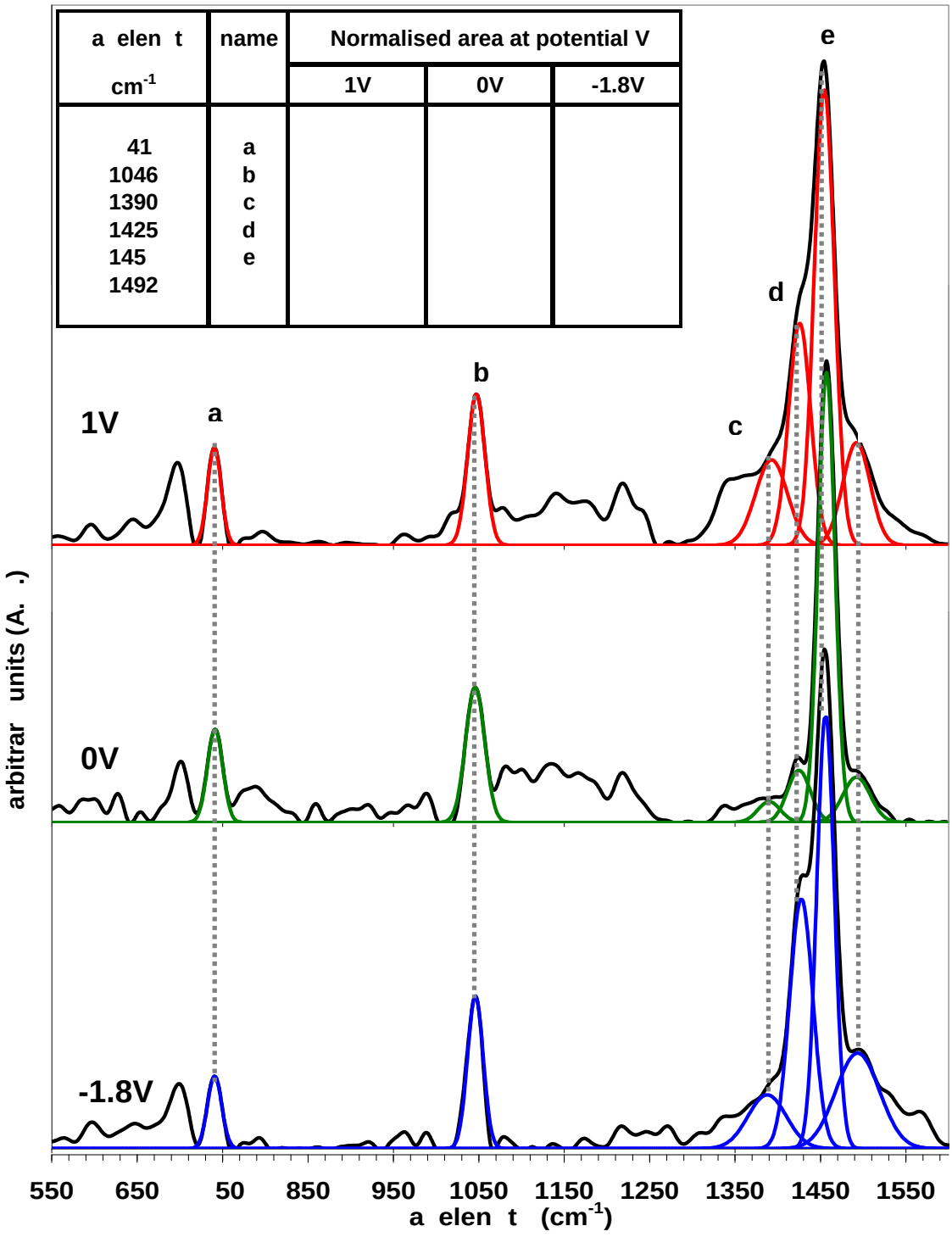

Figure 4.12- Raman spectra of PBiTh / TFSI in EMITFSI at various potentials. 635 nm excitation. Table inset shows peak areas at various applied potentials.

4.3.1.5 Summary of Results from Section 4.3.1

- CV responses of a P3PFTh / TFSI film in 0.1M EMITFSI / acetonitrile electrolyte produced desirable electrochemical features, but degraded rapidly over 5 cycles. Related experiments in pure EMITFSI electrolyte gave poor current response, making the system unsuitable for batteries.

- Other polythiophenes were investigated in pure EMITFSI to determine whether the lack of desirable observations was purely a function of the electrolyte. PBiTh / TFSI in pure EMITFSI did produce clear p- and n-doping features observed in CV and Raman spectra. However, the system was insufficiently stable for device applications. The option of optimising PBiTh / TFSI in ionic liquid for n-doping was not pursued in preference of investigating the interesting behaviour of P3PFTh in ionic liquid.

4.3.2 Studies of P3PFTh in Various Ionic Liquids

The possibility of finding an improved P3PFTh / dopant in ionic liquid match was first investigated by varying the ionic liquid. As the polymers in the preceding section were all grown from a 0.1 M acetonitrile solution of the final pure cycling ionic liquid (all grown from 0.1 M EMITFSI / acetonitrile, then cycled in pure EMITFSI), the same pattern was extended to CV studies of P3PFTh in the ionic liquids $BMIPF_6$ and $BMIBF_4$.

The CV of a P3PFTh / BF_4 film grown from 0.1 M $BMIBF_4$ / acetonitrile and cycled in pure $BMIBF_4$ is shown in Figure 4.13. The corresponding CV in $BMIPF_6$ is shown in Figure 4.14. These CVs may be compared with that in EMITFSI shown in the previous

section (Figure 4.3). None of the CVs displayed suitable current responses or cyclic stability to be considered in battery devices. The CV in $BMIPF_6$ was the only one that showed visible current magnitude response in the n-doping region.

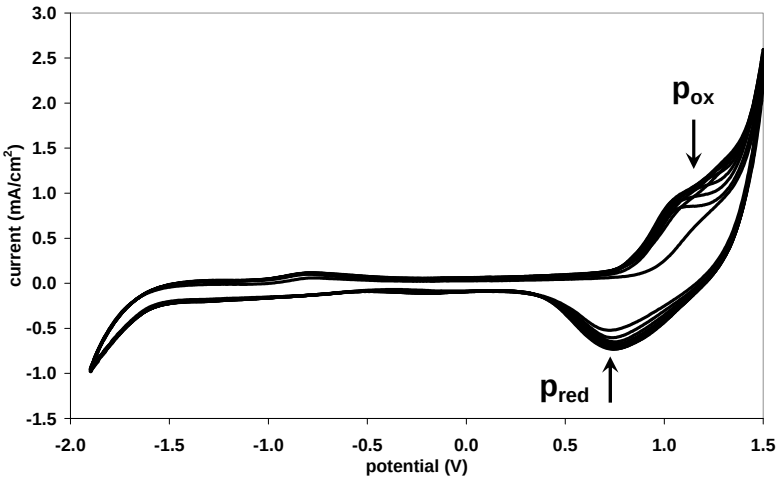

Figure 4.13- CV of P3PFTh / BF_4 film grown from 0.1 M $BMIBF_4$ / acetonitrile, and cycled in pure $BMIBF_4$. p_{ox} and p_{red} refer to p-doping processes described in Equations 4.1. Arrows indicate change in CV magnitude on subsequent cycles. Scan rate = 200 mV/s, 10 cycles.

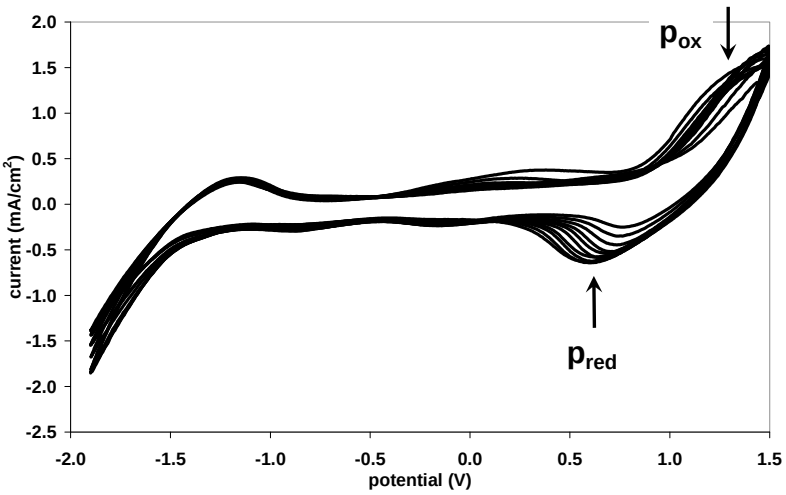

Figure 4.14- CV of P3PFTh / PF_6 film grown from 0.1 M $BMIPF_6$ / acetonitrile, and cycled in pure $BMIPF_6$. p_{ox} and p_{red} refer to p-doping processes described in Equations 4.1. Arrows indicate change in CV magnitude on subsequent cycles. Scan rate = 200 mV/s, 10 cycles.

Raman studies discussed in the previous section indicated the physical structure of the polymer was responsible for resisting ion movement. In the present section so far, the polymers were grown from electrolytes with the same ions that made up the ionic liquid used in cycling. One may consider that the ions present during growth should produce a polymer with physical pathways suitable to accommodate the movement of those ions in subsequent cycling, but this hypothesis is not supported by the corresponding CV results above.

To investigate the physical pathway notion closer, tetramethylammonium perchlorate ($TMAClO_4$) was examined as the electrolyte for the growth of P3PFTh films due to small anion and cation sizes. Three P3PFTh / ClO_4 films were subsequently grown from 0.1M $TMAClO_4$ in acetonitrile, and the resultant polymers were then separately cycled in $BMIBF_4$ (Figure 4.15), $BMIPF_6$ (Figure 4.16), and EMITFSI (Figure 4.17).

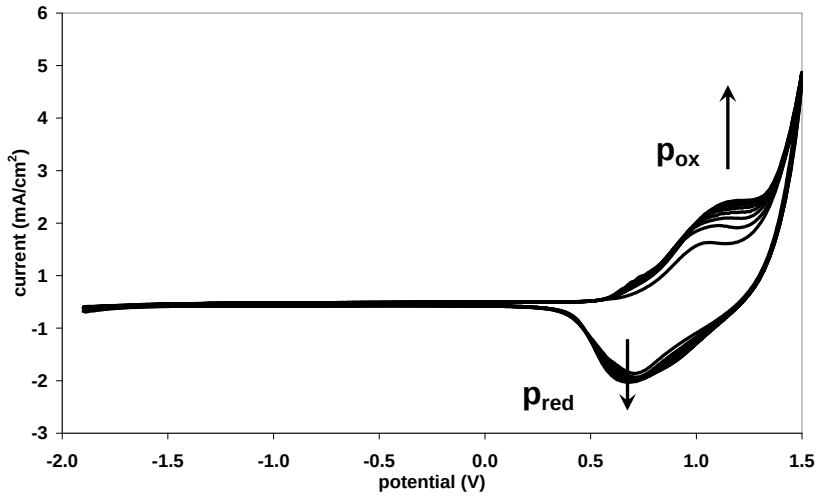

Figure 4.15- CV of P3PFTh / Cl 4 film grown from 0.1 M TMACl 4 / acetonitrile, and cycled in pure $BMIBF_4$. p_{ox} and p_{red} refer to p-doping processes described in Equations 4.1. Arrows indicate change in CV magnitude on subsequent cycles. Scan rate = 200 mV/s, 10 cycles.

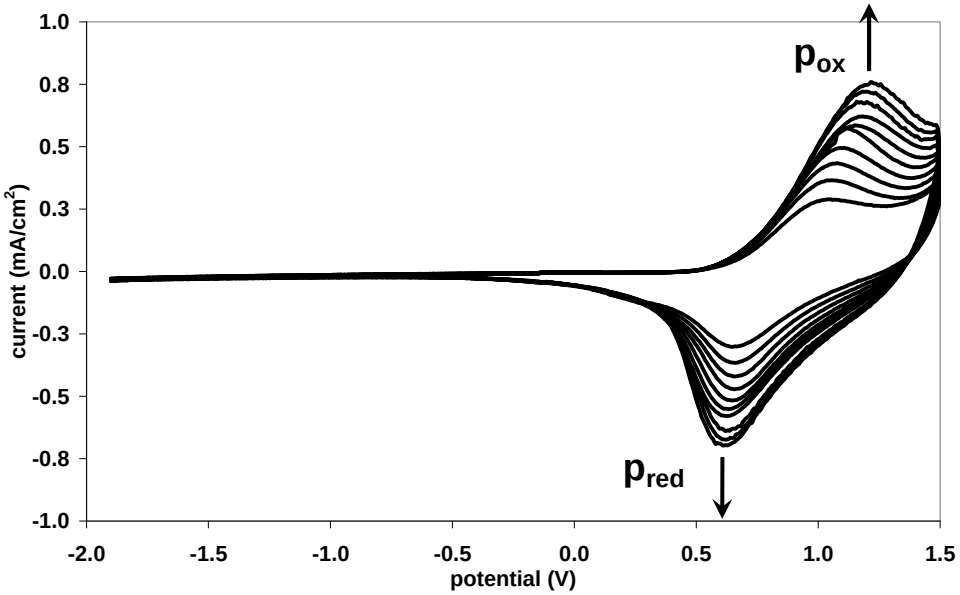

Figure 4.16- CV of P3PFTh / Cl 4 film grown from 0.1 M TMACl 4 / acetonitrile, and cycled in pure BMIPF6. pox and pred refer to p-doping processes described in Equations 4.1. Arrows indicate change in CV magnitude on subsequent cycles. Scan rate = 200 mV/s, 10 cycles.

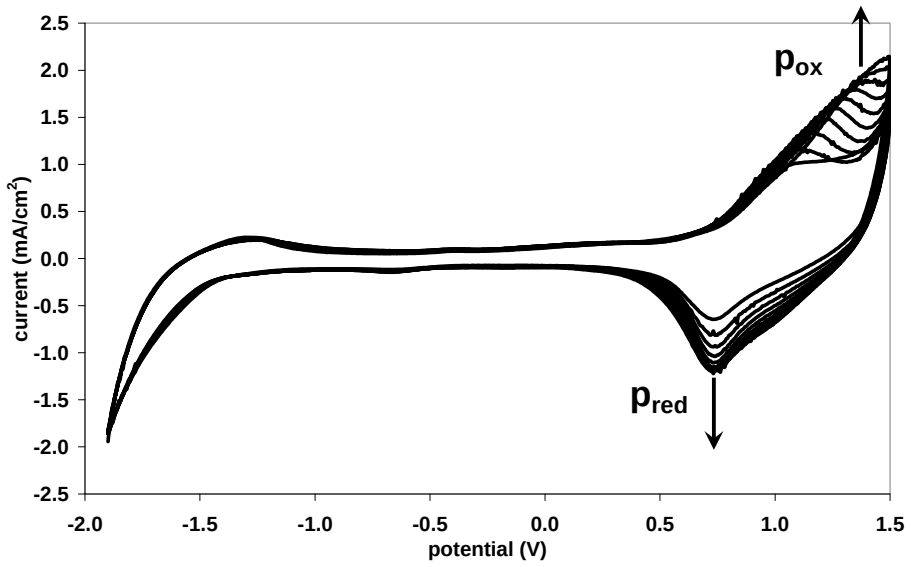

Figure 4.17- CV of P3PFTh / Cl 4 film grown from 0.1 M TMACl 4 / acetonitrile, and cycled in pure EMITFSI. pox and pred refer to p-doping processes described in Equations 4.1. Arrows indicate change in CV magnitude on subsequent cycles. Scan rate = 200 mV/s, 10 cycles.

The three initially identical films all displayed current magnitude increases on subsequent cycles, an observation absent from previous polythiophenes systems in this chapter. As seen in Figure 4.15 – 4.17, all systems exhibited very similar p-doping / dedoping potentials, at 1.2 V and 0.7 V, respectively. Only the EMITFSI cycled polymer showed a detectable level of current magnitude response in the n-doping region.

These results conflicted with simple notions of ionic migration being impeded by the size of an ion relative to voids in the conducting polymer. As the Raman spectral studies on other polythiophenes (PTerTh and PBiTh) showed, doping processes in ionic liquids are expected to occur via ion expulsion processes. Therefore, the n-doping process should occur with the expulsion of the anion from the polymer. The $TFSI^-$ anion is considerably larger than BF_4^- and PF_6^- used in the above comparison, so one would expect it to be the least mobile in a given polymer and least likely to support n-doping processes.

The results do, however, indicate that it should be possible to find the right growth and cycling conditions to achieve n-doping in P3PFTh / dopant with an ionic liquid electrolyte. Once the requirements of such conditions are understood, the stabilising effect of ionic liquids on n-doping processes could be properly investigated and exploited.

4.3.3 Structure-Electroactivity Relationships of P3PFTh

The preceding sections of this Chapter showed that the nature of the monomer solution for conducting polymer deposition, and the identity of the ionic liquid used in subsequent cycling, significantly influenced the nature of the CV response for the ICPs. Preliminary experiments on P3PFTh produced a small current response at n-doping potentials that were highly dependent on both the polymer growth and cycling media. Although none of the preceding P3PFTh systems produced the desired response for a battery device, the changes in CV obtained from varying the growth conditions and cycling electrolytes showed promise, as these parameters can be modified to tune the desired characteristics of a system.

Electrolytes consist of anions and cations that inevitably have an effect on the growth and subsequent CV responses of the particular system. By altering the anion or cation individually, it should be possible to isolate the effect of that alteration on the CV behaviour. If CVs are parameterised using the simulation techniques discussed in Chapter 2, the effect of ion structure on the system can be closely assessed. Identifying these trends provides a means by which structure-activity relationships can be identified and tailored towards desirable polymer properties.

Various salts were used to prepare acetonitrile-based electrolytes for P3PFTh films. Each film obtained was washed with acetone and after drying, subsequently transferred into particular post-monomer solution and the CV recorded. Each of the polymers was also grown in the same way and the post-growth CV recorded, but in electrolytes containing different ions. This procedure was conducted for more than 300 growth / CV

experiments, involving 12 different monomer solutions and 14 cycling electrolytes. The ions used are depicted in Table 4.3.

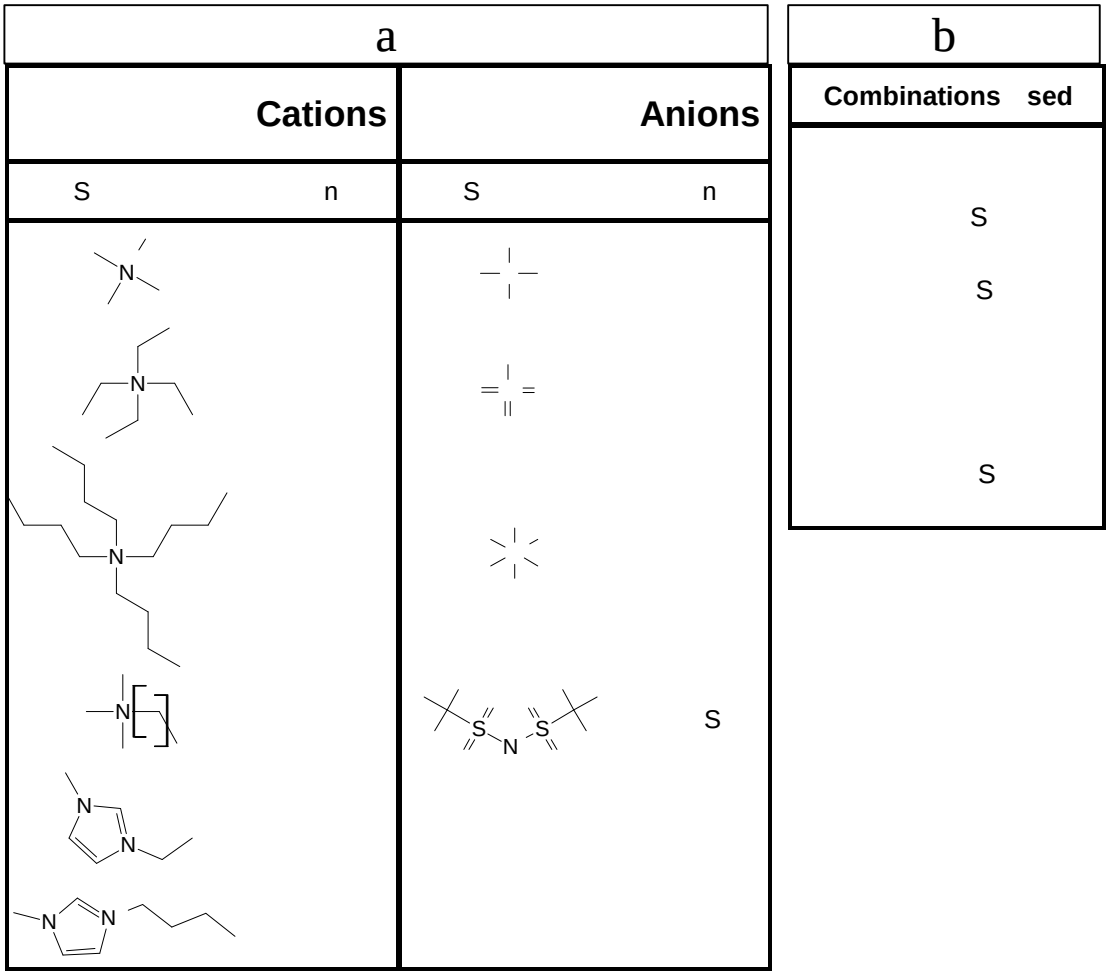

Table 4.3- (a) - structure and acronyms of ions used in the present study. (b) - the ion combinations used in electrolytes from the present study.

To facilitate global analysis of the CV responses, the CVs were first divided into four sectors (Figure 4.18), each identified by Equations 4.1 as distinct doping or dedoping processes. The Gaussian distributions functions outlined in Chapter 2 were conformed to the data of each CV sector by adjusting the Gaussian function parameters until a close fit was produced. The Gaussian function parameters thus produced could be used for further mathematical analysis and are present in the Appendix of this dissertation.

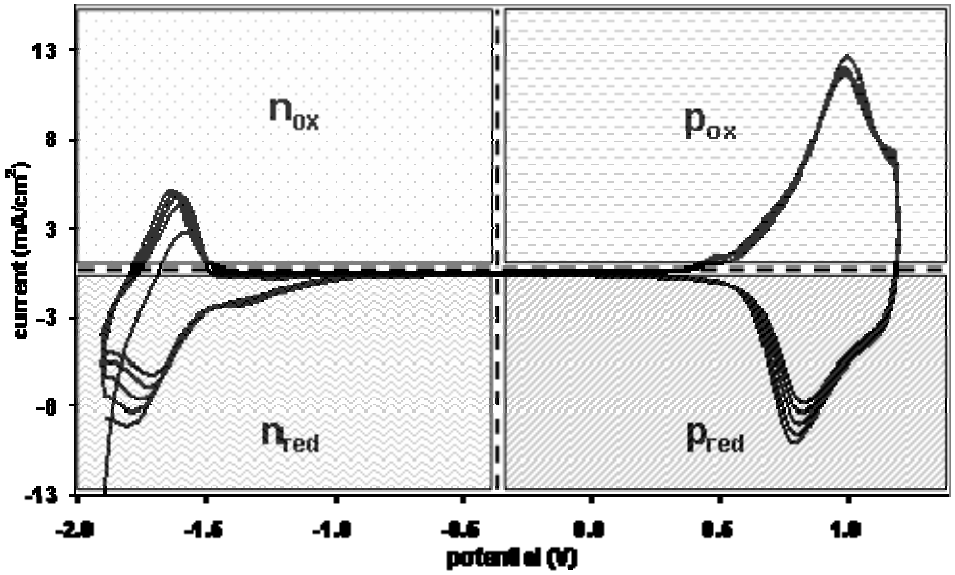

Figure 4.18- Diagrammatic of protocols used for decomposition and analysis of P3PFTh in various electrolytes. The annotation p_{ox} is used to denote a p-doping process, and the subscript "ox" to denote oxidation. Similarly, n_{red} denotes an n-doping process during reduction.

After deconvolution, each parameter set (such as Faradaic charge or peak potential) was recorded into matrices of CV sector data. The rows of the matrices were designated by cycling electrolyte, the columns designated by monomer solution and the intersecting values were the values derived from the CV result for that particular growth and cycling electrolyte combination. Statistical analysis provided in the next Section describes how structure-electroactivity relationships were thereby obtained for these systems.

4.4 Electrochemometrics – Use of Multidimensional Scaling

Chemometrics involves the use of statistical and / or mathematical methods on chemical data to reveal otherwise hidden relationships and patterns[132]. Electrochemometrics combines electrochemistry with chemometrics. Multidimensional scaling (MDS) was explored as a novel method to process the large amount of electrochemical data produced from the experimental matrix obtained in the previous section to reveal the structure-electroactivity relationships for the systems. MDS reveals how parameters

relate for simple interpretation on a two or more dimensional mapped representation[133]. Because of this utility, the method is used in an extremely broad range of fields where relational information is sought, from chemistry[134] to genetics[135], or human perception[136].

MDS works by clustering or pairing similar variables together on single or multiple dimension maps. Attention here shall be focussed on two dimensional maps. When two variables are dissimilar, MDS represents the dissimilarity by placing the variables far apart on the map. When two variables are similar, the distance between them on the MDS map is small. If many variables share similarities, they group together.

The real power of MDS arises when we have vast numbers of parameters with no clear view of which factors connect them. For a more complex example, if we took a map of Australia showing 500 towns spread roughly across the country, we could define the positions of towns on the map relative to each other by assigning a matrix of the distances between them without any particular problem - the map is absolute and we have a bird's eye view. However, if we were given the matrix of distances between towns it would be very difficult to manually re-construct the map, even though sufficient information is present.

MDS can accurately reconstruct a geographical map from the distance matrix (although the scale bar of the map would be arbitrary). The way it does this is by comparing the values of data points in pairs, iteratively, and arranging the data points through multiple dimensions so that the differences (in distance) is minimised[137] on the resulting projected two-dimensional map. The assignments of dimensions or axes on the MDS maps are open to interpretation, but can usually be determined with some logical thought on how the data are spread through the map.

Data was obtained and correlated from CV experiments following procedures described in Section 4.3.3. For the analysis of MDS maps herein, the spread or clustering of monomer solution data points (points that have white centres) is circled with a red line. The cycling electrolyte data points are marked by black centres, and circled with blue line. If there is 'justifiable logic' in the ordering of data points, their relative order is shown in greater detail with a respectively coloured box.

4.4.1 MDS Analysis of Peak Potentials in P3PFTh Systems

The MDS analyses of peak potential values from the P3PFTh CVs are shown in Figure 4.19. In the n-doping sectors, the data is separated into two approximately linear clusters. Identifying the data points, we find that the data along the D1 axis is strongly discriminated into clusters of growth (circled in red) and cycling (circled in blue) conditions identifying D1 as a cycle / growth discriminator. When the n-doping / dedoping distributions of the data points along the D2 axis are examined, one finds that the data is influenced by the nature of both growth and cycling conditions.

Closer analysis of the n-dedoping data along the D2 axis of Figure 4.19 n_{red} did not show a logical order of growth data points (circled in red) but an ordering was observed in the cycling electrolyte (circled in blue) with respect to the nature of the cations. More interestingly, the order of the cycling electrolytes showed that peak potentials are affected by both cation and anion nature with respect to the D2 axis (n_{red} = *cycling cation + anion sensitive*), with evidence that the cation entering the polymer during n-doping is affected by local anions in electrolyte. The affinity of the PF_6^- and BF_4^- anions on the cation was seen to be different in two groups, that of the tetraalkylammonium cations, and that of the imidazolium cations. The effect of the $TFSI^-$ anion was to cluster cations together, regardless of structure. The ClO_4^- anion

also brought two different cations (although both tetraalkylammonium) clustering together.

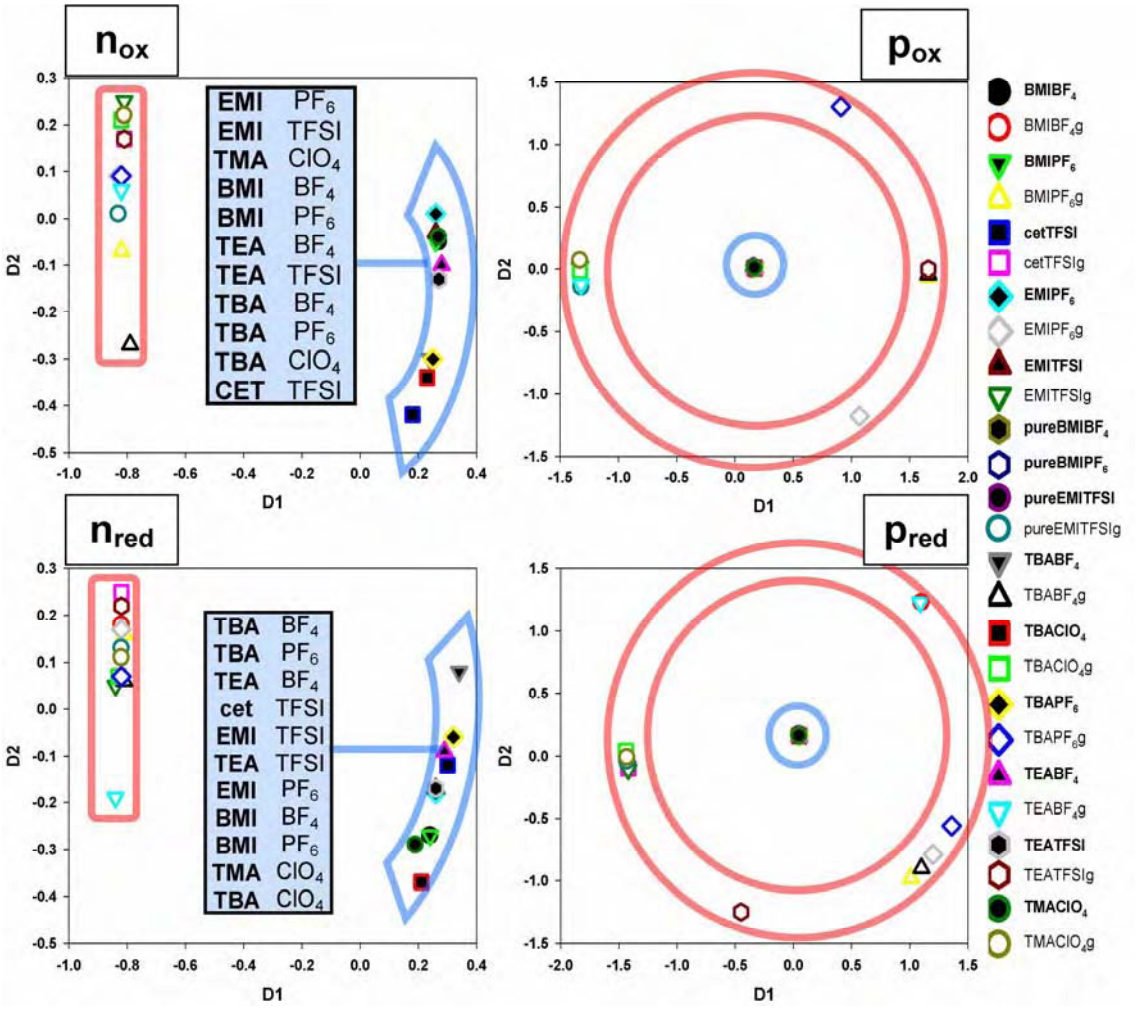

Figure 4.19- Multidimensional scaling analysis of peak potentials for each sector of P3PFTh in various growth and cycling electrolytes. The points circled in blue represent cycling electrolyte data, and the points circled in red represent monomer solution data. The inlaid tables show the resultant order of ions along the D2 axis. D1 is the cycle / growth discriminator axis.

Examining the n_{ox} sector of Figure 4.19 closely, the monomer solution (circled in red) did not produce a logical order in D2. The cycling electrolyte data (circled in blue), however, was distributed logically along the D2 axis, showing excellent discrimination of the cation size employed in post-growth CV. Discrimination along this axis of as

of the cation size employed in post-growth CV. Discrimination along this axis of as little as two carbon units of the cation was possible. When the van der Waals volume (VDW) of the cycling cations was plotted against the D2 cycling cation values, a straight line was produced in Figure 4.20 (n_{ox} = *cycling cation size sensitive*).

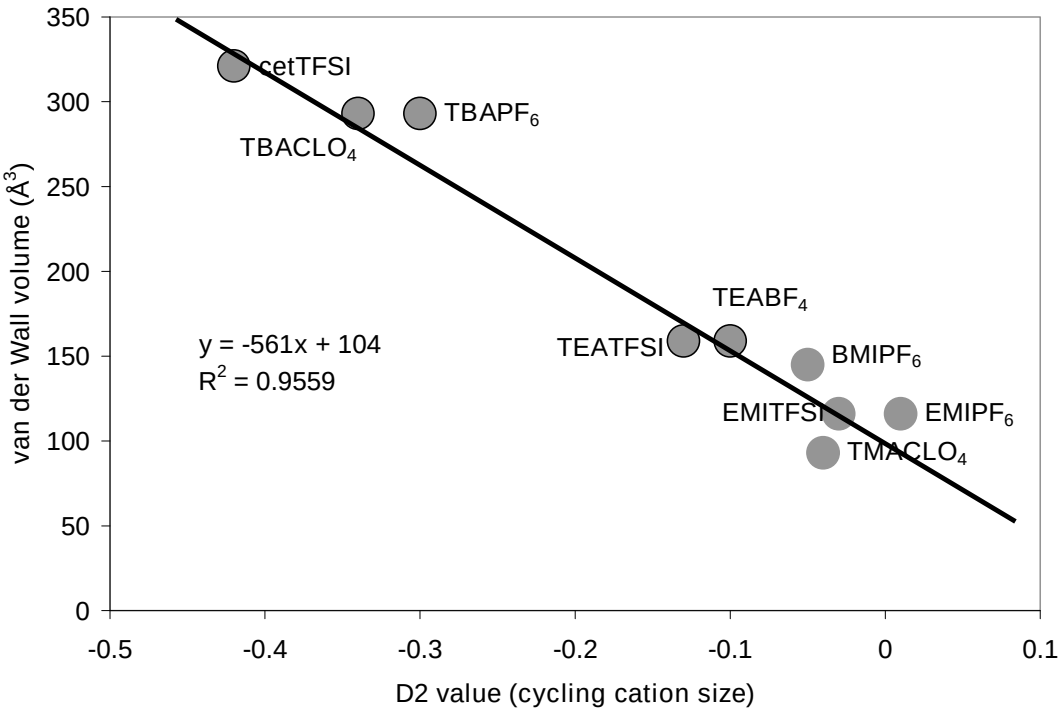

Figure 4.20- Plot of D2 (cycling cation size) from n_{ox} ***against VD volume of respective cations.***

The behaviour of p_{ox} and p_{red} related data observed in Figure 4.19 showed the greatest variance on cycling with respect to the growth conditions circled in red. This could not be readily correlated, and the significance of the axes cannot be clearly defined. The distributions produced by the cycling electrolytes was very small manifesting almost a single point of the MDS analysis (p_{ox} *and* p_{red} = *monomer solution sensitive*).

4.4.2 MDS Analysis of Faradaic Charge in P3PFTh Systems

MDS analysis of Faradaic charge extracted from the same set of CVs is depicted in Figure 4.21. The n_{ox} sector of Figure 4.21 shows that the Faradaic charge of the n-doping oxidation was most affected by growth conditions (circled in red), with the cycling electrolyte component clustering tightly together (circled in blue), producing little if any change in the system.

With the two exceptions of $TBAPF_6$ and EMITFSI, the resulting changes in P3PFTh n-doped oxidation process were dominated by the nature of the anion used in polymerisation, making D2 sensitive to the conditions used in growth for this set of data points (n_{ox} = *growth anion sensitive*). Such an observation suggested that the anion used in polymerisation established a structure in the polymer that was important with respect to Faradaic charge passed in the n-doping oxidation process with little regard for the cycling electrolyte. However, the exact characteristic of the growth anion responsible for discrimination could not be correlated to common physical data of the ions.

The trends in Figure 4.21 n_{red} showed close clustering with respect to the monomer solution, with large effects observed due to the cycling electrolyte. There was not, however, an easily distinguishable trend in the ordering of the electrolytes with respect to D2 (n_{red} = *cycling electrolyte sensitive*).

The order of results along the D2 axis of Figure 4.21 p_{ox} was dominated by the size and nature of the cycling cation (p_{ox} = *cycling cation sensitive*). Whilst such an observation may be expected for pure ionic liquid redox cycling, it also manifested for all of the other more common electrolyte examples. The values derived from ionic liquid electrolytes, however, clustered closely to one point, although they did not appear to differentiate from standard electrolytes. The monomer solution had the most effect in Figure 4.21 p_{red} (p_{red} = *growth cation sensitive*). This observation produced a relational map with similar distribution to the data relationships of Figure 4.21 n_{ox}.

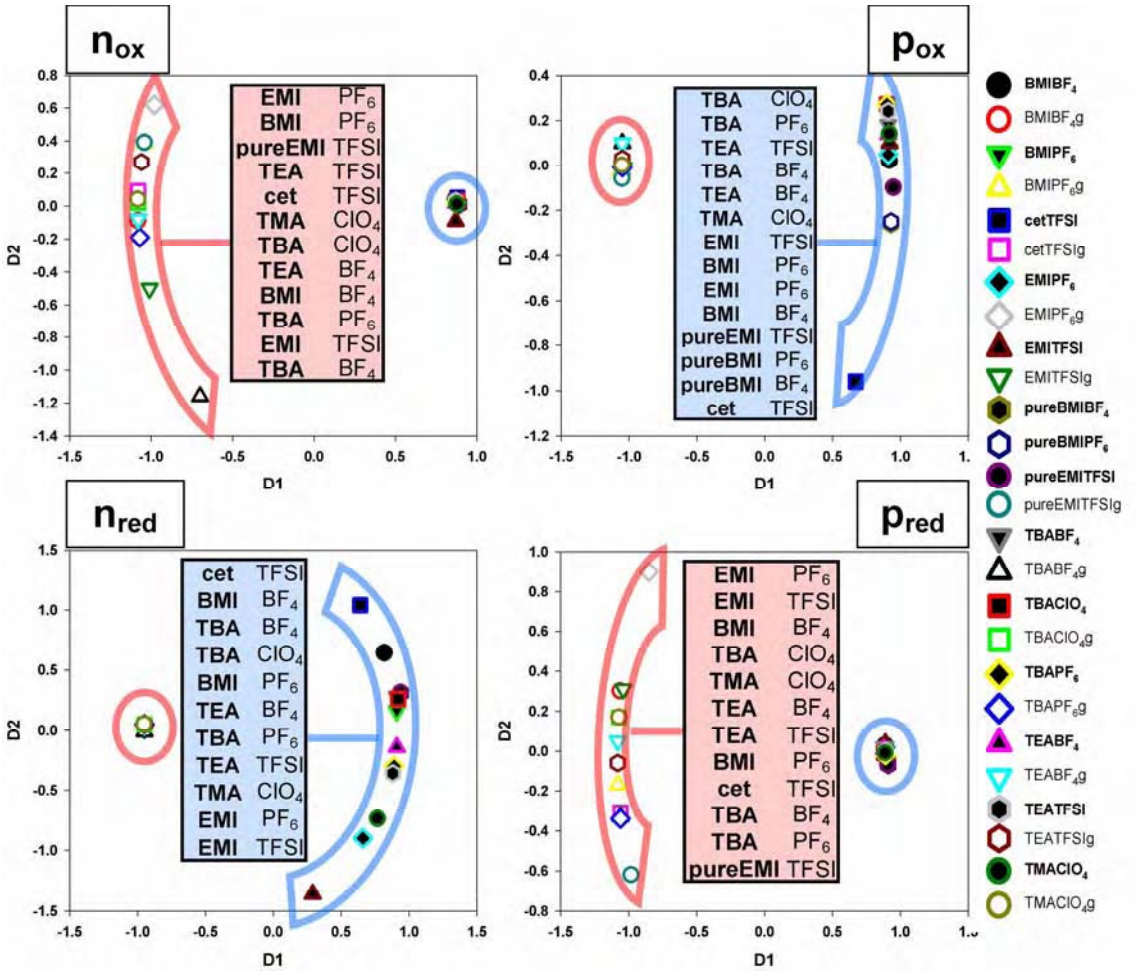

Figure 4.21- Multidimensional scaling analysis of Faradaic charge for each sector of P3PFTh in various growth and cycling electrolytes. The points circled in blue represent cycling electrolyte data, and the points circled in red represent monomer solution data. The inlaid tables show the resultant order of ions along the D2 axis. D1 is the cycle / growth discriminator axis.

Interestingly, it was found that the nature of the monomer solution dominated the processes where ions are expelled, and the cycling electrolyte dominated ion insertion processes. The ordering of electrolytes in Figure 4.21 n_{ox} suggested that the effect of cation expulsions was dominated by the growth anion, while Figure 4.21 p_{ox} suggested that the anion insertion process was dominated by the nature of the cycling electrolyte cation.

4.4.3 MDS Analysis of Surface Concentration in P3PFTh Systems

Surface concentration parameters, "Ns" were derived from Gaussian fits to experimental data, and the result of subsequent MDS analysis is shown in Figure 4.22. Figure 4.22 n_{ox} showed that the monomer solution produced the greatest variations in the n-doping oxidation process. The order of monomer solutions with respect to D2 is one which showed, with the exceptions of pure EMITFSI and $TBABF_4$, an ordering closely linked to the size and specific nature of the anion used in the monomer solution (*n_{ox} = growth anion sensitive*). Figure 4.22 n_{red} showed a close connection to the behaviour of p_{ox}. Both of these processes are ones that involve ion incorporation in classical electrolytes. With the exception of $TBAPF_6$, the order relative to D2 of cycling cations is simply reversed (*n_{red} = cycling cation sensitive*). Such an observation suggests that both ion insertion processes are closely linked.

The ion expulsion data in Figure 4.22 n_{ox} and Figure 4.22 p_{red}, showed growth condition dependence, with a degree of logical ordering of the growth anion in n_{ox} (*n_{ox} = growth anion sensitive*). A logical order could not be established in p_{red} (*p_{red} = monomer solution sensitive*). Figure 4.22 p_{ox} suggested that the cycling electrolyte was dominant in effect on p-doping oxidation. With the exception of pure EMITFSI as a cycling electrolyte, the trend observed with respect to D2 is dominated almost completely by the nature of the cation in the cycling electrolyte (*p_{ox} = cycling cation sensitive*).

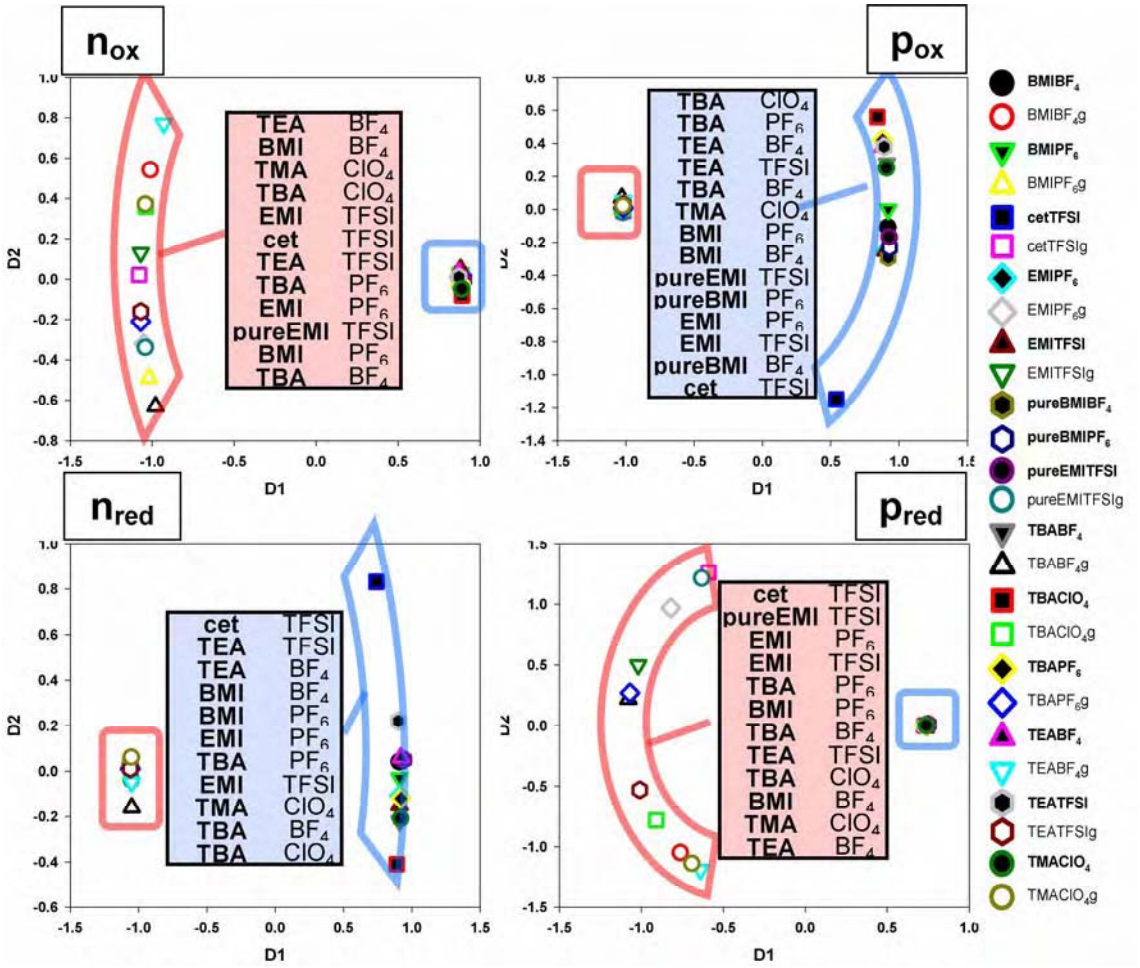

Figure 4.22- Multidimensional scaling analysis of Surface Concentration (N_s) for each sector of P3PFTh in various growth and electrolyte conditions. The points circled in blue represent cycling electrolyte data, and the points circled in red represent monomer solution data. The inlaid tables show the resultant order of ions along the D2 axis. D1 is the cycle / growth discriminator axis.

4.4.4 MDS Analysis of Peak Heights in P3PFTh Systems

Peak height parameters were extracted from the set of CVs and analysed with MDS to give Figure 4.23. With the exception of $TBABF_4$, Figure 4.23 n_{ox} showed that the system had a strong dependence on monomer solution, with the nature of the anion dominating the process. (n_{ox} = *growth anion sensitive*). Figure 4.23 p_{ox} showed that with respect to peak height of the p-doping region, the only systematic result which could be obtained was that the nature of the cycling electrolyte had the greatest effect on half-peak widths of CVs,

although further information could not be interpreted from the ordering of the points (p_{ox} = *cycling electrolyte sensitive*). Figure 4.23 n_{red} and Figure 4.23 p_{red} showed that cycling and growth conditions, respectively, dominated the peak heights of the CVs, although no anion or cation classes could be determined to dominate (n_{red} = *cycling electrolyte sensitive,* p_{red} = *monomer solution sensitive*).

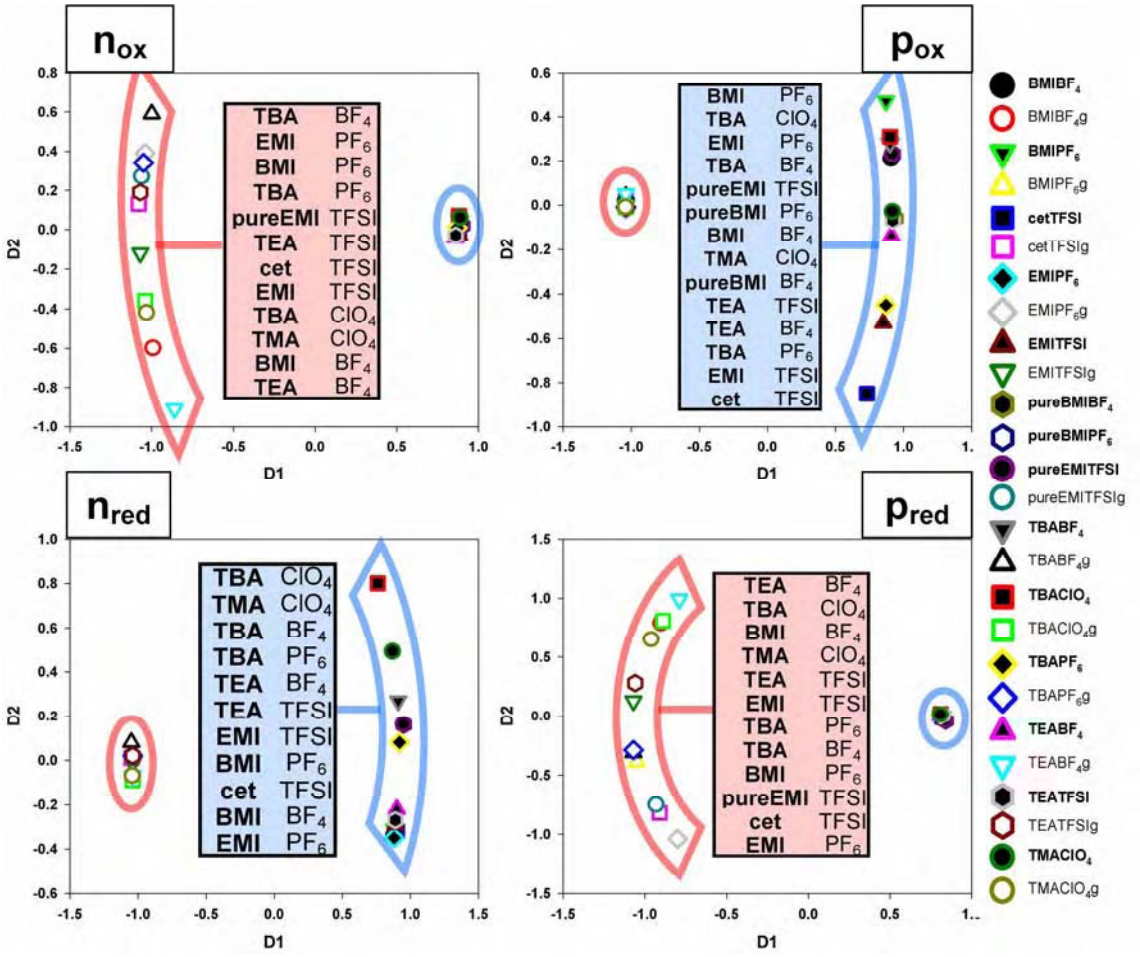

Figure 4.23- Multidimensional scaling analysis of Peak Heights for each sector of P3PFTh in various growth and electrolyte conditions. The points circled in blue represent cycling electrolyte data, and the points circled in red represent monomer solution data. The inlaid tables show the resultant order of ions along the D2 axis. D1 is the cycle / growth discriminator axis.

4.4.5 MDS Analysis of Half-Peak Widths in P3PFTh Systems

Half-peak widths were extracted from the sets of CVs and analysed with MDS (Figure 4.24). Half-peak width is a variable that should be independent of surface concentration, amount of polymer, peak height, and Faradaic charge observed. It is essentially a signature of the system with respect to kinetics.

Figure 4.24 n_{ox} showed excellent purely cation differentiation with respect to D2 for the cycling electrolyte. Figure 4.24 n_{red} showed that the process of cation insertion was completely dominated by the size and nature of the cation in the cycling electrolyte (n_{red} = *cycling cation sensitive*). Figure 4.24 p_{red} also showed that the monomer solution dominated the anion expulsion process, although its effect could not be readily correlated with ions size or the nature of the electrolyte (p_{red} = *monomer solution sensitive*).

Although both the growth and cycling electrolyte had an effect on the magnitude of half-peak width, only the cycling electrolyte produced results which could be calculated with ion size or class (n_{ox} = *cycling electrolyte sensitive*). The half-peak width was most affected by the nature of the cation in the cycling electrolyte, as seen by the ordering with respect to D2. Figure 4.24 p_{ox} showed that the monomer solution dominated the half-peak widths of the p-doping cation insertion process (p_{ox} = *monomer solution sensitive*), with the cycling electrolytes all appearing at the same point. No other obvious trends could be correlated with the positions of the growth points.

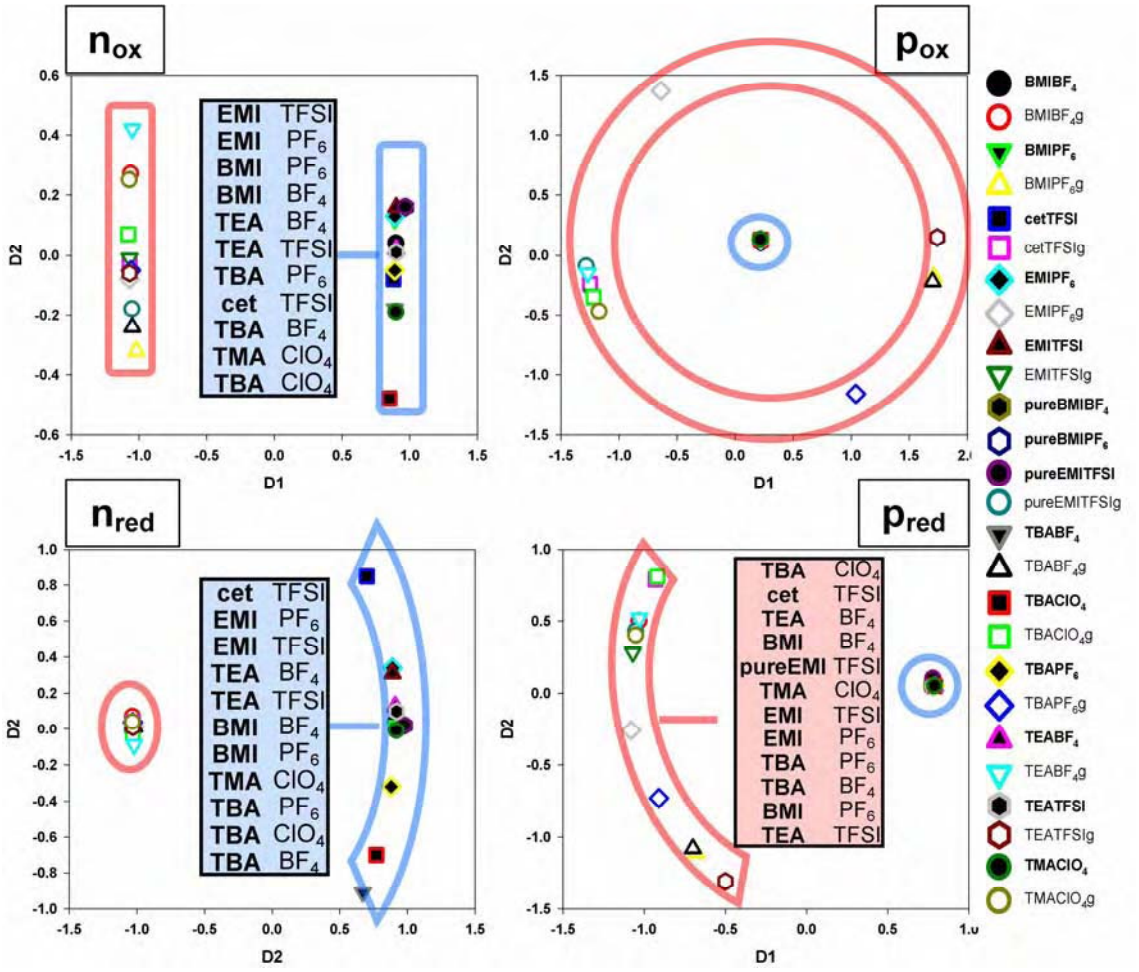

Figure 4.24- Multidimensional scaling analysis of Half-peak Width for each sector of P3PFTh in various growth and electrolyte conditions. The points circled in blue represent cycling electrolyte data, and the points circled in red represent monomer solution data. The inlaid tables show the resultant order of ions along the D2 axis. D1 is the cycle / growth discriminator axis.

4.5 General Conclusions

A system was sought for portable electrochemical storage cell applications employing n-doping of conducting polythiophenes in ionic liquids. The goal was to use the ionic liquid to stabilise the electrochemical processes to allow for a durable device. Initially, EMITFSI was chosen as the electrolyte for several n-doping candidates - P3PFTh,

P3MeTh, PBiTh and PTerTh, and the Raman spectra collected from the systems at various applied potentials.

- The electrochemical Raman spectra showed that both p- and n-doping processes occurred in the studied polymers via ion expulsion processes, which is the opposite of behaviour observed using classical electrolytes. The Raman studies also indicated that the polymer structure plays an important role in determining whether a polymer is capable of n-doping. PBiTh in EMITFSI was found to be capable of producing reasonable n-doping currents, but it lacked sufficient stability for applications in cyclical charge storage.

- P3PFTh exhibited distinctive n-doping during initial CV scans in an acetonitrile based electrolyte, but the system degraded very rapidly. However, the CV performed on this polymer in EMITFSI showed no significant n-doping current, nor were changes observed in the Raman spectra. By altering the nature of the monomer solution, and subsequent cycling ionic liquid, CV studies indicated that it should be possible to n-dope P3PFTh in ionic liquid if the right conditions are determined.

The studies were extended to a large experimental matrix allowing for the parametric decomposition via statistical distribution functions of CVs, as discussed in Chapter 2. The decomposed CV parameters were investigated with Multidimensional scaling analysis.

- The results indicated that growth conditions generally have the greatest effect on ion expulsion processes, and ion inclusion processes were most affected by the nature of cycling electrolyte. This analysis paves the way to produce polymers that are suitable for n-doping in ILs by targeting which ions are used in polymer growth for a corresponding cycling IL.

- Peak potentials were found to be sensitive to the cycling conditions for cation expulsion processes in the n-doping region of P3PFTh, whereas interplay of both the anion and cation were found to influence n-doping cation insertion during cycling.

- The Faradaic charge extracted from CV and analysed with MDS was found to be dominated by the nature of monomer solution with respect to the anion expulsion process of cycling in the n-doping region, and the p-doping anion insertion process was found to be dominated by the size and nature of the cation used in the cycling electrolyte.

- The value of derived surface concentration followed the same trends as observed with Faradaic charge processes. Half-peak widths of both the cation insertion and expulsion processes of the n-doping region were most affected by the nature of the cycling electrolyte, with an exclusive selectivity to the nature of the cation.

- Faradaic charge, surface concentration, and peak heights showed similar mechanistic effects, since ion expulsion processes were monomer solution dependent and ion insertion processes were cycling electrolyte dependent.

- A summary of results is presented in Table 4.4.

Property	**Tuneable Parameter**			
	n_{ox}	p_{ox}	p_{red}	n_{red}
potential	cycling cation	growth electrolyte	growth electrolyte	cycling anion
Faradaic charge	growth anion	cycling cation	growth electrolyte	cycling electrolyte
surface concentration	growth anion	cycling cation	growth electrolyte	cycling anion
peak height	growth anion	cycling electrolyte	growth electrolyte	cycling electrolyte
halfpeak width	cycling electrolyte	growth electrolyte	growth electrolyte	cycling cation

Table 4.4- Summary of results obtained with multidimensional scaling studies on electrochemical data obtained from growth and cycling electrolytes of P3PFTh.

Understanding how ions interact with a polymer is important in designing a system that utilises stabilising ionic liquids. Although no suitable n-doping system exploiting P3PFTh and ionic liquid was explicitly identified here, the data produced in this Chapter reveal structure-property relationships important to achieving n-doping of P3PFTh in ionic liquids n-doping by finding a suitable monomer solution / cycling ionic liquid combination.

4.6 References

[116] Levi, M. D., Y. Gofer and D. Aurbach. *"A synopsis of recent attempts toward construction of rechargeable batteries utilizing conducting polymer cathodes and anodes."* Polymers for Advanced Technologies, **2002** *13*: 697-713.

[117] Steinmueller, D., M. G. Ramsey and F. P. Netzer. *"Polaron and bipolaronlike states in n-doped bithiophene."* Physical Review B: Condensed Matter and Materials Physics, **1993** *47*: 13323-9.

[118] Yossef Gofer, Haripada Sarker, Jeffrey G. Killian, Theodore O. Poehler, Peter C. Searson. *"An all-polymer charge storage device."* Appl. Phys. Lett., **1997** *11*: 1582-1584.

[119] T.F. Otero, I. Cantero, B. Azcano. *"Optimization of poly-3-methylthiophene to be used in advance polymer batteries."* International Journal of Hydrogen Energy, **2000** *25*: 221-233.

[120] Borjas, Ricardo and Daniel A. Buttry. *"Eqcm studies of film growth, redox cycling, and charge trapping of n-doped and p-doped poly(thiophene)."* Chemistry of Materials, **1991** *3*: 872-8.

[121] Laforgue, A., P. Simon and J. F. Fauvarque. *"Chemical synthesis and characterization of fluorinated polyphenylthiophenes: Application to energy storage."* Synthetic Metals, **2001** *123*: 311-319.

[122] Geetha, S. and D. C. Trivedi. *"Studies on polypyrrole film in room temperature melt."* **2004** *88*: 388.

[123] Li, Ling and David M. Collard. *"Poly(3-perfluoroalkylthiophene)s."* Abstracts of Papers, 226th ACS National Meeting, New York, NY, United States, September 7-11, 2003, **2003**: PMSE-286.

[124] Naudin, Eric, Pierre Dabo, Daniel Guay, Livain Breau and Daniel Belanger. *"X-ray photoelectron spectroscopy studies of electronically conducting polymer in the n-doped state."* Polymeric Materials Science and Engineering, **1999** *80*: 629-630.

[125] Fu, Mingxiao, Gaoquan Shi, Fengen Chen and Xiaoyin Hong. *"Doping level change of polythiophene film during its electrochemical growth process."* Physical Chemistry Chemical Physics, **2002** *4*: 2685-2690.

[126] Shi, Gaoquan, Jingkun Xu and Mingxiao Fu. *"Raman spectroscopic and electrochemical studies on the doping level changes of polythiophene films during their electrochemical growth processes."* Journal of Physical Chemistry B, **2002** *106*: 288-292.

[127] Bazzaoui, E. A., G. Levi, S. Aeiyach, J. Aubard, J. P. Marsault and P. C. Lacaze. *"Sers spectra of polythiophene in doped and undoped states."* Journal of Physical Chemistry, **1995** *99*: 6628-34.

[128] Chen, Feng'en, Gaoquan Shi, Jiaxing Zhang and Mingxiao Fu. *"Raman spectroscopic studies on the structural changes of electrosynthesized polythiophene films during the heating and cooling processes."* Thin Solid Films, **2003** *424*: 283-290.

[129] Garreau, S., G. Louarn, J. P. Buisson, G. Froyer and S. Lefrant. *"In situ spectroelectrochemical raman studies of poly(3,4-ethylenedioxythiophene) (pedt)."* Macromolecules, **1999** *32*: 6807-6812.

[130] Hernandez, V., J. Casado and J. T. Lopez Navarrete. *"Density functional study on the structures and vibrational spectra of the radical cation and dication of a,a'-bis(aminomethyl)quaterthiophene."* Journal of Molecular Structure, **2000** *521*: 249-260.

[131] Casado, Juan, Victor Hernandez, Shu Hotta and Juan T. Lopez Navarrete. *"Ft-raman studies of charged defects created on methyl end-capped oligothiophenes by doping with nobf4."* Advanced Materials (Weinheim, Germany), **1998** *10*: 1458-1461.

[132] Lavine, Barry K. and Charles E. Davidson. *"Classification and pattern recognition [in chemometrics]."* Practical Guide to Chemometrics (2nd Edition), **2006**: 339-377.

[133] Agrafiotis, Dimitris K., Dmitrii N. Rassokhin and Victor S. Lobanov. *"Multidimensional scaling and visualization of large molecular similarity tables."* Journal of Computational Chemistry, **2001** *22*: 488-500.

[134] Feher, Miklos and Jonathan M. Schmidt. *"Metric and multidimensional scaling: Efficient tools for clustering molecular conformations."* Journal of Chemical Information and Computer Sciences, **2001** *41*: 346-353.

[135] Xu, Qiang. *"Visualization of protein fold space via nonmetric multidimensional scaling."* Protein and Peptide Letters, **2005** *12*: 473-475.

[136] Thomas, J. A. and W. A. Stock. *"The concept of happiness: A multidimensional scaling investigation."* Int J Aging Hum Dev FIELD Full Journal Title:International journal of aging & human development, **1988** *27*: 141-54.

[137] Ingwer Borg, Patrick J F Groenen. *"Modern multidimensional scaling."* Springer, **2005**.

CHAPTER 5
CHARGE STORAGE IN CONDUCTING POL ERS

5.1 Introduction

The history of Electrochemical Storage Cells (batteries) dates back to 1786, when Galvani made frogs legs twitch by connecting them to brass and iron plates[138]. In 1796 Volta made the first electrochemical stack using silver and zinc plates to produce electrical current[139]. By 1909, the invention of the tungsten filament globe pushed the development of batteries into portable sources of power[138].

Batteries now have vast importance in the modern world - from starting vehicles, to telecommunications and life support systems such as pacemakers[140]. Modern life makes use of batteries almost everywhere. Many electronic devices cannot function in their intended application without having batteries creating a global demand for this technology [141].

Modern batteries almost universally rely on a corrosive electrolyte coupled with toxic, flammable, explosive, corrosive or environmentally unsound electrodes and component materials[142]. As such, they are bundled into strong rigid, plastic and metal enclosures, to prevent hazardous exposure between the contents and outside environment. The bulky nature and packaging of current batteries must be improved for many applications, but this would require a departure from the general hazardous material constructs.

5.1.1 Environmental Considerations of Conducting Polymers

Conducting polymers can inherently store charge through redox processes within their structure. They can provide several benefits over many other materials for battery applications due to their low toxicity, especially when compared to heavy metals such as cadmium, nickel or lead, which persist in the environment and cause harm[143,144]. In addition, conducting polymers won't explode or burn when exposed to moisture, unlike lithium and hydride materials[142]. Conducting polymers are relatively non-toxic, even to the point of biocompatability[145], so for applications in portable electronics carried close to a person, they may be considered safe in the event of device leakage.

5.1.2 aterial Considerations of Conducting Polymers

Conducting polymers have other benefits over many materials for use in batteries[146,147,148]. Primarily, they are lightweight, enabling them to be easily carried, and hence more portable[143,149]. In addition, conducting polymers can be made processable and physically flexible. There are few other candidates which possess a degree of physical flexibility[150] and also the redox requirements to produce a charge storage device such as a battery. Flexibility introduces a new avenue in battery design, and can be quite beneficial for application in portable electronics. The shape of a battery can be easily manipulated or moulded more compactly for the space requirements of a device.

Conducting polymers also behave differently to almost all other forms of battery material because they do not undergo dissolution and redeposition; rather ions are readily diffused in and out of the polymer matrix. The reliance on ion flux rather than a

dissolution / deposition stage and the accompanying structural phase change is highly beneficial, as it is the failure of the redeposited material to regain its predissolution microstructure that causes these types of batteries to fail[151,152,153].

5.1.3 Ionic Liquids for Battery Use

Ionic liquids should always be considered as a prime candidate for use in any conducting polymer system. This recommendation stems from the electrochemistry demonstrated in various polymer systems[154] and the unique environmental aspects of these materials[155,156,157]. Additionally, the lack of vapour pressure[158,159,160], and the possibility of selecting hydrophobic salts[161,162,163] makes these substances quite attractive. They are also considered to be of low toxicity[164,165,166], although admittedly these materials are relatively new and current toxicity data is incomplete. Finally, the large electrochemical window in which ionic liquids can readily operate (4 V)[154,167,168] allows for their application in systems where there are few alternatives. The work contained in this Chapter aims at producing flexible conducting polymer batteries using ionic liquids

5.2 Experimental

There are many materials suitable as electrode substrates for flexible battery applications. Not all material combinations of ICP and substrate are suitable, nor are certain electrodes for every design. Therefore, a range of materials and substrates were chosen for investigations with different system constraints and are summarised in Table 5.1.

Substrates	Electroactive Polymers
fine stainless steel mesh	poly-3-methylthiophene doped with TFSI
Ni-Cu(-Pt) coated polyester	polyaniline doped with ferrocene sulfonic acid
Pt coated PVDF	polypyrrole doped with $LiClO_4$
carbon felt	polypyrrole doped with polystyrene sulphonic acid sodium salt
woven carbon textile	poly-3 4-ethylenedioxythiophene doped with polystyrene sulphonic acid sodium salt

Table 5.1- Substrates and active polymers used in battery designs.

5.2.1 Substrates

Fine stainless steel mesh was obtained from Metal Mesh Pty. Ltd. (Australia) and pre-treated with methods described later for specific devices. Ni-Cu-coated polyester was obtained as a free sample from Liard Industries (Canada) and used as received, or sputter coated with pure Pt in a Dynavac sputter coater for 60 mins each side in a vacuum of 2.3 x 10^{-3} mbar with argon purging, running at a current of 30 mA. Woven carbon fabric Zorflex was obtained as a free sample from Chemviron Carbon and used as received. PVDF membrane (0.45 m) was obtained from Millipore and sputter coated with pure Pt in a Dynavac sputter coater for 30 mins each side in a vacuum of 2.3 x 10^{-3} mbar with argon purging, running at a current of 30 mA. Carbon felt was obtained from Aldrich and used as received.

5.2.2 aterials

The monomers pyrrole (Merck), 3-methylthiophene (Aldrich), 3,4-ethylenedioxythiophene (Bayer) and aniline (Aldrich) were distilled under nitrogen prior to use. Acetonitrile (Ajax), $TBABF_4$ (Aldrich), polystyrene sulphonate sodium salt (PSS) *m.w. ca.* 70,000 (Aldrich), $LiClO_4$ (Aldrich), ferrocene (Aldrich), 98 w / w sulphuric acid (Ajax), 33 hydrochloric acid (Ajax), ammonium persulphate (Aldrich) and LiTFSI (3M) were used as received. EMITFSI was synthesised using the methods described in the Experimental Section of Chapter 3. Ferrocene sulphonic acid was synthesised following published procedure[169].

5.2.3 Chemical Synthesis of ICP Dispersions

Poly-3,4-ethylenedioxythiophene (PEDOT) / PSS dispersion was synthesised from 3,4-ethylenedioxythiophene (EDOT) (32.5 mmol) and polystyrene sulphonic acid sodium salt (PSS) (13.0 g) were mixed in 800 mL of water, and stirred with gentle heating until the solution went clear. The EDOT / PSS solution was allowed to cool to room temperature and a solution of ammonium persulphate (APS) (10.7 g, 52 mmol) in 200 mL water added. The solution was stirred for a further 10 mins and a solution of 50 mg of iron (II) ammonium sulphate in 20 mL water added, at which point the solution started to turn blue. Vigorous stirring was continued for 24 hours until the reaction was complete.

The dark blue PEDOT / PSS dispersion was then dialysed for 48 hours with 20 L portions of MilliQ water, changed twice daily, to produce a clean stable dispersion.

Polypyrrole / PSS dispersion also used the above procedure, but 2.2 g of pyrrole replaced the EDOT monomer. In addition, the pyrrole / PSS solution was cooled to 2.0° C, and the APS solution added over 30 mins with vigorous stirring. Dialysis was conducted as above.

5.2.4 General Electrochemistry

Electrochemistry was performed on a Radiometer Analytical PST050 potentiostat, interfaced to a PC running Voltamaster 4.6 software on Windows XP. A normal 3-electrode setup was used, using a special reference electrode comprising Ag / AgCl in EMITFSI. Connection to substrates was achieved using platinum sheet tipped alligator clips to prevent contact point interactions. All electrochemical investigations were performed using EMITFSI as the electrolyte. To obtain information about the potential stability of substrates, CVs were run on respective substrates at a scan rate of 200 mV/s at increasing potentials until a decomposition potential limit was reached, denoted by current density exceeding 4.0 mA/cm^2. Investigations of conducting polymers were conducted on a 0.02 cm^2 BASi Pt disk electrode.

5.2.5 Device Construction and Testing

Several variations of battery design were developed. Each battery was tested by cycling in conditions that may be encountered in existing devices; charging was achieved by application of controlled voltage and current, and discharge was performed across a load resistor. This type of testing protocol was adapted from the work of Killian *et. al.* [170].

5.2.6 Device Testing Procedure

In order to adapt the testing protocols of Killian *et. al.*[170], some custom equipment was required. The authors did not provide details of their equipment customisations, so new custom equipment was designed and built to automate the charge / discharge protocols.

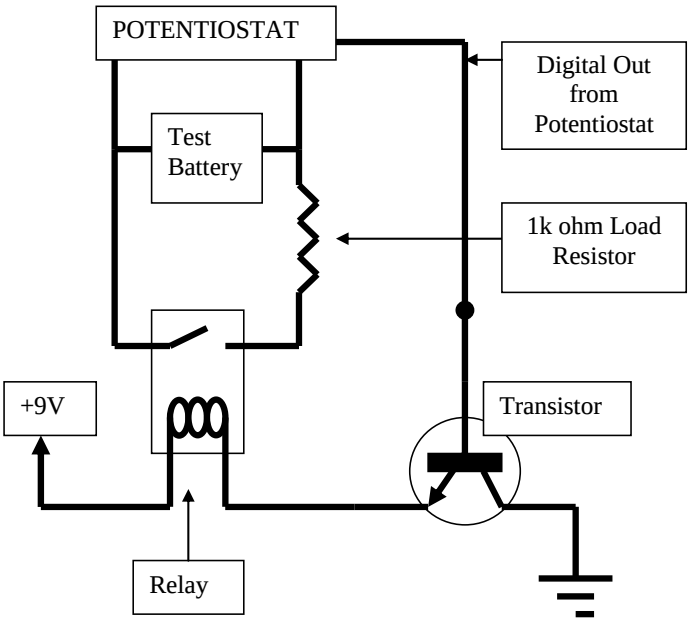

Figure 5.1- The interface built to automate the introduction of a load resistor into circuit during a battery discharge cycle.

General testing protocol consisted of

A) *- measuring open circuit potential*
B) *- galvanostatic charging until a prescribed potential was reached*
C) *- measuring the open circuit potential for a given amount of time*
D) *- discharge across a 1.0 k ohm resistor until given potential was reached*
E) *- the sequence repeated*

The Radiometer Analytical PST050 potentiostat used in this work has a voltage out facility that can trigger external equipment. The voltage out trigger of the potentiostat is controlled by the equipment software and may be programmed into control methods to activate when certain electrochemical parameters are satisfied.

A circuit was constructed to introduce a 1.0 k ohm resistor in parallel across the battery during a discharge cycle (Figure 5.1). During discharge, the potentiostat was used to record cell potential. The cell voltage record and predefined load resistance were thus applied using Ohms Law to determine current flow and charge capacity

5.2.7 Polypyrrole Unsealed embrane in Laminate Devices

To construct electrodes and a separator, Pt was sputter coated onto opposite sides of PVDF membrane measuring 16.0 cm^2. Sputter coating was performed for 30 mins at 30 mA at a pressure of on 2.3 x 10^{-3} mBar on either side of the membrane. This resulted in 2.8 x 10^{-4} g/cm^2 of Pt deposited on each side. The Pt electrodes on PVDF membrane were coated with PPy on each side with the use of two different anion monomer solutions as described below.

The cathode was prepared from 0.16 M pyrrole and 0.75 M $LiClO_4$ in acetonitrile. Potentiostatic growth was performed on one electrode of the Pt coated membrane at 800 mV until 1.7 C/cm^2 was passed. This produced a cathode deposit weight of 1.2 x 10^{-3} g/cm^2 after washing with acetonitrile and drying in air overnight.

The anode was prepared on the opposing side of the Pt coated membrane with 0.16 M Pyrrole 0.26 M PSS (sodium salt) in 3:1 H_2O / acetonitrile. Using the same electrochemical growth parameters as with the cathode, 6.3 x 10^{-3} g/cm^2 of the anode active material was deposited. The resultant double-coated PVDF was then trimmed to a convenient size and soaked in EMITFSI.

5.2.8 Polypyrrole Poly-3-methylthiophene in Sealed Laminate Devices

To construct the flexible PPy / P3MeTh battery, a fine stainless steel mesh was used for the electrode substrates. Polymers were grown electrochemically on the substrates, and 0.45 μm porosity PVDF membrane was employed as an electrode separator. The device was hermetically sealed under vacuum into a transparent polyethylene envelope to prevent interferences from atmospheric gasses.

Fine stainless steel mesh electrodes measuring 16.0 cm^2 were pre-treated by application of an isopropanol dispersion containing 10 w/w graphite powder. After excess graphite dispersion was wiped away, and the electrodes were dry, a negligible mass uptake was evident (in the order of $1.0x10^{-5}$ g/cm^2 graphite).

P3MeTh was grown onto the pre-treated substrates galvanostatically at 0.1 mA/cm^2 until 1.7 C/cm^2 was passed from a monomer solution of 0.10 M 3-methylthiophene and 0.50 M LiTFSI in propylene carbonate. Polypyrrole was deposited with the same electrochemical parameters as for the P3MeTh electrode. However, 0.10 M pyrrole / 0.50 M LiTFSI in propylene carbonate was used as the monomer solution. After washing the electrodes with acetonitrile and drying in air overnight, 1.3×10^{-2} g/cm^2 of P3MeTh / TFSI was present on the anode and 6.5×10^{-3} g/cm^2 of PPy / TFSI was present on the cathode.

The device was assembled by sandwiching the PVDF membrane between overlapping anode and cathode substrates, with the PVDF positioned such that direct electrical contact would not occur between the electrodes. The device was hermetically sealed under vacuum into a transparent polyethylene envelope to prevent interferences from atmospheric gasses.

5.2.9 Polyaniline Doped with Ferrocene Sulphonic Acid in Sealed Laminate Devices

Polyaniline doped with ferrocene sulphonic acid was grown electrochemically on a range of substrates to produce flexible battery devices. Anode and cathode materials were grown potentiostatically for 1 hour at 750 mV from 0.75 M ferrocene sulphonate, 0.30 M H_2SO_4 and 0.20 M aniline in deionised water on 16.0 cm^2 substrates in a three-electrode cell. After washing in acetonitrile and drying the substrates at 50° C for 2 hours, the Laird Industries Cu-Ni-coated polyester yielded 1.4 x 10^{-2} g/cm^2 conducting polymer, carbon felt yielded 3.1 x 10^{-2} g/cm^2, and carbon fibre textile (Zorflex) produced 2.2 x 10^{-2} g/cm^2 of the conducting polymer deposit. Device assembly was essentially identical to the one described in section 5.2.8 above.

5.2.10 Polypyrrole PEDOT from Pre-formed Dispersion in Sealed Laminate Devices

To investigate improvements in device manufacture, conducting polymers were deposited onto substrates from chemically pre-formed aqueous dispersions, rather then by electrochemical means.

Polymer dispersions of PPy / PSS or PEDOT / PSS were sprayed directly onto the stainless steel mesh electrodes (area of 10 cm^2) with a small hobby airbrush, until 2 x 10^{-3} g/cm^2 of respective polymer was deposited on each electrode. The cell was then assembled by placing the electrodes on top of each other, separated by a 0.45 m PVDF membrane, and the device laminated in a plastic sheath employing standard equipment often used in laminating library cards. Once the device was immobilised in plastic lamination, EMITFSI was injected via syringe through the plastic sheath. After

compression, excess EMITFSI was removed and the EMITFSI injection hole was further sealed with hot melt glue to ensure an atmospheric seal.

5.3 Results and Discussion

5.3.1 General Construction and Form of Flexible Conducting Polymer Batteries

In order to construct a conducting polymer battery, we should look at existing designs. Most batteries are composed of an anode and cathode of differing standard potentials that are immersed in an electrolyte and physically separated by an inactive porous material. The physical separator is required to prevent short-circuiting, but it should allow the movement of ions to maintain charge neutrality (Figure 5.2).

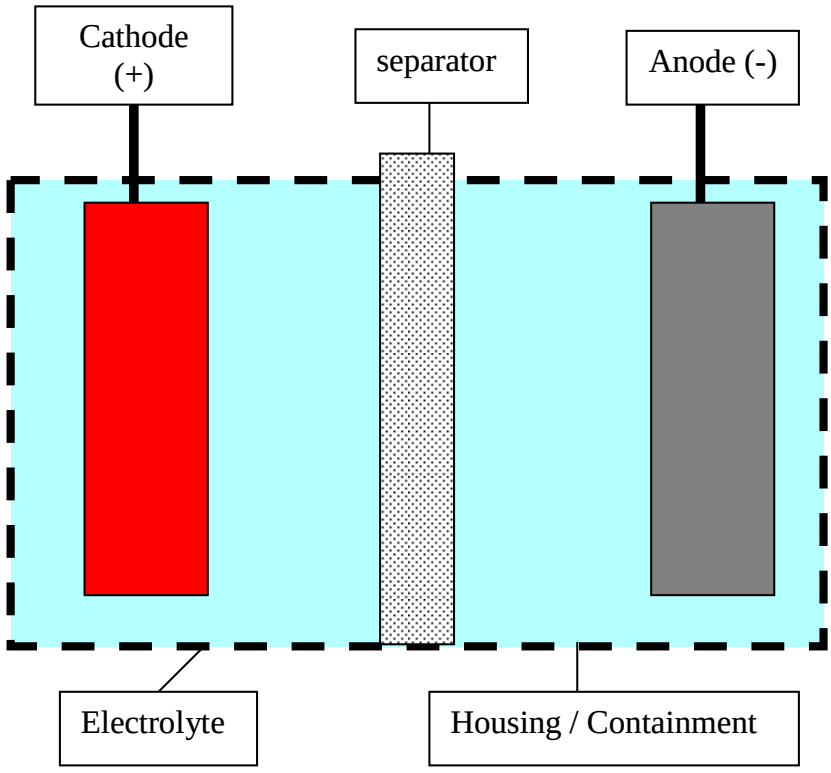

Figure 5.2- The general form of an electrical battery.

The electrode separation can also be achieved by attaching the electrodes onto opposing walls of a container. Ion movement is required exclusively between anode and cathode inside the battery. Finally, the electrolyte should be contained in some way. This general design has changed little, if at all, since its conception 200 years ago.

The simple design from Figure 5.2 has been adapted into a flexible form by using flexible substrates and enclosure materials. Because of the flexible nature of the design, a separator was necessary to prevent the electrodes from touching. In addition, a thin separator permitted the electrodes to get close to one another, thereby decreasing the effect of electrolyte resistance, allowing the cell to run at optimal efficiency. The concept is outlined in Figure 5.3.

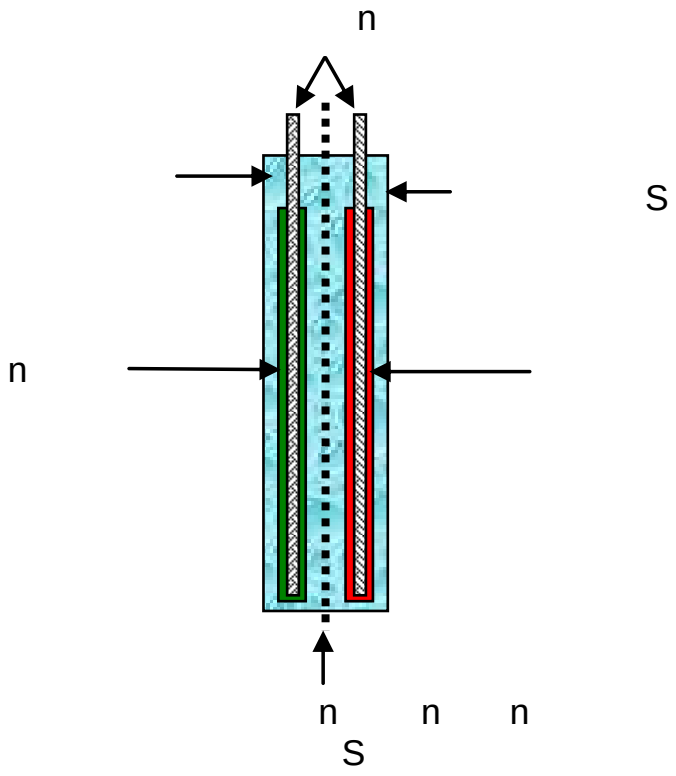

Figure 5.3- The general layout of a flexible battery

The use of ionic liquid electrolyte allows the device to be assembled at ambient air pressure, avoiding the need for complicated airtight adhesive sealing systems. Other more conventional electrolytes, when sealed, have the potential to develop vapour pockets, causing the device to separate and fail. Flexible substrates, separator and housing can be used to allow the device to be pliable and compliant overall. The whole device may be sealed and components held in place by ambient air pressure.

5.3.2 Electrode Substrates for Flexible Battery Devices

In order to achieve a flexible battery construction, all substrates contained within the battery clearly need to be flexible. Other researchers have pursued substrates compromising of metallic fibres[171], foils[172], conductive carbon paper[149,173], carbon fibre materials[170], and plasticised carbon[174]. For most battery designs investigated here, PVDF membrane was used as the physical separator. The choice of PVDF was due to the inertness of the substance, and a large porosity of 0.45 m that allowed sufficient ion flow.

5.3.2.1 Electrochemical Studies of Substrates

To determine the suitability of the proposed substrates in batteries, their electrochemistry was first evaluated in the intended device electrolyte, EMITFSI. Carbon felt was investigated as a flexible electrode substrate due to its ability to conduct electrons and its relatively large surface area. A small piece of carbon felt with external dimensions *ca.* 0.25 cm^2 was electrically connected in a three-electrode cell. It was

clamped on with Pt sheet-tipped alligator clips, and CVs were recorded in EMITFSI as shown in Figure 5.4.

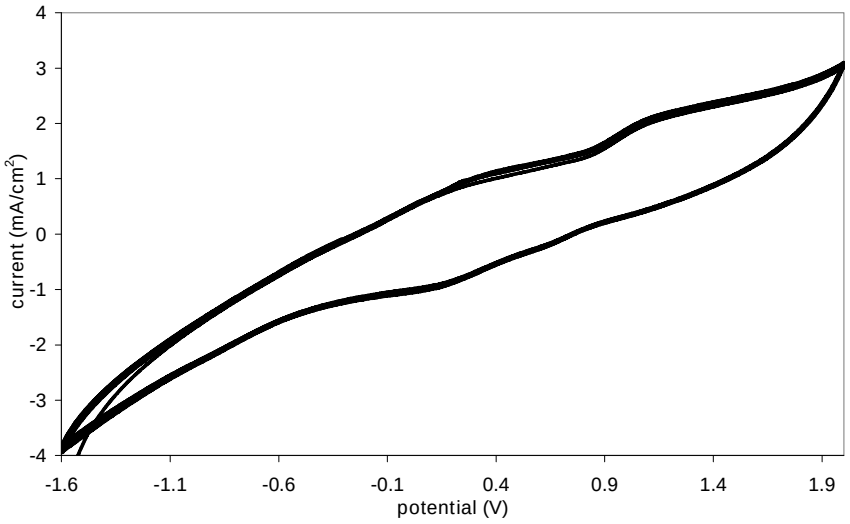

Figure 5.4- CVs obtained using a carbon felt working electrode in EMITFSI. Scan rate = 200 mV/s, 10 cycles.

Redox responses appeared around 0.0 V and +1.0 V. These peaks remained after five subsequent CV cycles. A large capacitive current was also observed. This was expected due to the large surface area of the substrate (in comparison to smooth electrodes). The slope observed in the current vs. potential scan was indicative of an internal resistance drop of 514 ohms/cm^2. Four-point probe conductivity measurements on this system did not produce meaningful results, as the required parameter of sample thickness varied significantly with applied pressure. This produced large variation in measured conductivity. Nevertheless, it was determined that this material was suitable for use in the potential range of -1.6 to +2.0 V, as the change in current magnitude response remained below 2.0 mA/cm^2 over a 0.5 V increment.

The CV from a small piece of Liard industries Ni-Cu-coated polyester electrode (0.25 cm^2) in EMITFSI is shown in Figure 5.5. A persistent electrochemical process was observed around 0.5 V (B and C), and a deteriorating process (signified by decreasing current magnitude) at -1.0 V (A) on subsequent cycles. The deteriorating process was thought to be due to the reduction of residual water[175] on the substrate surface.

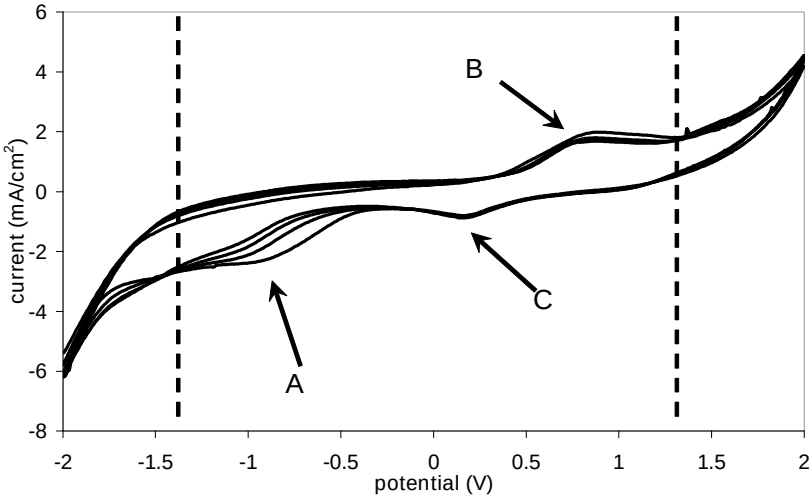

Figure 5.5- CV obtained using aird technologies Ni-Cu-coated polyester as a working electrode in EMITFSI. Dotted lines represent potential window and (A), (B) and (C) are features described in the text. Scan rate = 200 mV/s, 10 cycles

After 200 cycles, the CV had developed into the one shown in Figure 5.6 and the peak attributed to residual water was no longer apparent in the CV[175]. When removed from the electrolyte, the electrode material was visually unaltered. From these results, it was concluded that the bare substrate in EMITFSI should be stable during the experimental timeframe within the potential window of -1.4 to +1.4 V, suitable for use in battery cells.

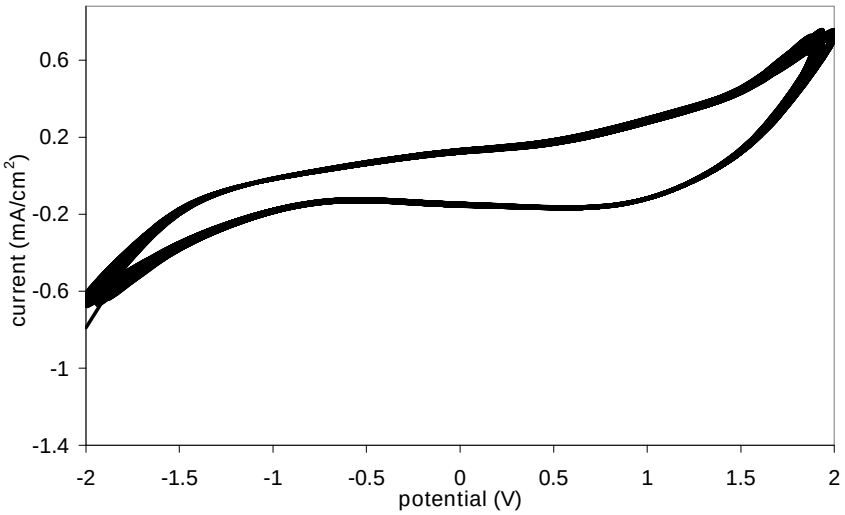

Figure 5.6- aird Technologies material as in Figure 5.4, but 200 cycles later.

The CV obtained from a piece of stainless steel mesh working electrode (0.25 cm^2) in EMITFSI is shown in Figure 5.7. The oxidation of stainless steel at 1.8 V is typically utilised in electropolishing of the metal to produce highly reflective surfaces for optical applications[176,177,178], and is thought to occur in ionic liquids via the direct dissolution of oxidised species at the interface of the ionic liquid and stainless steel.

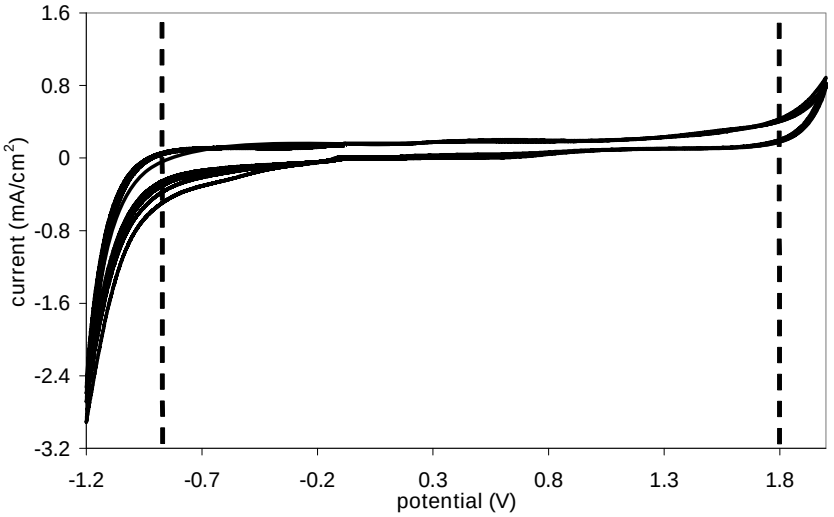

Figure 5.7- CVs obtained using fine stainless steel mesh working electrode in EMITFSI. Dotted lines represent potential stability range. Scan rate = 200 mV/s, 10 cycles.

The CV obtained for a piece of Zorflex fine carbon weave (0.25 cm^2) in EMITFSI is shown in Figure 5.8. The substrate appeared to provide a potential window higher than otherwise possible with glassy carbon and platinum electrodes. This large potential window was, however, put into doubt by the large slope of the CV, indicating a resistance of 600 ohm/cm^2 that may skew CV observations.

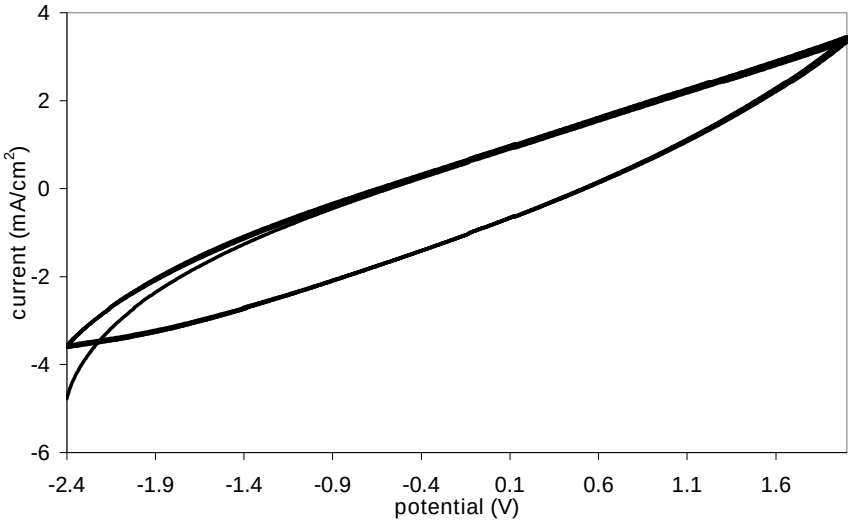

Figure 5.8- CV obtained using a orflex carbon fabric working electrode in EMITFSI. Scan rate = 200 mV/s, 10 cycles.

In addition, Chemviron claimed their Zorflex materials had a surface area of 2000 m^2/g, which could provide a significant area for electrochemical interaction. The CV response observed from such a material would therefore not resemble that observed from a localised disk electrode. One could envisage the system as a massive number of disk electrodes experiencing different potentials in a cell due to their connection by differing lengths of electroresistive material.

There were no electrochemical processes evident in Figure 5.8, even at potentials that were unstable when using glassy carbon electrodes. Although appreciable resistance was observed, the potential window of the material was larger than any observed for electroactive polymers in EMITFSI. Hence, the stability of the material deemed it suitable for use in battery designs.

5.3.3 Polypyrrole Unsealed embrane Laminate Device

A battery design was considered which had minimal components and no environmental shielding. PVDF membrane sputter coated on either side with Pt formed the electrodes and electrode separator (Figure 5.9). Polypyrrole redox materials, as described by Killian *et. al.*[170], were employed with the present configuration.

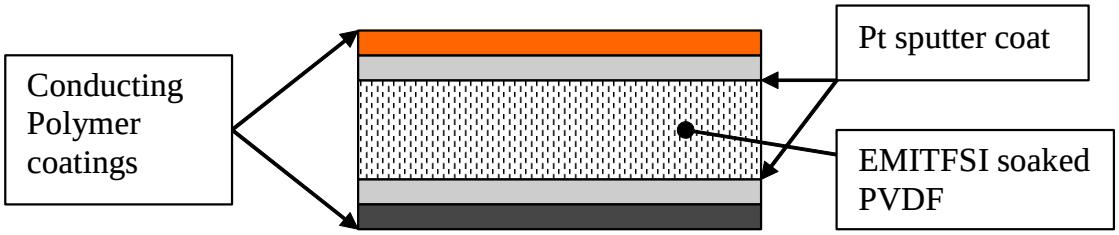

Figure 5. - The open-air membrane battery.

The original work of Killian *et.al.*[170] composed of a carbon fibre felt as the substrate and polyacrylonitrile based gel electrolyte. The conducting polymer materials were polypyrrole for both the anode and cathode, with PSS^- as a dopant for the anode and ClO_4 as the dopant for the cathode. The PSS^- dopant was large and immobile, delaying the oxidation of the material, in a process described as pseudo n-doping[170], although experimental evidence apparently increases p-doping potentials. The potential separation of the two polymers produced a potential gap in which to store charge. In the

present variant, PVDF soaked in EMITFSI was used as the electrolyte and sputter coated Pt as the electrode substrate material. This configuration has been shown to be efficient when applied in electromechanical actuators by Wallace *et. al*.[179].

Post growth CVs of the PPy polymers on Pt substrate are presented in Figure 5.10. The peaks were separated by 400 mV, due to the large negative stationary charge interaction of NaPSS.

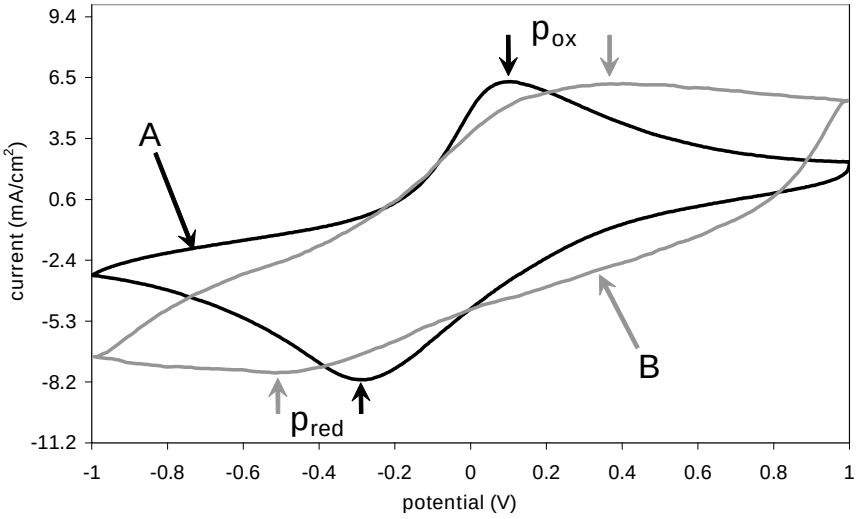

Figure 5.10- CVs of (A) - PPy / Cl 4, and (B) - PPy / PSS in EMITFSI on Pt sputter coated PVDF electrodes. p_{ox} and p_{red} denote p-doping oxidation and reduction processes, respectively. Third cycle of each CV. Scan rate = 200 mV/s.

Testing was performed by a charge cycle of 1.4 mA/cm^2 galvanostatically until a potential of 2.0 V was reached, followed by measuring open circuit potential for 5 minutes, then discharging across a 1.0 k ohm resistor, followed by 5 minutes of measurement of open circuit potential. Typical cell capacity was 20 15 mAh/g. Cell efficiency was 90 throughout as calculated from the charge / discharge curves as

shown in Figure 5.11. The data obtained as a function of cycle number from charge / discharge cycles is present in Figure 5.11.

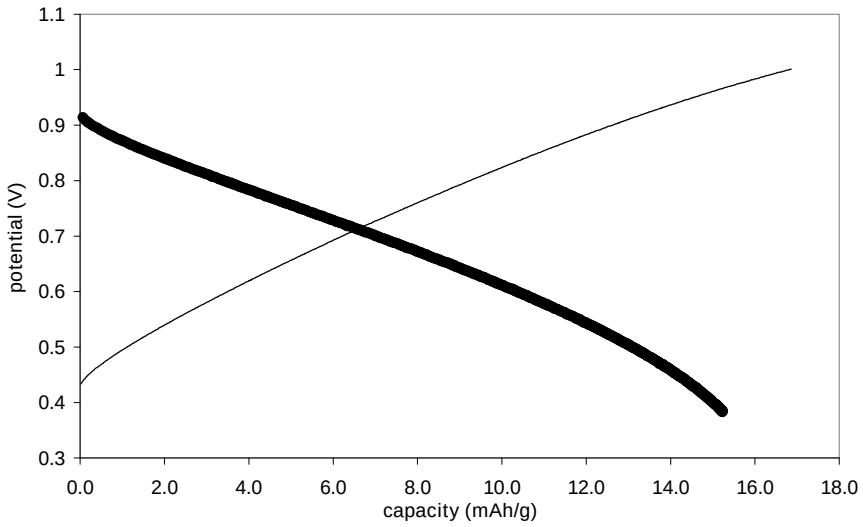

Figure 5.11- Typical charge / discharge curve of PPy / PSS PPy / iCl $_4$ in EMITFSI in a Pt coated PVDF membrane battery. The thick line represents a discharge cycle across a 1 k ohm resistor and the thin line represents a charge cycle.

Although EMITFSI usually produced stable electrochemistry in PPy, the cell capacity of the membrane battery reported here rapidly diminished upon successive charge / discharge cycles (Figure 5.12). The Killian *et. al*. device employed large surface area carbon felt electrodes, $LiClO_4$ gel electrolyte, and was prepared and sealed in a glove box under inert atmosphere. The ultimate charge capacity reported was 22 mAh/g and produced useable capacity over 100 cycles. The membrane battery from the work in this Chapter produced a maximum charge capacity *ca.* 21 mAh/g, placing it in the realm of charge capacity reported [170], although stability of the current work was lower.

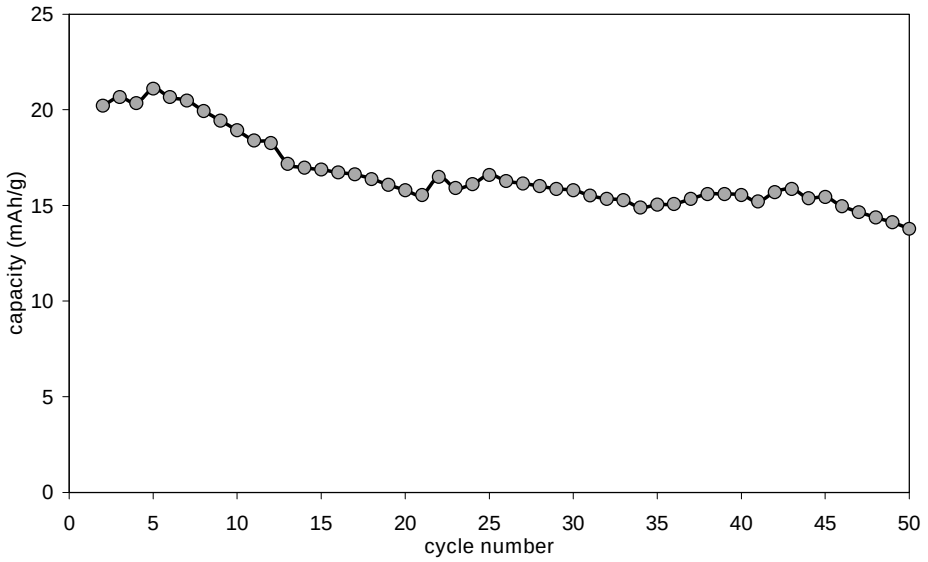

Figure 5.12- Charge capacity as a function of cycle number of PPy / PSS PPy / Cl $_4$ ***in EMITFSI in a Pt coated PVDF membrane battery.***

There are two possible explanations for the instability observed in the membrane battery of the present work. Firstly, the membrane battery was exposed to atmospheric conditions, where the ingress of water and oxygen has been reported to be detrimental to conducting polymer stability[180,181,182,183]. Secondly, the active area of the membrane battery configuration here would be small relative to the surface area of a carbon felt. A large electroactive surface area allows for greater efficiency of redox reactions, and may play a role in storing electrical double layer charge that can contribute to cell capacity.

5.3.4 Polypyrrole Poly-3-methylthiophene in a Sealed Laminate Device

Given the stability results in the previous Section, it was decided that a flexible ICP battery should be sealed from the atmosphere, and that the current collectors should be on the outside of the polymer. Subsequent adaptations were made to the assembly and a

design produced where the electroactive polymers were deposited onto a conductive substrate and the device sealed hermetically.

From CV data, a system of polymers was selected with large electrical potential separation. The system chosen was that of PPy / TFSI, and P3MeTh / TFSI for the opposing electrodes. The system showed high stability when cycled in EMITFSI and produced an anodic and cathodic separation of *ca.* 1.0 V.

In order to achieve consistent and even coatings on the stainless steel mesh electrodes, several adaptations were required. Firstly, the mesh was very flexible, so it had to be held in place, otherwise it would curl and bend interfering with cell geometry and producing uneven films. Consequently, the stainless steel mesh was mounted under tension across a flat glass surface to control the geometry of the substrate in the electrochemical polymer growth cell. It was subsequently observed that the stainless steel mesh in this configuration produced uneven films, from the build-up of polymer between the stainless steel mesh and mounting glass. This problem was resolved by tensioning the mesh over a spacer to provide a small gap between the mesh and mounting glass, as depicted in Figure 5.13.

Firstly, the fine stainless steel mesh was taped taut to a sheet of glass at its ends. Stainless steel rods were then inserted behind the mesh and were held in place by the tightness of the material, somewhat like a bridge on a guitar neck. The rods pushed the stainless steel mesh away from the glass, preventing problematic deposits from behind the mesh. The entire assembly was placed in a monomer solution for polymer deposition.

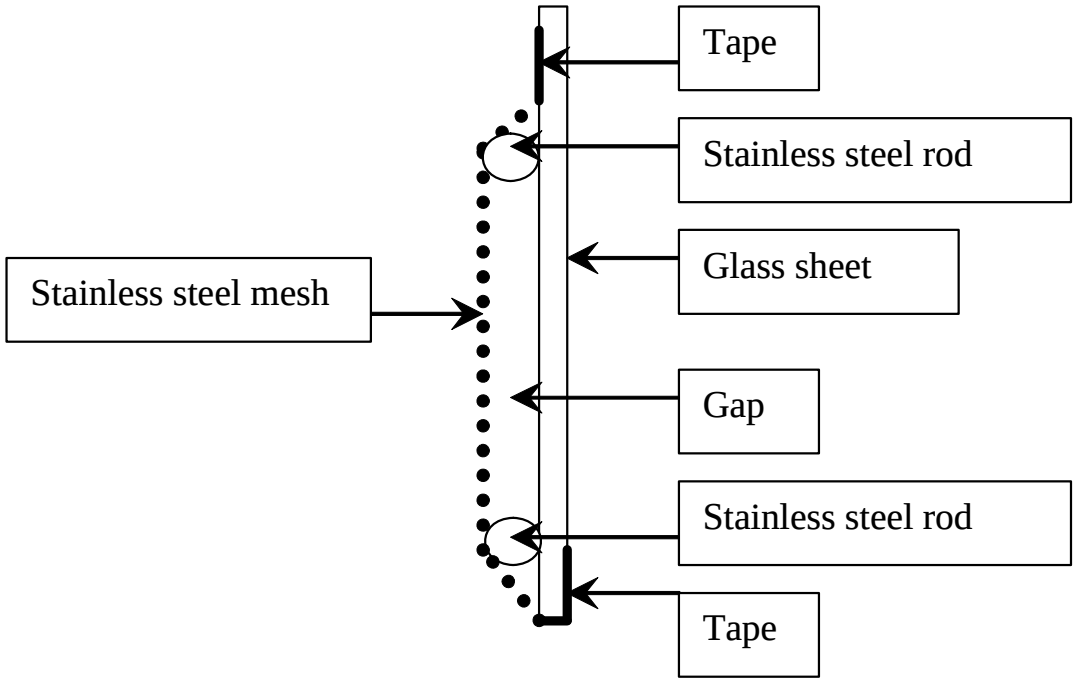

Figure 5.13- The rig required to deposit conducting polymer onto fine stainless steel mesh, side view.

Although the assembly in Figure 5.13 made many provisions for problems encountered in early experiments, it was still a significant problem to achieve even polymer coating from the monomer solutions. Areas of the substrate randomly nucleated the polymer growth, producing uneven coatings. Attempts to produce an evenly nucleating surface on the mesh substrate included abrasive sanding, Pt sputter coating, acid baths and flame treatment, but even growth was not produced.

Consistent film growth was ultimately achieved by rubbing fine graphite powder mixed with isopropanol gently into the mesh - a messy but a very effective procedure. The graphite powder coating facilitated the polymer deposition by providing ample nucleation sites. Conducting polymers were deposited galvanostatically at 1 mA/cm^2 for two minutes. Resultant post-growth CVs are presented in Figure 5.14.

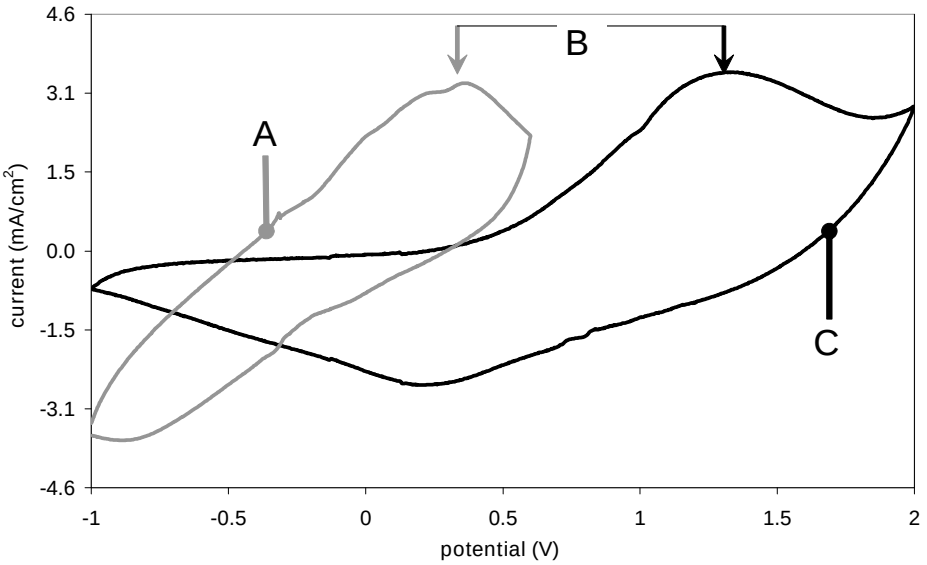

Figure 5.14- CVs of A – PPy / TFSI and C - P3MeTh / TFSI in EMITFSI on fine stainless steel mesh electrodes. B shows the separation of 1.0 V between the PPy and the P3MeTh oxidation peaks. Third cycle of each CV shown. Scan rate = 200 mV/s.

To produce the cell, sheets of fine stainless steel mesh coated with electroactive polymer were placed facing each other, and separated by a PVDF membrane. The result, after full assembly and sealing as described in the Experimental section, is shown in Figure 5.15.

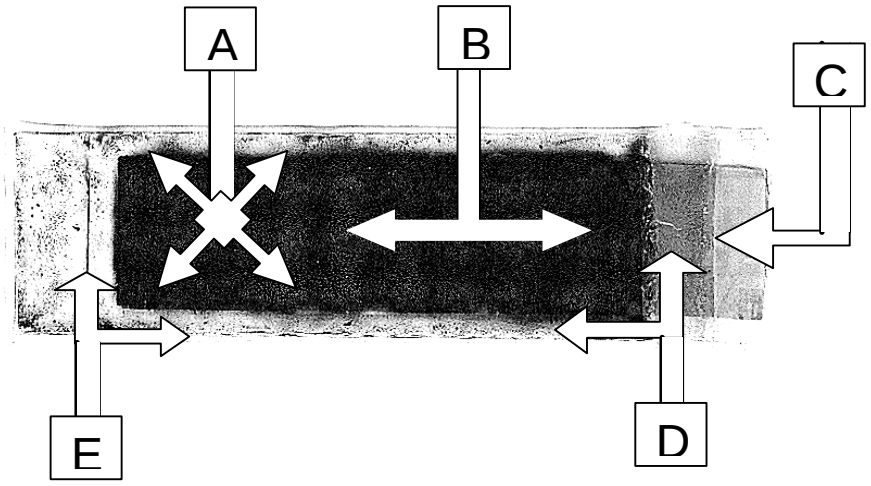

Figure 5.15- A picture of the PPy / TFSI P3MeTh / TFSI assembled battery.

Testing was performed via a charge cycle by applying a constant current of 2.0 mA until a potential of 2.0 V was reached, followed by the measurement of open circuit potential for 5 minutes. The device was then discharged across a 1k ohm resistor until a potential of 0.5 V was reached, followed by 5 minutes of measuring open circuit potential. A representative cycle shown in Figure 5.16.

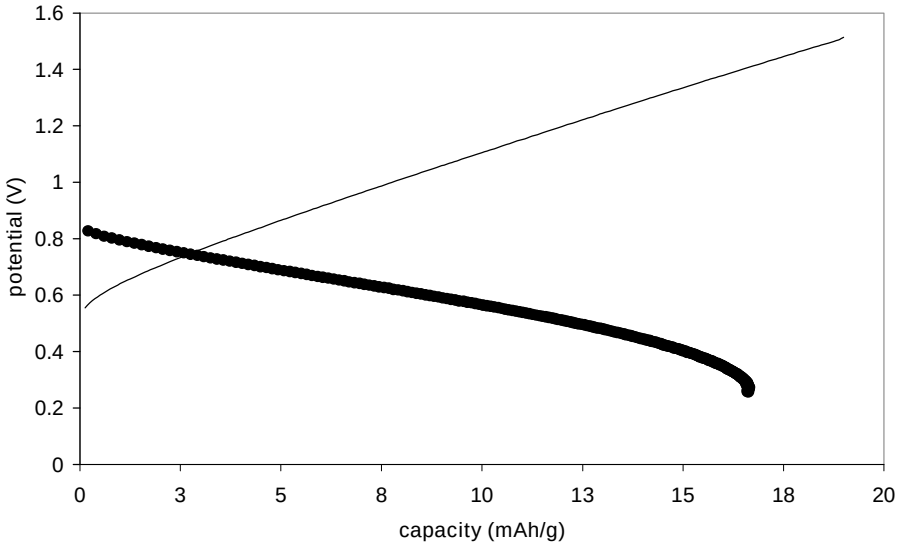

Figure 5.16- Typical charge / discharge curve of a PPy / TFSI P3MeTh / TFSI in EMITFSI in a fine stainless steel mesh battery. The thick line represents a discharge cycle across a 1 k ohm resistor and the thin line represents a charge cycle.

Cell efficiency was calculated at 90 during cycling as determined from the charge / discharge data shown in Figure 5.16. The charge / discharge curves show almost identical development. Most notably, a well-defined operating potential was not achieved. The potential dropped in a near-linear fashion from an initial 0.8 to 0.3 V at the end of the discharge. Although the system could be used to power modern semiconductor electronics by attaching these cells in series and controlling output with voltage regulator circuits, it would be preferred to have a cell capable of producing a more stable output to decrease the requirement for additional components.

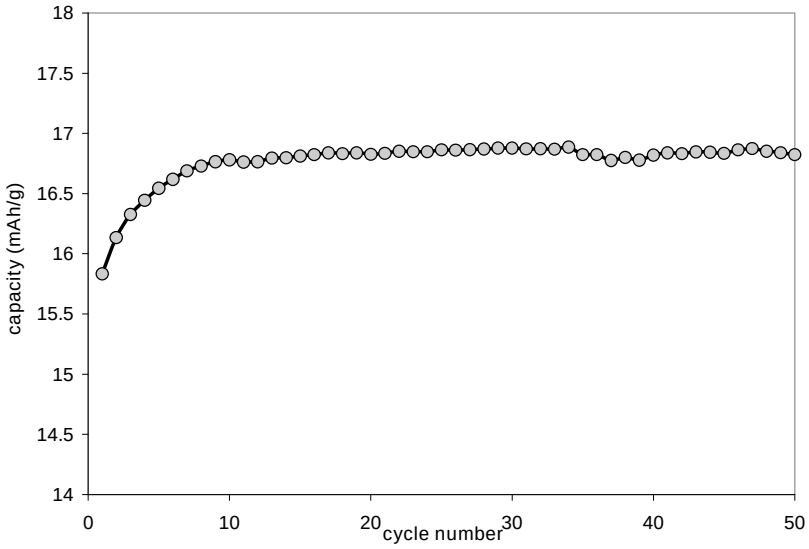

Figure 5.17- Charge capacity as a function of cycle number of PPy / TFSI P3MeTh / TFSI in EMITFSI on fine stainless steel mesh battery.

Typical cell capacity was calculated to be 16.8 mAh/g over 50 cycles for the PPy : P3MeTh battery (Figure 5.17). The new configuration of the cell, along with improvements in the conducting polymers chosen, resulted in a system with increased system stability. The loss of charge capacity per cycle was negligible, which is a significant improvement over the losses experienced in the previous membrane cell.

The problems experienced with electrodeposition of an active polymer were overcome after examining many variables, and a workable system was established. The flexibility of the new system was improved with the use of a stainless steel substrate which, allowed layers to have some ‘free-play’ between each other, and permitted electrode movement during charge and discharge cycling. The fact that the system was hermetically sealed also improved the durability of the electrochemistry with respect to the charge and discharge cycling. This promising arrangement showed benefits that could be transferred to other systems.

5.3.5 Polyaniline Doped with Ferrocene Sulphonic Acid in Sealed Laminate Devices

The sealed laminate assembly developed in the previous section was adapted to utilise a relatively new ICP system using ferrocene sulphonic acid ($FcHSO_3$) doped polyaniline[169]. This polymer was selected because of its desirable electrochemical current response in neutral environments and very high reported charge capacity of 126 mAh/g. The existence of two redox peaks in polyaniline systems was considered an advantage, with the possibility of producing a stable cell potential using aniline for both the anode and cathode.

The polymer was initially tested on a Pt disk electrode to establish its suitability with EMITFSI electrolyte. Deposition was by CV (100 mV/s, -0.2 V to 1.1 V for 20 cycles) as depicted in Figure 5.18. During growth, $FcHSO_3$ redox peaks at around 0.5 V and 0.3 V were pronounced and dwarfed the redox peaks of polyaniline. The rapid growth of the $FcHSO_3$ peaks was indicative of the incorporation of this electroactive component into the polymer.

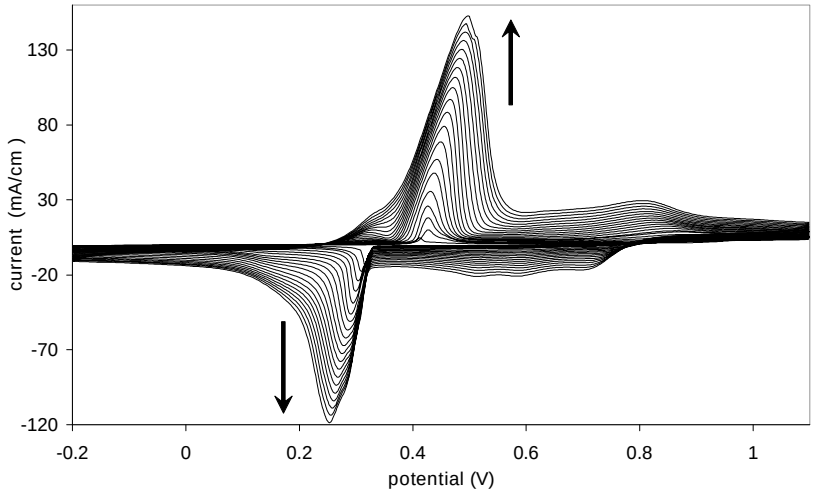

Figure 5.18- Example of CV growth of PAn / Fc S 3 on Pt disk electrode. Arrows indicate direction of current magnitude response on subsequent cycles. Scan rate = 200 mV/s.

The polymer was removed, washed in methanol, dried and put into EMITFSI electrolyte where electrochemistry was tested by CV at 200 mV/s, -0.2 to 1.1 V for 20 cycles (Figure 5.19). Electrochemical current magnitudes of the polymer in Figure 5.19 were also pronounced in the neutral EMITFSI medium. Although a well-defined and large separation in charge potentials was not observed, a battery design could still be produced to exploit the large charge storage capability, as indicated by the current magnitude separation of the cathodic and anodic components.

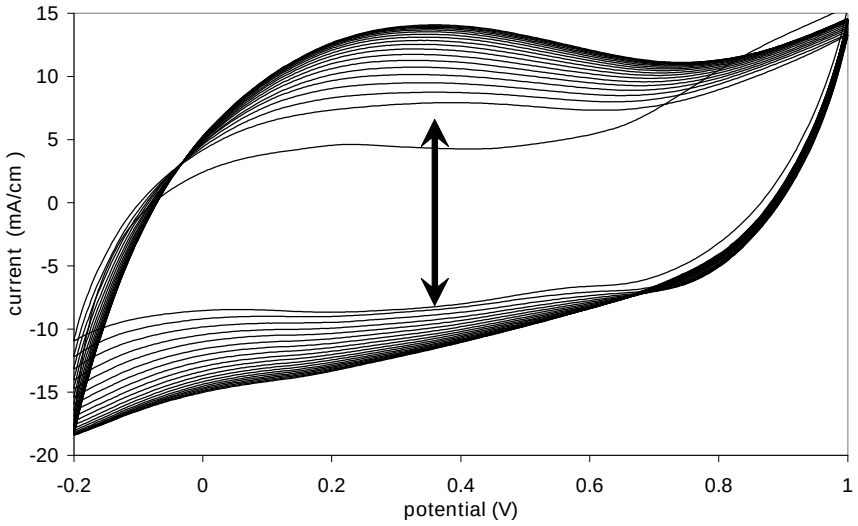

Figure 5.1 - CV of PAn / Fc S 3 on Pt disk electrode in EMITFSI. Arrows indicate direction of current magnitude response on subsequent cycles. Scan rate = 200 mV/s.

Polyaniline doped with $FcHSO_3$ was therefore considered a worthwhile redox material to investigate in battery construction. The obvious choice of electrode substrate was fine stainless steel mesh so that design characteristics used in the P3MeTh / PPy battery could be directly transferred to this system. Unfortunately, the fine stainless steel mesh was quite unstable at the potentials required for polymerisation in the highly acidic $FcHSO_3$ monomer solution. Therefore, a range of substrates was investigated in PAn / $FcHSO_3$ batteries and the results presented in the following sections.

5.3.5.1 Polyaniline Doped with Ferrocene Sulphonic Acid on (Pt)-Ni-Cu-Coated Polyester in a Sealed Laminate Device

Laird Technologies Ni-Cu-coated polyester substrate was chosen as another possible substrate with which to produce a polymer-based battery. From Section 5.3.2, a potential range over 2.8 V was possible with this material in EMITFSI. The CV in EMITFSI showed a large separation between oxidative and reductive components, indicative of a large active surface area that could be beneficial for use as an electrode substrate. The particular substrate chosen was 3027-235, which is a random compressed weave textile that was stiff and rigid. This choice simplified electrochemical deposition, as the substrate could be easily held in place without the need of a frame or additional support.

A piece of substrate measuring 14.0 x 2.5 cm was used for the electrochemical deposition of polymer. 8.0 cm of the substrate was dipped into the monomer solution (making a deposition area of 20.0 cm^2). Various protocols were employed for polymer deposition. Firstly, the monomer solution was stirred slowly and a current of 3 A applied for 16 hours. The fabric was removed, to find the deposition had failed, and all metal had simply corroded away revealing the supporting polyester (Figure 5.20).

Figure 5.20- Galvanostatic deposition of polyaniline doped with ferrocene sulphonic acid onto aird Industries Ni-Cu-coated polyester at 3 μA/cm^2 over 16 hours.

The same conditions as above were then applied but deposition time reduced to 2 hours. The resulting coating was deemed unsuitable for reproducible testing. Most of the metallic coating appears intact; however, the deposition was very patchy (Figure 5.21).

Figure 5.21- Galvanostatic deposition of polyaniline doped with ferrocene sulphonic acid onto aird Industries Ni-Cu-coated polyester at 3 μA/cm^2 over 2 hours.

Potentiostatic deposition was also investigated as a possible means of depositing the desired polymer. A potential of 750 mV was applied for 1 hour onto the substrate, but this stripped the metal off the polyester (Figure 5.22). Under these conditions, the remaining metallic coating had corroded away and the substrate lost all conductivity.

Figure 5.22- Potentiostatic deposition of polyaniline doped with ferrocene sulphonic acid onto aird Industries Ni-Cu-coated polyester at 750 mV over 1 hour.

The substrate itself appeared to be unaffected by the monomer solution, but the metallic coating was unstable at the potentials required to deposit the polymer (Figure 5.23). In order to stimulate the growth of conducting polymer before the substrate degraded, a thin protective layer of Pt was sputter-coated onto the substrate before any electrochemistry was conducted. The pre-treatment of the substrate in this way

produced viable coatings. The presence of a thin Pt layer over the other two metals allowed the polymer to nucleate cleanly, and prevented the substrate metal from being corroded away.

Figure 5.23- Potentiostatic deposition of polyaniline doped with ferrocene sulphonic acid onto aird Industries Pt-Ni-Cu-coated polyester at 750 mV over 1 hour.

Pairs of electrodes were made using the above conditions, with a deposition time of 1 hour. After washing the polymer-coated substrate in water and drying in a vacuum oven, the polymer became brittle. A small piece of actively coated material was cut away from these main electrodes, and the CV measured in EMITFSI (Figure 5.24). The p_{ox} and p_{red} current magnitude peaks had a potential separation of 0.8 V, which was deemed suitable for investigation in a battery assembly.

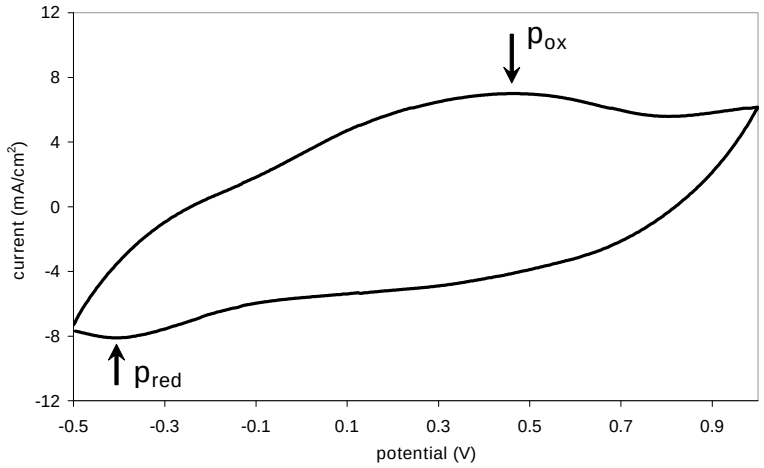

Figure 5.24- CV of PAn / Fc S 3 on iard Industries Pt-Ni-Cu-coated polyester in EMITFSI. Third cycle of CV shown. Scan rate = 200 mV/s.

The polymer-coated substrates were assembled in the laminated configuration described in the Experimental section, with both anode and cathode made of the same material in the same conditions.

A representative charge / discharge curve from the device is depicted in Figure 5.25. The CV of the material combination observed in Figure 5.24 suggested that the charge discharge / curve of a battery made with both anode and cathode of this same material would not produce a well-defined discharge potential, as the current was stored across a range of potentials. As a result, the device rapidly dropped in potential in the first 0.5 mAh/g from 1.00V to 0.65V, and then slowly fell in potential to the discharge limit of 0.55 V.

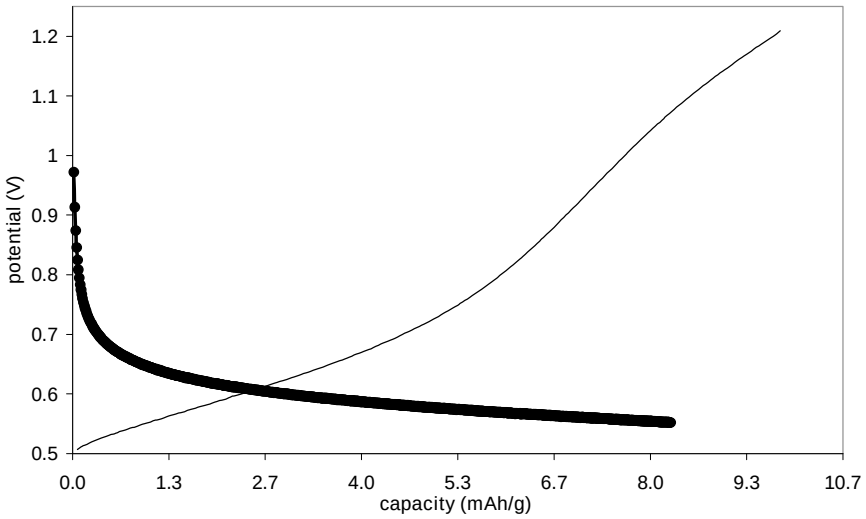

Figure 5.25- Typical charge / discharge curve of PAn / Fc S 3 PAn / Fc S 3 on Pt-Ni-Cu-coated polyester in EMITFSI battery. The thick line represents a discharge cycle across a 1 k ohm resistor and the thin line represents a charge cycle.

The charge capacity as a function of cycle number is shown in Figure 5.26. This reveals the relatively poor initial capacity of 13 mAh/g rapidly declining over 30 cycles to zero. The charge capacity decline was indicative of substrate degradation, as suggested by the difficulty in growth of polyaniline onto the substrate in oxidative and acidic conditions.

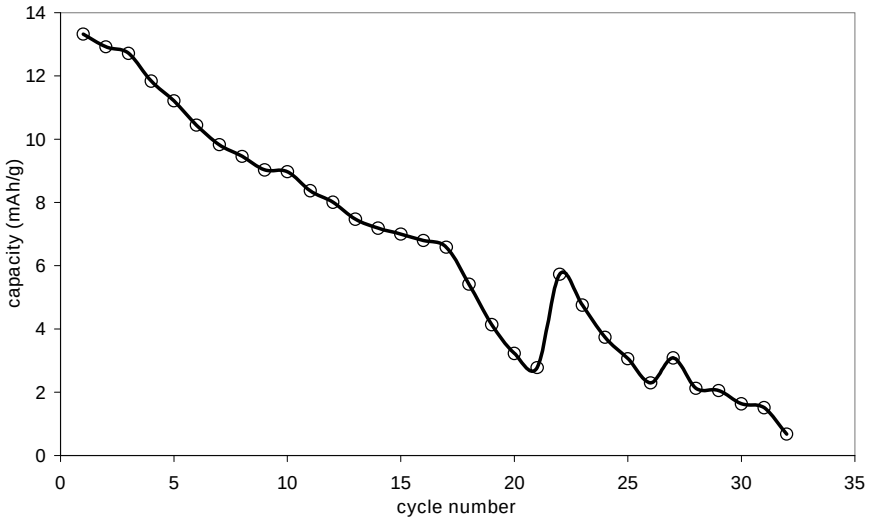

Figure 5.26- Charge capacity as a function of cycle number of PAn / Fc S 3 PAn / Fc S 3 on Pt-Ni-Cu-coated polyester in EMITFSI battery.

5.3.5.2 Polyaniline Doped with Ferrocene Sulphonic Acid on Carbon Felt in a Sealed Laminate Device

The construction of a sealed laminate battery using PAn / $FcHSO_3$: PAn / $FcHSO_3$ on Pt-Ni-Cu-coated polyester in EMITFSI proved to be problematic. After issues of the monomer solution causing significant degradation of the substrate were mostly overcome, the resulting battery was found to be unstable, quickly degrading in charge storage performance over some 30 cycles. A different substrate was therefore chosen with improved stability. In this section of the study, carbon felt was used.

PAn / $FcHSO_3$ was coated onto carbon felt in the same manner as the successful polymer deposition described in the previous Section, *i.e.* - via application of a constant potential of 0.75 V to the substrate surface in the monomer solution for 1 hour using a 3 electrode cell. After washing the substrate in water and drying, a small piece of

electroactive-coated substrate was cut away from the bulk electrode and its CV measured (Figure 5.27).

The CV in Figure 5.27 exhibited several redox peaks, three on the anodic side and two on the cathodic side. Polyaniline in acidic electrolyte usually produces a total of two doping and two dedoping processes[184] observable electrochemically. To complicate assignments of this system, $FcHSO_3$ was also incorporated into the material that may have similar redox potentials to the polyaniline system. $FcHSO_3$ also provides protons to the polyaniline so that polyaniline may access all its electrochemical states in a surrounding neutral bulk media. As such, definitive assignments of the a - e peaks are difficult to resolve due to the large interdependencies of the system. The important observation from this CV is that there are current magnitude peaks separated by useable magnitude potentials to provide a driving force for a battery.

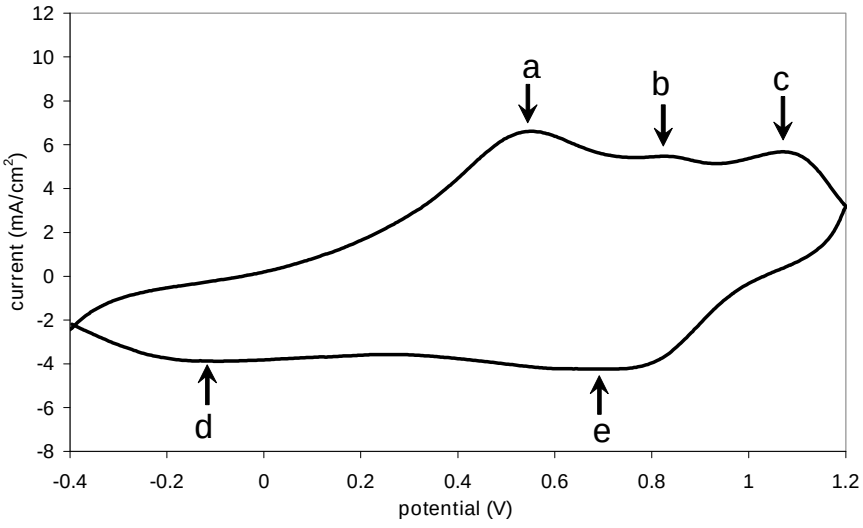

Figure 5.27- CV of PAn / Fc S 3 on carbon felt in EMITFSI. Third cycle of CV shown. Current density peaks a - e are discussed in text. Scan rate = 200 mV/s.

The battery was assembled from the rest of the electrode material used above and subjected to charge / discharge cycles. Representative cycles are shown in Figure 5.28. A large external charging potential (up to 3.5 V) was necessary to produce any significant charge storage due to the poor conductivity of the substrate introducing a large internal resistance drop. The large internal resistance drop translated to smaller potential magnitudes experienced at the active polymer surface, hence poor stimulation of the redox activity of the polymer.

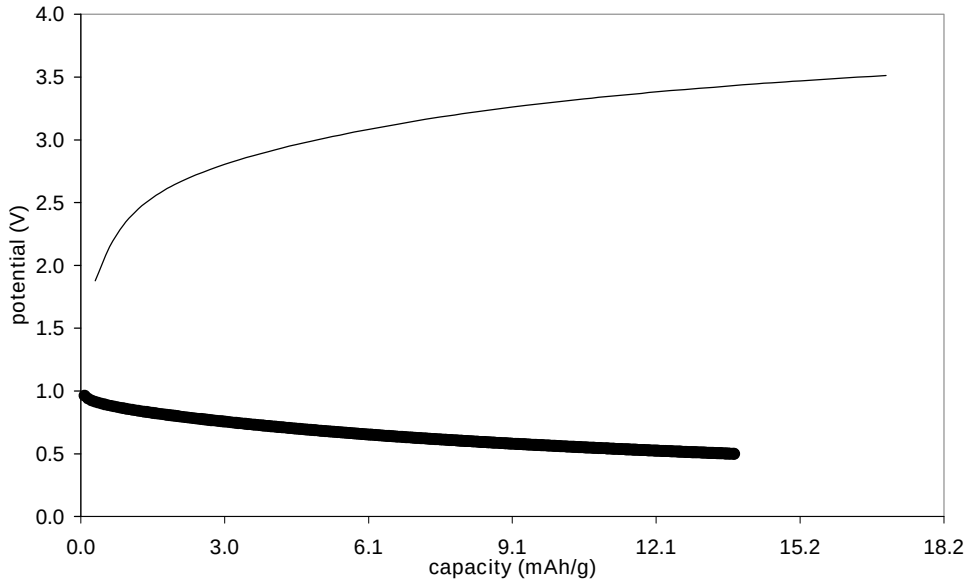

Figure 5.28- Typical charge / discharge curve of a PAn / Fc S 3 PAn / Fc S 3 on carbon felt in EMITFSI battery. The thick line represents a discharge cycle across a 1 k ohm resistor and the thin line represents a charge cycle.

The cycle stability of the system is shown in Figure 5.29. A maximum charge capacity of 18 mAh/g was achieved after 5 cycles, after which the charge capacity slowly degenerated to 10 mAh/g over 27 cycles. The maximum charge capacity observed was somewhat higher than with the Pt-Ni-Cu-coated polyester substrate system, and the

charge capacity did not degrade as rapidly, showing improvement of carbon felt over Pt-Ni-Cu-coated polyester.

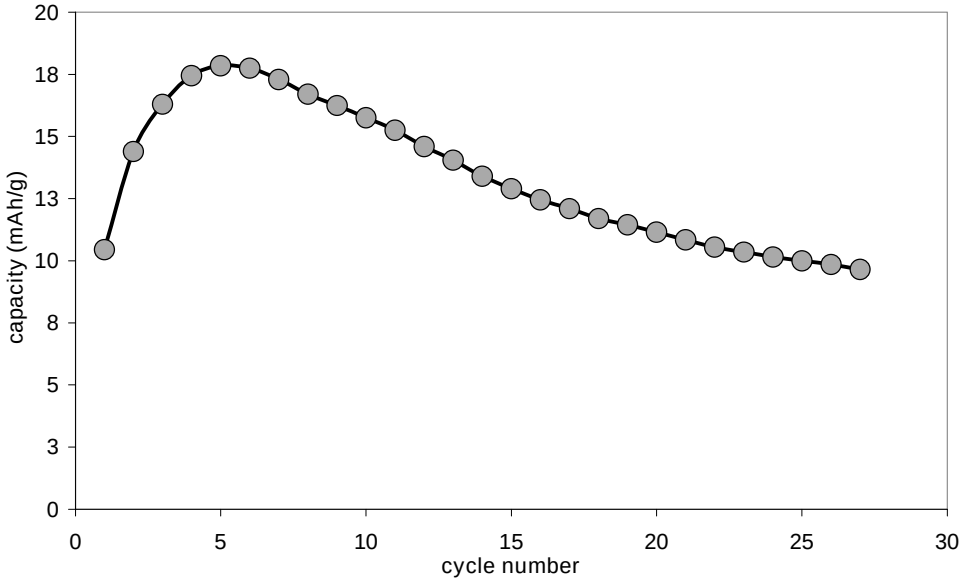

Figure 5.2 - Charge capacity as a function of cycle number of a PAn / Fc S 3 PAn / Fc S 3 on carbon felt in EMITFSI battery.

5.3.5.3 Polyaniline Doped with Ferrocene Sulphonic Acid on orflex Carbon Fabric in a Sealed Laminate Device

The performance of two PAn / $FcHSO_3$ batteries using different electrode substrates was investigated in the previous Sections, with each system showing a level of improvement concerning battery manufacturability, stability and charge capacity. For additional device performance enhancement, another substrate was chosen, namely Chemviron Zorflex, in the form of a finely woven carbon fabric. PAn / $FcHSO_3$ was grown electrochemically onto the Zorflex substrate using the same method as other PAn

/ $FcHSO_3$ electrodes in preceding Sections (0.75 V for 1 hour). After washing and drying the prepared electrodes, a small sample of electroactive area was cut away, and its CV recorded in EMITFSI (Figure 5.30).

The CV in Figure 5.30 is similar to that obtained for the carbon-felt system in Figure 5.27. However, there is an important difference: the oxidation peaks a-c do not overlap in potential with peaks d and e. The oxidation and reduction processes are therefore discrete, and one would expect that a battery device made from the system employing anode and cathode of the same material would produce a discrete potential of discharge.

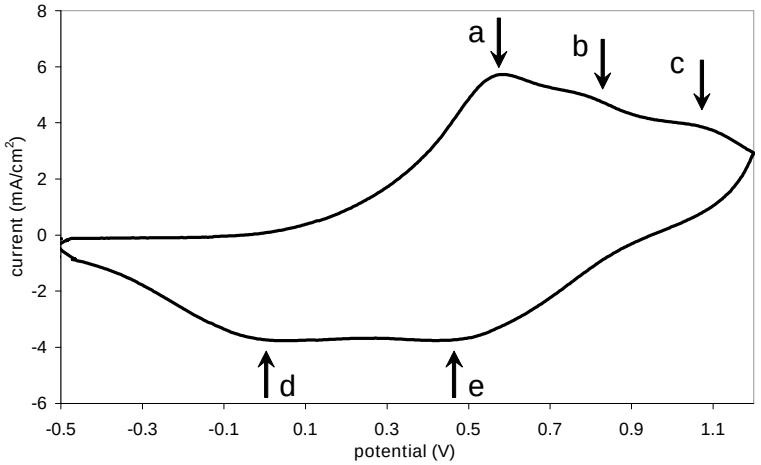

Figure 5.30- CV of PAn / Fc S 3 on orflex woven carbon fabric. Current density peaks a - e are discussed in text. Third cycle of CV shown. Scan rate = 200 mV/s.

The electrodes produced with PAn / $FcHSO_3$ on Zorflex were assembled into a battery device using the techniques described in the Experimental section of this Chapter using EMITFSI as the electrolyte. The resulting charge discharge curve is shown in Figure 5.31.

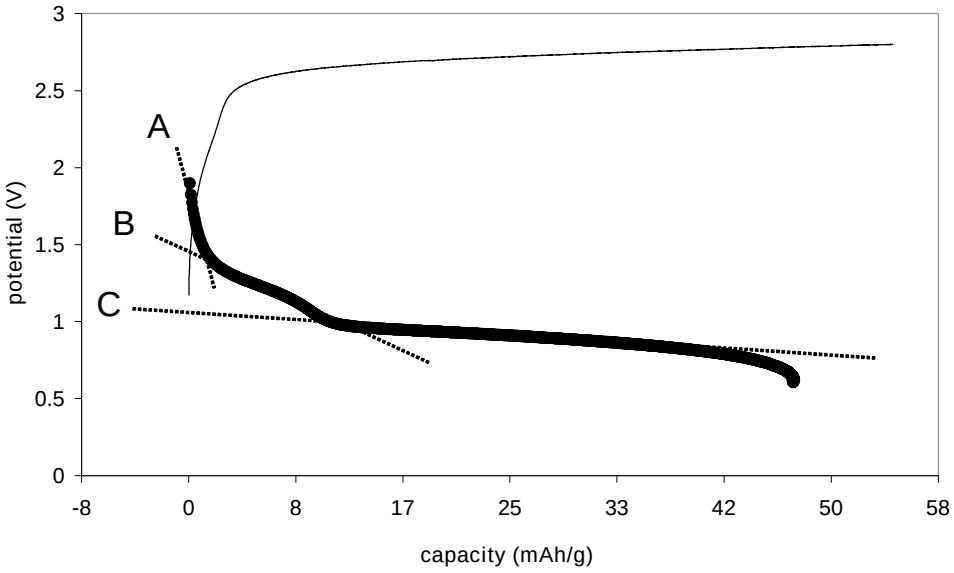

Figure 5.31- Typical charge / discharge curve of a PAn / Fc S 3 PAn / Fc S 3 on orflex carbon fabric in EMITFSI battery. Annotations A, B and C show the effect of distinguishable processes further discussed in the text. The thick line represents a discharge cycle across a 1 k ohm resistor and the thin line represents a charge cycle.

The charge / discharge curve in Figure 5.31 shows excellent battery characteristics with respect to supporting a relatively constant discharge potential. Three processes are apparent in the discharge curve. Process A is most likely due to a capacitive effect of Helmholtz layer formation. Process A is clearly defined in this particular example due to the comparatively large surface area of the substrate (2000 m^2/g), allowing a significant double layer to form.

Process B is likely to be due to the electroactivity of excess $FcSO_3^-$ ions near the polymer surface, which would be easier to access by diffusion than the electroactive population of $FcSO_3^-$ inside of the polymer. The stable plateau (designated process C) would come from a combination of the electroactivity of PAn and $FcHSO_3$. The battery

produced in this configuration had excellent initial charge capacity of 58 mAh/g, which degraded over 60 cycles to 15 mAh/g.

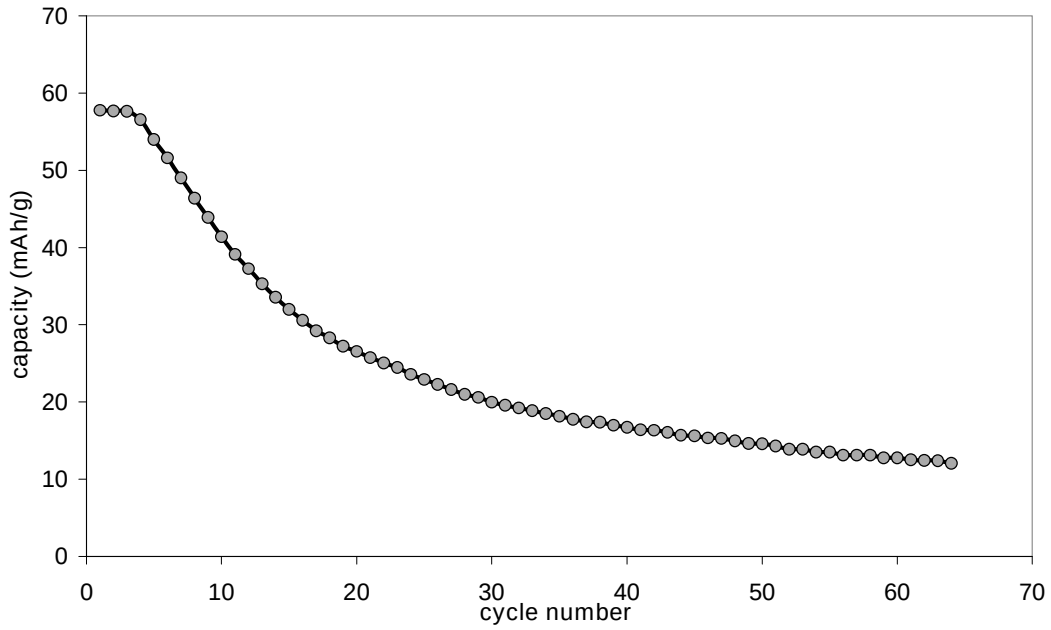

Figure 5.32- Charge capacity as a function of cycle number of PAn / Fc S 3 PAn / Fc S 3 on orflex carbon fabric in EMITFSI battery.

Using Zorflex fabric has therefore improved PAn / $FcHSO_3$ battery performance in comparison to equivalent systems composed of Pt-Ni-Cu-coated polyester or carbon felt. The Zorflex-based battery has the highest initial charge capacity of the systems studied so far in this Chapter, but suffers from poor stability. This can be attributed to the poor mechanical properties of PAn / $FcHSO_3$ and the possibility of leaching $FcHSO_3$ dopant into the bulk battery electrolyte causing loss of its electroactivity and associated charge capacity.

5.3.6 Polypyrrole PEDOT from Pre-formed Dispersion in a Sealed Laminate Device

In designing the next battery, a different strategy was pursued, namely that of a pre-formed polymer dispersion. Standard lamination equipment (as used to protect library cards and photographs) were also employed to assemble the battery cell. Pre-formed polymers in the form of dispersions have many benefits over electrochemical deposition. As we have witnessed in previous designs, the polymers grown directly onto a substrate suffered from uneven deposition, substrate degradation and adherence issues. In addition, the polymers used here should have good physical characteristics that add to the stability of a produced device.

A common conducting polymer dispersion consists of PEDOT doped with polystyrene sulphonate in aqueous medium. This polymer dispersion can be employed in spray coating, spin coating, silk screening and dip coating[185]. The method used to produce this dispersion[186], with PSS as a dispersant and polyelectrolyte, was found to be a simple and effective procedure. Polypyrrole / PSS dispersion was successfully made after slight modification to the synthesis method (altering the monomer and performing polymerisation at 0 to 2° C).

Each polymer was initially tested by cyclic voltammetry on fine stainless steel mesh as depicted in Figure 5.33. Both polymers showed promise for charge storing applications, as evidenced by the large current magnitudes occupying a large region of potential. To construct a battery, stainless steel mesh electrodes were chosen because they have good electrochemical resistance, and good conductivity.

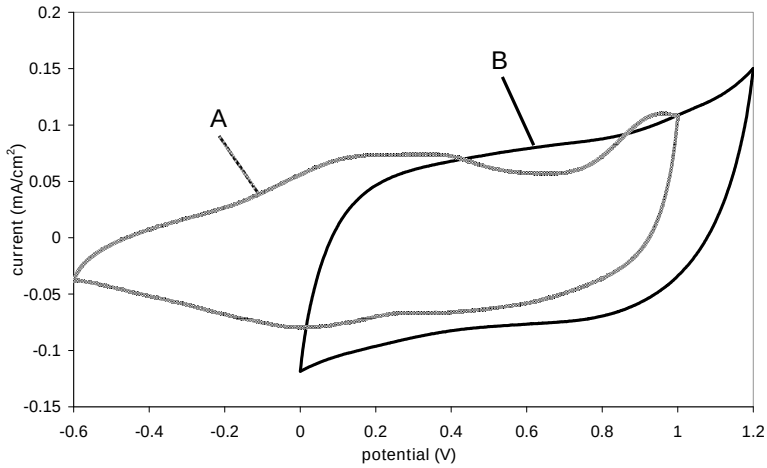

Figure 5.33- CV of A – PED T / PSS and B – PPy / PSS in EMITFSI on fine stainless steel mesh. Third cycle of each scan shown. Scan rate = 200 mV/s.

The battery was charged at various currents up to a potential of 2.0 V, and discharged across a 1 k ohm resistor until a potential of 300 mV was reached. A typical charge / discharge curve is shown in Figure 5.34.

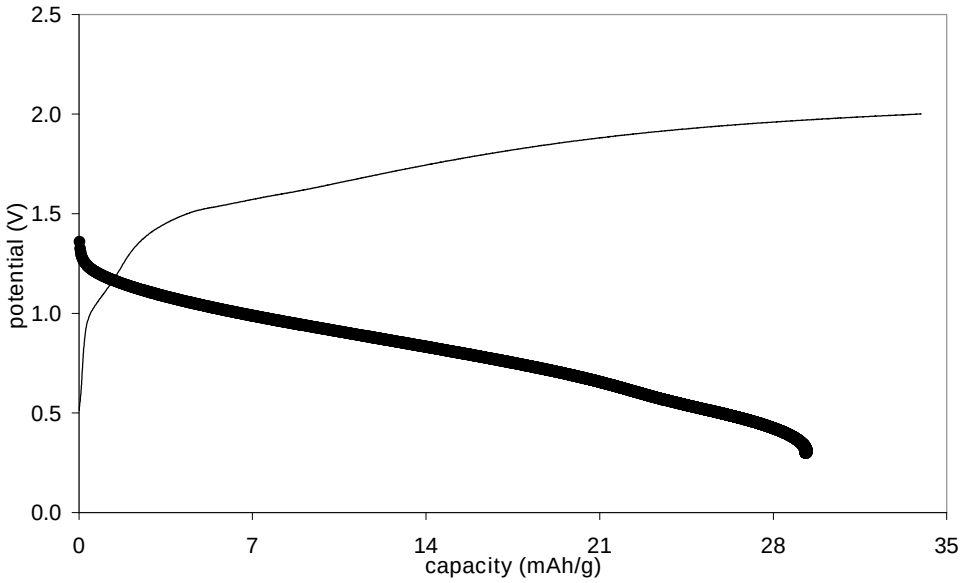

Figure 5.34-Typical charge / discharge curve of a PPy / PSS PED T / PSS on fine stainless steel mesh in EMITFSI battery. The thick line represents a discharge cycle across a 1 k ohm resistor and the thin line represents a charge cycle.

The charge capacity was determined at different charging rates with a pause of 24 hours between each set. The charge capacity of each cycle is depicted in Figure 5.35. Two sets of 1mA charge rates were used, to see if a rest cycle would restore its capacity. From Figure 5.35, it is seen that the initial charge capacity from the second 1 mA charge increased to 46 mAh/g, from a previous value of 42 mAh/g, although the charge capacity degradation was much faster on consecutive cycles.

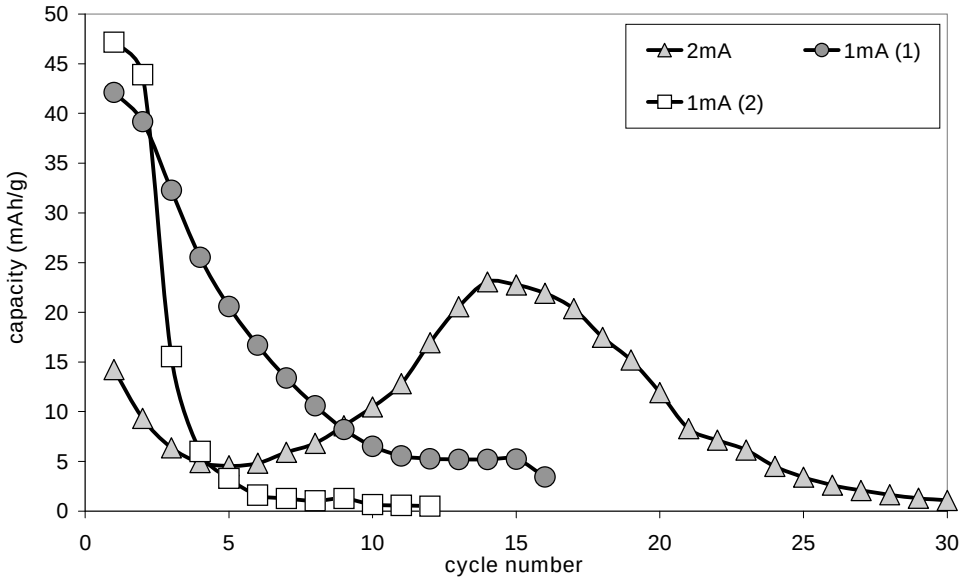

Figure 5.35- Charge capacity Vs cycle number of a PED T / PSS PPy / PSS battery, at different charge rates.

The battery described in this Section was capable of storing charge up to a capacity of 46 mAh/g. A freshly made battery needs to be cycled several times before it reaches its peak capacity at a given charge rate. Also, unlike the PPy : P3MeTh battery constructed in Section 5.2.8, the charge capacity degraded rapidly on consecutive cycles without prolonged resting periods.

After leaving the battery to sit on the shelf for 24 hours, the charge capacity was significantly restored, but upon continuous cycling it degraded rapidly. Such behaviour may be due to slow redox processes within the system that continue once the battery is

not subjected to a load. In this case, the effect would probably occur within each polymer separately, as the charge state of the polymer becomes uniform.

The charge capacity of 46 mAh/g of this device was in excess of the theoretical 21 mAh/g, that should be possible for polypyrrole, but other processes are likely to come into play, such as pronounced non-Faradaic effects. This has been observed in different systems that use nanoparticles, where dominating electrical double layer results in combination with the very high surface area.

5.4 General Conclusions

- The PPy in EMITFSI open-air membrane configuration was found capable of producing a battery comparable to a system utilising the same polymeric materials and solvent based electrolytes[170] of 21 mAh/g. However, the stability of the system, although reasonable could be improved by sealing the cell from the atmosphere.

- A flexible conducting polymer cell was produced consisting of PPy : P3MeTh, EMITFSI electrolyte and fine stainless steel mesh electrodes. A charge capacity of 17 mAh/g was achieved. The system was hermetically sealed preventing atmospheric damage, and it compromised of durable components, without the loss of physical flexibility. Charge capacity, once established did not change over 50 cycles, and represented the most stable of the systems studied.

- The performance of PAn / $FcHSO_3$ on various substrates in battery configurations was also investigated. Fine stainless steel mesh was found to be

an inappropriate electrode material for electrochemical polymerisation, due to its lack of stability in polymer growth solutions on application of polymerisation potential. Ni-Cu-coated polyester, as an electrode material, after further coating with Pt, was found suitable for growth of PAn / $FcHSO_3$. The PAn / $FcHSO_3$ on Pt-Ni-Cu-coated polyester produced a battery with very poor electrochemical cycling stability and a maximum charge capacity of 14 mAh/g.

- Carbon felt and carbon fabric (Zorflex) were investigated as substrates for the PAn / $FcHSO_3$ based PESC systems. The poor conductivity of the substrates required that a large potential be applied to charge the battery to compensate for internal resistance effects. The charge capacity and stability of the carbon felt and Zorflex system had a maximum charge capacity of 58 mAh/g and showed improvements over the Pt-Ni-Cu-coated polyester.

- A battery was constructed using chemically formed dispersions of polypyrrole and PEDOT deposited on fine stainless steel mesh, using EMITFSI as an electrolyte. A maximum charge capacity of 46 mAh/g was observed, which was attributed to both Faradaic and non-Faradaic processes. Although charge capacity degraded rapidly on continuous cycles, the battery recovered its charge capacity if left without external load for 24 hours.

- Of the design types explored, the easiest to build and process control was the system utilising stainless steel mesh and polymer dispersions. Where many other systems exhibited corrosion and un-even growth during polymer deposition, the process of applying the electroactive materials with an airbrush is far more

appealing if such a system is to be scaled for commercialisation. At this point in the developmental stage, the PPy / P3MeTh battery produced the greatest charge capacity, but it is expected that the dispersion-produced battery could also reach the same or better stability as manufacturing procedures are refined.

Although many publications claim very high charge capacities[143] of up to 300 mAh/g for polyaniline, these values are hard to believe. The state-of-the-art commercial lithium polymer batteries hold only 200 mAh/g. An unusually high charge capacity for a conducting polymer battery in a publication can usually be traced back to a misunderstanding of the abstract or title. All too often, the charge capacity refers to the material alone[169,187,188], and not to an actual physical device constructed from it. Where authors actually constructed and tested devices, the charge capacities were much more realistic[170,189] and comparable to the results obtained in this Chapter (*ca.* 20 mAh/g).

5.5 References

[138] Piccolino, Marco. *"The bicentennial of the voltaic battery (1800-2000): The artificial electric organ."* Trends in Neurosciences, 2000 *23*: 147.

[139] Bond, Alan M. *"200 years of practical electroanalytical chemistry: Past, present and future directions illustrated by reference to the on-line, on-stream and off-line determination of trace metals in zinc plant electrolyte by voltammetric and potentiometric techniques."* Analytica Chimica Acta, 1999 *400*: 333.

[140] Stone, Charles and Anne E. Morrison. *"From curiosity to "power to change the world(r)"."* Solid State Ionics, 2002 *152-153*: 1.

[141] Cullen, Bob. *"Global market for industrial lead acid batteries--past, present and future."* Journal of Power Sources, *In Press, Corrected Proof*.

[142] Felix B. Dias, Lambertus Plomp, Jakobert B.J. Veldhuis. *"Trends in polymer electrolytes for secondary lithium batteries."* Journal of Power Sources, 2000 *88*: 169-191.

[143] Petr Nova K, Klaus Mu Ller, K. S. V. Santhanam, Otto Haas. *"Electrochemically active polymers for rechargeable batteries."* Chem. Rev., 1997 *97*: 207-281.

[144] Rydh, Carl Johan and Bo Svard. *"Impact on global metal flows arising from the use of portable rechargeable batteries."* The Science of The Total Environment, 2003 *302*: 167.

[145] E. De Giglio, M.R. Guascito, L. Sabbatini, G. Zambonin. *"Electropolymerization of pyrrole on titanium substrates for the future development of new biocompatible surfaces."* Biomaterials, 2001 *22*: 2609-2616.

[146] S. A. Hashmi, R. J. Latham, R. G. Linford &W. S. Schlindwein. *"Conducting polymer-based electrochemical redox supercapacitors using proton and lithium ion conducting polymer electrolytes."* Polymer International, 1998 *47*: 28-33.

[147] Scrosati, Bruno. *"Conducting polymers: Advanced materials for new design, rechargeable lithium batteries."* Polymer International, 1998 *47*: 50-55.

[148] Gurunathan, K., A. Vadivel Murugan, R. Marimuthu, U. P. Mulik and D. P. Amalnerkar. *"Electrochemically synthesised conducting polymeric materials for applications towards technology in electronics, optoelectronics and energy storage devices."* Materials Chemistry and Physics, 1999 *61*: 173.

[149] Yossef Gofer, Haripada Sarker, Jeffrey G. Killian, Theodore O. Poehler, Peter C. Searson. *"An all-polymer charge storage device."* Appl. Phys. Lett., 1997 *71*: 1582-1584.

[150] Saunier, J., F. Alloin, J. Y. Sanchez and G. Caillon. *"Thin and flexible lithium-ion batteries: Investigation of polymer electrolytes."* Journal of Power Sources, 2003 *119-121*: 454.

[151] Harman, Charles M. Hart, Louis. *"Accelerated life cycle testing and analysis for early failure prediction using two types of lead/acid batteries."* Journal of Power Sources, 1992 *37*.

[152] Ruetschi, Paul. *"Aging mechanisms and service life of lead-acid batteries."* Journal of Power Sources, 2004 *127*: 33-44.

[153] Urquidi-Macdonald, Mirna. Bomberger, Neil A. *"Predicting failure of secondary batteries."* Journal of Power Sources, 1998 *74*: 87-98.

[154] Lu, W. Fadeev, A. G. Qi, B. H. Smela, E. Mattes, B. R. Ding, J. Spinks, G. M. Mazurkiewicz, J. Zhou, D. Z. Wallace, G. G. Macfarlane, D. R. Forsyth, S. A. Forsyth, M. *"Use of ionic liquids for pi-conjugated polymer electrochemical devices."* Science, 2002 *297*: 983-987.

[155] Seddon, K. R. *"Ionic liquids for clean technology."* Journal of Chemical Technology & Biotechnology, 1997 *68*: 351-356.

[156] Brennecke, J. F. and M. A. Stadtherr. *"A course in environmentally conscious chemical process design."* Computers & Chemical Engineering, 2000 *24*: 1375-1380.

[157] Fuchigami, T. and H. Ishii. *"Electroorganic synthesis towards environmentally friendly processes 4. Organic electrolytic reactions in ionic liquids (room temperature molten salts) [japanese]."* Electrochemistry, 2002 *70*: 46-50.

[158] Salazar, Jose and Romano Dorta. *"Pentylpyridinium tribromide. A vapor pressure free room temperature ionic liquid analogue of bromine."* Synlett, 2004: 1318-1320.

[159] Marsh, K. N., A. Deev, A. C. T. Wu, E. Tran and A. Klamt. *"Room temperature ionic liquids as replacements for conventional solvents - a review [review]."* Korean Journal of Chemical Engineering, 2002 *19*: 357-362.

[160] Schafer, T., C. M. Rodrigues, C. A. M. Afonso and J. G. Crespo. *"Selective recovery of solutes from ionic liquids by pervaporation - a novel approach for purification and green processing."* Chemical Communications, 2001: 1622-1623.

[161] Quinn, B. M., Z. F. Ding, R. Moulton and A. J. Bard. *"Novel electrochemical studies of ionic liquids."* Langmuir, 2002 *18*: 1734-1742.

[162] Huddleston, J. G., A. E. Visser, W. M. Reichert, H. D. Willauer, G. A. Broker and R. D. Rogers. *"Characterization and comparison of hydrophilic and hydrophobic room temperature ionic liquids incorporating the imidazolium cation."* Green Chemistry, 2001 *3*: 156-164.

[163] Fuller, J., A. C. Breda and R. T. Carlin. *"Ionic liquid-polymer gel electrolytes from hydrophilic and hydrophobic ionic liquids."* Journal of Electroanalytical Chemistry, 1998 *459*: 29-34.

[164] Skladanowski, A. C., P. Stepnowski, K. Kleszczynski and B. Dmochowska. *"Amp deaminase in vitro inhibition by xenobiotics: A potential molecular method for risk assessment of synthetic nitro- and polycyclic musks, imidazolium ionic liquids and n-glucopyranosyl ammonium salts."* Environmental Toxicology and Pharmacology, 2005 *19*: 291.

[165] Cull, S. G., J. D. Holbrey, V. Vargas-Mora, K. R. Seddon and G. J. Lye. *"Room-temperature ionic liquids as replacements for organic solvents in multiphase bioprocess operations."* Biotechnology & Bioengineering, 2000 *69*: 227-233.

[166] Matsumoto, Michiaki, Kenji Mochiduki and Kazuo Kondo. *"Toxicity of ionic liquids and organic solvents to lactic acid-producing bacteria."* Journal of Bioscience and Bioengineering, 2004 *98*: 344.

[167] Yang, Chunhe, Qingjiang Sun, Jing Qiao and Yongfang Li. *"Ionic liquid doped polymer light-emitting electrochemical cells."* Journal of Physical Chemistry B, 2003 *107*: 12981-12988.

[168] Fung, Y. S. and R. Q. Zhou. *"Room temperature molten salt as medium for lithium battery."* Journal of Power Sources, 1999 *82*: 891-895.

[169] Shan, Dan and Shaolin Mu. *"Electrochemical characteristics of polyaniline synthesized in the presence of ferrocenesulfonic acid."* Synthetic Metals, 2002 *126*: 225.

[170] J. G. Killian, B. M. Coffey, F. Gao, T. O. Poehler, P. C. Searson. *"Polypyrrole composite electrodes in an all-polymer battery system."* Journal of the Electrochemical Society, 1996 *143*: 936-942.

[171] Ahn, Soonho, Youngduk Kim, Kyung Joon Kim, Tae Hyung Kim, Hyungkeun Lee and Myung H. Kim. *"Development of high capacity, high rate lithium ion batteries utilizing metal fiber conductive additives."* Journal of Power Sources, 1999 *81-82*: 896.

[172] Barbic, P. A., L. Binder, S. Voss, F. Hofer and W. Grogger. *"Thin-film zinc/manganese dioxide electrodes based on microporous polymer foils."* Journal of Power Sources, 1999 *79*: 271.

[173] Yazici, M. S., D. Krassowski and J. Prakash. *"Flexible graphite as battery anode and current collector."* Journal of Power Sources, 2005 *141*: 171.

[174] Passerini, Stefano, Jose Mauricio Rosolen and Bruno Scrosati. *"Plasticized carbon electrodes of interest for lithium rocking chair batteries."* Journal of Power Sources, 1993 *45*: 333.

[175] Sweeny, Brendan K. and Dennis G. Peters. *"Cyclic voltammetric study of the catalytic behavior of nickel(i) salen electrogenerated at a glassy carbon electrode in an ionic liquid (1-butyl-3-methylimidazolium tetrafluoroborate, bmim+bf4-)."* Electrochemistry Communications, 2001 *3*: 712-715.

[176] Abbott, Andrew P., Glen Capper, Katy J. Mckenzie, Andrew Glidle and Karl S. Ryder. *"Electropolishing of stainless steels in a choline chloride based ionic liquid: An electrochemical study with surface characterisation using sem and atomic force microscopy."* Physical Chemistry Chemical Physics, 2006 *8*: 4214-4221.

[177] Abbott, Andrew P., Glen Capper, Katy J. Mckenzie and Karl S. Ryder. *"Voltammetric and impedance studies of the electropolishing of type 316 stainless steel in a choline chloride based ionic liquid."* Electrochimica Acta, 2006 *51*: 4420-4425.

[178] Abbott Andrew, P., Glen Capper, J. Mckenzie Katy, Andrew Glidle and S. Ryder Karl. *"Electropolishing of stainless steels in a choline chloride based ionic liquid: An electrochemical study with surface characterisation using sem and atomic force microscopy."* Physical chemistry chemical physics: PCCP, 2006 *8*: 4214-21.

Bennett, Matthew, Donald Leo, Gordon Wallace and Geoff Spinks (2005). Ionic solvents with good electrochem. Stability, low viscosity, and low vapor pressure used in ionic polymer transducers, sensors and actuators. Application: US US, (USA). 19 pp.

[180] Zhou, Dezhi, Geoffrey M. Spinks, Gordon G. Wallace, Churat Tiyapiboonchaiya, Douglas R. Macfarlane, Maria Forsyth and Jiazeng Sun. *"Solid state actuators based on polypyrrole and polymer-in-ionic liquid electrolytes."* Electrochimica Acta, 2003 *48*: 2355.

[181] Mazeikiene, R. and A. Malinauskas. *"Kinetics of the electrochemical degradation of polypyrrole."* Polymer Degradation and Stability, 2002 *75*: 255.

[182] Liu, Yu-Chuan and Bing-Joe Hwang. *"Enhancement of conductivity stability of polypyrrole films modified by valence copper and polyethylene oxide in an oxygen atmosphere."* Thin Solid Films, 2000 *360*: 1.

[183] Novak, Petr. *"Limitations of polypyrrole synthesis in water and their causes."* Electrochimica Acta, 1992 *37*: 1227.

[184] Ryu, Kwang Sun, Kwang Man Kim, Seong-Gu Kang, Jinsoo Joo and Soon Ho Chang. *"Comparison of lithium//polyaniline secondary batteries with different dopants of hcl and lithium ionic salts."* Journal of Power Sources, 2000 *88*: 197.

[185] L. Groenendaal, F. Jonas D. Freitag H. Pielartzik J. R. Reynolds. *"Poly(3,4-ethylenedioxythiophene) and its derivatives: Past, present, and future."* Advanced Materials, 2000 *12*: 481-494.

[186] Louwet, F., L. Groenendaal, J. Dhaen, J. Manca, J. Van Luppen, E. Verdonck and L. Leenders. *"Pedot/pss: Synthesis, characterization, properties and applications."* Synthetic Metals, 2003 *135-136*: 115.

[187] Sung, Joo-Hwan, Se-Joon Kim and Kun-Hong Lee. *"Preparation of compact polyaniline films: Electrochemical synthesis using agar gel template and charge-storage applications."* Journal of Power Sources, 2004 *126*: 258.

[188] Veeraraghavan, Basker, Jason Paul, Bala Haran and Branko Popov. *"Study of polypyrrole graphite composite as anode material for secondary lithium-ion batteries."* Journal of Power Sources, 2002 *109*: 377.

[189] K.S. Hwang, C.W. Lee, T.H. Yoon, Y.S. Son. *"Fabrication and characteristics of a composite cathode of sulfonated polyaniline and ramsdellite mno for a new rechargeable lithium polymer battery."* Journal of Power Sources, 1999 *79*: 225-230.

APPENDIX

The results contained herein refer to the data obtained from Chapter 4, Section 4.3.3 and are the result of parametric decomposition of the CVs of P3PFTh grown and cycled in various electrolytes.

Peak Height (mA/cm^2)

Process	Growth Electrolyte	Cycling Electrolyte													
n_{ox}		$BMIBF_4$	$BMIPF_6$	cetTFSI	$EMIPF_6$	EMITFSI	$TBABF_4$	$TBACIO_4$	$TBAPF_6$	$TEABF_4$	TEATFSI	$TMACIO_4$	$PureBMIBF_4$	$PureBMIPF_6$	PureEMITFSI
	$BMIBF_4$	13.6763	13.7888	9.2633	9.8188	13.8635	7.0593	n/a	7.3205	20.3395	23.8920	1.6405	n/a	n/a	n/a
	$BMIPF_6$	6.1240	6.8895	5.2570	7.3550	7.3550	8.5085	10.9010	9.4145	11.7990	13.7100	6.1695	n/a	n/a	n/a
	cetTFSI	11.4170	11.4170	8.0905	11.2260	11.2860	10.8405	7.9245	13.6570	18.3100	12.8870	7.0840	n/a	n/a	n/a
	$EMIPF_6$	12.8080	12.8080	9.0075	10.6015	3.0765	15.7605	10.2660	7.1550	11.3165	16.8410	9.0805	n/a	n/a	n/a
	EMITFSI	9.9060	14.0335	10.6575	11.6415	14.3280	12.7280	7.0035	15.5635	23.6730	21.6120	6.6885	n/a	n/a	n/a
	$TBABF_4$	4.1730	8.2005	0.7355	5.4330	3.5565	12.7395	7.3515	8.1680	8.1045	10.6470	10.6470	n/a	n/a	n/a
	$TBACIO_4$	16.2090	13.5075	13.4325	12.1170	14.7135	16.7325	1.1155	21.9765	23.4715	20.5290	1.1405	n/a	n/a	n/a
	$TBAPF_6$	9.7955	9.7955	11.3680	7.6765	10.3415	13.6085	9.6060	10.7170	12.2480	12.2480	6.1240	n/a	n/a	n/a
	$TEABF_4$	15.8480	12.6480	1.5810	11.7715	11.7715	n/a	n/a	6.5835	19.1790	18.8190	n/a	n/a	n/a	n/a
	TEATFSI	10.0155	10.0155	9.4860	7.1145	7.1145	9.4860	10.6015	13.8635	15.4945	18.7565	6.0585	n/a	n/a	n/a
	$TMACIO_4$	14.2575	12.3825	13.9280	7.8345	13.6080	7.8050	n/a	14.1115	21.7100	23.2155	6.6330	n/a	n/a	n/a
	PureEMITFSI	11.8100	9.6915	13.3875	10.0705	11.7075	14.0910	13.4505	15.3720	18.4730	18.4730	10.8880	n/a	n/a	n/a
p_{ox}		$BMIBF_4$	$BMIPF_6$	cetTFSI	$EMIPF_6$	EMITFSI	$TBABF_4$	$TBACIO_4$	$TBAPF_6$	$TEABF_4$	TEATFSI	$TMACIO_4$	$PureBMIBF_4$	$PureBMIPF_6$	PureEMITFSI
	$BMIBF_4$	28.2336	28.7153	27.3135	35.0880	32.2400	32.2560	27.0640	29.5320	30.8160	27.1170	24.3320	1.9125	0.4272	1.9071
	$BMIPF_6$	20.6720	19.3830	17.0950	17.3580	19.2660	20.5530	12.8790	15.6510	22.2720	16.4140	16.4000	n/a	2.7878	n/a
	cetTFSI	27.2080	27.2080	24.7080	29.4030	27.5760	27.5760	22.6100	20.3490	22.8690	22.1650	21.2100	8.2656	5.2416	10.9188
	$EMIPF_6$	24.6120	23.3280	24.0100	27.0710	40.1120	20.5640	21.8890	31.2800	37.6360	28.5390	18.2250	5.4999	4.9290	n/a
	EMITFSI	36.3720	38.0700	33.0220	42.2180	34.5540	28.7250	40.6600	36.8940	35.4400	34.1600	28.3140	6.0334	7.5348	14.4900
	$TBABF_4$	22.8420	23.8140	10.6490	19.4110	15.7170	21.6240	27.0400	22.1760	35.9370	19.0240	19.0240	n/a	1.3080	n/a
	$TBACIO_4$	33.3840	30.6600	31.7100	33.4320	30.8040	29.9520	29.2600	36.7780	37.6550	35.3340	27.5880	2.1450	5.5680	1.5504
	$TBAPF_6$	27.5880	25.9160	26.7520	22.9320	30.2250	23.7460	28.9100	32.6270	33.3360	25.9280	25.5450	n/a	5.2992	3.8916
	$TEABF_4$	31.0230	33.0480	10.4500	38.0380	27.1810	30.0050	30.0050	28.9100	29.6100	32.1480	24.0120	5.9596	0.5138	2.6082
	TEATFSI	27.0400	20.9560	25.1140	26.9280	28.5600	28.5600	27.3360	31.8960	34.9970	29.5320	26.0680	n/a	n/a	n/a
	$TMACIO_4$	27.7760	24.9570	29.0160	33.0220	27.6330	26.7270	24.8320	37.1840	32.6160	28.3520	30.6000	3.5574	1.1728	2.9477
	PureEMITFSI	26.0360	28.2080	27.7830	28.1700	23.3160	21.3200	19.7680	19.2080	30.6240	20.2370	21.5730	12.0428	6.8226	16.2006

Peak Height (mA/cm^2)

Process	Growth Electrolyte	Cycling Electrolyte													
n_{red}		$BMIBF_4$	$BMIPF_6$	cetTFSI	$EMIPF_6$	EMITFSI	$TBABF_4$	$TBACIO_4$	$TBAPF_6$	$TEABF_4$	TEATFSI	$TMACIO_4$	$PureBMIBF_4$	$PureBMIPF_6$	PureEMITFSI
	$BMIBF_4$	28.9358	28.9358	19.3572	31.0752	32.6592	17.2752	17.2752	18.3552	28.1432	31.5732	15.2892	n/a	n/a	n/a
	$BMIPF_6$	24.6432	24.9872	11.4432	11.4432	25.2472	16.3812	12.9332	16.6222	23.3772	20.9572	8.4272	n/a	n/a	n/a
	cetTFSI	27.3122	27.1152	15.9432	25.4592	26.5932	16.6842	11.5872	14.6652	23.2832	27.1352	14.9872	n/a	n/a	n/a
	$EMIPF_6$	28.0602	25.6312	19.4552	33.0372	20.5042	17.2992	14.4992	24.0672	21.9032	30.4112	14.9742	n/a	n/a	n/a
	EMITFSI	26.7582	30.2802	19.0212	34.9112	28.0112	13.8882	15.6832	19.8592	33.8672	32.4032	17.2172	n/a	n/a	n/a
	$TBABF_4$	24.8542	21.3902	1.5092	24.4902	24.4902	20.4152	18.3872	21.0912	20.9712	21.6832	21.6832	n/a	n/a	n/a
	$TBACIO_4$	34.0632	32.5242	28.4202	33.6472	33.6472	21.0372	2.7602	24.7672	31.3632	35.9142	7.2432	n/a	n/a	n/a
	$TBAPF_6$	32.3972	32.3972	20.7832	26.4882	29.5212	19.6612	17.3052	25.2672	25.2672	25.2672	17.9242	n/a	n/a	n/a
	$TEABF_4$	41.4652	41.4652	10.0772	39.8272	39.8272	12.0032	7.2912	17.8432	27.8142	31.4382	14.6772	n/a	n/a	n/a
	TEATFSI	27.0392	21.2182	21.2182	26.4812	26.4812	18.5592	17.6712	23.6412	27.0912	31.9872	15.4732	n/a	n/a	n/a
	$TMACIO_4$	37.1732	32.7952	20.6272	33.2992	31.4072	14.2662	5.4002	20.7152	33.4022	30.7632	11.9952	n/a	n/a	n/a
	PureEMITFSI	29.4882	33.2672	20.9412	33.0252	25.9722	23.3312	21.0602	20.2912	27.6232	26.3572	17.1292	n/a	n/a	n/a
p_{red}		$BMIBF_4$	$BMIPF_6$	cetTFSI	$EMIPF_6$	EMITFSI	$TBABF_4$	$TBACIO_4$	$TBAPF_6$	$TEABF_4$	TEATFSI	$TMACIO_4$	$PureBMIBF_4$	$PureBMIPF_6$	PureEMITFSI
	$BMIBF_4$	16.7206	15.2277	17.6172	15.9572	18.0692	21.7512	23.0652	16.5072	21.4292	18.2972	18.3112	1.3816	0.3014	1.1758
	$BMIPF_6$	8.1592	8.3472	9.8612	8.3472	7.1232	12.0032	11.0352	9.0992	12.4872	9.6632	10.1472	n/a	1.0822	n/a
	cetTFSI	8.7912	8.7912	12.6312	9.0992	9.0992	11.9592	12.5632	8.9392	9.3832	7.9632	12.8592	3.9967	4.6990	6.6102
	$EMIPF_6$	1.8520	1.8590	1.8590	1.8590	1.8590	1.8590	1.8590	1.8590	1.8590	1.8350	1.8350	n/a	n/a	n/a
	EMITFSI	13.7332	15.4012	18.9152	17.3732	14.2892	23.1572	25.2672	20.1392	20.7952	20.4672	17.1312	2.7472	4.7336	7.4496
	$TBABF_4$	7.9872	10.2752	2.1392	9.6152	5.9792	11.2812	14.7212	11.0112	16.8072	7.4892	7.4892	n/a	0.8636	n/a
	$TBACIO_4$	20.0192	16.7552	17.9872	16.1392	17.1872	18.7592	22.6972	20.7952	20.7952	20.7152	23.4112	1.5680	4.6848	1.3888
	$TBAPF_6$	6.1272	7.0312	15.1232	8.6152	11.6312	15.1032	13.8012	16.2532	13.5292	11.3632	14.2932	n/a	3.1164	1.5364
	$TEABF_4$	18.7252	16.0272	9.9792	18.5472	16.7832	23.2092	23.2092	20.7532	20.7532	19.6512	22.2272	2.7832	0.5024	1.7360
	TEATFSI	13.7712	11.3552	15.6792	11.4552	12.7872	14.5992	17.0632	15.4012	17.0632	17.0632	14.8472	n/a	n/a	n/a
	$TMACIO_4$	18.1792	14.7212	17.6172	18.1712	16.7072	20.1912	22.3392	22.3392	18.5952	16.8072	18.4212	3.0060	1.1304	2.3184
	PureEMITFSI	11.1552	8.8032	11.9952	10.6032	10.6032	10.8992	13.5192	15.3912	17.8872	12.4352	16.7912	7.1736	4.5864	9.6632

Peak Current Potential (V)

Process	Growth Electrolyte	Cycling Electrolyte													
n_{ox}		$BMIBF_4$	$BMIPF_6$	cetTFSI	$EMIPF_6$	EMITFSI	$TBABF_4$	$TBACIO_4$	$TBAPF_6$	$TEABF_4$	TEATFSI	$TMACIO_4$	$PureBMIBF_4$	$PureBMIPF_6$	PureEMITFSI
	$BMIBF_4$	1.6700	1.6600	1.6000	1.7000	1.6800	1.6000	1.6000	1.6000	1.6300	1.6300	1.6700	n/a	n/a	n/a
	$BMIPF_6$	1.6700	1.6700	1.6700	1.6700	1.6700	1.6700	1.7000	1.7000	1.6600	1.6800	1.6800	n/a	n/a	n/a
	cetTFSI	1.6700	1.6700	1.6400	1.6700	1.6700	1.6200	1.5700	1.6300	1.6500	1.6500	1.6800	n/a	n/a	n/a
	$EMIPF_6$	1.6600	1.6600	1.6400	1.6500	1.6500	1.6300	1.6300	1.6400	1.6600	1.6600	1.6600	n/a	n/a	n/a
	EMITFSI	1.6600	1.6600	1.6000	1.6600	1.6600	1.5800	1.5800	1.5700	1.6300	1.6400	1.6600	n/a	n/a	n/a
	$TBABF_4$	1.6800	1.6800	1.8200	1.6700	1.6800	1.7000	1.7000	1.6900	1.6700	1.6700	1.6700	n/a	n/a	n/a
	$TBACIO_4$	1.6500	1.6600	1.6000	1.6700	1.6700	1.6100	1.6100	1.5900	1.6300	1.6300	1.6300	n/a	n/a	n/a
	$TBAPF_6$	1.6600	1.6600	1.6400	1.6900	1.6700	1.6400	1.6400	1.6400	1.6600	1.6600	1.6600	n/a	n/a	n/a
	$TEABF_4$	1.6400	1.6700	1.6300	1.6900	1.6900	1.6900	1.6900	1.5900	1.6200	1.6500	1.6500	n/a	n/a	n/a
	TEATFSI	1.6700	1.6700	1.6100	1.6900	1.6900	1.6400	1.6100	1.6200	1.6500	1.6500	1.6700	n/a	n/a	n/a
	$TMACIO_4$	1.6700	1.6700	1.6100	1.6800	1.6700	1.5900	1.5900	1.6000	1.6500	1.6300	1.6700	n/a	n/a	n/a
	PureEMITFSI	1.6700	1.6600	1.6600	1.6600	1.6600	1.6700	1.6500	1.6600	1.6500	1.6500	1.6600	n/a	n/a	n/a
p_{ox}		$BMIBF_4$	$BMIPF_6$	cetTFSI	$EMIPF_6$	EMITFSI	$TBABF_4$	$TBACIO_4$	$TBAPF_6$	$TEABF_4$	TEATFSI	$TMACIO_4$	$PureBMIBF_4$	$PureBMIPF_6$	PureEMITFSI
	$BMIBF_4$	1.0600	1.0800	1.0600	1.1000	1.0500	1.0700	1.0900	1.0600	1.0600	1.0500	1.1500	1.0900	1.3200	1.2300
	$BMIPF_6$	1.0300	1.0200	1.0200	0.9900	1.0000	1.0900	1.0000	1.0400	1.0500	1.0100	1.1300	n/a	1.4600	n/a
	cetTFSI	1.0400	1.0400	1.0400	1.0400	1.0400	1.0400	1.0100	1.0100	1.0200	1.0400	1.1000	1.1700	1.3600	1.1300
	$EMIPF_6$	1.0000	1.0200	1.0300	1.0300	1.1800	1.0300	1.0200	1.0400	1.1400	1.0300	1.0900	1.2700	1.2400	n/a
	EMITFSI	1.1100	1.0700	1.0700	1.0700	1.0600	1.0500	1.0800	1.0400	1.0400	1.0400	1.1300	1.2200	1.3200	1.3100
	$TBABF_4$	1.0400	1.0500	1.1100	1.0300	1.0300	1.0500	1.1200	1.0400	1.1600	1.0400	1.0400	n/a	1.1300	n/a
	$TBACIO_4$	1.0500	1.0600	1.0500	1.0800	1.0400	1.0500	1.0800	1.0400	1.0800	1.0600	1.1700	1.0800	1.4400	1.0900
	$TBAPF_6$	1.0400	1.1300	1.0200	1.1400	1.0400	1.0200	1.0500	1.0500	1.0700	1.0500	1.1100	n/a	1.2100	1.2900
	$TEABF_4$	1.0800	1.0900	1.0300	1.1000	1.0700	1.0900	1.0900	1.0600	1.0600	1.0900	1.1700	1.3900	0.9800	1.1600
	TEATFSI	1.0100	1.0600	1.0300	1.0600	1.0900	1.0900	1.0400	1.0500	1.0800	1.0500	1.1400	n/a	n/a	n/a
	$TMACIO_4$	1.0400	1.0600	1.0400	1.0900	1.0400	1.0500	1.0700	1.0700	1.0400	1.0500	1.1500	1.1200	1.1700	1.3000
	PureEMITFSI	1.0200	1.0200	1.0100	1.0100	1.0100	1.0100	1.0000	1.0300	1.0700	1.0000	1.0500	1.3100	1.3100	1.0400

Peak Current Potential (V)

Process	Growth Electrolyte	Cycling Electrolyte													
n_{red}		$BMIBF_4$	$BMIPF_6$	cetTFSI	$EMIPF_6$	EMITFSI	$TBABF_4$	$TBACIO_4$	$TBAPF_6$	$TEABF_4$	TEATFSI	$TMACIO_4$	$PureBMIBF_4$	$PureBMIPF_6$	PureEMITFSI
	$BMIBF_4$	1.8270	1.8270	1.8450	1.8450	1.8660	1.8390	1.8390	1.7770	1.8480	1.8480	1.8520	n/a	n/a	n/a
	$BMIPF_6$	1.8520	1.8590	1.8590	1.8590	1.8590	1.8590	1.8590	1.8590	1.8590	1.8350	1.8350	n/a	n/a	n/a
	cetTFSI	1.8280	1.8280	1.8280	1.8280	1.8280	1.8210	1.7400	1.7680	1.8450	1.8580	1.8580	n/a	n/a	n/a
	$EMIPF_6$	1.8340	1.8340	1.8340	1.8520	1.8520	1.8390	1.8390	1.8570	1.8600	1.8680	1.8570	n/a	n/a	n/a
	EMITFSI	1.8570	1.8410	1.8410	1.8590	1.8490	1.7660	1.8630	1.8040	1.8480	1.8720	1.9140	n/a	n/a	n/a
	$TBABF_4$	1.8660	1.8870	1.8870	1.8890	1.8890	1.8560	1.9050	1.8570	1.8870	1.8680	1.8680	n/a	n/a	n/a
	$TBACIO_4$	1.8540	1.8660	1.8200	1.8470	1.8470	1.8250	1.8250	1.8250	1.8510	1.8680	2.0000	n/a	n/a	n/a
	$TBAPF_6$	1.9010	1.9010	1.8310	1.8700	1.8760	1.8400	1.8550	1.8550	1.8550	1.8550	1.8970	n/a	n/a	n/a
	$TEABF_4$	1.8970	1.8970	1.8160	1.8710	1.8710	1.7600	1.9740	1.7880	1.8330	1.8720	1.9310	n/a	n/a	n/a
	TEATFSI	1.7910	1.7680	1.7680	1.8500	1.8500	1.8400	1.8280	1.8560	1.8560	1.8560	1.8820	n/a	n/a	n/a
	$TMACIO_4$	1.8950	1.8800	1.8580	1.8740	1.8740	1.7770	1.7770	1.8200	1.8720	1.8720	1.8920	n/a	n/a	n/a
	PureEMITFSI	1.8390	1.8730	1.8730	1.8650	1.8650	1.8550	1.8550	1.8350	1.8450	1.8450	1.8890	n/a	n/a	n/a
p_{red}		$BMIBF_4$	$BMIPF_6$	cetTFSI	$EMIPF_6$	EMITFSI	$TBABF_4$	$TBACIO_4$	$TBAPF_6$	$TEABF_4$	TEATFSI	$TMACIO_4$	$PureBMIBF_4$	$PureBMIPF_6$	PureEMITFSI
	$BMIBF_4$	0.7975	0.7900	0.7625	0.7925	0.8150	0.7925	0.7825	0.7775	0.7950	0.7700	0.7275	0.7500	0.7950	0.7950
	$BMIPF_6$	0.8550	0.8225	0.7800	0.8200	0.8200	0.8200	0.8200	0.8200	0.8200	0.8200	0.7925	n/a	0.6750	n/a
	cetTFSI	0.7925	0.7925	0.7900	0.7900	0.7900	0.8125	0.7725	0.7725	0.7925	0.7500	0.7275	0.7400	0.2925	0.6675
	$EMIPF_6$	0.4078	0.4826	0.5008	0.5008	0.3898	0.3268	0.5420	0.3956	0.3786	0.4654	0.4016	n/a	0.5008	n/a
	EMITFSI	0.8350	0.8400	0.8025	0.8375	0.8200	0.8100	0.8025	0.8025	0.8025	0.7825	0.7400	0.7425	0.5025	0.6550
	$TBABF_4$	0.8475	0.8700	0.8425	0.8425	0.8425	0.8425	0.8350	0.8175	0.8450	0.8150	0.8150	n/a	0.7475	n/a
	$TBACIO_4$	0.7925	0.7925	0.7600	0.7900	0.7600	0.7900	0.7825	0.7825	0.7900	0.7775	0.7200	0.8000	0.2925	0.7625
	$TBAPF_6$	0.8150	0.8500	0.7700	0.8225	0.8225	0.8275	0.8275	0.8500	0.8600	0.8425	0.7700	n/a	0.6125	0.7600
	$TEABF_4$	0.8175	0.8175	0.8175	0.8175	0.8175	0.8175	0.8175	0.8025	0.8025	0.8050	0.7625	0.7800	0.7350	0.7675
	TEATFSI	0.7975	0.7975	0.7650	0.8325	0.8325	0.8625	0.8225	0.8425	0.8275	0.7925	0.7925	n/a	n/a	n/a
	$TMACIO_4$	0.8325	0.7950	0.7725	0.8125	0.7800	0.8025	0.7750	0.7950	0.8150	0.7575	0.7575	0.7050	0.6250	0.7450
	PureEMITFSI	0.7575	0.7550	0.7450	0.7525	0.7525	0.7800	0.7700	0.8050	0.8050	0.7600	0.7300	0.6550	0.6075	0.7475

Peak Width at Half Height (V)

Process	Growth Electrolyte	Cycling Electrolyte													
n_{ox}		$BMIBF_4$	$BMIPF_6$	cetTFSI	$EMIPF_6$	EMITFSI	$TBABF_4$	$TBACIO_4$	$TBAPF_6$	$TEABF_4$	TEATFSI	$TMACIO_4$	$PureBMIBF_4$	$PureBMIPF_6$	PureEMITFSI
	$BMIBF_4$	0.1446	0.1434	0.1636	0.1678	0.1616	0.1586	0.0002	0.1980	0.1232	0.1324	0.0804	n/a	n/a	n/a
	$BMIPF_6$	0.1722	0.1722	0.3508	0.1792	0.1792	0.2632	0.2658	0.2658	0.2010	0.1922	0.1922	n/a	n/a	n/a
	cetTFSI	0.1616	0.1616	0.1792	0.1408	0.1402	0.1338	0.1496	0.1352	0.1440	0.1432	0.1488	n/a	n/a	n/a
	$EMIPF_6$	0.1646	0.1646	0.2194	0.1616	0.1286	0.1756	0.1540	0.1842	0.1514	0.1722	0.1596	n/a	n/a	n/a
	EMITFSI	0.1596	0.1596	0.1854	0.1472	0.1472	0.1656	0.1318	0.1440	0.1448	0.1464	0.1380	n/a	n/a	n/a
	$TBABF_4$	0.1894	0.1768	0.1792	0.1456	0.1112	0.1966	0.2330	0.2580	0.1464	0.1732	0.1732	n/a	n/a	n/a
	$TBACIO_4$	0.1464	0.1464	0.1472	0.1522	0.1522	0.1182	0.1182	0.1380	0.1292	0.1156	0.1156	n/a	n/a	n/a
	$TBAPF_6$	0.1480	0.1480	0.1854	0.2232	0.1656	0.1646	0.1646	0.1722	0.1722	0.1722	0.1722	n/a	n/a	n/a
	$TEABF_4$	0.1330	0.1666	0.1666	0.1456	0.1456	0.0002	0.0002	0.1402	0.1236	0.1260	0.0002	n/a	n/a	n/a
	TEATFSI	0.1448	0.1448	0.1666	0.1666	0.1666	0.1666	0.1616	0.1616	0.1616	0.1616	0.1522	n/a	n/a	n/a
	$TMACIO_4$	0.1386	0.1596	0.1514	0.1514	0.1550	0.1688	0.0002	0.1214	0.1214	0.1192	0.1192	n/a	n/a	n/a
	PureEMITFSI	0.2232	0.1768	0.2460	0.1440	0.1688	0.2058	0.2058	0.2058	0.1854	0.1854	0.1936	n/a	n/a	n/a
p_{ox}		$BMIBF_4$	$BMIPF_6$	cetTFSI	$EMIPF_6$	EMITFSI	$TBABF_4$	$TBACIO_4$	$TBAPF_6$	$TEABF_4$	TEATFSI	$TMACIO_4$	$PureBMIBF_4$	$PureBMIPF_6$	PureEMITFSI
	$BMIBF_4$	0.3228	0.3362	0.3352	0.3228	0.3268	0.2940	0.3310	0.3078	0.3078	0.3352	0.4276	0.3512	0.3700	0.2694
	$BMIPF_6$	0.4078	0.4826	0.5008	0.5008	0.3898	0.3268	0.5420	0.3956	0.3786	0.4654	0.4016	n/a	0.5008	n/a
	cetTFSI	0.3680	0.3680	0.3786	0.3628	0.3440	0.3440	0.4078	0.4078	0.3628	0.3268	0.4348	0.4590	0.7238	0.3908
	$EMIPF_6$	0.4496	0.4574	0.3840	0.5206	0.3580	0.3396	0.3190	0.3580	0.3396	0.2908	0.5420	0.4526	0.4250	n/a
	EMITFSI	0.3042	0.3114	0.3152	0.3152	0.2974	0.3440	0.3078	0.2786	0.2974	0.2700	0.3628	0.4236	0.5228	0.4772
	$TBABF_4$	0.3114	0.3486	0.2846	0.3190	0.3268	0.3228	0.3898	0.4574	0.3628	0.4016	0.4016	n/a	0.4028	n/a
	$TBACIO_4$	0.3078	0.3008	0.2908	0.3310	0.2908	0.2816	0.3152	0.2544	0.2974	0.2908	0.3628	0.4054	0.8232	0.4078
	$TBAPF_6$	0.3628	0.3152	0.3152	0.4826	0.3268	0.3440	0.3190	0.3190	0.2846	0.2846	0.3352	n/a	0.5146	0.7006
	$TEABF_4$	0.3440	0.3228	0.3152	0.3152	0.3732	0.3732	0.3732	0.3190	0.3114	0.3114	0.3786	0.4156	0.2666	0.4066
	TEATFSI	0.3898	0.3898	0.3042	0.3228	0.3228	0.3228	0.3228	0.2974	0.2974	0.3078	0.3840	n/a	n/a	n/a
	$TMACIO_4$	0.2940	0.3114	0.2816	0.3152	0.2908	0.2908	0.3396	0.2940	0.2908	0.2974	0.3228	0.4276	0.5290	0.6014
	PureEMITFSI	0.4654	0.4016	0.3840	0.4208	0.3786	0.4016	0.3732	0.3840	0.3786	0.3190	0.3114	0.4276	0.4808	0.3268

Peak Width at Half Height (V)

Process	Growth Electrolyte	Cycling Electrolyte													
n_{red}		$BMIBF_4$	$BMIPF_6$	cetTFSI	$EMIPF_6$	EMITFSI	$TBABF_4$	$TBACIO_4$	$TBAPF_6$	$TEABF_4$	TEATFSI	$TMACIO_4$	$PureBMIBF_4$	$PureBMIPF_6$	PureEMITFSI
	$BMIBF_4$	0.2800	0.2800	0.4654	0.2646	0.3486	0.2700	0.2700	0.2756	0.2594	0.2646	0.2362	n/a	n/a	n/a
	$BMIPF_6$	0.3228	0.3396	0.4420	0.4420	0.3152	0.3008	0.4420	0.3440	0.3628	0.3042	0.2876	n/a	n/a	n/a
	cetTFSI	0.2672	0.2448	0.4826	0.2816	0.2646	0.3268	0.3228	0.3628	0.3078	0.3078	0.2672	n/a	n/a	n/a
	$EMIPF_6$	0.3352	0.3310	0.4496	0.3486	0.2018	0.4142	0.3580	0.3580	0.3152	0.2876	0.3114	n/a	n/a	n/a
	EMITFSI	0.2728	0.2846	0.3352	0.2280	0.2700	0.4496	0.3898	0.3078	0.2700	0.2700	0.2786	n/a	n/a	n/a
	$TBABF_4$	0.3042	0.3042	0.3840	0.3840	0.3840	0.3898	0.3898	0.3898	0.3228	0.2940	0.2940	n/a	n/a	n/a
	$TBACIO_4$	0.2568	0.2568	0.2568	0.2404	0.2404	0.3532	0.3532	0.3532	0.2496	0.2620	0.2620	n/a	n/a	n/a
	$TBAPF_6$	0.3310	0.3310	0.4208	0.3352	0.3008	0.3310	0.3152	0.2940	0.2940	0.2940	0.3190	n/a	n/a	n/a
	$TEABF_4$	0.3190	0.3190	0.3190	0.2594	0.2594	0.5312	0.5312	0.4016	0.2908	0.2908	0.2908	n/a	n/a	n/a
	TEATFSI	0.2846	0.3440	0.3440	0.2756	0.2756	0.3152	0.3310	0.3310	0.3228	0.3228	0.3440	n/a	n/a	n/a
	$TMACIO_4$	0.3310	0.3310	0.4496	0.2786	0.2786	0.3268	0.3268	0.3078	0.2974	0.3228	0.3228	n/a	n/a	n/a
	PureEMITFSI	0.3190	0.3580	0.3486	0.3008	0.3114	0.3580	0.3840	0.3532	0.2786	0.2620	0.2876	n/a	n/a	n/a
p_{red}		$BMIBF_4$	$BMIPF_6$	cetTFSI	$EMIPF_6$	EMITFSI	$TBABF_4$	$TBACIO_4$	$TBAPF_6$	$TEABF_4$	TEATFSI	$TMACIO_4$	$PureBMIBF_4$	$PureBMIPF_6$	PureEMITFSI
	$BMIBF_4$	0.2372	0.2276	0.2378	0.2296	0.2902	0.1926	0.1702	0.1820	0.2078	0.2146	0.1354	0.4196	0.4196	0.3182
	$BMIPF_6$	0.3036	0.2968	0.2378	0.2968	0.3108	0.2722	0.2722	0.2722	0.2722	0.2564	0.2182	n/a	0.4066	n/a
	cetTFSI	0.2968	0.2968	0.2378	0.2722	0.2722	0.2182	0.2182	0.2182	0.2078	0.2614	0.1926	0.5630	0.3830	0.3620
	$EMIPF_6$	n/a	n/a	n/a	n/a	n/a	n/a	n/a	n/a	n/a	n/a	n/a	n/a	n/a	n/a
	EMITFSI	0.2666	0.2378	0.2564	0.2564	0.2564	0.2378	0.2336	0.2146	0.2078	0.2112	0.1984	0.3260	0.5398	0.3430
	$TBABF_4$	0.3430	0.2666	0.1724	0.3260	0.3260	0.2780	0.2666	0.2968	0.2336	0.2780	0.2780	n/a	0.5186	n/a
	$TBACIO_4$	0.2422	0.2422	0.2256	0.2514	0.2514	0.2514	0.2078	0.2078	0.2078	0.2722	0.1396	0.5880	0.3430	0.3036
	$TBAPF_6$	0.2968	0.3522	0.2422	0.2722	0.3036	0.3036	0.3036	0.2902	0.2902	0.3108	0.2378	n/a	0.4480	0.3944
	$TEABF_4$	0.2378	0.2614	0.2614	0.2614	0.2968	0.2146	0.2146	0.2146	0.2146	0.2468	0.2182	0.4638	0.4196	0.3036
	TEATFSI	0.2182	0.2182	0.2336	0.2968	0.2968	0.2780	0.2378	0.2378	0.2378	0.2378	0.2378	n/a	n/a	n/a
	$TMACIO_4$	0.2666	0.2666	0.2378	0.2378	0.2902	0.2336	0.2112	0.2112	0.2112	0.2336	0.1846	0.3944	0.4196	0.3182
	PureEMITFSI	0.1984	0.2514	0.2614	0.2336	0.2336	0.2514	0.2514	0.2722	0.2564	0.2840	0.2182	0.4480	0.4480	0.2564

Faradaic Charge (mC/cm^2)

Process	Growth Electrolyte	Cycling Electrolyte													
n_{ox}		$BMIBF_4$	$BMIPF_6$	cetTFSI	$EMIPF_6$	EMITFSI	$TBABF_4$	$TBACIO_4$	$TBAPF_6$	$TEABF_4$	TEATFSI	$TMACIO_4$	$PureBMIBF_4$	$PureBMIPF_6$	PureEMITFSI
	$BMIBF_4$	5.9525	5.9610	4.5780	4.8887	7.8622	4.8183	3.0432	5.4277	8.9784	10.7875	3.9183	n/a	n/a	n/a
	$BMIPF_6$	5.2669	5.5998	5.9968	3.8421	3.8421	6.2520	7.8860	6.8107	6.8751	7.6091	3.4241	n/a	n/a	n/a
	cetTFSI	5.4155	5.4155	4.6435	5.1578	5.1602	4.7770	3.9511	5.9283	8.2273	5.9114	3.6089	n/a	n/a	n/a
	$EMIPF_6$	6.6046	6.6046	6.0066	5.4666	1.7953	8.4849	5.0973	4.2486	5.5037	8.8677	4.7110	n/a	n/a	n/a
	EMITFSI	5.0929	7.0082	6.1388	5.5178	14.1106	6.2586	2.7460	6.6658	10.1625	9.3692	2.7310	n/a	n/a	n/a
	$TBABF_4$	2.2859	4.2162	0.3179	2.3329	17.8460	7.1366	4.7677	5.8165	3.4985	5.3919	5.3919	n/a	n/a	n/a
	$TBACIO_4$	8.3087	7.1914	7.1518	6.7872	7.9120	7.3982	2.6304	10.2379	10.3320	8.5561	2.6380	n/a	n/a	n/a
	$TBAPF_6$	5.6993	5.6993	7.2785	8.5705	9.2182	6.6097	4.6657	5.4324	6.1817	6.1817	3.0908	n/a	n/a	n/a
	$TEABF_4$	6.2600	6.1777	0.7784	5.0325	5.0325	n/a	n/a	2.7438	7.0570	7.0444	n/a	n/a	n/a	n/a
	TEATFSI	5.7286	5.7286	5.9056	4.8873	4.8873	5.9242	6.3072	7.7946	8.5756	10.0928	4.2460	n/a	n/a	n/a
	$TMACIO_4$	7.2560	7.1120	7.4942	4.9668	7.5176	5.1626	2.8530	6.6215	9.2686	9.6611	4.1066	n/a	n/a	n/a
	PureEMITFSI	7.5237	5.0143	9.3401	4.2857	5.8019	8.3506	8.0332	9.1475	10.0239	10.0239	6.1306	n/a	n/a	n/a
p_{ox}		$BMIBF_4$	$BMIPF_6$	cetTFSI	$EMIPF_6$	EMITFSI	$TBABF_4$	$TBACIO_4$	$TBAPF_6$	$TEABF_4$	TEATFSI	$TMACIO_4$	$PureBMIBF_4$	$PureBMIPF_6$	PureEMITFSI
	$BMIBF_4$	21.9287	21.7419	21.4449	24.6936	25.7075	22.6777	19.8074	21.8322	22.7903	21.6584	18.2204	1.9445	0.3911	1.4635
	$BMIPF_6$	19.5255	20.9431	19.4822	20.5763	18.7798	15.1497	15.9469	14.5937	19.7815	17.9963	12.7006	n/a	3.8705	n/a
	cetTFSI	24.0599	24.0599	22.3083	25.7370	23.2003	23.2003	22.5122	20.2610	20.6070	17.9553	18.8517	10.2503	9.2434	12.0700
	$EMIPF_6$	26.6580	24.9094	22.2469	31.2539	23.7472	17.3894	17.8932	27.1053	24.7829	21.4585	19.5201	6.2213	5.4692	n/a
	EMITFSI	24.1806	28.2617	24.7292	31.6159	24.7907	23.7819	29.3243	26.4789	26.7378	23.9350	20.2685	6.7852	8.8909	16.2305
	$TBABF_4$	17.8445	19.9076	6.7400	19.8613	18.3176	17.0857	21.0422	22.9743	23.2743	17.9357	17.9357	n/a	1.4827	n/a
	$TBACIO_4$	25.4554	22.5968	23.1723	25.4271	22.8497	21.3564	21.4707	24.6028	26.4805	25.3978	17.2067	2.4843	9.6919	1.8003
	$TBAPF_6$	24.1483	16.6574	21.6681	19.9949	24.4845	20.5539	22.6371	25.5476	23.1526	18.6379	18.2417	n/a	6.9771	5.8974
	$TEABF_4$	24.2663	24.1412	8.3549	26.6461	23.0319	24.3700	24.3700	22.2534	22.3933	22.8723	15.5335	5.2587	0.4070	2.9502
	TEATFSI	26.0339	18.6795	19.5479	20.9147	20.8628	20.8628	21.9412	23.7023	24.6113	22.5182	18.9154	n/a	n/a	n/a
	$TMACIO_4$	20.7780	18.8744	20.9951	23.6991	20.4975	19.5310	19.6384	26.4615	24.1938	21.0687	18.6959	4.2693	1.6300	5.4883
	PureEMITFSI	28.1541	27.3993	26.4587	28.7040	21.9663	20.9885	18.6505	17.7975	26.2207	16.9258	16.5942	12.4461	7.6828	15.5019

Faradaic Charge (mC/cm^2)

Process	Growth Electrolyte	Cycling Electrolyte													
n_{red}		$BMIBF_4$	$BMIPF_6$	cetTFSI	$EMIPF_6$	EMITFSI	$TBABF_4$	$TBACIO_4$	$TBAPF_6$	$TEABF_4$	TEATFSI	$TMACIO_4$	Pure$BMIBF_4$	Pure$BMIPF_6$	PureEMITFSI
	$BMIBF_4$	18.0924	18.0924	17.0868	20.5331	21.1352	13.4647	13.4647	16.1651	18.5496	20.6005	11.1362	n/a	n/a	n/a
	$BMIPF_6$	19.7938	20.2276	13.5751	13.5751	19.4626	13.9253	14.7297	15.1427	20.0492	17.7193	9.7219	n/a	n/a	n/a
	cetTFSI	20.4574	19.3666	19.1937	19.9676	19.9285	16.1830	14.1161	17.0678	18.8390	20.3748	12.4610	n/a	n/a	n/a
	$EMIPF_6$	23.5789	21.7832	16.4412	21.5052	18.8143	15.8740	12.4510	18.1071	15.1274	18.2506	15.8688	n/a	n/a	n/a
	EMITFSI	16.8963	20.3467	15.3232	30.0447	32.1931	13.7006	10.7743	13.6352	18.2996	26.2070	17.2634	n/a	n/a	n/a
	$TBABF_4$	13.7100	18.7956	4.7395	31.2254	38.8334	14.3656	10.7273	26.6789	22.9728	23.4141	23.4141	n/a	n/a	n/a
	$TBACIO_4$	18.2259	16.5685	17.2779	17.6625	17.6625	16.0499	2.9321	18.7270	16.7081	18.3063	2.2834	n/a	n/a	n/a
	$TBAPF_6$	17.3388	17.3388	17.7514	16.5396	16.3761	13.7575	11.2242	15.1432	15.1432	15.1432	9.8757	n/a	n/a	n/a
	$TEABF_4$	21.5972	21.5972	7.8269	19.7629	19.7629	14.4953	5.5062	16.4397	17.7532	17.2114	6.4019	n/a	n/a	n/a
	TEATFSI	19.0420	18.0778	18.0778	15.3747	15.3747	12.5891	12.9150	15.4966	17.2876	20.2400	9.8074	n/a	n/a	n/a
	$TMACIO_4$	20.3117	19.2485	17.2180	17.4012	16.4665	11.8472	5.0755	14.5562	18.5558	18.3399	7.1429	n/a	n/a	n/a
	PureEMITFSI	19.6791	21.4208	13.5400	19.0736	15.6196	16.3088	15.6404	15.0789	15.4675	14.0818	8.0693	n/a	n/a	n/a
p_{red}		$BMIBF_4$	$BMIPF_6$	cetTFSI	$EMIPF_6$	EMITFSI	$TBABF_4$	$TBACIO_4$	$TBAPF_6$	$TEABF_4$	TEATFSI	$TMACIO_4$	Pure$BMIBF_4$	Pure$BMIPF_6$	PureEMITFSI
	$BMIBF_4$	13.5293	10.2676	12.4210	12.0186	15.3107	14.0458	13.4600	10.7102	14.9906	13.4320	9.1522	1.3316	0.3094	0.9845
	$BMIPF_6$	8.9066	9.0392	8.6850	7.9629	7.1703	10.3540	9.5819	8.0377	12.4200	9.7432	8.7850	n/a	0.8708	n/a
	cetTFSI	10.0337	10.0337	11.3792	9.7783	9.7783	10.2170	10.6265	8.2794	8.2796	11.9786	8.5748	4.6477	1.1852	4.8005
	$EMIPF_6$	20.6720	19.3830	17.0950	17.3580	19.2660	20.5530	12.8790	15.6510	22.2720	16.4140	16.4000	n/a	2.7878	n/a
	EMITFSI	14.0190	14.0818	17.5879	16.3597	21.5699	16.2684	20.7593	15.5147	15.5244	15.5330	15.2162	2.1840	2.7658	4.9646
	$TBABF_4$	8.4033	8.5597	3.1964	11.0982	6.7955	10.9358	13.2901	11.3196	13.9598	8.7963	8.7963	n/a	0.9573	n/a
	$TBACIO_4$	14.3356	11.9983	12.0468	11.9839	12.7928	13.9294	14.0109	12.8368	12.8325	16.6157	9.7382	2.0203	0.9914	1.0791
	$TBAPF_6$	5.2998	7.0222	10.8480	6.8688	10.2574	13.3045	12.1576	13.6682	11.3472	10.1851	10.0729	n/a	2.2414	1.4449
	$TEABF_4$	13.1447	12.3106	7.6651	14.2463	14.5098	14.7531	14.7531	13.2054	13.2054	14.3083	14.4015	3.0196	0.4753	1.3579
	TEATFSI	8.9069	7.3443	10.8621	9.8722	11.0201	11.7670	11.9715	10.7781	11.9645	12.0059	10.4467	n/a	n/a	n/a
	$TMACIO_4$	14.1954	11.5579	12.4135	12.7625	14.2333	13.9519	14.0113	13.9981	11.6380	11.6481	10.1192	2.5456	0.8012	1.8178
	PureEMITFSI	11.6847	8.0545	10.7800	8.8502	8.8502	9.6003	10.0554	12.3041	13.5075	10.4016	11.4911	5.9185	3.2423	6.4795

Surface Concentration ($x10^{23}$ cm^{-3})

Process	Growth Electrolyte	Cycling Electrolyte												
n_{ox}		$BMIBF_4$	$BMIPF_6$	cetTFSI	$EMIPF_6$	EMITFSI	$TBABF_4$	$TBACIO_4$	$TBAPF_6$	$TEABF_4$	TEATFSI	$TMACIO_4$	$PureBMIBF_4$	$PureBMIPF_6$	PureEMITFSI
	$BMIBF_4$	1.5000	1.5000	1.1500	1.2500	1.7000	0.8500	n/a	1.1000	1.9000	2.4000	0.1000	n/a	n/a	n/a
	$BMIPF_6$	0.8000	0.9000	1.4000	1.0000	1.0000	1.7000	2.2000	1.9000	1.8000	2.0000	0.9000	n/a	n/a	n/a
	cetTFSI	1.4000	1.4000	1.1000	1.2000	1.2000	1.1000	0.9000	1.4000	2.0000	1.4000	0.8000	n/a	n/a	n/a
	$EMIPF_6$	1.6000	1.6000	1.5000	1.3000	0.3000	2.1000	1.2000	1.0000	1.3000	2.2000	1.1000	n/a	n/a	n/a
	EMITFSI	1.2000	1.7000	1.5000	1.3000	1.6000	1.6000	0.7000	1.7000	2.6000	2.4000	0.7000	n/a	n/a	n/a
	$TBABF_4$	0.6000	1.1000	0.1000	0.6000	0.3000	1.9000	1.3000	1.6000	0.9000	1.4000	1.4000	n/a	n/a	n/a
	$TBACIO_4$	1.8000	1.5000	1.5000	1.4000	1.7000	1.5000	0.1000	2.3000	2.3000	1.8000	0.1000	n/a	n/a	n/a
	$TBAPF_6$	1.1000	1.1000	1.6000	1.3000	1.3000	1.7000	1.2000	1.4000	1.6000	1.6000	0.8000	n/a	n/a	n/a
	$TEABF_4$	1.6000	1.6000	0.2000	1.3000	1.3000	n/a	n/a	0.7000	1.8000	1.8000	n/a	n/a	n/a	n/a
	TEATFSI	1.1000	1.1000	1.2000	0.9000	0.9000	1.2000	1.3000	1.7000	1.9000	2.3000	0.7000	n/a	n/a	n/a
	$TMACIO_4$	1.5000	1.5000	1.6000	0.9000	1.6000	1.0000	n/a	1.3000	2.0000	2.1000	0.6000	n/a	n/a	n/a
	PureEMITFSI	2.0000	1.3000	2.5000	1.1000	1.5000	2.2000	2.1000	2.4000	2.6000	2.6000	1.6000	n/a	n/a	n/a
p_{ox}		$BMIBF_4$	$BMIPF_6$	cetTFSI	$EMIPF_6$	EMITFSI	$TBABF_4$	$TBACIO_4$	$TBAPF_6$	$TEABF_4$	TEATFSI	$TMACIO_4$	$PureBMIBF_4$	$PureBMIPF_6$	PureEMITFSI
	$BMIBF_4$	6.9200	7.3300	6.9500	8.6000	8.0000	7.2000	6.8000	6.9000	7.2000	6.9000	7.9000	0.5100	0.1200	0.3900
	$BMIPF_6$	6.4000	7.1000	6.5000	6.6000	5.7000	5.1000	5.3000	4.7000	6.4000	5.8000	5.0000	n/a	1.0600	n/a
	cetTFSI	7.6000	7.6000	7.1000	8.1000	7.2000	7.2000	7.0000	6.3000	6.3000	5.5000	7.0000	2.8800	2.8800	3.2400
	$EMIPF_6$	8.4000	8.1000	7.0000	10.7000	10.9000	5.3000	5.3000	8.5000	9.7000	6.3000	7.5000	1.8900	1.5900	n/a
	EMITFSI	8.4000	9.0000	7.9000	10.1000	7.8000	7.5000	9.5000	7.8000	8.0000	7.0000	7.8000	1.9400	2.9900	5.2500
	$TBABF_4$	5.4000	6.3000	2.3000	4.7000	3.9000	5.3000	8.0000	7.7000	9.9000	5.8000	5.8000	n/a	0.4000	n/a
	$TBACIO_4$	7.8000	7.0000	7.0000	8.4000	6.8000	6.4000	7.0000	7.1000	8.5000	7.8000	7.6000	0.6600	3.4800	0.4800
	$TBAPF_6$	7.6000	6.2000	6.4000	8.4000	7.5000	6.2000	7.0000	7.9000	7.2000	5.6000	6.5000	n/a	2.0700	2.0700
	$TEABF_4$	8.1000	8.1000	2.5000	9.1000	7.7000	8.5000	8.5000	7.0000	7.0000	7.6000	6.9000	1.8800	0.1040	0.8050
	TEATFSI	8.0000	6.2000	5.8000	6.6000	7.0000	7.0000	6.7000	7.2000	7.9000	6.9000	7.6000	n/a	n/a	n/a
	$TMACIO_4$	6.2000	5.9000	6.2000	7.9000	6.1000	5.9000	6.4000	8.3000	7.2000	6.4000	7.5000	1.1550	0.4710	1.3460
	PureEMITFSI	9.2000	8.6000	8.1000	9.0000	6.7000	6.5000	5.6000	5.6000	8.8000	4.9000	5.1000	3.9100	2.4900	4.0200

Surface Concentration ($x10^{23}$ cm^{-3})

Process	Growth Electrolyte	Cycling Electrolyte												
n_{red}		$BMIBF_4$	$BMIPF_6$	cetTFSI	$EMIPF_6$	EMITFSI	$TBABF_4$	$TBACIO_4$	$TBAPF_6$	$TEABF_4$	TEATFSI	$TMACIO_4$	$PureBMIBF_4$	$PureBMIPF_6$	PureEMITFSI
	$BMIBF_4$	6.1500	6.1500	6.8400	6.2400	8.6400	3.5400	3.5400	3.8400	5.5400	6.3400	2.7400	n/a	n/a	n/a
	$BMIPF_6$	6.0400	6.4400	3.8400	3.8400	6.0400	3.7400	4.3400	4.3400	6.4400	4.8400	1.8400	n/a	n/a	n/a
	cetTFSI	5.5400	5.0400	5.8400	5.4400	5.3400	4.1400	2.8400	4.0400	5.4400	6.3400	3.0400	n/a	n/a	n/a
	$EMIPF_6$	7.1400	6.4400	6.6400	8.7400	3.1400	5.4400	3.9400	6.5400	5.2400	6.6400	3.5400	n/a	n/a	n/a
	EMITFSI	5.5400	6.5400	4.8400	6.0400	5.7400	4.7400	4.6400	4.6400	6.9400	6.6400	3.6400	n/a	n/a	n/a
	$TBABF_4$	5.7400	4.9400	0.4400	7.1400	7.1400	6.0400	5.4400	6.2400	5.1400	4.8400	4.8400	n/a	n/a	n/a
	$TBACIO_4$	6.6400	6.3400	5.5400	6.1400	6.1400	5.6400	0.7400	6.6400	5.9400	7.1400	1.4400	n/a	n/a	n/a
	$TBAPF_6$	8.1400	8.1400	6.6400	6.7400	6.7400	4.9400	4.1400	5.6400	5.6400	5.6400	4.3400	n/a	n/a	n/a
	$TEABF_4$	10.0400	10.0400	2.4400	7.8400	7.8400	4.8400	2.9400	5.4400	6.1400	6.9400	3.2400	n/a	n/a	n/a
	TEATFSI	5.8400	5.5400	5.5400	5.5400	5.5400	4.4400	4.4400	5.9400	6.6400	7.8400	4.0400	n/a	n/a	n/a
	$TMACIO_4$	9.3400	8.2400	7.0400	7.0400	6.6400	3.5400	1.3400	4.8400	7.5400	7.5400	2.9400	n/a	n/a	n/a
	PureEMITFSI	7.1400	9.0400	5.5400	7.5400	6.1400	6.3400	6.1400	5.4400	5.8400	5.2400	3.7400	n/a	n/a	n/a
p_{red}		$BMIBF_4$	$BMIPF_6$	cetTFSI	$EMIPF_6$	EMITFSI	$TBABF_4$	$TBACIO_4$	$TBAPF_6$	$TEABF_4$	TEATFSI	$TMACIO_4$	$PureBMIBF_4$	$PureBMIPF_6$	PureEMITFSI
	$BMIBF_4$	3.0100	2.6300	3.1800	2.7800	3.9800	3.1800	2.9800	2.2800	3.3800	2.9800	1.8800	0.4400	0.0960	0.2840
	$BMIPF_6$	1.8800	1.8800	1.7800	1.8800	1.6800	2.4800	2.2800	1.8800	2.5800	1.8800	1.6800	n/a	0.3340	n/a
	cetTFSI	1.9800	1.9800	2.2800	1.8800	1.8800	1.9800	2.0800	1.4800	1.4800	1.5800	1.8800	1.7080	1.3660	1.8160
	$EMIPF_6$	0.9955	0.9951	0.9476	0.9873	0.9958	0.9714	0.9733	0.9967	0.9861	0.9951	0.9824	n/a	0.9900	n/a
	EMITFSI	2.7800	2.7800	3.6800	3.3800	2.7800	4.1800	4.4800	3.2800	3.2800	3.2800	2.5800	0.6800	1.9400	1.9400
	$TBABF_4$	2.0800	2.0800	0.2800	2.3800	1.4800	2.3800	2.9800	2.4800	2.9800	1.5800	1.5800	n/a	0.3400	n/a
	$TBACIO_4$	3.6800	3.0800	3.0800	3.0800	3.2800	3.5800	3.5800	3.2800	3.2800	4.2800	2.4800	0.7000	1.2200	0.3200
	$TBAPF_6$	1.3800	1.8800	2.7800	1.7800	2.6800	3.4800	3.1800	3.5800	2.9800	2.6800	2.5800	n/a	1.0600	0.4600
	$TEABF_4$	3.3800	3.1800	1.9800	3.6800	3.7800	3.7800	3.7800	3.3800	3.3800	3.6800	3.6800	0.9800	0.1600	0.4000
	TEATFSI	2.2800	1.8800	2.7800	2.5800	2.8800	3.0800	3.0800	2.7800	3.0800	3.0800	2.6800	n/a	n/a	n/a
	$TMACIO_4$	3.6800	2.9800	3.1800	3.2800	3.6800	3.5800	3.5800	3.5800	2.9800	2.9800	2.5800	0.9000	0.3600	0.5600
	PureEMITFSI	1.6800	1.6800	2.3800	1.8800	1.8800	2.0800	2.5800	3.1800	3.4800	2.6800	2.7800	2.4400	1.5600	1.8800